CRANFIELD UNIVERSITY

CHIARA PALLA

DEVELOPMENT OF DRAG AUGMENTATION SYSTEMS FOR DE-ORBITING SMALL SATELLITES

SCHOOL OF AEROSPACE, TRANSPORT AND MANUFACTURING
Space Research Group

PhD
Academic Year: 2016–2017

Supervisor: Dr Jenny Kingston
June 2017

CRANFIELD UNIVERSITY

SCHOOL OF AEROSPACE, TRANSPORT AND
MANUFACTURING
Space Research Group

PhD

Academic Year: 2016–2017

CHIARA PALLA

Development of Drag Augmentation Systems for De-orbiting
Small Satellites

Supervisor: Dr Jenny Kingston
June 2017

This thesis is submitted in partial fulfilment of the
requirements for the degree of PhD.

Abstract

The adoption of the ISO 24113 by ESA in 2014 has set an important milestone for the path towards an evolution and worldwide compliance of the Space Debris Mitigation (SDM) requirements.

Small spacecraft classes have limited propulsion capabilities or even they are not provided with propulsion subsystem to achieve a controlled re-entry. This issue brings the need to develop affordable de-orbiting technologies with a limited reliance on the system level performance, ideally largely passive methods.

The main aim of this research is to develop passive drag augmentation systems (DAS) for de-orbiting small spacecraft at the end of life, enabling them to comply with SDM requirements.

After a feasibility study for the potential commercial use of DAS, the satellites' need for passive de-orbiting technologies is investigated through market forecast and future scenarios of spacecraft compliance to the 25 years re-entry requirement.

Spacecraft subsystems failures are analysed statistically to assess how they might impact the end of mission phase and to guide in the de-orbiting strategy selection.

The applicability of current Cranfield DAS design is assessed by developing a simple model for preliminary drag area calculation, validating it with STELA and DRAMA, and calculating the additional area needed vs the area provided by DAS for a spacecraft sample.

The requirements for DAS are analysed considering the customer's needs with respect to the internal design drivers. A design parameters analysis is performed to evaluate the scalability of the DAS and their compatibility with satellite platforms. The parametric study together with the requirements analysis provide useful input to explore new concepts based on the heritage designs.

In parallel, the De-Orbit Mechanism (DOM) technological demonstrator is developed from prototype model up to flight model, after undergoing qualification test campaign. The DOM will fly on board the upcoming ESA ESEO mission.

This research will enable a commercial DAS products offering that will be an attractive solution for small satellite integrators, allowing them to meet debris mitigation requirements.

Keywords: space debris mitigation, Clean Space, de-orbiting, drag augmentation

Acknowledgements

To my supervisor, Dr Jenny Kingston, goes my deep gratitude for having guided me during this journey and being able to maintain that balance between instructing and encouraging.

Her energy and enthusiasm have shown me the bright side of the research.

Also, I would like to thank Dr Steve Hobbs for the fruitful discussions and feedback on my research work.

Nobody better than my office colleagues can understand what takes to achieve this goal. Thanks to them for the exchanges of ideas and for sharing the passion for Space.

Knowledge would not be enough without the close friends who share my values, reasons, and feelings.

Simply always there to support me, during cheerful and challenging times, thanks to my family who encouraged me to embark this journey.

Contents

List of Figures

List of Tables

List of Abbreviations

AO	Announcement of Opportunity
AOCS	Attitude & Orbit Control System
ATOX	Atomic Oxygen
ATP	Area Time Product
ATT	Attitude & Thrusters
BB	Building Block
BC	Ballistic Coefficient
CAGR	Compound Annual Grow Rate
CDF	Concurrent Design Facility
DAS	Drag Augmentation System
DOM	De-Orbit Mechanism
DRAMA	Debris Risk Assessment and Mitigation Analysis
EBB	Elegant Bread Board
ECSS	European Cooperation for Space Standardization
EoL	End of Life
EoM	End of Mission
ESA	European Space Agency
ESEO	European Student Earth Orbiter
FMECA	Failure Mode Effects and Criticality Analysis

FS	Flight Spare
GEO	Geostationary Earth Orbit
GTO	Geostationary Transfer Orbit
HDMR	Hold-Down and Release Mechanism
IADC	Inter-Agency Space Debris Coordination Committee
LEO	Low Earth Orbit
LSI	Large System Integrator
MECH	Mechanism & Structures
MEO	Medium Earth Orbit
MOD	Mean of Date
MSFC	Marshall Space Flight Center
NGSO	Non-Geosynchronous Orbits
OBDH	On-board Data Handling
OSCAR	Orbital SpaceCraft Active Removal
PAY	Payload
PDU	Power Distribution Unit
PFM	Protoflight Model
POW	Power
SDM	Space Debris Mitigation
SSO	Sun Synchronous Orbit
STELA	Semi-analytic Tool for End of Life Analysis
S/C	Spacecraft
TLE	Two Line Element
TRL	Technology Readiness Level
TTC	Telemetry Tracking & Command
UNCOPUOS	United Nations Committee on the Peaceful Uses of Outer Space

UNK   Unknown

VDA   Vapour-deposited Aluminium

Chapter 1

Introduction

This chapter presents the rationale and significance of the "problem" which frames the whole doctoral research. The objectives of the research work are here described and their connection with the thesis structure is shown. The novelties of this PhD are introduced through the publications and showing how they relate to the objectives.

1.1   Problem statement

Space missions in Low Earth Orbit (LEO) are severely affected by the build-up of orbital debris. For this reason the European Space Agency (ESA) established the Clean Space initiative in 2012 to redesign the way industry operates and ensure it operates in a safely and sustainable way on space environment.

The international awareness of the problem is reflected in the IADC (Inter-Agency Space Debris Coordination Committee) debris mitigation guidelines [IADC, 2007], which indicate the removal of space systems that interfere with the LEO region not later than 25 years after the End of Mission.

The adoption of the ISO 24113 by ESA in 2014 [ESA Director General's Of-

fice, 2014] has set an important milestone for the path towards an evolution and worldwide compliance of the Space Debris Mitigation (SDM) requirements. Different countries have so far implemented the SDM within their National Space Law as a condition for the launch licence/authorization (e.g.: France, UK, Canada, USA), some have other SDM mechanism implementation, but many other still do not have any SDM provision implemented in their law. The trend seems anyway that future Space Laws will likely to be strict with SDM compliance [Petros, 2016].

According to CNES [Dolado-Perez et al., 2014] approximately 60% of LEO objects are currently compliant with the 25 years residual lifetime guideline/requirement and there is a general trend to increase the efforts or at least "attempt" for post mission disposal.

However, small classes of satellites show degraded adherence levels; according to the estimation of the ESA Space Debris Office [Frey et al., 2016] the lowest compliance rates is for objects with mass between 10 and 1000 kg (around 30%).

Considering that the future population in LEO will be dominated by space missions with mass below 1000 kg with a large share in the commercial sector [Doncaster and Shulman, 2016], the implications of non-compliances within these satellite classes should not be underestimated.

Micro and smaller spacecraft have limited propulsion capabilities or even they are not provided with propulsion subsystem to achieve a controlled re-entry, so they need different de-orbit strategies. This issue brings the need to develop affordable de-orbit technologies with a limited reliance on the system level performance of the host satellite, ideally largely passive methods.

Passive disposal strategies which take advantage of aerodynamic drag as the de-orbit force are particularly attractive because they are independent of spacecraft propulsion capabilities.

Drag augmentation devices, also known as drag sails, have demonstrated achievement of high TRL in the last few years, with some concepts already on-orbit [Kuwahara et al., 2013], [Kingston et al., 2014], [Rasse, 2015].

However, despite the high TRL, these devices are not yet strictly commercial products and a family design for de-orbiting different range of spacecraft has not been developed yet.

1.2   Research aim and objectives

The main aim of this research work is to develop a range of drag augmentation systems (DAS)[1] for de-orbiting small spacecraft at the end of life, enabling them to comply with SDM requirements.

A set of objectives were defined at the beginning of the research to help in achieving the main goal. Table 1.1 summarizes the main objectives of the PhD and how to achieve them.

---

[1]The heritage design and level of maturity of DAS at Cranfield is described in detail in Chapter 3

Table 1.1: PhD objectives.

	OBJECTIVE	How to achieve it?
1	Assess the feasibility for potential commercial use of DAS	Identify current legislation on SDM, preliminary markets forecast, review of disposal methods for satellites, options attractive for people and companies.
2	Identify and review the state of the art on drag de-orbiting	Overview of current methods and mechanisms, Cranfield technology background evaluation.
3	Determine the need for passive de-orbiting in the future	STELA validation for re-entered S/C, future launches database development, STELA simulations for satellites' decay, identify S/C compliances with SDM.
4	Assess satellites' subsystems failures	Database of subsystems failures, statistical analysis of subsystems reliabilities, reliabilities vs. de-orbit strategies, trade-off analysis to guide strategy decision.
5	Assess the applicability of DAS design	Simple model for preliminary drag area, validate model with STELA and DRAMA, calculate additional area needed vs area provided by DAS for S/C sample.
6	Analyse requirements of DAS.	Definition of target spacecraft from previous objectives; compliance of baseline design vs. requirements; interface and operational capabilities; performance analyses.
7	Evaluate the scalability for a DAS family	Design parameters analysis, compatibility with S/C platforms, derived DAS design for different range of satellites.
8	Develop DOM payload technological demonstrator	Design phases (starting from PDR), testing, and delivery. Work performed in parallel.

1.3   Thesis outline

The thesis is divided into nine chapters. Fig. 1.1 presents an overview of the different chapters and how they relate to the PhD objectives. As can be seen, the work in each chapter contributes to the others. The Critical Evaluation (Chapter 8) draws together the research outcomes and the Conclusions (Chapter 9) summarize the achievements.
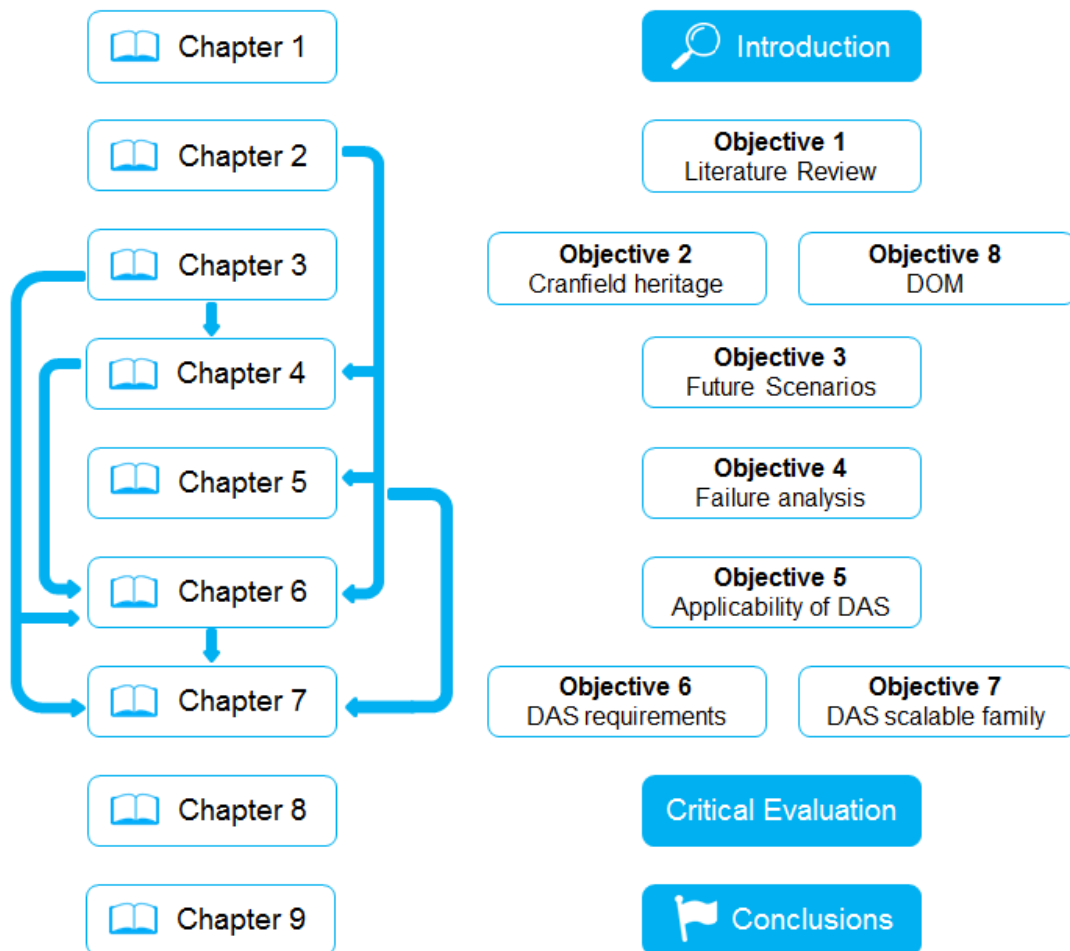
Figure 1.1:   Thesis outline diagram.

1.4   Novelties and publications

This section gives an overview of the novelties by presenting the journal articles and the conference papers produced.

Journal articles:

[1] Palla C. and Kingston J., *Forecast analysis on satellites that need de-orbit technologies: future scenarios for passive de-orbit devices*, CEAS Space Journal, 2016. DOI:10.1007/s12567-016-0120-x

[2] Palla C., Peroni M., Kingston J., *Failure analysis of satellite subsystems to define suitable de-orbit devices*, Acta Astronautica, 2016. DOI:10.1016/j.actaastro.2016.07.021

Conference papers (only as main author listed here) included in the proceedings:

[1] Palla C. and Kingston J., *How many satellites need de-orbit technologies? Future scenarios for passive de-orbit devices*, 5th CEAS Air and Space Conference, 7-11 September 2015, Delft, Netherlands.

[2] Palla C., Kingston J., Peroni M. *Failure analysis of satellite subsystems to define suitable de-orbit devices*, 66th International Astronautical Congress, 12-16 October 2015, Jerusalem, Israel. Paper ID: IAC-15-A6.4.1.

[3] Palla C. and Kingston J., *Applicability of drag augmentation systems to enable future LEO spacecraft compliance with debris mitigation guidelines*, 67th International Astronautical Congress, 26-29 September 2016, Guadalajara, Mexico. Paper ID: IAC-16-A6.4.5.

[4] Palla C. and Kingston J., *Development of a family of scalable drag augmentation systems*, IEEE Aerospace Conference, 4-11 March 2017, Big Sky, Mon-

tana, USA.

[5] Palla C., Kingston J., Hobbs S., *Development of commercial drag-augmentation systems for small satellites*, 7th European Conference on Space Debris, 18-21 April 2017, ESA/ESOC, Darmstadt, Germany.

As can be seen, the publications match with the objectives of the PhD.

The first article considers the potential target market for passive de-orbiting. This is a different perspective, because most of the studies in the literature concentrate on the technical development of the de-orbit device, with little or no discussion of the wider market need.

The second article is novel as it explores which de-orbit strategy is more appropriate based on reliability data and using a targeted classification of satellites.

The conference papers produced in 2016 and 2017 focus on the applicability of the DAS design with respect to the market need and on the further development of the DAS technology to be suitable for a broader range of satellites.

In addition, in the framework of the PhD, a proposal to ESA AO on CleanSat was prepared and successful accepted:

- *Drag-Augmentation System Modules for LEO Satellites*, CleanSat's technology assessment and concurrent engineering in support of LEO platform evolutions, AO/1-8287/15/NL/MT, July 2015.

The research novelties will be discussed in greater details in the Critical Evaluation Chapter.

Chapter 2

Literature Review

This chapter is intended to give an overview of the relevant background and key aspects for the research work performed.

This encompasses the space debris environment and the debris mitigation actions, both in terms of regulations and de-orbiting technologies, current and future projections on spacecraft market, a brief literature on the survivability, an overview of the models used in the decay analyses.

2.1 Space debris environment

The 60 years of space activities with more than 7200 satellites already launched have produced more than 20000 human-made objects larger than 10 cm (currently in orbit) [ESA Clean Space, 2016], making space debris a substantial problem for future space missions.

Space debris, as defined by Inter-Agency Space Debris Coordination Committee (IADC) and reported in [Klinkrad, 2006] are *"all man made objects including fragments and elements thereof, in Earth orbit or re-entering the atmosphere, that are*

non functional".
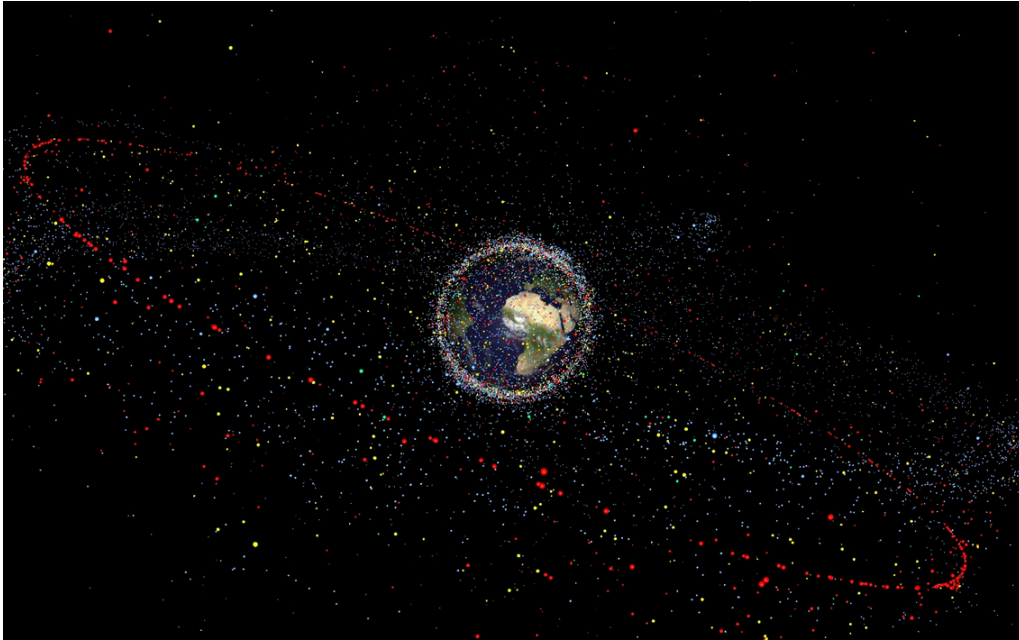
Figure 2.1: Trackable objects in orbit around the Earth, the size of the debris is exaggerated compared to the Earth (Courtesy of ESA).

The US Space Surveillance Network regularly tracks and keeps catalogued more than 20000 orbiting objects, including items larger than approximately 5 to 10 cm in LEO and 30 cm to 1 m at GEO [ESA Space Debris Office, 2017].

The tracking and cataloguing of objects is carried out by ground-based radars and optical measurements. The observable size of space debris objects from Earth is due to radar sites limitations on power and wavelengths. According to [ESA Space Debris Office, 2017] ground-based search radars can actually detect objects down to 1 cm size, however, the orbits of these objects can not be determined with sufficient accuracy to be predictable and neither they can be correlated with specific launch or break-up event.

At the reference epoch 1 January 2017 the total number of observable objects was 18753 [Frey and Lemmens, 2017]. More than 65% of these objects are orbiting

in LEO and about 5% in GEO.

Scientific models estimate the total number of debris objects to be in the order of 29000 for objects larger than 10 cm, 740000 for size >1 cm and more than 160 million for size >1 mm [Klinkrad, 2015].
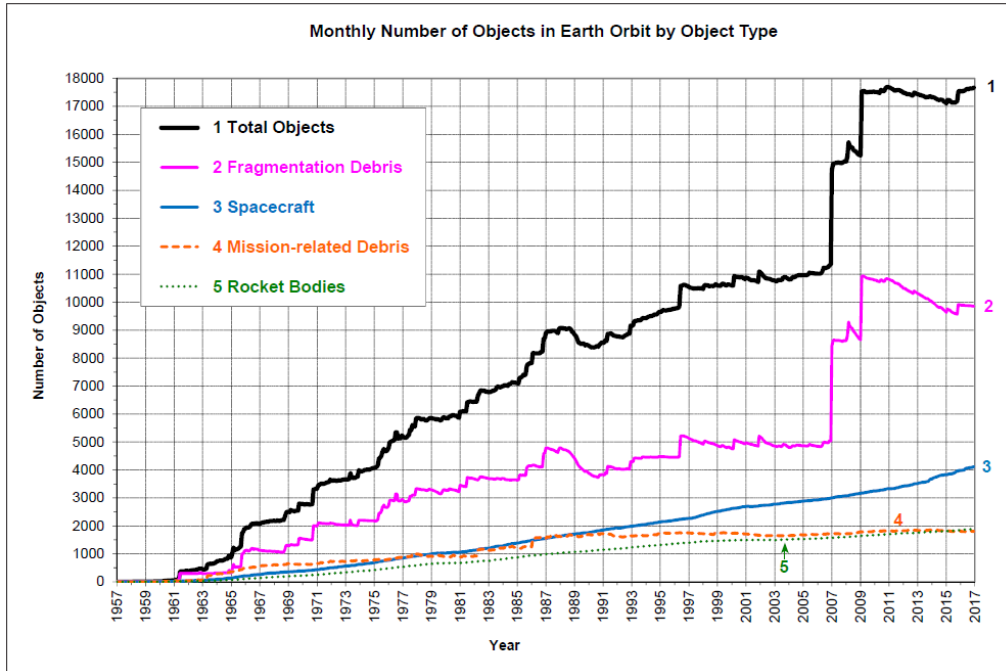
Figure 2.2:   Monthly numbers of catalogued objects in Earth Orbit by Object Type NASA Orbital Debris QN, Issue 1, Feb 2017.

The catalogued orbit population includes operational satellites only for the 6%; 38% instead are decommissioned satellites, upper stages rockets, mission-related object; the remaining population is composed by in-orbit fragmentations objects, recorded since 1961.

The potential sources for the formation of space debris are:

- Explosions (which account for 42% of the total)

- Hypervelocity collisions

11

- Deteriorations of spacecraft

- Solid rockets firings

- Unknown sources

The problem of a potential creation of *"debris belt"* was identified by D. J. Kessler back in 1978 [Kessler and Cour-Palais, 1978]. Kessler developed a model which took into account the major source and sink terms driving the growth of satellite population in orbit. His predictions, considering a continuing trend at that time, were:

- Collisional breakups as a new source of debris, possibly before 2000.

- A debris flux higher than natural meteoroid flux in certain orbital regions.

- An exponential growth of the debris flux even without any new insertion in orbit, this is the well known cascade effect or Kessler syndrome.

Fig. 2.2 shows a jump in the curve of number of objects in 2009, precisely on February the 10th. This is due to the catastrophic collision between the Iridium 33 and Cosmos 2251 satellites at an altitude of 790 km. This represents the first clear example of what Kessler predicted in 1978.

In his review of the *"significance of the Kessler syndrome today"* [Kessler, 2009] Kessler affirmed there are minor differences, despite the fact that all existing data and analysis support the major conclusions presented in [Kessler and Cour-Palais, 1978]. The main difference was between the predicted growth rate compared with the actual growth rate, which is less. This was due to the reduction of accidental explosions in orbit, an abnormal high solar activity, and the declining economy of the USSR. The growth rate would have been even lower, had it not been for

the intentional Chinese anti-satellite test in 2007. As can be seen in Fig. 2.2, this produced over 2000 of catalogable fragments.

As for the debris distribution, in 2013 the peak densities were around the altitude of 800 km (see Fig. 2.3) with inclination peaks near 72°, 82° and 97° [Klinkrad, 2015].
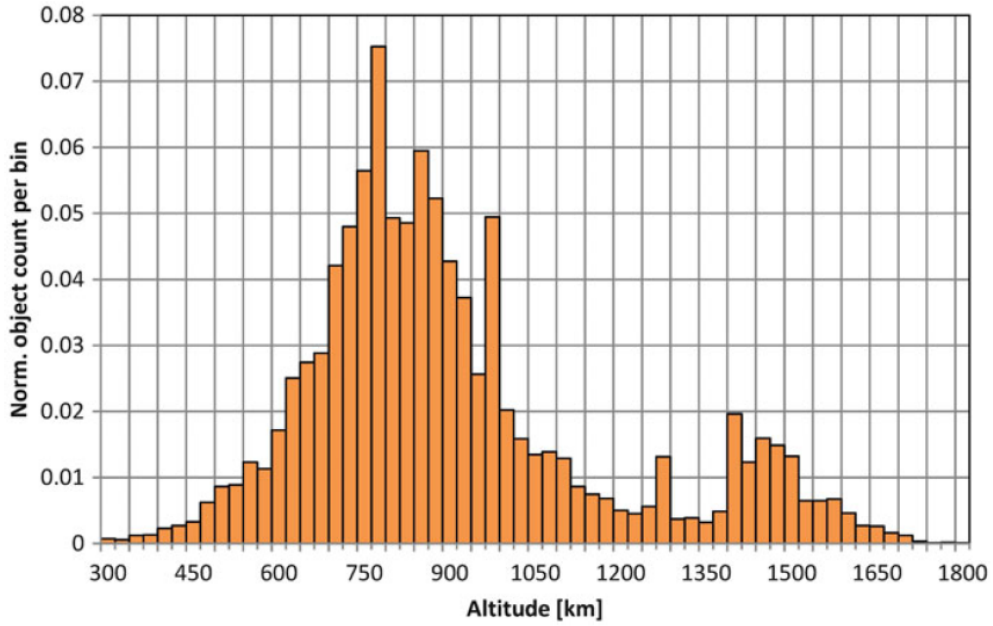
Figure 2.3: Altitude distribution of catalog-size objects (>10 cm) in LEO in November 2013. The normalized count is in fractions per 50 km altitude bin for a total of 12170 objects [Klinkrad, 2015].

A key point for the estimation of the future population will be the estimation of fragments derived from collisions and or explosions. This will strongly depend on on-orbit breakups, non-fragmentations debris sources, constellation deployments, models of future traffic. As Kessler presented in the 7th Space Debris Conference, improved models need to be supported by increased measurements and the maximum acceptable debris environment, including the probability of maintaining it, need to be addressed.

The natural mechanisms opposing to the increase of space debris are the atmo-

spheric drag and the solar radiation pressure, however the solely natural de-orbit, without any proper planned strategy, can take a very long time. In addition from high altitudes there is a migration of the debris to lower operational orbits.

2.2   Space debris mitigation

The most effective way of averting the predicted "Kessler syndrome", and stabilizing the space debris environment, is then reducing the mass in regions with high densities of space debris. This can be achieved by means of international efforts and collaboration among the different space actors through mitigation measures and official regulations.

Chobotov in [Chobotov, 2002] asserts that mitigation measures shall focus on limiting sources of debris in the future. The different strategies encompass passivation of spacecraft and upper stages, de-orbiting of rocket bodies and EoL orbiting items, re-orbiting techniques, and collision avoidance study together with shielding technologies. In a nutshell these represent the focus of ESA Clean Space.

2.2.1   Clean Space

Space debris represents a major risk to future space missions, this is why ESA, within the Clean Space initiative, is establishing requirements to mitigate the production of new space debris.

ESA started the Clean Space initiative in 2012 to redesign the way industry operates and ensure it operates in a safe and sustainable way both on terrestrial and space environments. Due to its broad range activities, the initiative was introduced as a cross-cutting theme within ESA's Technology programmes as part of Agenda 2015 [ESA, 2014a].

Figure 2.4: Clean Space logo (Courtesy of ESA).

Clean Space was originally implemented in four main branches: Eco-design, Green technologies, Space debris mitigation, and Technologies for space debris remediation. More recently the Clean Space activities evolved into three different branches, which reflect the "solutions" to address the challenge of a cleaner and sustainable space (and space industry).

According to [ESA, 2016] the three branches, graphically represented in Fig. 2.5, are:

- EcoDesign: designing to address environmental impacts and foster green technologies;

- CleanSat: designing to reduce the production of space debris;

- eDeorbit: removing a large piece of space debris from orbit.

In particular, CleanSat represents the programmatic response of ESA to support the European space industry with the worldwide market demand for SDM compliant solutions [Antonetti et al., 2015b]. ESA Clean Space is coordinating the CleanSat programme, which is addressing three key areas for spacecraft to be launched:

- Design for Demise: to ensure spacecraft comply with the casualty risk on

15
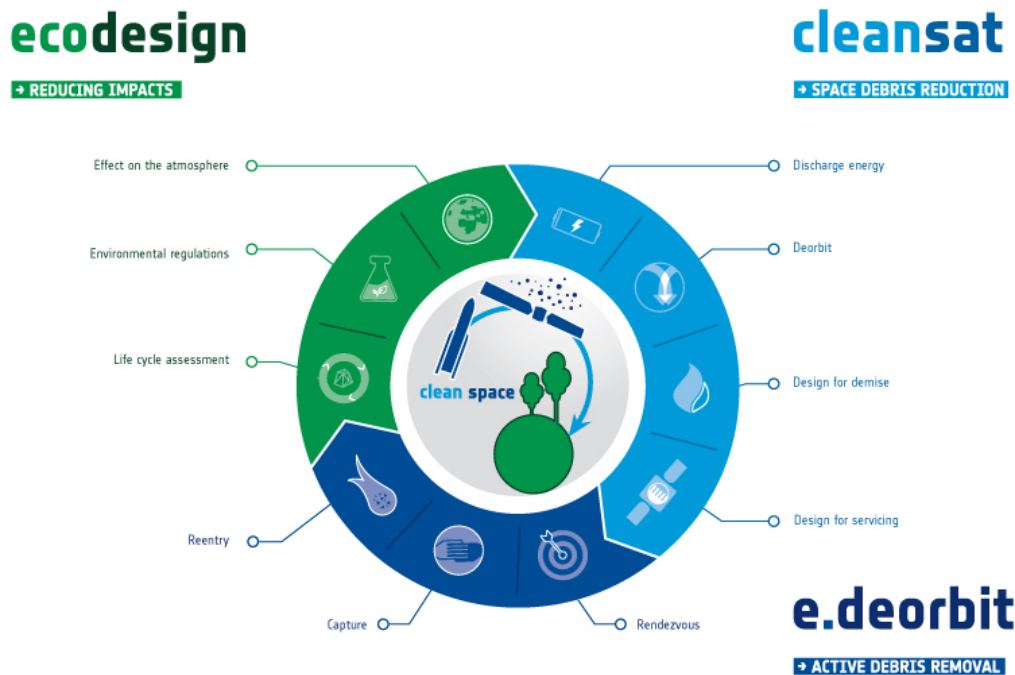
Figure 2.5: Clean Space branches infographics (Courtesy of ESA).

ground (shall not exceed 10^{-4} [ESA SDM WG, 2015]) and that they demise upon re-entry.

- De-orbiting systems: to remove satellites in LEO within 25 years after the end of mission, ideally without reducing mission efficiency.

- Passivation: to permanently deplete or make safe all source of stored energy on-board (mainly propulsion and power subsystems).

CleanSat is supporting LEO platform evolution through technology assessment and concurrent engineering studies [ESA, 2015a] to mature and develop suitable "building blocks" (BB) that will help satellite designers and manufacturers make their future satellites compliant with current best practice guidelines and regulations.

2.2.2 Legislation

The first concerns on space debris date back to the 70's, mainly at NASA level [Brooks et al., 1974]. However, as Bonnal pointed out [Bonnal, 2016], there were no recommendations but just facts and first models on collision and debris propagation.

Between the late 60's and 70's the basis for space flight regulatory environment were established under the United Nations Committee on the Peaceful Uses of Outer Space (UNCOPUOS). Four main international treaties were derived from the activities of UNCOPUOS and ratified by the major space-faring nations [BSI Standards Publication, 2011a]. These were the Outer Space Treaty (1967), the Rescue Agreement (1968), the Liability Convention (1972), and the Registration Convention(1975). Particularly relevant for the subsequent space debris legislation were the Outer Space Treaty and the Liability Convention. The treaties introduced and addressed issues on the international responsibility for national activities in space and associated liabilities for launching State.

As mentioned before, the problem and potential cascading effect was identified by Kessler in 1978 [Kessler and Cour-Palais, 1978]. In this work we see for the first time recommendations on "de-orbit" at the end of mission and avoiding explosions and collisions.

As showed by Bonnal [Bonnal, 2016], in the 80's there was a general dissemination of the information at international level on space debris environment and modelling through journal articles and agencies reports.

In Europe the first standard does not appear before 1988, when the ESA-PSS-01-40 Issue 2 was issued. The document was not specific on space debris, but included associated requirements as controlled re-entry, de-orbiting, collision risk and passivation.

17

National standards followed (e.g.: France, Germany, Russia) with a relatively good coherence. This led the way to the preparation of International standards. The first official meeting of the Inter-Agency Space Debris Coordination Committee (IADC) took place in Moscow in 1993. The IADC includes four Working Groups (Measurements, Environment and Database, Protection, Mitigation) and a Steering Group with technical experts from 13 different countries (and including ESA).

NASA, instead, issued the specific standard *Guidelines and Assessment Procedures for Limiting Orbital Debris* in 1995 [NASA Safety Standard, 1995]. In the NASA standard appears also (probably among the first) the end of life disposal *"to limit the orbital lifetime after mission completion to 25 years or maneuvering to a disposal orbit"*.

The IADC established a set of guidelines, known as IADC Space Debris Mitigation Guidelines, which were unanimously approved in 2002 and then revised in 2007 [IADC, 2007].

On the basis of the IADC Guidelines the UNCOPUOS of United Nations elaborated their official guidelines in 2007.

The lengthy process that brought to the high level standard *ISO 24113 Space Systems − Space Debris Mitigation Requirements* passed through European SDM Standards in 1998 and European Code of Conduct in 2003. The first formal issue was in February 2010.

ESA adopted the ISO 24113 [BSI Standards Publication, 2011a] as requirements for its missions [ESA Director General's Office, 2014] in March 2014.

As mentioned before, different countries implemented space law within their national regulations (see Table 2.1), however the first law directly related to space debris was the French Space Operations Act [Republique Française, 2008] this has become mandatory since 2010 [Lazare, 2013].

Table 2.1: Overview of SDM legislation, extracted from [Antonetti et al., 2015a].

INTERNATIONAL LAWS, REGULATIONS and GUIDELINES		
IADC Space Debris Mitigation Guidelines		Voluntary
Outer Space Treaty		Voluntary
ISO 24113		Voluntary
Space Liability Convention		Voluntary
EUROPEAN REGULATIONS and GUIDELINES		
European Code of Conduct for SDM		
ESA/ADMIN/IPOL(2014)2 - SDM for Agency Projects		Mandatory for
ECSS-U-AS-10C - Adoption Notice of ISO 24113		ESA's missions
ESSB-HB-U-002 - ESA SDM Compliance Verification Guidelines		
EUROPEAN NATIONAL LAWS and GUIDELINES		
FRANCE	Space Operation Act (loi n. 2008-518)	Mandatory
UK	UK Outer Space Act	Mandatory
GERMANY	DLR-RF-PS-001(6.0)	Mandatory
AUSTRIA	Austrian Outer Space Act	Mandatory
BELGIUM	Law on Activities of Launching, Flight Operation or Guidance of Space Objects	Mandatory
US REGULATIONS and GUIDELINES		
FEDERAL	U.S. Government Orbital Debris Mitigation Standard Practices	Voluntary
	U.S. National Space Policy	Voluntary
	DoD Directive 3100.10 "Space Policy"	Mandatory
	DoD Directive 3100,12 "Space Support"	Mandatory
NASA and other U.S. entities	"NASA Procedural Requirements for Limiting Orbital Debris" - NPR 8715.6	Mandatory for institutional mission
	"NASA Process for Limiting Orbital Debris" - NPR 8719.14	
	FAA 14 CFR 417.139 "Safety at end of launch"	
	FCC 47 USC Sec. 301	
	NOAA 15 CFR Section 960.11 "Spacecraft Disposal and Orbital Debris Mitigation Plan"	
OTHER NATIONAL LAWS and GUIDELINES		
CANADA	Canadian Remote Sensing Space System Regulations	Mandatory
JAPAN	JAXA Management Requirements (JMR-003B)	Mandatory
RUSSIA	GOST R52925-2008: "General Requirements on Space Systems for the Mitigation of Human- Produced near-Earth Space Population"	Mandatory

2.2.2.1   SDM requirements

The recent adoption of ISO 24113 Space System − Space Debris Mitigation Require-
ments [BSI Standards Publication, 2011a] in the ESA Policy ESA/ADMIN/IPOL(2014)2
ensures that a standard approach [ESA SDM WG, 2015] on space debris mitigation
requirements for ESA projects is established.
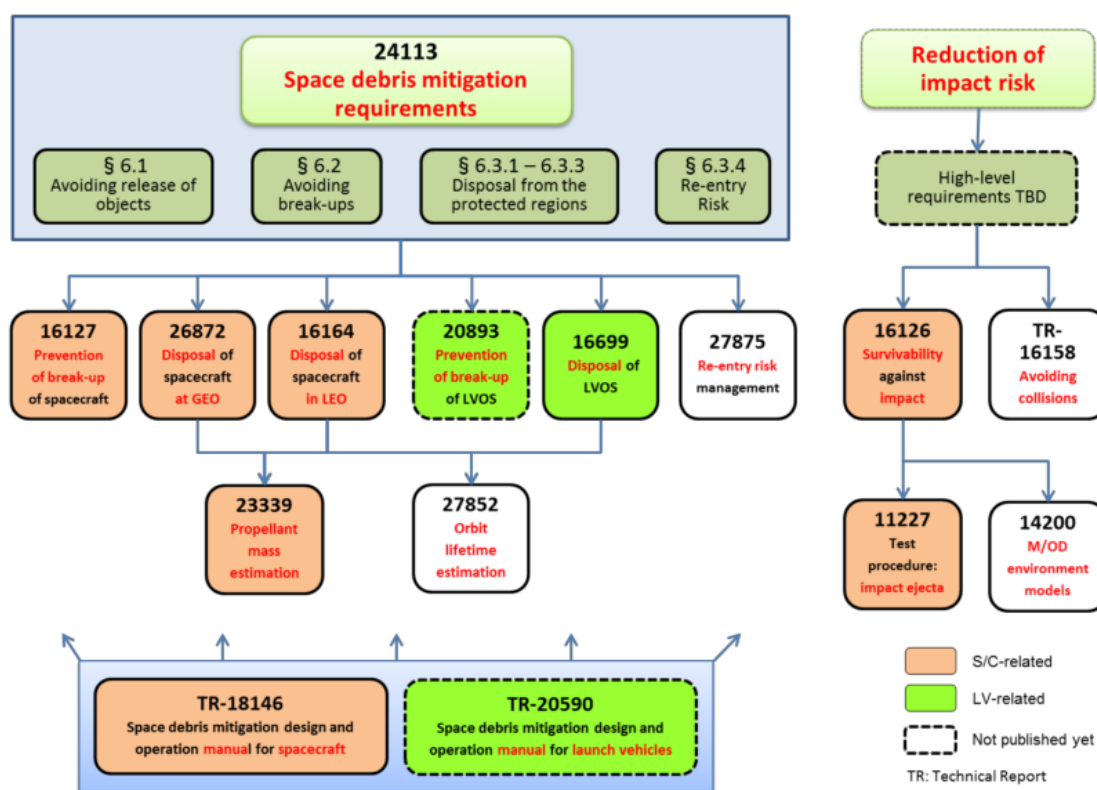
Figure 2.6: Current structure of ISO Debris Standards (Courtesy of UK Space
Agency).

The International Standard defines two protected regions with regards to space
debris as identified in the IADC mitigation guidelines [IADC, 2007]: Low Earth
Orbit (LEO) and Geosynchronous Earth Orbit (GEO) regions.

LEO region is a spherical region that extends from the Earth's surface up to an
altitude (Z) of 2000 km. GEO region ($Z_{GEO} = 35786$ km) is a segment of a spherical
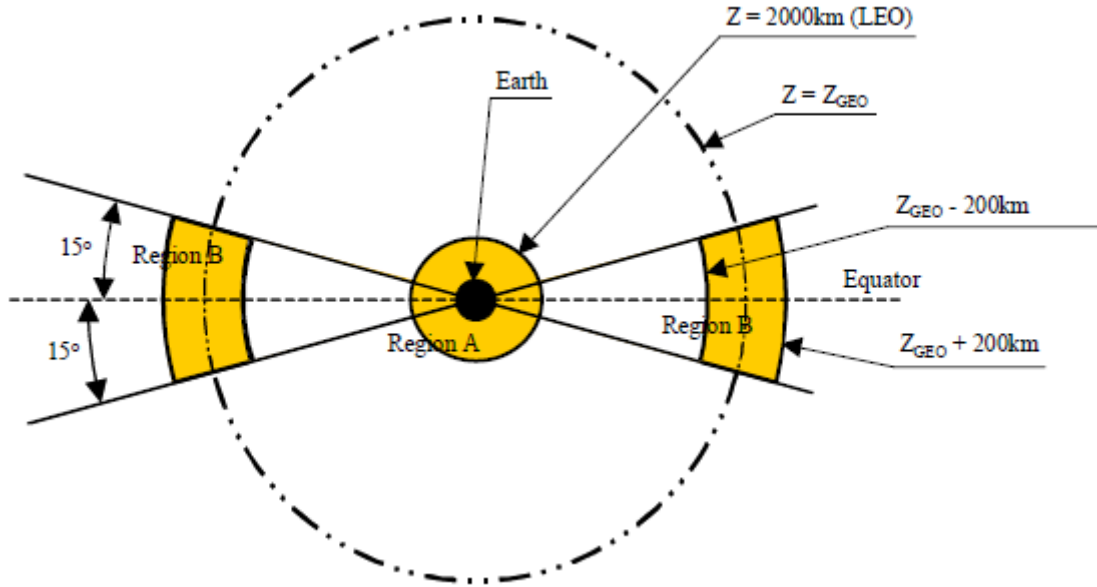
Figure 2.7: Protected regions [IADC, 2007].

shell defined with a lower altitude equal to Z$_{GEO}$ - 200 km, an upper altitude equal to Z$_{GEO}$ + 200 km and a latitude range [-15 degrees, +15 degrees].

The removal of spacecraft or orbital stages after the End of Mission (EoM) from these two protected regions is required. In particular the probability of successful disposal of the space system shall be at least 0.9 when the disposal is executed (Req. 6.3.1.1).

Focussing on the LEO region, the main requirements about the space systems removal define the clearance time for de-orbit (Req. 6.3.3.1) and the disposal manoeuvre approach to be adopted after the EoM (Req. 6.3.3.2).

The time limit, in which the removal shall occur, is 25 years after the EoM, this is a result of the studies performed on space debris population in LEO [ESA SDM WG, 2015] and a compromise between the debris growth and the cost burden for implementing mitigation measures.

After the EoM, the disposal manoeuvre shall be accomplished by one of the

following approaches [BSI Standards Publication, 2011a]:

(a) controlled re-entry,

(b) controlled manner into a targeted re-entry with a well-defined impact footprint on the surface of the Earth,

(c) controlled manner to an orbit with a shorter orbital lifetime (compliant with 6.3.3.1),

(d) by deploying a device augmenting the orbital decay so that the remaining orbital lifetime is compliant with the 25 years,

(e) natural orbital decay so that the remaining orbital lifetime is compliant with 6.3.3.1,

(f) controlled manner to an orbit with a perigee altitude sufficiently above the LEO protected region that long-term perturbation forces do not cause it to re-enter the LEO protected region within 100 years.

2.2.2.2 Future of SDM regulations

A general intention to change the Space Debris Mitigation guidelines in law in the near future can be perceived within the main space agencies and in different countries. As can be seen in Table 2.1, some countries already implemented SDM in their national regulations (to be noted: different countries have different needs on their national legislation) and also NASA and ESA made the SDM requirements mandatory for their missions. Nevertheless some discrepancies remain and the rules are not yet applied in a satisfactory level today.

Some of the current evolutions on SDM, under consideration at IADC level, encompasses: the probability of successful disposal operations ($\geq 90\%$) and of break-up during operational phase ($\leq 10^{-3}$); a maximal duration of 25 year in GEO region; the zone above 2000 km to be no longer used as graveyard when object coming from LEO; possible specific rules concerning Mega-constellations.

At the moment the ISO is under heavy revision; this process is expected to take some time hopefully reaching a convergence.

As Bonnal suggested, the ISO 24113 appears to be the most promising way for the future. The standard has been approved at international level and jointly prepared by industrials, operators, and agencies. Furthermore it could be applicable universally to any contract in the future (both manufacturers and operators).

2.3 De-orbiting strategies

The approaches identified in the SDM disposal requirements lead to different de-orbiting strategies. The de-orbiting methods for LEO clearance within 25 years can be divided in two main categories: active and passive [Innocenti and Soares, 2013].

It is worth noting also the possibility of using the natural decay, when EoM disposal manoeuvre is not required.

2.3.1 Active de-orbit

Active de-orbit strategies make use of propulsion to accomplish the disposal. They need the spacecraft bus subsystems to be fully operational at the EoM, from the power supply to the attitude control (AOCS) on-board and TT&C.

2.3.1.1   On-board propulsion

Among the active methods there are chemical propulsion and electric propulsion.

The active direct de-orbit is basically achieved applying a velocity change to the spacecraft to reduce the perigee altitude. The velocity change required to de-orbit a S/C in a circular orbit according to [Wertz and Larson, 1999] is:

$$\Delta V_{de-orbit} \approx V \left[1 - \sqrt{\frac{2(R_E + H_p)}{2R_E + H_p + H_i}} \right] \tag{2.1}$$

At initial altitude H_i and with orbital velocity V, R_E as Earth Radius and H_p as final altitude of perigee (see Fig. 2.8). The altitude of perigee here imposed to consider a successful re-entry in the atmosphere is 60 km.
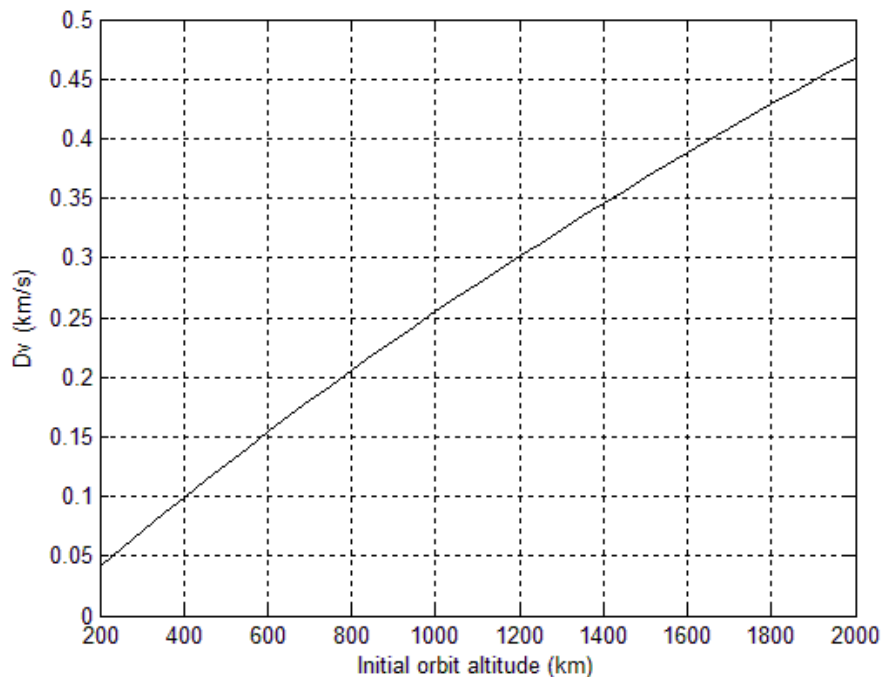
Figure 2.8: Change in velocity required vs initial altitude for direct re-entry with perigee altitude of 60 km.

Considering the same range of altitudes and the same final H_p, the propellant

mass required for direct re-entry, in terms of dry mass m_0 of the spacecraft can be calculated as follows:

$$m_p = m_0(e^{\Delta V/V_0} - 1) \tag{2.2}$$

In Fig. 2.9 the mass fraction of propellant (mono and bi-propellant) required for de-orbit can be seen. The exhaust velocity assumed is 2 km/s for mono-propellant hydrazine, 3 km/s for bi-propellant hydrazine/N2O4.

As pointed out in ISO 24113:2011, controlled re-entry is the first in order of preference for removing a spacecraft from the LEO protected region. This can be achieved by the spacecraft propulsion capabilities and, as stated in [ESA Director General's Office, 2014], it is mandatory when the on-ground casualty risk exceeds 10^{-4}. This de-orbit method is needed for large spacecraft which do not fully demise during re-entry, so there is the risk of fragments made of materials with high melting points (e.g.: titanium, stainless steel) to reach the ground.

On-board propulsion is a space-proven technology; however this strategy can strongly limit operational lifetime, as propellant mass is dedicated to the de-orbiting (up to 20% of the spacecraft mass [Taylor and Hobbs, 2013], see Fig. 2.9).

In addition, previous reliability studies have identified the propulsion subsystem as one of the major contributors driving satellite failures (see Fig. 2.10) [Castet and Saleh, 2009]. It has also been seen that this subsystem experiences significant degradation on orbit and even when it (partially) fails, it is likely to have major effect on mission capability [Castet and Saleh, 2010].
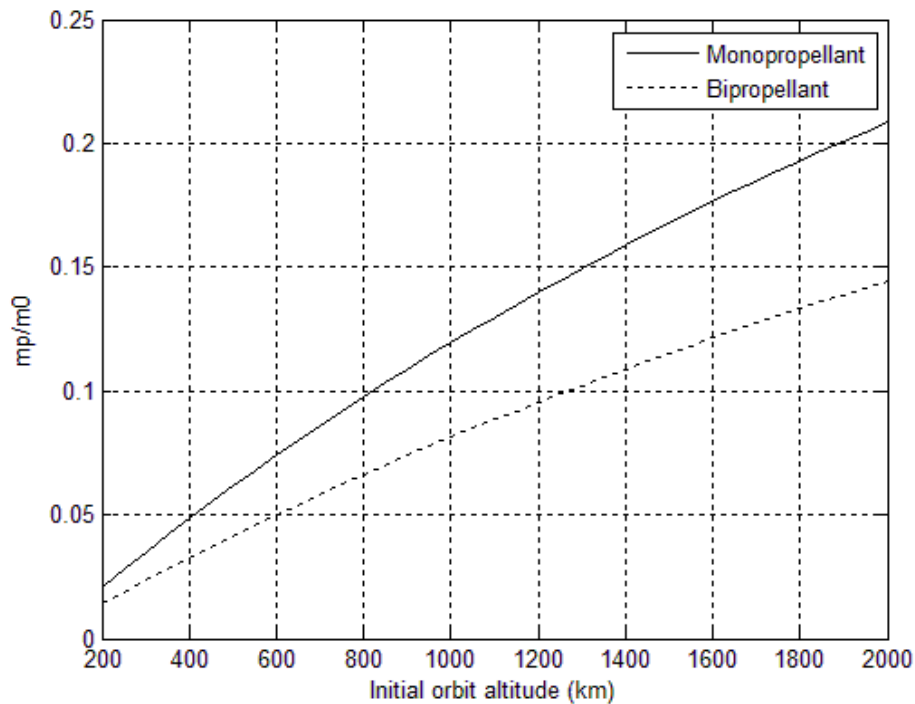
Figure 2.9: Propellant mass fraction required vs initial circular orbit altitude for direct re-entry with perigee altitude of 60 km.

2.3.1.2 Independent device

D-Orbit$^{\text{TM}}$ smart propulsive device [Rossettini, 2015] can also be included in the propulsive methods; however this decommissioning device, currently at qualification level, is quite independent from the spacecraft itself, in fact it has its own electronics, communications, attitude and propulsion subsystems [D-Orbit, 2015]. This device just needs a power line from the spacecraft host to charge one of the two batteries provided. The de-orbit manoeuvre is accomplished by means of a solid rocket motor [Antonetti et al., 2015b].
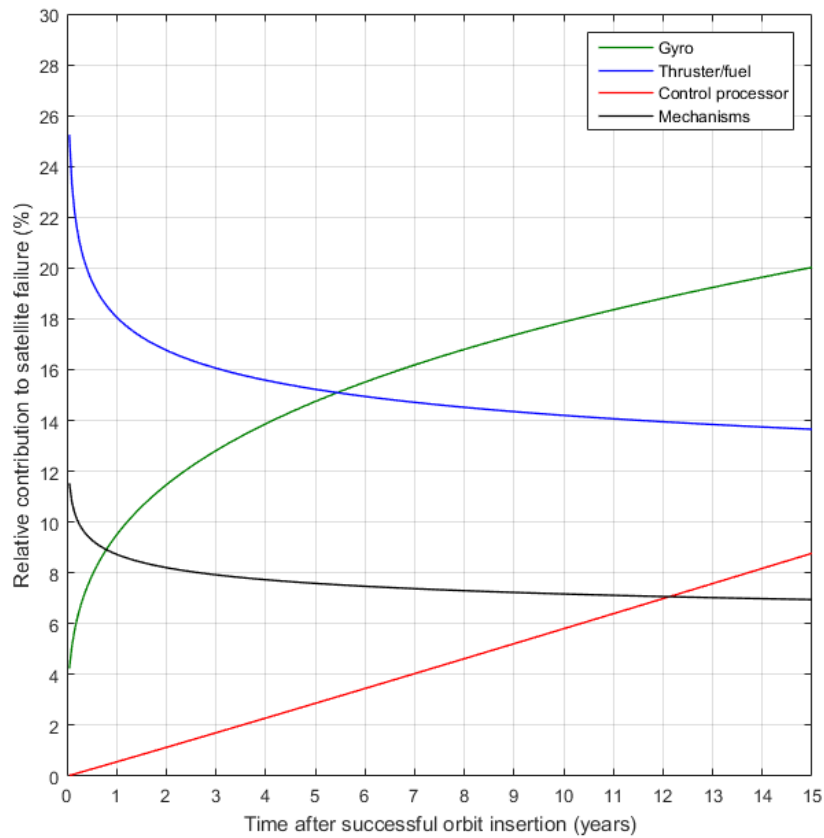
Figure 2.10: Relative contribution of subsystems (gyro/reaction wheel, thruster/fuel, control processor, mechanisms/structures) to satellite failure, obtained from Weibull parameters of [Castet and Saleh, 2009].

2.3.2   Passive de-orbit

Passive disposal strategies are independent from spacecraft propulsion capabilities. They take advantage of external perturbation forces (atmospheric drag, solar radiation pressure, Earth's magnetic field), governing the orbital lifetime, to decrease the satellite's altitude and have a faster re-entry.

Considering the future of SDM requirements and regulations (see section 2.2.2.2), it will be mandatory to have post mission disposal strategies for all satellites, including micro and smaller classes. Furthermore, micro (10-100 kg) and smaller spacecraft are, in general, not provided with propulsion capabilities to achieve a controlled re-entry, so they need different de-orbit disposal methods.

The most promising passive methods take advantage of electromagnetic drag (tethers) or aerodynamic drag (drag augmentation devices) as de-orbit force.

2.3.2.1   Tethers

The tether, i.e.: a conductive wire, is designed to be deployed from the satellite at the EoL. The tether takes advantage of three characteristics of the Sun-Earth system: the Earth magnetosphere, the Earth ionosphere and the Gravity gradient [Urgoiti, 2016] .

The electrodynamic tether collects electrons from the ionosphere at its anodic end (the conductive tether itself left bare) and emits electrons through a plasma contactor at the cathodic end [Zanutto et al., 2012].

The electrodynamic drag exploits the Lorentz force produced from the interaction of the electric current that circulates in the tether, and the Earth's magnetic field. The Lorentz force depends on the tether design, the orbit and the ionosphere characteristics. As a consequence the induced decay rate is greater at low altitudes

because of higher density of the ionospheric plasma, in addition the maximum efficiency is achievable for equatorial orbits while for high inclinations is less or not at all effective, as described in [Pardini et al., 2009].

$$\mathbf{F} = \int\limits_{0}^{L} I(l)d\mathbf{l} \times \mathbf{B} \tag{2.3}$$

As can be seen from the equation, the tether length has a strong impact in its design, in fact the shorter the tether the longer the de-orbit time needed. The study presented in [Pardini et al., 2009] confirms that the tether is a technology with good potential as mitigation measure, but still in progress and with various problems to be solved before adopting it as a practical solution.

In the family of tethers for de-orbiting an interesting concept, the electrostatic plasma brake, has been proposed by the Finnish Meteorological Institute. The plasma brake has been analysed as Building Block concept within the CleanSat programme [Janhunen and Toivanen, 2016].

This type of tether enhances the drag between the spacecraft and the natural plasma flow in the ionosphere using negative tether polarity. According to [Janhunen and Toivanen, 2016] the plasma brake seems to be an efficient and safe way of de-orbiting primarily small masses, although scaling to higher masses could be possible. Benefits of the system include low mass, low power consumption, and reduced area-time-product (ATP); disadvantages are the reduced effect at high latitudes, the length, and the TRL of the technology.

2.3.2.2 Drag augmentation devices

The governing force for this de-orbit strategy is the aerodynamic drag, which is caused by the interaction of the residual atmosphere with the satellite's surface.

The drag force acts in the opposite direction of velocity, its effect is a change in semi-major axis and, in the case of non-circular orbits, eccentricity of the orbit over time. It is only of second order magnitude as compared to the first order Earth's oblateness perturbation.

$$F_{drag} = -\frac{1}{2}C_d A \rho v^2 \qquad (2.4)$$

Where C_d is the coefficient of drag, A is the surface area normal to the velocity vector, ρ is the density of the atmosphere. For 700 km orbit, the order of magnitude is $10^{-6} N/m^2$, considering average atmospheric density value.

Drag augmentation devices increase the area-to-mass ratio of the spacecraft, augmenting the surface area normal to the velocity vector, and in this way they allow to reduce the natural orbit decay.

These devices are at high TRL with some concepts already on-orbit [Kuwahara et al., 2013], [Kingston et al., 2014], [Rasse, 2015]; in addition there are other projects at late stage, such as AEOLDOS [Harkness et al., 2014].

Based on the main design concept, passive drag augmentation strategies can be divided into two categories:

- Ultrathin envelope or balloon (Fig. 2.11): as described in [Nock et al., 2013], they consist of a thin envelope inflated using gases, so that the shape resembles a balloon. Because the outside pressure is very low, just a small amount of gas is required to keep the balloon inflated. Nevertheless a gauge system is required to maintain the inflation as the altitude decreases or because of gas leaks due to particle impacts. In order to avoid the constant inflation, the rigidized option, through a mechanical or chemical process, has been investigated as well. Advantages of this concept are the large cross sectional area and the

low mass, disadvantages include the deformation by collision and the need for constant inflation during re-entry. Nock describes them when considering the Area Time Product (ATP).
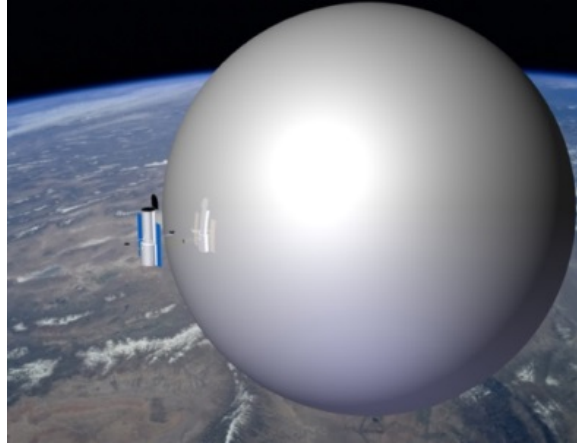
Figure 2.11: Example of ultrathin envelope (Courtesy of Global Aerospace Corporation).

- Boom supported film aerobrake or drag sails (Fig. 2.12): in this concept a very thin surface (the sail) is deployed and supported by boom arms. This strategy is very similar to the concept of solar sail, which would instead need an active control to make use of the solar radiation pressure to alter the spacecraft orbit. This concept can also be in the form of a drag tether, as IDEAS onboard Microscope [Rasse, 2015], where the booms are much longer than the width of the sail. Key advantages are the low mass and volume.

Cranfield University has recent experience in design and development of aerodynamic drag-based de-orbiting devices of the aerobrake concept type (Icarus-1 [Kingston et al., 2014] on UK's TechDemoSat-1, DOM [ESA Education, 2014] for ESEO, Icarus-3 on Carbonite-1 [SSTL, 2015]).

Aerobrakes are promising, there is a consistent heritage in their design and current work in progress, in addition they will lead to a reduction in debris collision
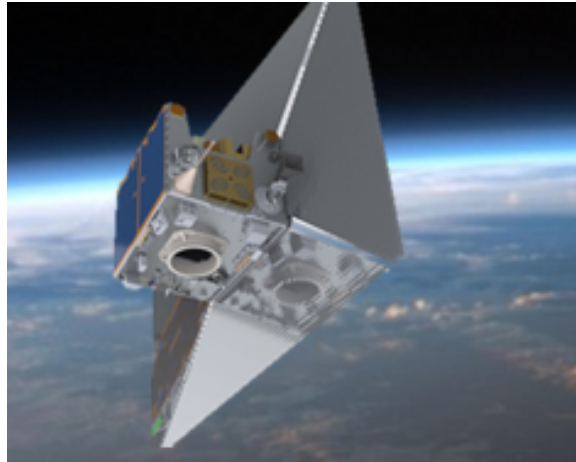
Figure 2.12: Example of boom supported film aerobrake: Icarus-1 on TechDemoSat-1 (Courtesy of SSTL).

risk as shown in [Visagie et al., 2015].

2.3.3   Comparison among the different strategies

A summary of the main advantages and disadvantages of the de-orbiting strategies described in the previous sections is shown in Table 2.2.

In the table only the general features are shown for the sake of comparison. Indeed, the selection on the de-orbiting strategy is very dependent of the specific mission and different factors need to be considered (see Trade-off analysis in Chapter 5).

2.4   Spacecraft market

In 2013 the commercial space transportation forecast [FAA, 2013] for Non-Geosynchronous Orbits (NGSO) predicted an average of 13 NGSO launches per year for the 2013-2022 period, significantly higher compared to a 5 launches per year in the previous 10 years.

Table 2.2: Main advantages and disadvantages of de-orbiting strategies.

Strategy	Advantages	Disadvantages
On-board propulsion	• controlled re-entry; • very short re-entry time; • space-proven technology	• system complexity; • spacecraft fully operative; • additional propellant mass
Independent propulsion	• different level of independences from S/C; • very short re-entry time	• still to be tested on-board; • system complexity
Tether	• low mass; • low power consumption	• very long wire (km length), control for deployment; • reduced effect at high latitudes; • low TRL
Balloon	• large cross sectional area; • low mass	• deformation by collision; • constant inflation needed
Aerobrake	• low mass; • low volume; • high TRL	• decay time

The mass varies significantly in the commercial NGSO market and it is worth to note the increasing number of micro and nanosats for scientific research and remote sensing as for commercial telecommunications.

Despite risks and difficulties in the predictions, the potential growing of small satellite classes (<200 kg) is confirmed by different sources, such as [Foust, 2008]

and [Christensen et al., 2010] who detected an existent demand of average 12 S/C of microsatellite mass class per year from 2000 to 2010.

The main interest in small classes of spacecraft is due to their limited propulsion capabilities or absence of propulsion subsystem. These features make them a target for the application of passive de-orbit devices, considering that the propulsive de-orbit has high cost in terms of mass and launch requirements [Nock et al., 2013] for S/C that does not require a nominal propulsion subsystem.

2.4.1 Small satellites market

According to the FAA, in the decade 2003-2012 almost 300 microsats[1] and smaller class satellites were launched using both commercial and non-commercial launch vehicles.

Moreover, in 2014 SpaceWorks Projection [Buchen and DePasquale, 2014] reflected a significant increase in the global launch demand for nano/microsatellites, comparing to the previous decade, with a CAGR (Compound Annual Grow Rate)

---

[1]Note that for FAA microsats mass is 10-200 kg

Figure 2.13: Number of commercial spacecraft per mass classes in near-term manifest 2013-2014, derived from FAA data [FAA, 2013].
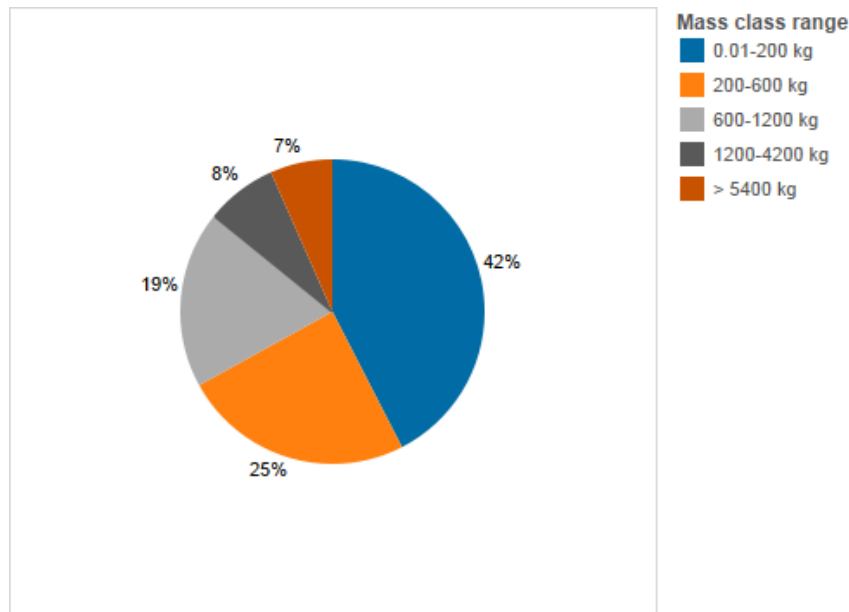
Figure 2.14: Distribution of commercial spacecraft masses in 2013-2014, derived from FAA data [FAA, 2013].

equal to 23.8% average over 2014-2020.

The satellites considered in the assessment by SpaceWorks are in the mass range 1 to 50 kg and the dataset was developed from public announcements, and quantitative and qualitative adjustments.

Looking at the updated 2016 report by SpaceWorks [Doncaster and Shulman, 2016], the CAGR expected for nano/microsatellite still continue to grow over the next 6 years (2016-2022) with an average of 13% per year. The historical average growth was of 39% per year over the last 5 years (2010-2015). The main driver for this growth is the eruption of commercial companies and start-up activities.

According to [Doncaster and Shulman, 2016] the projections based on announced spacecraft and future plans of programmes indicate as many as 3000 nano/microsatellites will require a launch in the next six years (see Fig. 2.15).

The forecasts look very promising because, quantities aside, they suggest that
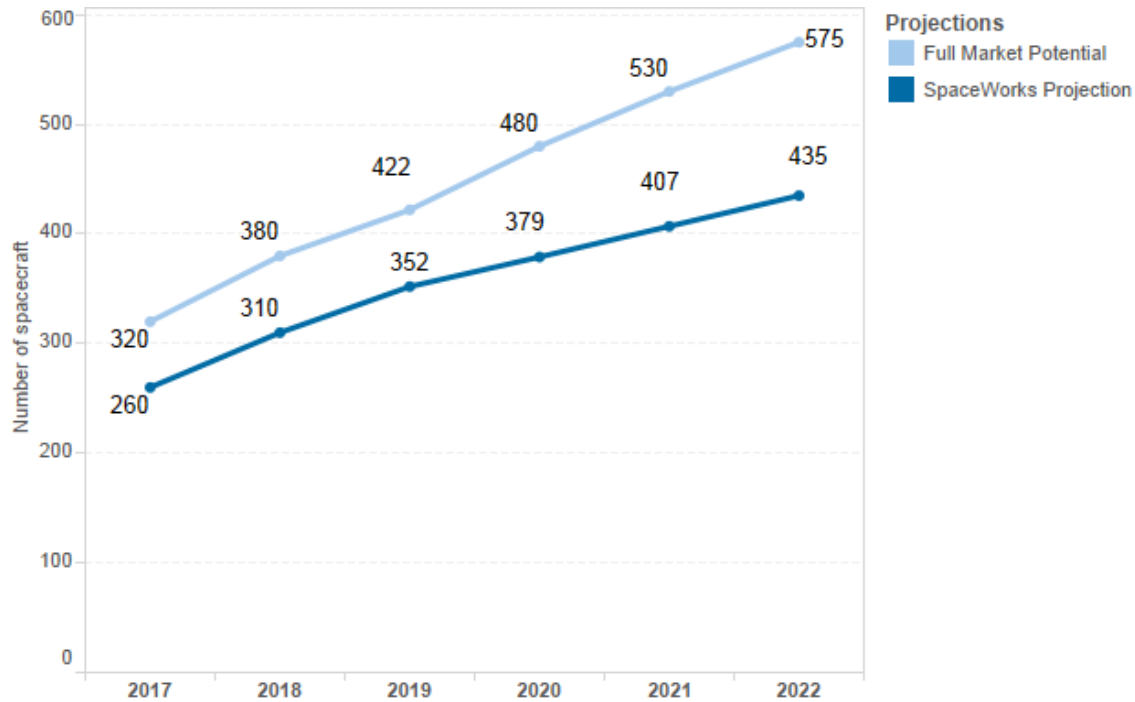
Figure 2.15: SpaceWorks forecast and Full Market Potential projections according to Gompertz logistic curve for (1-50)kg satellites, derived from [Doncaster and Shulman, 2016] data.

the commercial sector will have a meaningful impact on the small satellite classes on which a passive de-orbit device can be selected as de-orbiting strategy (see Chapter 4).

2.5   Survival analysis

In this section elements of the survival analysis are introduced. This is to give an overview of the statistics tools that will be used in the methodology for the Failure analysis of satellites' subsystems (Chapter 5).

The survival analysis is the study of the time between two specific events: the initial event and the terminal event. The data collected can be complete observations (i.e. the terminal event occurred) and/or censored ones (i.e. terminal event has not

occurred).

The analysis of a population sample of mechanical component (e.g.: spring) is different from analysing the survival probability of patients being given a new medical treatment [Peroni and Kingston, 2015]. In the first case the sample can be tested until the last component eventually fails. In the second case we are dealing with people, who sometimes during the period of observation quit the treatment, or die for a different reason, or they are still alive by the end of the observation. This second case is closer to the situation where satellite failures are being studied, because some satellites may reach planned end of life during the period of observation, and hence leave the population without suffering a failure.

Such analysis needs a different approach, this was developed by Kaplan and Meier.

2.5.1   Kaplan-Meier analysis

Kaplan-Meier analysis, developed in 1958 [Kaplan and Meier, 1958], is largely used in medicine to estimate a survival curve from a population sample; a good example is given by [Tripepi and Catalano, 2004].

One of the key features of the Kaplan-Meier analysis is the management of incomplete observations, i.e. the right-censored data. This happens when no information is available about one element of the sample after a specific time, for example a patient who quits the treatment. The analysis also works when subjects begin the study in different time instants, because their lifetimes can be shifted to a common zero position and then compared.

As can be seen from the example in Table 2.3 the probability $R(t)$ of surviving at any time t (or the Reliability at time t) is calculated from the cumulative probability

$(1 - F(t_i))$ of surviving to each of the previous time intervals, i.e. the product of current and previous probabilities. The failure probability $F(t)$ is then given by $(1 - R(t))$.

Table 2.3: Kaplan-Meier table example: $F(t)$ is the Failure probability, $R(t)$ is the Reliability. Note t_i is the time interval.

Time	Lost	Censored	Subjects	$F(t_i)$	$1 - F(t_i)$	$R(t)$	$F(t)$
2	1	0	10	0.100	0.900	0.900	0.100
6	1	0	9	0.111	0.888	0.800	0.200
7	1	1	7	0.143	0.857	0.686	0.314
8	1	0	6	0.167	0.833	0.571	0.429
9	2	0	5	0.400	0.600	0.343	0.657

The data of cumulative reliability presented in Table 2.3 are summarized in Fig. 2.16 which makes use of the Kaplan-Meier plot.
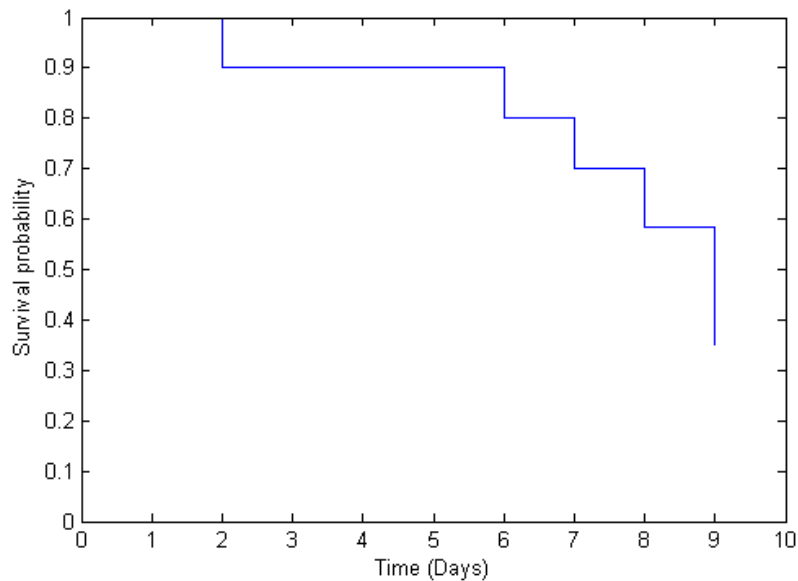
Figure 2.16: Example of Kaplan-Meier plot with MATLAB.

The Kaplan-Meier estimator is a non-parametric analysis. So from the step function it is difficult to calculate the failure rate. A link with a parametric function

is then necessary. For the purpose of the analysis performed the curve that fits the reliability data is the Weibull distribution.

The Weibull distribution is widely used in science and engineering to describe components' lives (or failures), strengths of brittle materials, etc. It is an example of a minimum extreme value distribution.

2.6 Modelling tools

In this section an overview of the atmospheric density, cross-sectional area and solar cycle models used in the decay analyses (see Chapters 4, 6, 7) is given. These models are embedded in the STELA [CNES, 2013] and DRAMA [ESA, 2014b] software tools.

2.6.1 Atmospheric models

Atmospheric drag models and data usage, affecting the propagation of near-Earth orbiting satellites, is extensively discussed by Vallado and Finkleman in the journal article *"A critical assessment of satellite drag and atmospheric density modeling"* [Vallado and Finkleman, 2014].

In this work they seek to clarify the uncertainty sources affecting the atmospheric drag to guide the researchers to a consistent approach for the calculations of the effects on the satellite decay. As confirmed in [Wertz et al., 2011], although the physics of atmospheric drag is well understood, its prediction is difficult for two main reasons:

- the attitude of the spacecraft can affect the drag by as much as an order of magnitude;

- the variation of the atmospheric density vs altitude is very dependent upon the solar activity levels, this can vary by two orders of magnitude.
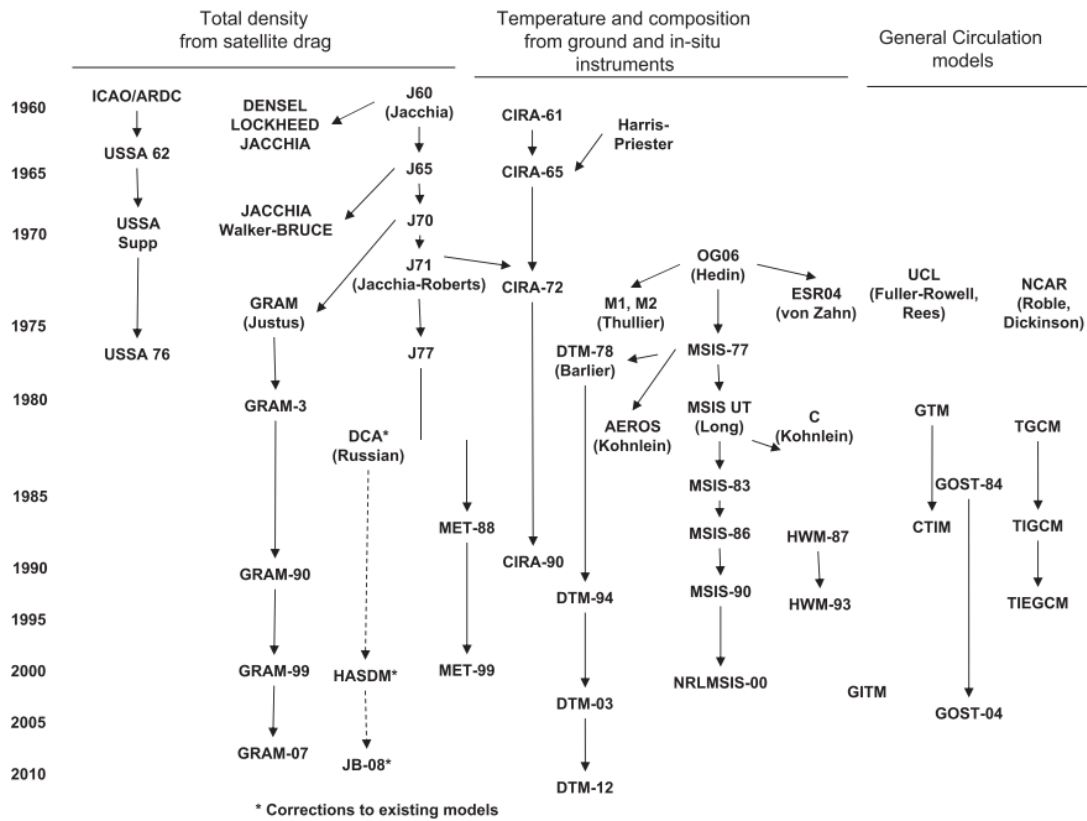
Figure 2.17: Development of atmospheric models chart from [Vallado and Finkleman, 2014].

As summarized by Vallado, the most common assumptions adopted in the atmospheric models development (see Fig. 2.17 for an overview of the models) are here listed.

- The lower atmosphere rotates with the Earth.

- The composition of sea level atmosphere is 78.11% nitrogen, 20.955% oxygen, 0.934% argon, 0.0006% helium, and hydrogen.

- The shape of the temperature profiles is constant with respect to basic models.

40

- The models account for atmospheric drag variation including effects on the 27-day Solar cycle rotation, upper atmosphere winds, magnetic storm variations, irregular short-periodic variations, tides and atmospheric composition.

- The index $F_{10.7}$ (i.e.the solar radio flux at 10.7 cm) is believed to be the major factor in the heating of the upper atmosphere.

- All the input parameters are available for historical, present and future use; their uncertainties are known with a certain precision for future predictions.

- The interpolation of the indices does not introduce weak time dependence errors in the solution.

- The atmospheric model selected is appropriate for the orbital class of satellite considered.

The main input parameters for the atmospheric models usually are: time and day of the year, altitude and geographic location of the satellite, solar flux index ($F_{10.7}$) and the geomagnetic index (A_P).

As can be seen in Fig. 2.17 a wide range of models have been developed, aside the improvements and the more accurate predictions, this is because no single model is the best for all applications. Indeed, the propagation differences between density models are equivalent in magnitude as a different treatment in the input data [Vallado and Finkleman, 2014]. Moreover, using one or two fixed parameters may improve the results, but only if the underlying conventions and assumptions are well known.

The NRLMSISE-00 model is the standard atmospheric model used in the space industry and it is already implemented in STELA and DRAMA. The NRLMSISE-00 is also one of the most accurate above 500 km of altitude.

2.6.2 Estimating cross-sectional area

The cross-sectional area is a parameter needed for the determination of the atmospheric drag. The cross-sectional drag area is the object area projection on the plane orthogonal to the flow direction [ESA SDM WG, 2015]. The determination of the cross-sectional area should take in account all the uncertainties that cannot be predicted with sufficient accuracy, in particular, as described in [ESA SDM WG, 2015], it should be considered:

- Object geometrical configuration: i.e. configuration at the beginning of the mission, at end of the operational phase, etc.

- Object attitude: i.e. stabilization, uncontrolled stabilization, aerodynamics stabilization effects, random tumbling, or any other damping effects.

If the attitude of the object, i.e. the spacecraft (in our case), cannot be predicted (as in most of the cases during the orbital decay), the user should assume the spacecraft is randomly tumbling. In other words, as explained in ISO 27852 [BSI Standards Publication, 2011b], the user shall calculate a mean cross-sectional area assuming that the attitude of the spacecraft varies uniformly with respect to the velocity direction. The mean area is then obtained by integrating the cross-sectional area across a uniform distribution of attitude of the spacecraft.

Tools to compute the mean cross-sectional area of complex geometries are available both in CNES's STELA (Mean Area Tool) and ESA's DRAMA (CROC).

In case a detailed model is not available, the composite flat-plate model may be used. This model considers a factor of 2 when calculating the mean surface area, e.g. for the case of a plane sheet with area S, it can be demonstrated that the mean surface area is S/2 when averaged over all possible viewing angles [BSI Standards

Publication, 2011b]. The same applies when considering a parallelepiped-shaped spacecraft. As reported in [BSI Standards Publication, 2011b], this model has an accuracy within 20% for tracked objects.

Nevertheless, as we mentioned before, under certain conditions the spacecraft attitude during the decay can be stabilized under gravity gradient effects or aerodynamic drag. The gravity gradient could occur for satellites with large length to diameter ratio. The aerostability, i.e. drag-induced passive attitude stabilization, can occur for spacecraft with large aero-torque moment. This can happen when the centre of gravity and the centre of pressure are suitably far apart and the aerodynamic drag force is suitably large. If aerostability can be achieved the orbital lifetime is minimized [Hobbs et al., 2013]. This is possible if the aerostability is properly implemented in the design of the spacecraft as in the case of Icarus-1 sail for TechDemoSat-1 [Hobbs et al., 2013]; nevertheless perturbations due to changes in atmospheric density may lead to periods of tumbling.

The hypothesis and models just described were used in the decay simulations, performed with STELA and DRAMA, to estimate the cross-sectional drag area of spacecraft. The specific cases and input parameters will be presented in the following chapters.

2.6.3 Predicting solar flux

The solar flux is a relevant parameter to determine the atmospheric density. The prediction of the $F_{10.7}$ values poses significant challenges, and moreover introduces significant uncertainty, as confirmed by Vallado in [Vallado and Finkleman, 2014].

Vallado showed that for a 45 day forecast predictions are good around a solar minimum but have a lot of variability around solar maximum.

Indeed, the solar flux prediction represents one of the largest contributing factors to differences in the atmospheric modelling. Vallado showed that the F10.7 can easily vary by 30-50 units, which results into an altitude difference of about 1 to 10 km.

For this reason, in this section the models embedded in the software tools STELA and DRAMA are presented to show the main differences and how these can affect the simulation of spacecraft decay.

2.6.3.1 Solar cycle models in STELA

In STELA the user can select one of the following three models for the solar flux predictions.

Mean constant

As described in STELA User manual [CNES, 2013], this model computes the normalized solar activity from the ballistic coefficient of the spacecraft and altitude of the apoapsis of the initial orbit. In this way the mean constant solar activity is a function of these two parameters but remains constant with respect to the time.

This has been tuned, through a statistical approach, to achieve a 25 years re-entry duration as a mean value (see [Fraysse et al., 2012]). Considering a 25 years orbit lifetime computed with the value obtained, the real lifetime computed statistically with several past solar cycles, and several initial dates in the first cycle would have a mean value of 25 years.

Constant equivalent solar activity is computed at the extrapolation beginning using the following formulas:

$$
\begin{aligned}
A_P &= 15 \\
F_{10.7} &= 201 + 3.25 \log\left(\frac{C_d S}{m}\right) - 7\log(Z_a)
\end{aligned}
\tag{2.5}
$$

Constant (user defined)

This model has only two specific inputs: a user defined constant solar flux (in SFU) and the geomagnetic index A_P.

Variable from input file

These values, given in the *stela_solar_activity* file, are past measurements (from 1956) and future mean prediction given by NOAA and NASA. The file goes up to year 2318.

It contains the following values:

- Date (JD1950 and seconds)
- daily solar flux $F_{10.7}$ (SFU)
- eight 3 hr A_P geomagnetic activity index for the current day

2.6.3.2   Solar cycle models in DRAMA

In DRAMA, within the OSCAR component, there are four methods available. These are recommended by different standards (ISO 27852:2011, ECSS E-ST-10-04C, French Space Operations Act).

Latest prediction

This model is recommended by the ISO 27852:2011 [BSI Standards Publication, 2011b]. It takes into account up-to-date solar and geomagnetic activity data from input files as provided by ESA or an user-defined file.

As described in [ESA SDM WG, 2015], the future behaviour of the current sunspot cycle is performed with the McNish-Lincoln forecast.

The method is similar to MSFC [Niehuss et al., 1996], which is also recommended by ISO. It utilizes a predicted $F_{10.7}$ solar activity profile generated by a model such as [Niehuss et al., 1996] coupled with a stochastic or similar generation of corresponding

$F_{10.7}$ and A_P values, e.g. [Woodburn and Lynch, 2005]. The method then takes into account:

- 13-Month smoothed Solar Flux: MSFC Lagrangian Linear Regression Technique for estimation of future $F_{10.7}$ uses all the observed data for all observed cycles; measured average $F_{10.7}$ extended back to 1749.

- 13-Month smoothed Geomagnetic index: it was extended back to 1884 using mean monthly magnetic character figure (Ci) data.

- Modified McNish-Lincoln Linear Regression Method MMLLRT.

For the "Best-Case/Worst-Case" scenario, one may specify a confidence interval, where the mean value for solar and geomagnetic activity is always the latest prediction scenario.

ECSS sample solar cycle

This method is recommended by the ECSS E-ST-10-04C [ECSS Secretariat, 2008]. This repeats the activity from the 23rd cycle, finding the starting point based on the position within the cycle at the start epoch with constant A_P index for $F_{10.7}$ bands (see Table 6-3 in [ECSS Secretariat, 2008]).

Constant solar flux

This is the same as STELA Mean constant, developed within the framework of the French Space Operation Act [Republique Française, 2008].

Monte-Carlo sampling

This method is also recommended by the ISO 27852:2011 [BSI Standards Publication, 2011b].

This is a random draw approach, generating daily activity based on up to six different solar cycles (completed) measured so far. The measurements of the solar cycle started in 1947.

The number of cycles that the user can select is then from 1 to 6. It draws a complete triad ($F_{10.7}$, $Avg_{10.7}$, A_P) from one sample. If, for example, the number 4 is entered, OSCAR will use the last 4 cycles 20-23 for the sampling process. The SDM Handbook [ESA SDM WG, 2015] suggests to use at least 5 sampled cycles.

2.7   Summary

From the literature review study performed the following points emerged:

- the IADC guidelines are not legally binding but recommended, however different countries and agencies have started implementing them as requirements, then de-orbit technologies at an advanced TRL will be needed;

- advantages and disadvantages of de-orbiting strategies, active vs. passive de-orbit;

- drag augmentation devices are promising, Cranfield has heritage in them, however a design applicable to different spacecraft hasn't been developed yet (this will be presented in the following chapters);

- a potential growth of micro and smaller satellites is confirmed by different projections, making them a target for passive de-orbiting devices.

Moreover an overview of the following was given:

- elements of the survival analysis needed for the subsystems' reliability study;

- variety and uncertainties affecting the solar flux forecast models.

Chapter 3

Cranfield Passive De-orbit Systems

In this chapter the passive de-orbit systems developed at Cranfield will be presented.

Cranfield Space Research Group has developed experience in design, build, and test of Drag Augmentation Systems (DAS) payloads, based on deployable Kapton sails using stored energy for deployment.

The DAS developed, which fall in the category of boom supported film aerobrake, are the Icarus-1 and Icarus-3 payloads, and the De-Orbit Mechanism (DOM) (originally named as Icarus-2).

Icarus-1 was built and delivered before the beginning of this research, so its design and solutions implemented were a starting point.

Icarus-3 was designed during the PhD, the involvement in the project included analyses of the de-orbiting.

The development of the DOM, instead, was performed from the PDR review up to the delivery of the PFM. In the first year of the PhD the project was brought forward from a prototype model, designed by MSc students of 2013, to the engineering

model; after this, design modifications, planning and performing of test campaign followed, and then building and testing of the flight model.

The main objective of the DAS is "*to increase the satellite drag to the point where the resultant force causes a decrease in orbital altitude which results in atmospheric re-entry within 25 years of EoL.*"

The main requirements used internally during the design process and applicable to all Cranfield DAS are:

- Reliability: ensuring the proper function of the DAS device.

- Low mass: the DAS mass must be less than the propellant mass required for de-orbit.

- Low cost: use of COTS, avoidance of complex systems to ensure commercial viability.

- Simple design: to be easily assembled and interfaced with the satellite.

- Simple interfaces: to ensure minimum impact on the host satellite and minimal power required for the deployment.

- Testability: to be easily testable in 1g and to ensure test repeatability.

- Safety: avoiding risk of premature deployment and any risk of damage to the host satellite.

- Scalability: to ensure it can be compatible to a wide range of commercial satellite platforms.

- No additional debris production: the DAS shall not create debris when being deployed and should not fragment when struck by space debris.

3.1   Icarus-1

Icarus-1, which is on-board the UK's TechDemoSat-1 [Kingston et al., 2014] (launched on 8th July 2014), represents the first DAS payload developed by Cranfield Space Research Group. It is expected to be deployed at EoM due in 2017/2018.

The general principle of the payload is to deploy drag sails at the end of TechDemoSat-1 mission to ensure that the spacecraft is removed from orbit within 25 years as recommended by IADC debris mitigation guidelines for LEO and now required for ESA missions [ESA Director General's Office, 2014].

3.1.1   Icarus design

The device consists of a thin C-section aluminium frame (905 mm x 698 mm), fitted around one of the external panels of the spacecraft (see Fig. 3.1), in which the lightweight sails and booms are stowed and restrained by a band.
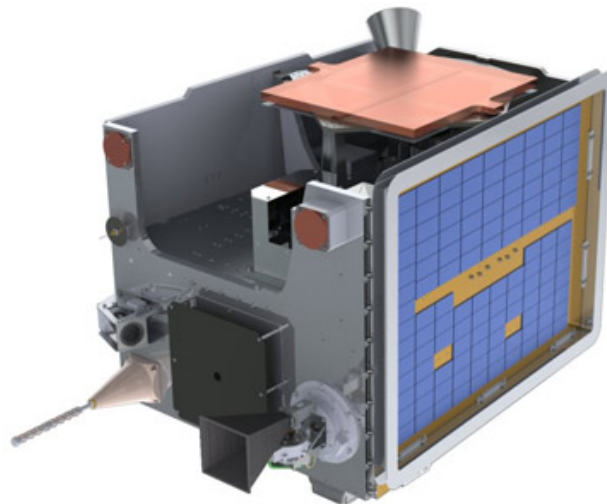
Figure 3.1: The TechDemoSat-1 satellite with Icarus frame (Courtesy of SSTL).

The sails (5 m^2 total drag area) are made of Aluminized-Kapton and with trape-zoidal shape, one each side of the rectangular frame (four in total). Each sail is

attached at four points, two points at the frame and on the tip of two booms that are either side of the sail. The general layout of the stowed and deployed configuration is shown in Fig. 3.2 and Fig.3.3 . Advantages of this concept are that the entire deployed surface is directly useful for drag augmentation, and that it can be used on panels with protruding elements, such as antennas.

Figure 3.2: Icarus-1 in stowed configuration. The payload is mounted to an aluminium mechanical ground support equipment plate for assembly and test.

The deployment is achieved by cutting the band, which allows the stored energy in copper-beryllium tape spring hinges to unfold the lightweight booms and sails.

Once deployed the trapezoidal sails form a shallow square-based pyramid thanks to the booms layout; this dihedral shape should provide an aerostable configuration [Hobbs et al., 2013].

The design based on the stored energy required the development of a hold-down and release mechanism (HDRM) to ensure that both the booms and the sails would not release unintentionally during the AITV, launch phase and operational mission.

As described in [Kingston et al., 2014], the specific requirements for the HDRM for the TechDemoSat-1 mission were:

1. The HDRM shall prevent unintentional release of the booms and sails through launch and operations, until the end of the mission (mission life is 3 to 5 years).
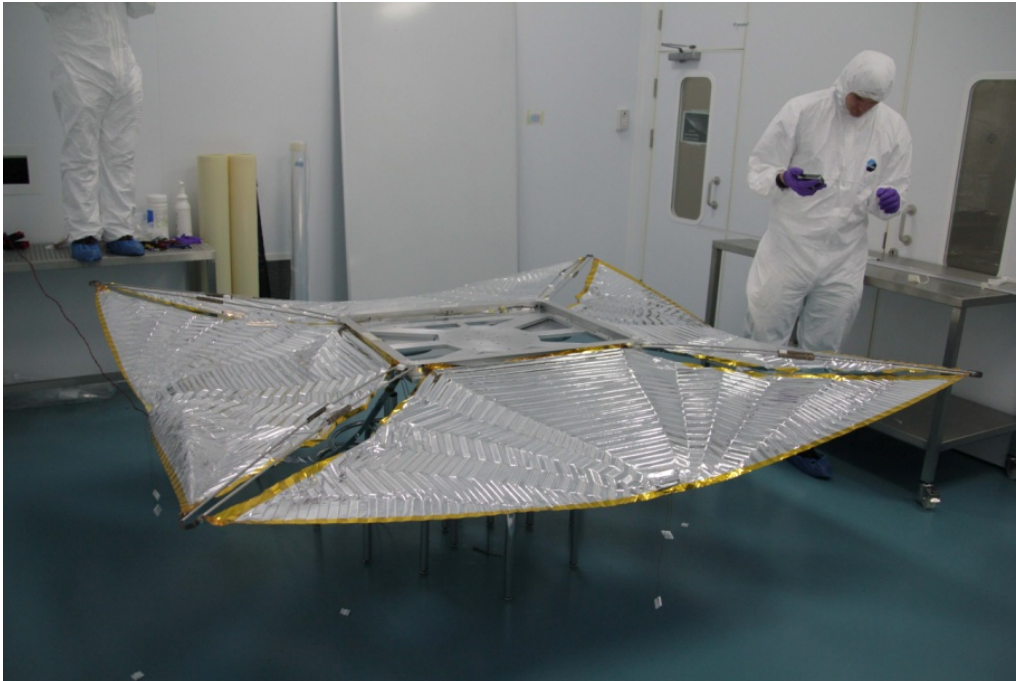
Figure 3.3: Icarus-1 in deployed configuration.

2. The HDRM shall allow the booms and sails to release freely on command with $P_{success} \geq 90\%$.

3. Release shall be effected with no damage incurred to the sail material.

4. Release shall be effected with no release of debris.

5. The HDRM design shall be tolerant of 3 failures/inadvertent commands before accidental deployment.

Considering the requirements above, the HDRM selected was based on a flexible Kevlar band that would pass around the C-section frame and be tensioned to provide a clamping effect on the stowed sails and booms. Moreover, the band protects the sails and booms against unexpected micrometeoroid or debris.

The clamp band release and deployment sequence is shown in Fig. 3.4. The band

was designed to be cut at two points simultaneously to allow a smooth release of the booms and sails.
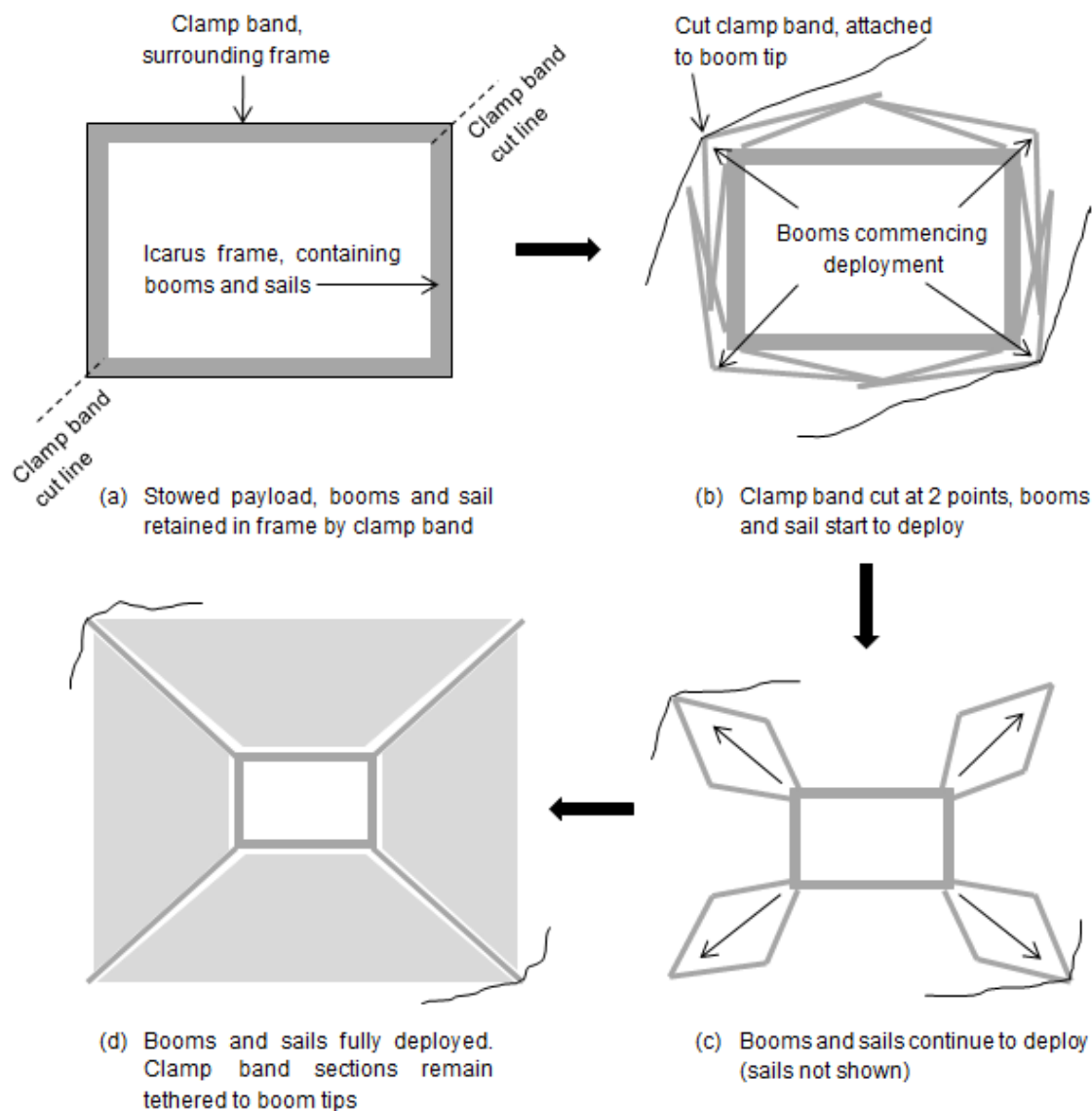
Figure 3.4: Clamp band release and sail deployment sequence [Kingston et al., 2014].

The actuator selected to achieve the release was the CYPRES[TM] cutter, a small commercial electro-explosive device used for release of parachute safety reserves ([Airtec, 2017]). The choice was dictated by cost constraints and high reliability at

the same time [Kingston et al., 2014].

Figure 3.5: CYPRES$^{\text{TM}}$ cutters. The cord to be cut passes through the hole near the end of the unit.

Table 3.1: Characteristics of the CYPRES$^{\text{TM}}$ cutter.

Parameter	Value/Specification
Mass	18 g
Dimensions	65 mm length x 8 mm diameter
Internal resistance	1.1 - 1.8 Ω (temperature dependent, increases with temperature)
Firing current	0.8 A for 10 ms
No-fire current	0.18 A for 10 s
Operating temperature	-50 to +90 °C (tested in thermal-vacuum)
Propellant	Nitrocellulose (max 40 mg)
Initiator	Lead picrate (max 7 mg)
Principle of operation	A defined electric current initiates a hermetically sealed gas generator, which fires a piston blade through the cutting hole, severing the cord(s)

The configuration consisted of four CYPRES$^{\text{TM}}$ cutters, two per opposite corners of the frame. At the two cut lines (see Fig. 3.4) of the clamp band, the band was connected by two sets of redundant Kevlar cords to allow the actuators to cut the band. Each set of cords passes through a single cutter, giving two cutters at each

of the two cut lines. Opposite pairs of cutters (1 & 3, 2 & 4) are activated by each of the two switches. Closing the first switch cuts only one of the cord pairs at each corner; the clamp band is still secure as the cord cutters are redundant. This operation is the a "mechanical arming" of the release mechanism. Closing the second switch cuts the remaining cords, achieving the "mechanical fire" operation and deploying the booms and sails.

A three-failure tolerant deployment sequence of mechanical plus electrical arm and fire operations is thus achieved. The clamp band can therefore tolerate accidental closing of 3 out of 4 activation switches and still safely contain the booms and sails. In addition, ARM and FIRE commands must also be received within a defined time interval to be accepted, reducing in this way the risk of accidental firing.

3.2   Icarus-3

The second frame concept developed and delivered is Icarus-3 (Fig. 3.8) DAS payload. It was designed, tested and qualified by Cranfield Space Research Group for Carbonite-1, an Earth observation technology demonstration satellite from SSTL, launched on 10th July 2015 [SSTL, 2015].

The spacecraft is in a circular sun-synchronous orbit at an altitude of 650 km. The mission had a target life of 1 year, however this was extended so the spacecraft is still currently on its operational mission. The deployment of the Icarus-3 sail is expected in the current year 2017.

Icarus-3 is based on four trapezoidal Kapton sails, folded and stowed for launch and the active mission duration into an aluminium box-frame structure that fits around one of the spacecraft panel. The sails are deployed at end-of-life by means of stored energy in copper-beryllium tape spring hinges and folded lightweight booms.
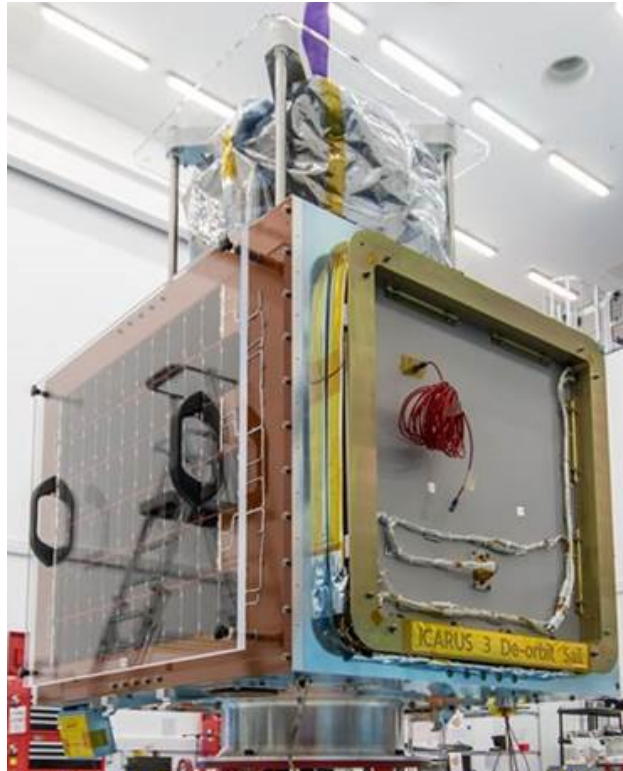
Figure 3.6: The Carbonite-1 satellite with Icarus-3 payload integrated (Courtesy of SSTL).

The design is based on Icarus-1 DAS payload [Kingston et al., 2014].

The involvement of this PhD in the project was performing orbit decay calculation and report delivery (Icarus3-STELA_Analysis_v1.1. 2014) to SSTL for the satellite Carbonite-1 with Icarus-3.

3.2.1   Design modifications

Icarus-3 design is similar to Icarus-1, but smaller to match the satellite panel (see Fig. 3.6). An easier sail fold pattern was used and other improvements were made to reduce complexity and increase reliability. This has permitted the development of the de-orbit payload in a short time frame.

The main modifications implemented in the design, as identified in the internal
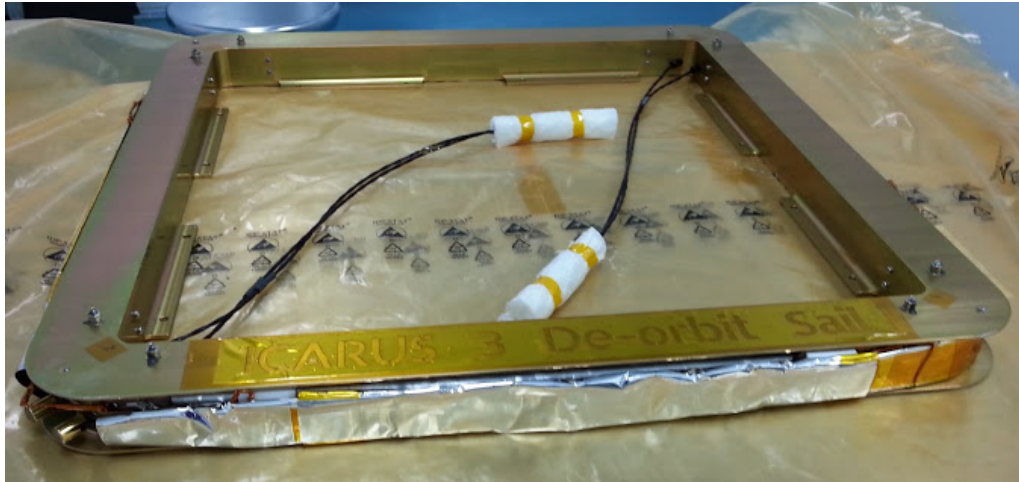
Figure 3.7: Icarus-3 in stowed configuration before delivery. Note the the connectors for the actuators for the two corners.

technical report prepared by J. Longley [Longley, 2015], were on:

- dimensions of the frame,

- spring mechanism,

- number of spring hinges,

- tensioning mechanism,

- sail fold pattern,

- Teflon hinges,

- interfaces with the spacecraft.

As mentioned before Icarus-3 is smaller and lighter (490 mm x 490 mm frame, 2 m^2 total drag area) compared to Icarus-1 (905 mm x 698 mm frame, 5 m^2 total drag area). Icarus-1 was probably approaching the upper limit of this design (at least under 1g test deployment conditions).
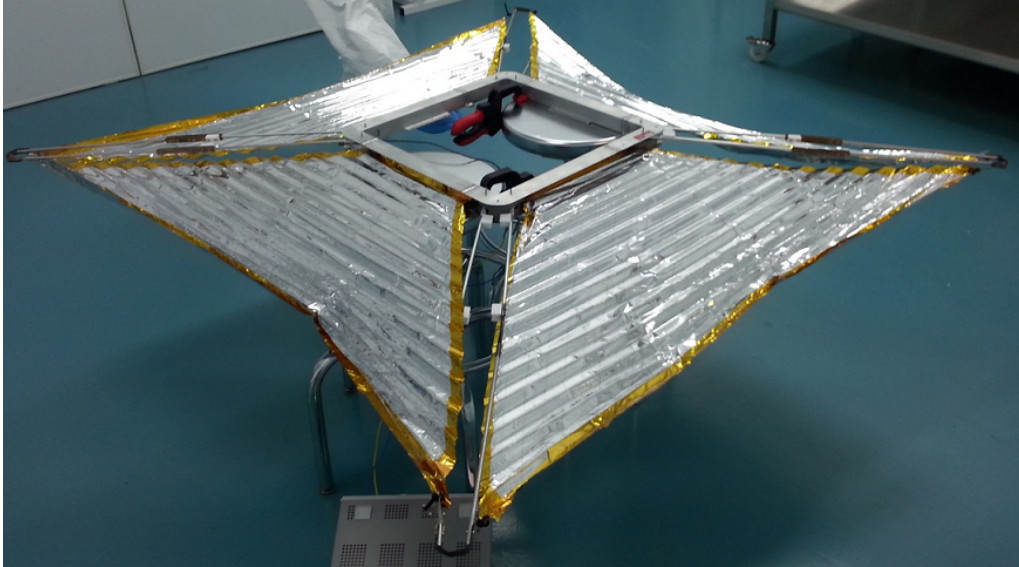
Figure 3.8: Icarus-3 in deployed configuration inside the clean room.

The spring mechanism was enhanced to include a torsion spring at the root. This is particularly useful in the early phase of deployment when there is little torque provided by the tape springs.

The number of mid-boom tape spring hinges per boom was reduced due to the smaller mass to be deployed. More tape springs per boom ensure higher elastic force, but, on the other side, they are difficult to fold into the stowed position and tend to buckle. While Icarus-1 had at least four (i.e. two tape springs either side of the boom) Icarus-3 used only three, with two outside and one inside.

The tensioning mechanism was also modified using a trucker's hitch knot, instead of rolling the clampband around a rod and then stopping the rod from rotating. This ensured sufficient tension and a faster tying process.

The sail fold pattern of Icarus-1 needed diagonal folds, allowing the "wings" of the trapezoid to fit into the base, i.e. as the sail unfolded out from the frame, it also expanded sideways. This pattern was very time consuming and complicated to fold, even though it should allow more sail film to be stored. For Icarus-3 a simpler

fold pattern of horizontal folds was selected and the "wing" excess was folded back on top of the centre.

The Teflon hinge parts were changed to allow smoother rotation of the booms and limit the vertical movement.

Finally, considering the interfaces, Icarus-3 electrical harness was connected to the spacecraft inside the frame, Icarus-1, instead, connected on the outside, necessitating a hole in one of the frame corners with no actuators.

3.2.2 De-orbit analysis

The de-orbit analyses were performed with STELA software tool. The analysis aimed to demonstrate that the Carbonite-1 satellite, with the Icarus-3 payload, is going to be compliant with the 25 years re-entry requirement. The demonstration of the compliance was needed for SSTL to obtain the launch licence from UK Space Agency, as required by the UK Outer Space Act [United Kingdom, 1986].

3.2.2.1 Initial conditions

The STELA simulations performed were set with maximum simulation duration of 50 years. If 50 years is exceeded the simulation stops automatically.

The main input parameters for STELA simulations were the orbit parameters (mean value in the reference frame Celestial MOD), the object characteristics, the atmospheric model adopted, the solar activity type.

It was assumed the sail deployment on 1st January 2016, at the end of the nominal imaging mission. Regarding Parameters Advanced section the default parameters, already set in STELA were adopted (see Table 4.3).

Table 3.2: STELA Input conditions for the final simulations performed.

STELA Input parameters	
Orbit Parameter	
Date	2016-01-01T12:00:00.000
zp [km]	650.00
za [km]	650.00
i [deg]	97.99
RAAN [deg]	0.00
ω [deg]	0.00
M [deg]	0.00
Object Parameter	
Mass [kg]	80.00
Reflectivity Area [m^2]	Depending on configuration selected
Reflectivity coeff	1.50
Drag Area [m^2]	Depending on configuration selected
Drag coefficient	2.2 (constant)
Atmospheric Model	
NRLMSISE-00	
Solar Activity	
Variable solar flux vs time	

3.2.2.2   Spacecraft configurations

The mean cross sectional area was needed as input condition. The computation of mean area was obtained with STELA Mean Area Tool drawing a simplified model of the spacecraft. Four different configurations were drawn for the simulations (see Fig. 3.9).

In Table 3.3 the calculated mean cross sectional areas for the different configurations are presented.

61
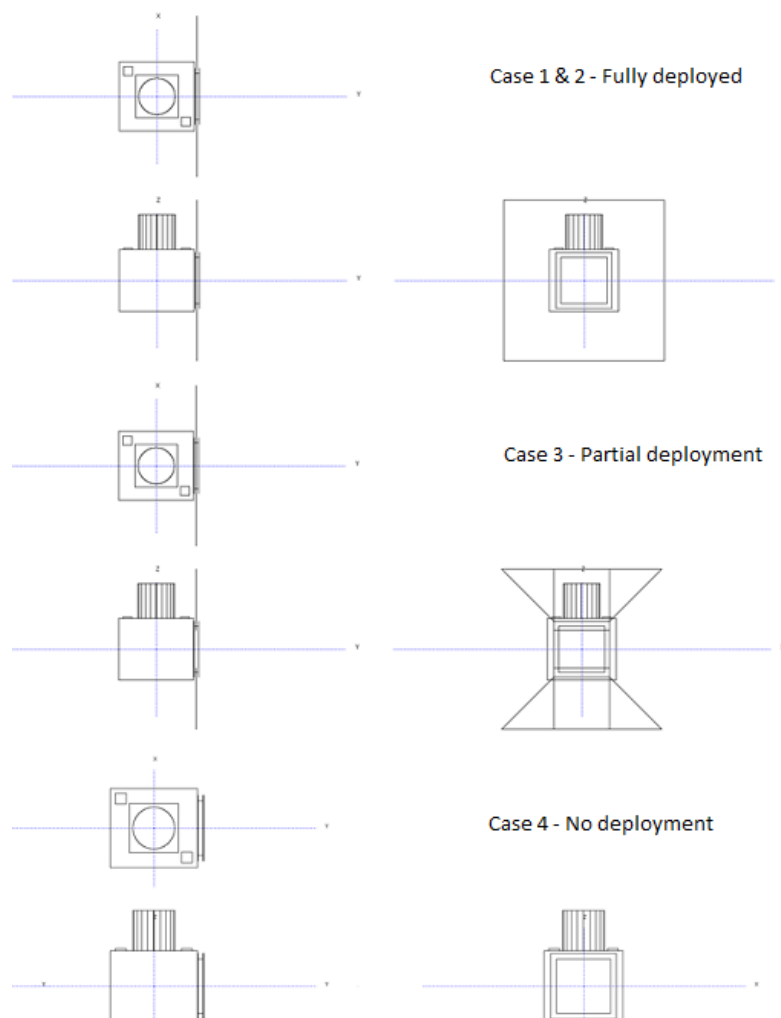
Figure 3.9: Configurations of Icarus-3 and spacecraft for de-orbit simulations.

Table 3.3: Mean cross sectional areas and area to mass ratios for different configurations.

Case	Area (m^2)	Mass (kg)	A/m (m^2/kg)	Configuration
1	1.96	80	0.025	Sail fully deployed and aero-stable
2	1.25	80	0.016	Sail fully deployed and random tumbling
3	0.92	80	0.012	Partial deployment and random tumbling
4	0.60	80	0.008	No sail/Deployment failure and random tumbling

3.2.2.3   Results

The simulations performed demonstrate that without the Icarus-3 payload, the spacecraft is not compliant with the 25 years re-entry requirement. As can be seen from Table 3.4 with the Icarus-3 sail fully deployed, the spacecraft is compliant with a large margin (both in aero-stable and random tumbling conditions), even when considering the variable solar cycle model (see section 2.6.3).

The estimation of the de-orbit time was performed by SSTL with the dedicated software tool DRAMA (ESA software) and DAS (NASA software). The results obtained were in accordance with the STELA simulations.

Table 3.4: Results of STELA de-orbit time for final simulations performed.

Case	Area (m^2)	Mass (kg)	A/m (m^2/kg)	De-orbit time (years)
1	1.96	80	0.025	12.17
2	1.25	80	0.016	18.45
3	0.92	80	0.012	27.32
4	0.60	80	0.008	38.74

Cases were also considered where the sail is only partially deployed (a fairly extreme case of only 50% deployment), with this condition there is a marginal non-compliance (see also Fig. 3.10). However, the simulations were made using a conservative case whereby the simulation starts at Year 0 (launch year) and at Year 1 (after the expected nominal imaging mission) with the sail in its final configuration. In reality, (assuming no on-board propulsion), the satellite altitude will reduce slightly over its lifetime before the sail is deployed. This will have two effects: firstly the de-orbit once the sail is deployed will start from a slightly lower initial altitude, and secondly that the next solar maximum will be reached earlier in the simulation, which is likely to reduce the de-orbit time. This was not simulated as the lifetime of the satellite was not given.

It should also be noted that the projected sail area of about 2 m^2 used in the random tumbling calculation was conservative; CAD modelling of the final payload design indicates a sail area of slightly over 2 m^2.

The case of aero-stability, i.e. the sail provides stability, was also analysed; the results showed, as expected, faster de-orbit time with respect to the other cases.
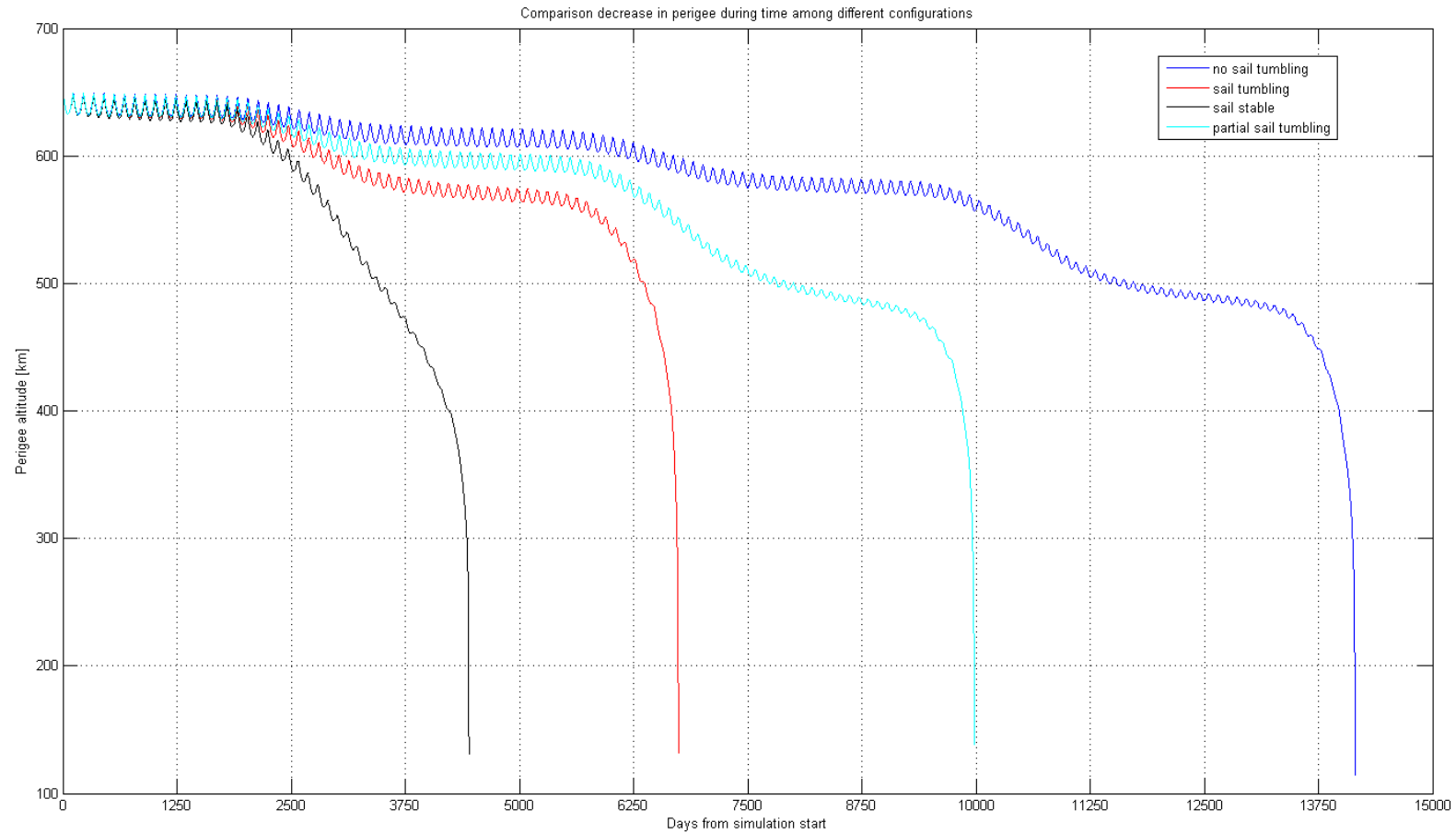
Figure 3.10: Perigee altitude vs time for the four different configurations with constant drag coefficient and variable solar flux.

If we observe Fig. 3.10 we can notice a periodic oscillation of the altitude of perigee during the decay. This is always detected in STELA when computed the altitude of perigee, nevertheless, this is compensated by the altitude of apogee. As can be seen in Fig. 3.11 a sudden drop in the apogee corresponds to a rise in the perigee, while the average altitude continues to decrease.

Oscillations of perigee and apogee are due to the eccentricity variation, this can happen as confirmed by real data, however, not in the form of the periodic oscillations we have seen here, which are due to the STELA semi-analytical model.
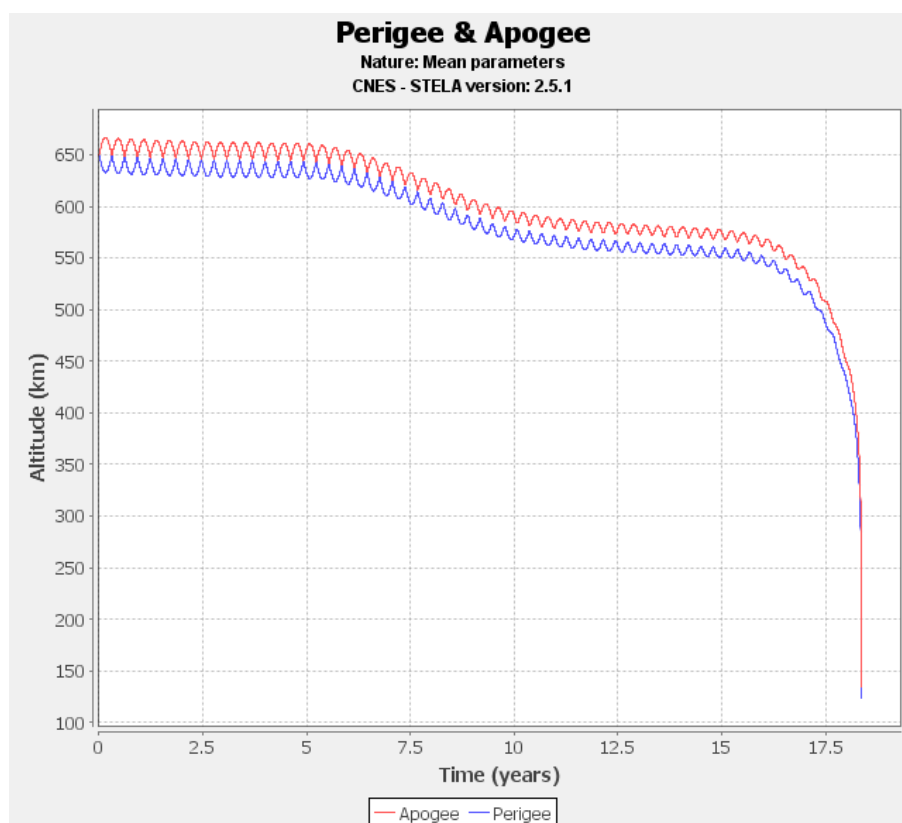
Figure 3.11: Perigee and apogee altitudes vs time for configuration with sail tumbling with variable solar flux.

The work performed allowed to gain further confidence in the use of STELA Tool. This was particularly useful considering the piece of research on the Future

scenarios (presented in Chapter 4) where STELA was used extensively to calculate the decay times.

Understanding the influences of the input parameters and how they affect the results (e.g.: drag coefficient variation, solar flux cycle) is a fundamental aspect. In addition, the modelling of the spacecraft from available CAD drawings was a good practise to determine how to simplify the geometry, without compromising integrity of the results.

3.3   DOM

The De-Orbit Mechanism technological demonstrator, which is going to be delivered in June 2017, will fly on board the upcoming ESEO mission [ESA Education, 2014], an ESA-funded educational mission (launch expected in 2018). The device is designed to deploy a drag sail at the end of the satellite mission thus enlarging the effective satellite area and hence, allowing the satellite an accelerated orbit decay and re-entry back to Earth. The design is based on Cranfield Space Research Group heritage in drag augmentation de-orbit systems (e.g.: Icarus 1 on the TechDemoSat-1, launched in 2014).

The development of the De-Orbit Mechanism for the ESEO mission has been a useful input for the research area. The main aim was in fact to reach a scalable design capable of de-orbiting a range of satellites with no need for significant re-engineering.

3.3.1   ESEO Mission

ESEO is a microsatellite mission to Low Earth Orbit, according to ALMASpace ESEO mission analysis report 2013 [AlmaSpace, 2013], the target orbit is a circular

Sun-Synchronous Orbit with 10:30 LTAN and an altitude of 523 km. ESEO is an ESA Education Office project with SITAEL (former ALMASpace) as industrial prime contractor and 7 payloads expected on-board being developed, integrated, and tested by teams of European university students.

Figure 3.12: ESEO spacecraft, DOM is on the right panel (Courtesy of ALMAS-pace).

The primary objective is indeed to give European students hands-on space project experience [ESA Education, 2014]. The ESEO satellite has the following mission objectives:

O.1 to take pictures of the Earth and/or other celestial bodies from Earth orbit for educational outreach purposes;

O.2 to provide dosimetry and space plasma measurement in Earth orbit and its effects on satellite components;

O.3 to test technologies for future satellite missions.

The DOM fits in the realization of the third objective.

3.3.2   DOM design

The DOM is a self-contained unit of less than 0.5 kg, mounted on the side panel of the ESEO satellite. It houses tape spring booms, aluminized Kapton sails, and a release mechanism. The sails are deployed at the end of the ESEO mission by closing a series of relay switches and thereby activating two CYPRES^{TM} cord cutters, which allow the release of the sails and booms.

The DOM does not have flight or qualification heritage at full system level; however it draws on qualification heritage from Icarus-1 for the CYPRES^{TM} cord cutters, aluminized-Kapton sails, and using stored-energy tape spring for deployment.

CAD drawings of the main structural elements of the DOM are reported in Appendix A.

3.3.2.1   Structural configuration

The DOM device deploys four individual sail quadrants, developing a total effective sail area of 0.5 m^2 (each sail is 0.125 m^2).

When stowed, the sail and deployment mechanism are contained within a volume envelope of 140 mm x 80 mm x 56 mm. This volume is partially embedded within the panel of the ESEO satellite, as shown in Fig. 3.15.

The booms and the sails are rolled up around a central spool in the middle of the device and held in position by Kevlar cords. Thus, the device is compactly stored in a single unit before actuation.

This design utilises a configuration with four boom arms of equal length, spaced
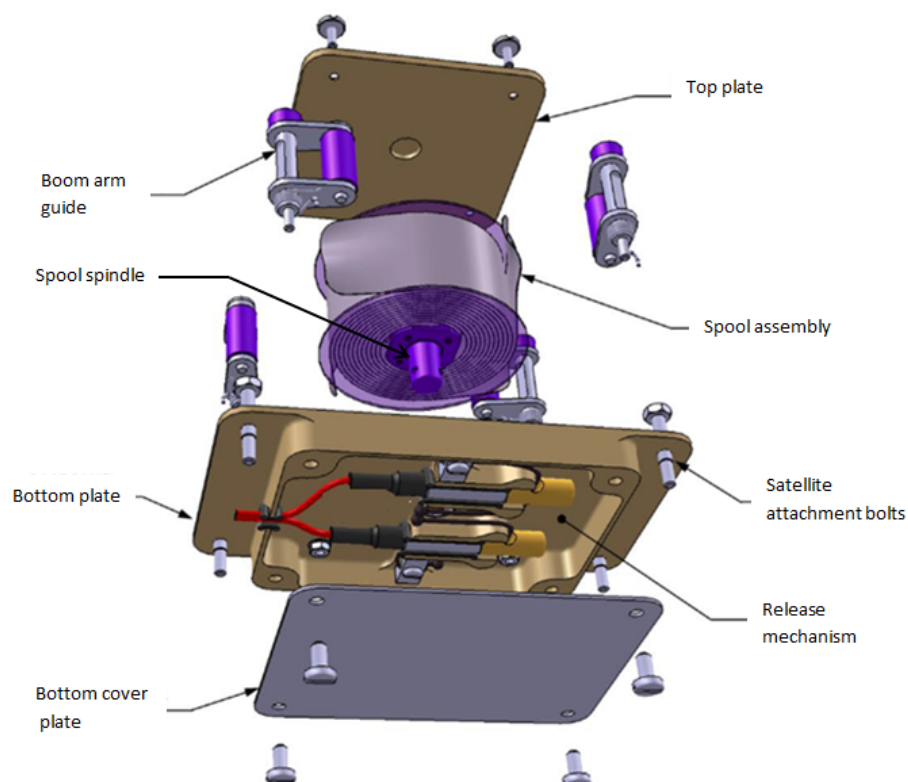
Figure 3.13: DOM exploded view, modified from [Taylor and Hobbs, 2013].

by 90° around a central spool. The sail quadrants are attached to four individual thin sectioned boom arms with a chord-wise, semi-circular profile.

The booms are attached at their root to a single free rotating spool, which rotates within the centre of the housing. In the stowed configuration the booms are wrapped around the spool, deforming their profile and adding spring energy to the system.

The booms are prevented from unravelling by the boom guides. The spool is prevented from rotating by the release mechanism.

The general configuration of the mechanism is shown in Fig. 3.13.
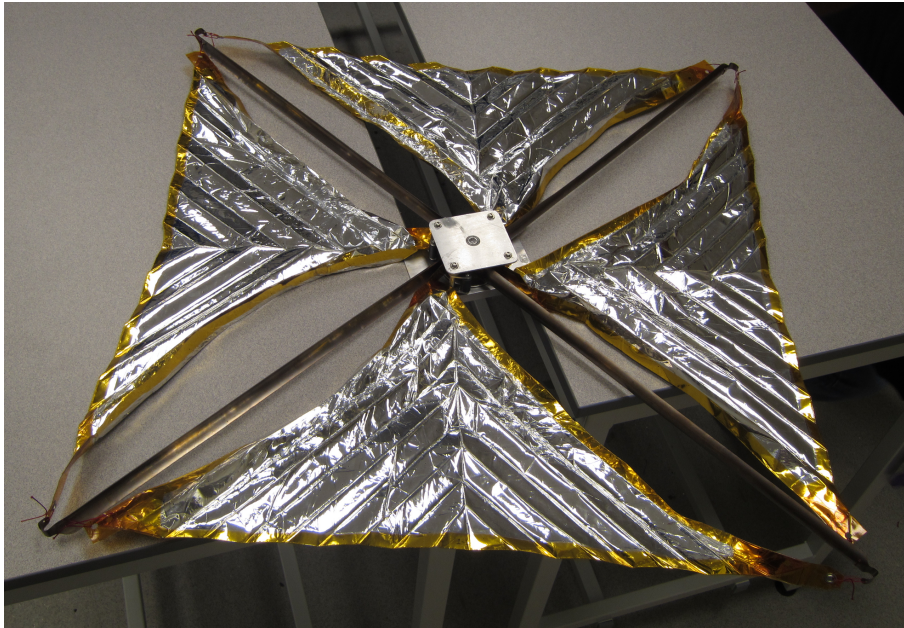
Figure 3.14: DOM EBB in deployed configuration.
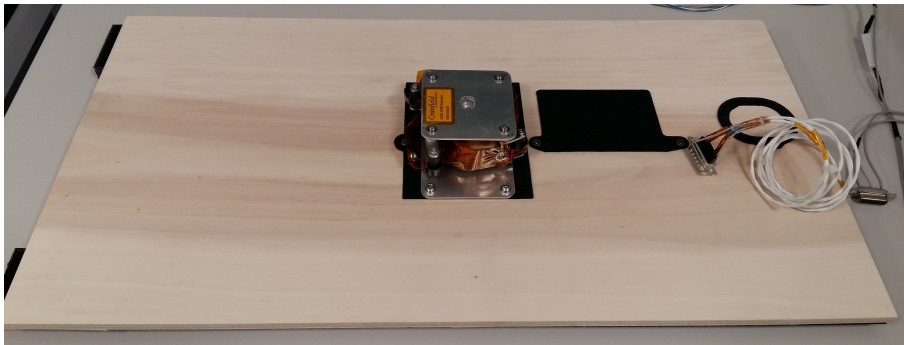
Figure 3.15: DOM EBB in stowed configuration on the ESEO mock-up panel.

3.3.2.2 Sails

Each of the sail quadrants is folded to a pattern developed from bio-mimetic "Miura-ori" studies [Tanizawa and Miura, 1978]. The pattern allows for deployment (see Fig. 3.16) in two perpendicular directions from a single point of origin.

The thickness of the aluminized-kapton used is 25 micron.

As mentioned before, the sails are stowed between the booms and wrapped

71

around the central spool to form the spool assembly. The depth of the sail fold is limited by the width of the booms.

The sails are attached at the tips of the booms and at the booms/spool interface. Snagging problems, associated with multiple attachment locations, were prevented by minimizing the number of attachment points.

Figure 3.16: Sail deployment process for DOM prototype.

3.3.2.3   Booms

Due to the Cranfield heritage, the material selected for the tape spring booms was an alloy of copper-beryllium.

The length of the booms is defined as a function of the angle of revolutions around the central spool, number of booms, and the sail area. A more detailed analysis is performed in Chapter 7.

The transverse radius of curvature of the booms, r, is defined by the radius of the central spool, R, where r=R, to achieve a smooth stowed profile when wrapped around the spool.

The width of the booms drives the height of the final assembly and the maximum depth of the fold of the sail pattern.

The booms deploy with a constant torque of the order of 0.1 Nm, this is the

steady-state bending moment calculated for a tape spring coiled onto a spool of radius approximately equal to its curvature [Seffen and Pellegrino, 1999]. In this way the booms fold naturally and jamming is prevented during deployment.

3.3.2.4   Release mechanism

The Release Mechanism consists of a Kevlar retaining cord attached to the Spool, two CYPRES^{TM} cord cutter actuators and two sets of cord clamps.

After stowing of the booms and sails, the retaining cord is threaded through the hole in the bottom spindle of the spool, through the actuators and through the cord clamps. The cord clamps are then tightened, securely clamping the cord in place and preventing rotation of the spool.

The release mechanism assembly is shown in Fig.3.17.
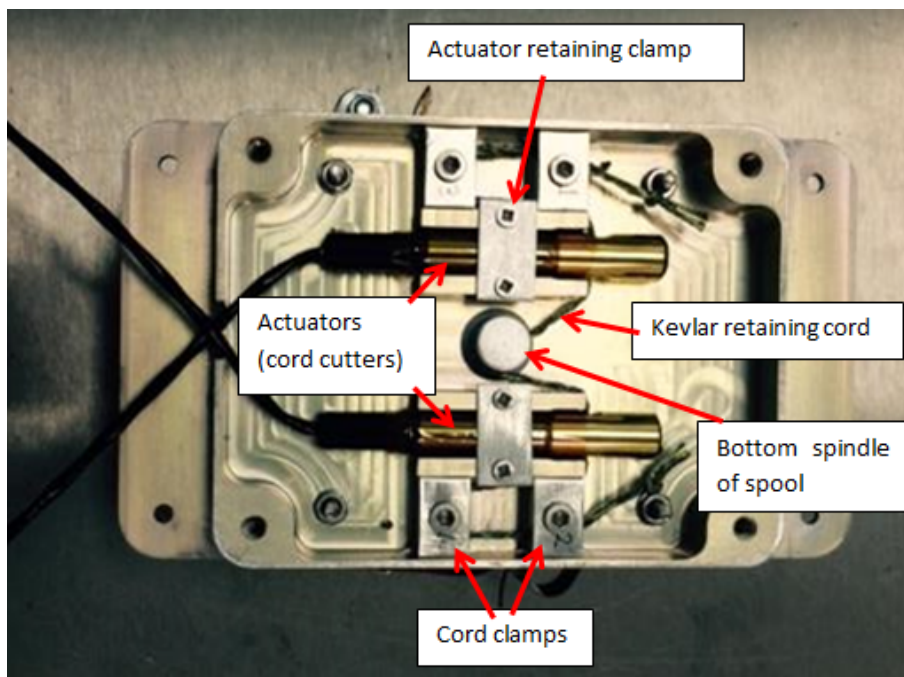
Figure 3.17: Release mechanism assembly of DOM.

Deployment is achieved by firing the two actuators in sequence. This cuts the

cord and allows the spool to freely rotate and the booms and sails to deploy. In the nominal case, firing a single actuator will cause deployment, both are used to give additional reliability.

3.3.2.5 Electrical architecture

The electrical diagram for the de-orbit device is presented in Fig 3.18.

The ECSS safety requirements for triple redundancy of critical systems are implemented on the satellite side. On the DOM payload side, redundancy is implemented via the use of two separate actuators, either of which is independently capable of cutting the retaining cord and releasing. The nominal operational sequence is to fire both actuators in sequence, to fully assure deployment.
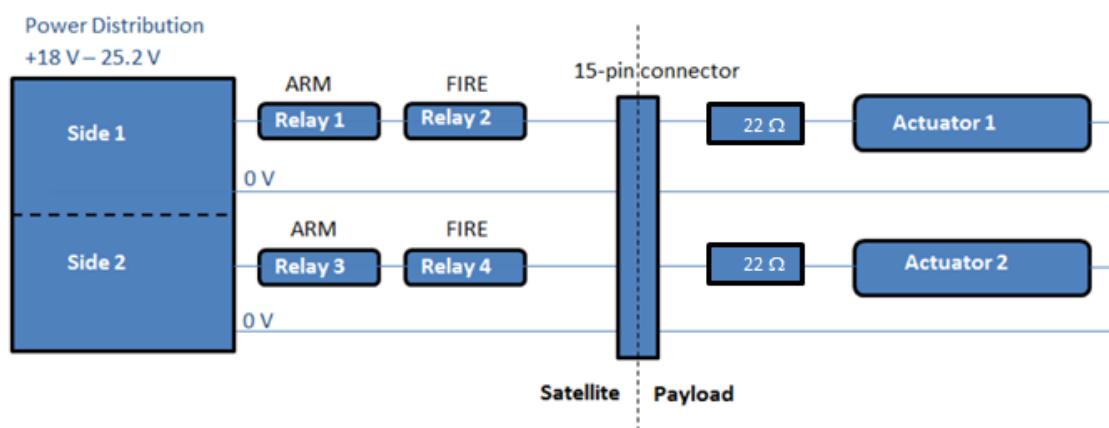
Figure 3.18: Electrical circuit diagram of DOM.

The firing sequence is as follow:

1. Close relay 1 ARM (primary): Sail safe.

2. Close relay 2 FIRE (primary): First actuator fires, cutting restraining cord and deploying sail.

3. Close relay 3 ARM (redundant): Used if sail is not deployed after primary ARM-FIRE sequence.

4. Close relay 4 FIRE (redundant): Second actuator fires, cutting restraining cord and deploying sail.

The 22 Ohm resistor, which is used in series with each actuator, is needed to cope with the ESEO PDU voltage requirement.

Once the deployment-command is sent, by closing a series of relay switches and thereby activating two CYPRES^{TM} cord cutters, the Kevlar cords are cut and the strain energy, stored in the boom arms during the coiling process, is transferred into kinetic energy about the central spool, resulting in deployment.

3.3.3   De-orbit analysis

The analyses were aimed to demonstrate the DOM payload performances on the ESEO spacecraft decay, and, from predicted differences in the orbital elements pre and post deployment, to allow deployment of the DOM to be confirmed.

Considering the orbit altitude (523 km), the ESEO satellite is anyway compliant with the 25 years re-entry requirement after the End of Mission.

3.3.3.1   Initial conditions

The orbit parameters (set in the reference frame Celestial Mean of Date) at the beginning of the mission (see Table 3.5) were given by ALMASpace. The planned mission duration is 0.5 year plus 1 year of extended mission. In this way the Non-Operational phase starts on 01/03/2017 @ 00:00:00.000 UTC. This date was set for the simulations considering the DOM sail deployed, after the EoM. The initial

orbital parameters are the ones obtained after 1.5 year of operational mission with natural decay.

Table 3.5: STELA Input conditions for DOM decay performance evaluation

STELA Input parameters	
Orbit Parameter	
Date	2015-09-01T00:00:00.000
zp [km]	517.38
za [km]	535.00
i [deg]	97.48
RAAN [deg]	137.34
ω [deg]	67.74
M [deg]	292.26
Object Parameter	
Mass [kg]	49.75 (including 10% margin)
Reflectivity Area [m^2]	Depending on configuration selected
Reflectivity coeff	Depending on configuration selected
Drag Area [m^2]	Depending on configuration selected
Drag coefficient	2.2 (constant)
Atmospheric Model	
NRLMSISE-00	
Solar Activity	
Variable solar flux vs time	

The reflectivity coefficient (1+Solar Reflectivity), used to compute the solar radiation pressure force, was calculated considering the Solar Reflectivity of the six external sides of the spacecraft, as provided by ALMASpace. An average value was obtained for the whole external surface of the spacecraft, this changes when the sail is deployed as it covers one panel (Radiator Panel).

3.3.3.2 Spacecraft configuration

As in the case of Icarus-3 on Carbonite-1, the mean cross sectional area was needed as input condition. The computation of mean area was obtained with STELA

Mean Area Tool drawing a simplified model of the spacecraft. The mean area was calculated considering the random tumbling orientation model and the fixed orientation on the Y axis - direction of observation.

Three different configurations were drawn for the simulations:

- Configuration 1: ESEO without sail, as during operational mission.

- Configuration 2: ESEO with sail deployed, to be deployed at EoM.

- Configuration 3: ESEO with sail deployed with different orientation angle.

The area obtained for Configuration 1 (see Table 3.6) in Random Tumbling mode has been used as input parameter for the simulation without sail, just natural decay. The two areas obtained for Configuration 2 (random, fixed orientation) represent the drag areas for the two simulations after the EoM. Configuration 3, given the non-significant difference with Configuration 2 has not been used in the simulation.

Table 3.6: Mean cross sectional areas for the DOM-ESEO configurations.

Config.	Mean Area Random Tumbling [m^2]	Area Fixed Orientation Y [m^2]
1	0.2850	0.2270
2	0.3774	0.5058
3	0.3756	0.5007

3.3.3.3 Results

A total of three simulations were performed. The first simulation was set with starting date as the originally expected launch date (01/09/2015) and Configuration 1, the other two instead had input date the correspondent start date for non-operational mission (01/03/2017), input parameters at 1.5 years after launch date, and Configuration 2 (one for the case of stable configuration, one for random tumbling conditions).
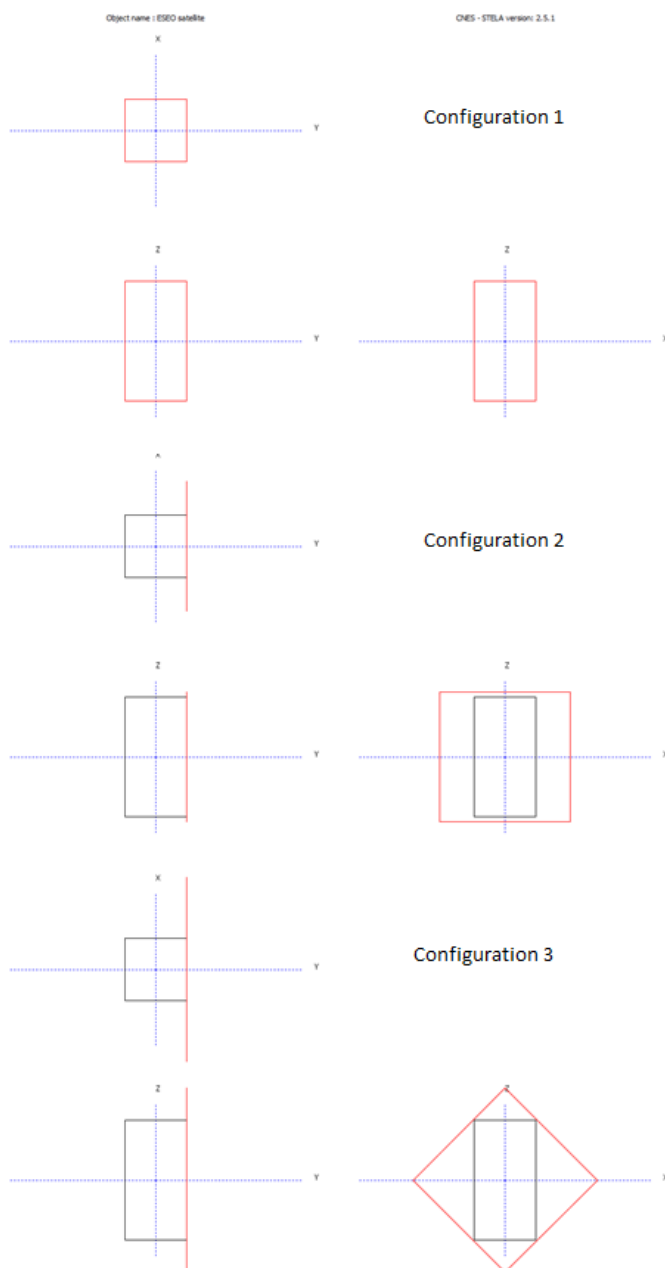
Figure 3.19: Configurations of DOM and ESEO spacecraft for de-orbit simulations.

The simulations performed demonstrate that without the DOM payload, the spacecraft natural decay is longer despite the ESEO is anyway compliant with wide margin with the 25 years rule. With the DOM sail fully deployed, the spacecraft will
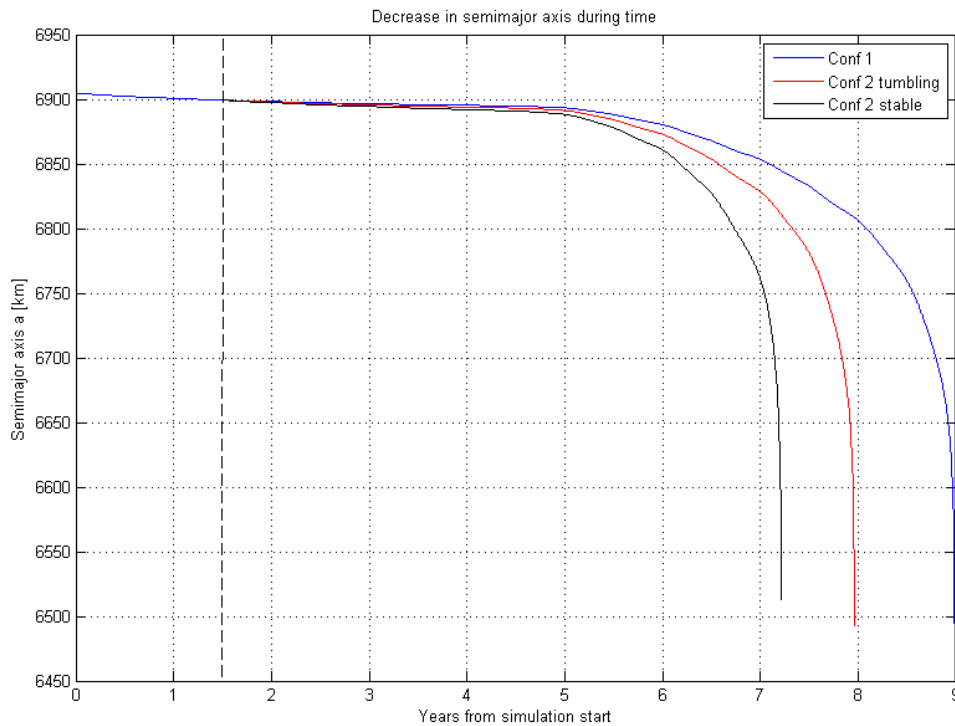
Figure 3.20: Semi-major axis vs time for three different configurations (no sail, sail tumbling, sail stable) with constant drag coefficient and variable solar flux.

re-enter in less than 6.5 years after the EoM (see Fig. 3.20). It has been assumed no on-board propulsion, so the satellite altitude reduces slightly over the 1.5 year operational lifetime before the sail is deployed.

The case of the sail in a stable configuration with respect to the direction of velocity has also been analysed. In this case the drag area is larger than the random tumbling area and the results show, as expected, faster de-orbit time (5.71 years) with respect to the other cases.

The differences between decay without and with DOM sail deployed will be more evident after 5 years from the EoM, when the altitude decreases around 500 km and the drag effect will be stronger. Nevertheless, after a couple of months from the EoM, the effect of the increased drag area will be noticeable monitoring the orbital

elements and comparing them with simulations data.

It is suggested to perform additional up-to-date simulations just before the planned EoM with the correct orbital elements to obtain the most accurate predictions of the trajectory with/without the deployed DOM sail.

3.3.4   Verification and testing

In this section the verification approach and test programme implemented for the DOM payload of the ESEO project is described. This is to give an overview of the methods and control necessary to define and accomplish the test and verification of the DOM payload.

The Test Plan document describes in detail the test program to ensure the DOM unit conforms to the design, manufacturing and requirements. The test campaign must demonstrate that the specific functional, performance and environmental requirements imposed on the ESEO satellite, subsystems and units are properly implemented. This guarantees capacity to provide all performances required during the mission, free from material and workmanship defects.

3.3.4.1   Model philosophy

The philosophy was defined by the ESEO mission requirements and constraints. The DOM payload followed a Hybrid philosophy with a proto-qualification approach. This philosophy is a compromise between the Prototype and Protoflight philosophies [Ley et al., 2009].

The Hybrid philosophy was suggested and selected since most of the components had qualification heritage from the Icarus DAS (CYPRES cord cutters, stored-energy tape spring deployment mechanisms, aluminized Kapton sails). In addition
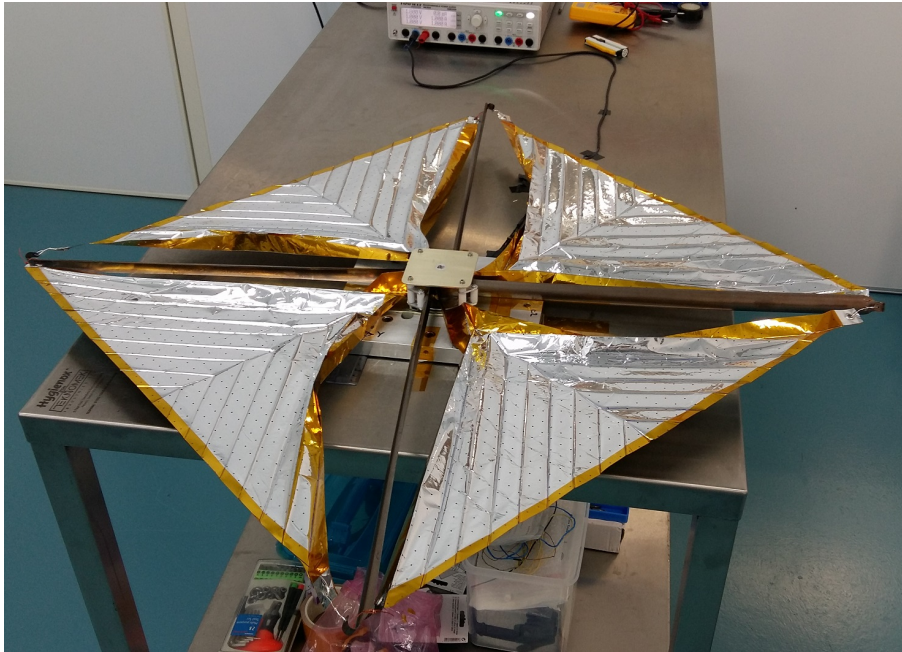
Figure 3.21: DOM PFM in deployed configuration after deployment test performed in the Clean room.

the DOM made use of materials with significant space flight heritage. For these reasons only acceptance tests were executed on the protoflight model at system level.

Four distinct models were built:

- Prototype Model: used in prototyping for functional deployment tests.

- EBB (Elegant Breadboard Model): which is almost identical to the Protoflight Model in form and function (there may be minor differences in materials and internal layout), and was subject to functional testing and mechanically tested at qualification levels. EBB is shown in Fig. 3.14.

- PFM (Protoflight Model): this will fly after test at qualification level with acceptance duration. PFM is shown in Fig. 3.21.

- FS (Flight Spare): this model has the same configuration of the EBB.

Considering the overall test philosophy, this focused on two areas:

1. Unit performance: tests for specific components or system elements that were identified as risk areas (e.g.: spool mechanism, booms, etc.).

2. Full system performance: tested at qualification and acceptance levels.

3.3.4.2   Verification approach

As stated in the ECSS-E-ST-10-02C [ECSS Secretariat, 2009a] the supplier conducts three main identification steps when generating the verification approach:

- "What" are the products and requirements subject of the verification process;

- "How" to verify them by considering the methods stated in the technical specification;

- "When" to implement by applying the chosen verification strategy.

These steps were applied to the DOM Verification approach in an iterative process and agreed by the supplier (Cranfield) together with ALMASpace and ESA.

Verification methods   The requirements verification for the DOM payload was accomplished with the following methods, as reported in [ECSS Secretariat, 2009a]:

- test (including demonstration);

- analysis (including similarity);

- review of design;

- inspection.

In the following section only the requirements verified by Test will be presented. The full compliance matrix was compiled and reported in the DOM Experiment Interface Document Part B.

Verification strategy   The Verification strategy in the different categories of technical requirements is defined in the Verification matrix (Table A.1). The Verification matrix lists line by line the different type of requirements applicable for the DOM payload and in the columns the different system level with their status (of verification).

3.3.4.3   Test Programme

The Test Programme for the DOM is reported here in the form of block diagrams.
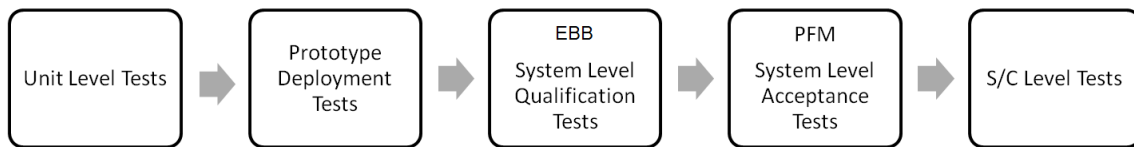
Figure 3.22: Test sequence block diagram for HW models.
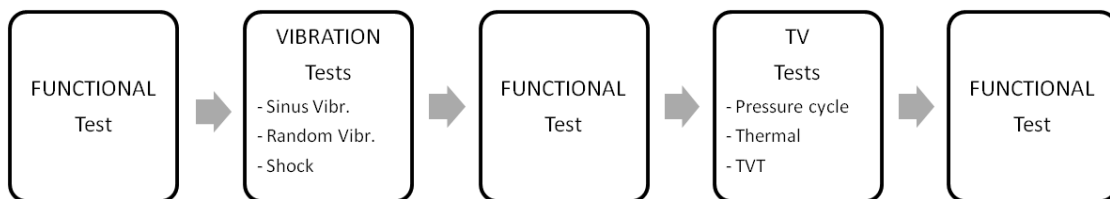
Figure 3.23: Test sequence block diagram for System Level Tests.

The first diagram (Fig. 3.22) shows the test sequence for the different HW models and specifies their different levels of testing. The Unit Level Tests aimed to prove the functionality of the different parts/components of the DOM: tape spring

characterization, boom guide mechanism, actuators characterization, sail re-folding and stowing process. After the Unit Level Tests the whole prototype was assembled and Multi-Deployment Tests on it were performed. Upon the completion of the manufacture of the EBB, a refinement of the prototype model, the System Level tests started.

The second diagram (Fig.3.23) shows the test sequence for the tests performed at System Level, first for the EBB model and then for the PFM model.

Test Plan   The Test Plan was developed to identify the tests to be carried out on the DOM.
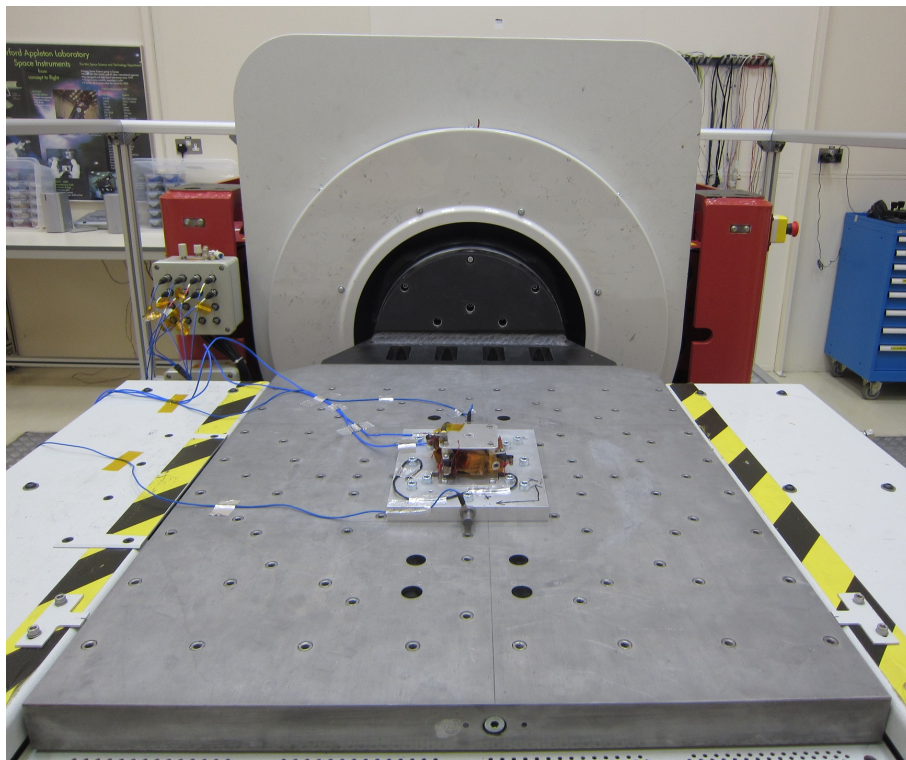
Figure 3.24: DOM EBB model set up for Vibration test on lateral axis at RAL Space facility.

All Test Procedures describe in detail, "step by step", in dedicated documents

Table 3.7: Overview on the test performed on the DOM.

Test Type	Objective	Brief description of test & test articles used
Functional Tests	To demonstrate the functionalities of the payload or components function. To verify deployment of booms and sails in 1g environment, and characterise mechanism behaviour.	Unit level test of component function (cord cutters, boom, mechanism, sail) and deployment system level tests to verify the functionality of the DOM. (Prototype, EBB & PFM)
Vibration Test	To verify that structural integrity of payload is maintained during launch phase, and that no hazard is posed to ESEO satellite.	Sinusoidal Vibration and Random Vibration on all three axes. (EBB at qualification level & PFM at acceptance level)
Vacuum Test	To ensure that the depressurisation during launch phase has no billowing effect on the sail.	DOM is subjected to depressurisation with maximum rate of 5 kPa/s. (EBB)
Thermal Test	To demonstrate the deployability of the device after being subjected to the thermal conditions to similar to the space environment.	DOM is subjected to the thermal conditions it will experience within the space environment, but at ambient pressure (hot case and cold case). (EBB)
Thermal Vacuum Test	To prove the results of the Vacuum Test and Thermal Cycle test at the same time	DOM is subjected to the thermal and vacuum conditions they will experience within the space environment and functionality demonstrated at hot and cold extremes. (Cord cutters, PFM)

(e.g. DOM-TPRO-Vibration v1.0) associated with each test type (a summary is presented in Table 3.7). This was to ensure the reliability and correct functioning of the DOM. After performing each test a dedicated Test Report (e.g. DOM-TREP-

Vibration v1.0) was drafted.

The Test Plan was created in accordance with a number of ECSS standards and each test was designed to demonstrate some requirements as set by either ALMAS-pace or the Cranfield ESEO team.

3.4   Concepts comparison

In this section the two different design concepts are compared against each other. The two DAS concepts have the following common features:

- Drag augmentation achieved by deploying lightweight film sails supported by rigid booms;

- Deployment achieved using stored spring energy;

- No use of complex electronics or autonomy;

- Technologies used compatible with low-cost manufacturing and testing facilities.

A summary of the main physical properties of the three DAS developed is given in Table 3.8.

Table 3.8:   Main physical properties of DAS developed.

Physical property	Icarus-1	Icarus-3	DOM
Mass (kg)	3.5	2.3	0.5
Sail area (m^2)	5	2	0.5
Frame/Structure (mm)	700 x 900	490 x 490	140 x 80

Both the Icarus and DOM designs meet the requirements presented at the beginning of the chapter, however, for some of them there are relevant differences in

the way they comply. These are the followings:

- Reliability: based on the rigour of the qualification and test campaign the DAS have undergone;

- Area;

- Mass;

- Deployable area to mass ratio;

- Scalability: the ability of the design concepts to be scaled in dimensions;

- Versatility: the ability of the design concepts to be adapted to different satellite configurations;

- Maturity of the design: the TRL of the concepts.

In Table 3.9 the limitations and advantages of the Icarus and DOM design concept are presented considering the parameters just described.

A colour code was used to identify the advantages (white unshaded cells) and limitations (grey shaded cells) in the designs as well as to determine if the limitation constraints come from the customer (darker grey) or the supplier, i.e. Cranfield University (lighter grey).

Table 3.9 shows that the DOM has more advantages than the Icarus concept. The limitations due to Cranfield's constraints affect both Icarus and DOM more than the ones due to the customer (e.g.: spacecraft manufacturer). The limitations due to internal Cranfield constraints need to be reduced or mitigated to have potential for a wider satellites' market and flexibility with respect to the spacecraft characteristics.

Table 3.9: Comparison Icarus concept vs DOM concept, note: table modified from Grinham [Grinham and Kingston, 2016].

Icarus Concept	DOM Concept
Qualification required less rigorous, less stored energy for deployment.	Passed an ECSS/ESA qualification campaign, greater deployment force margin.
Sail area constrained by shortest panel length.	Sail area constrained by boom length, not possible to manufacture longer booms in house.
Maximises useful sail area, no overlapping with satellite panel.	Overlapping sail area with satellite panel, once deployed can obstruct it.
Higher mass due to aluminium frame structure.	Very light and compact unit.
Frame less mass efficient. Ratio deployed surface and system mass improves with increasing size.	Self-contained unit is more compact and better A/m ratio from smaller size.
Scalability is limited due to panel side length constraints, difficult to scale down.	Expected to be more scalable (up and down).
Frame not very flexible in its placement location, more difficult to be adapted to different satellite configurations.	Being a small, light, self-contained unit provides opportunity for more than one DOM to be mounted onto a satellite.
TRL is 8-9, it is on-orbit in two active missions, awaiting for deployment at EoM.	TRL is 8, FM built and qualified, still not launched.

Chapter 4

Future Scenarios for Passive De-orbit Systems

This chapter is derived from the journal article *Forecast analysis on satellites that need de-orbit technologies: future scenarios for passive de-orbit devices* [Palla and Kingston, 2016b].

The chapter presents the investigation performed on the future spacecraft market for passive de-orbit systems in LEO. The main aim was to aid in defining top-level requirements for the design of such devices. The investigation was performed by considering the compliances of projected future satellites with the IADC de-orbit time, to quantify the number of spacecraft that are compliant or non-compliant with the guidelines/requirements and, in this way, determine their need for the previously discussed devices.

4.1   Methodology

In this section, the tools, models, and workflow adopted to quantify the compliances of projected future satellites with the 25 years de-orbit time are presented. The study was performed by using the SpaceTrak^{TM} database [Seradata, 2014] which provided future launch schedules, and reliability and trend information for launch vehicles and spacecraft types; the de-orbit analysis was carried out by means of simulations with STELA, the semi-analytic orbit propagator designed by CNES [Fraysse et al., 2012].

The main phases of this work encompassed:

- the evaluation of orbital data of satellites re-entered (TLE) with respect to STELA simulation;

- developing and updating of the future launch schedules database;

- division in satellite classes, types and orbits;

- performing STELA simulations for the de-orbit analysis of future satellites.

4.1.1   Database of future launches

SpaceTrak^{TM} provides an up-to-date database on satellites and launch vehicles and it has become the most used reference source for launch providers, satellite insurances, operators and manufacturers in the space sector. For the purpose of this study, all the future satellites in LEO with a stated launch date (the range is 2015-2020) were extracted, it is to be noted that suborbital vehicles and cargo missions were not considered since they were out of the objectives of this work.

Following the database classification, the satellites in LEO were divided into three different subgroups: Polar Orbit, Sun-Synchronous Orbit (SSO), and LEO in

Table 4.1: Summary of data available for the analysis on future launches 2015-2020 (last update April 2015). Satellites are divided depending on the orbit type (group).

Group	Total with launch year	Data missing for mass	Data missing for orbit	Data missing for area
LEO (not SSO/Polar)	143	19	31	39
SSO	135	24	42	61
Polar	93	2	9	9

general not fitting with the first two groups. For each spacecraft in the sample, the key parameters collected from the database were: (1) S/C name, (2) S/C bus, (3) Future launch date, (4) Mass, (5) Apogee, (6) Perigee, (7) Inclination.

Due to the uncertainty on the future launches and the information publicly available, the database was not complete for the orbit parameters and the spacecraft characteristics, including geometry. For this reason, the missing data were collected from different sources, the main ones were Gunter's Space Page [Krebs, 2015] and Earth Observation Portal [ESA, 2015b] or from the same SpaceTrak$^{\text{TM}}$ database (e.g.: previous satellites of the same bus type, same constellation, etc.). In addition, the geometry of the spacecraft, which was not contained in the SpaceTrak$^{\text{TM}}$ database, was added since this was needed for the calculation of the drag surface.

4.1.2   STELA tool

STELA reflects the standard concerning the protection of LEO and GEO regions (lifetime and protected regions crossing of disposal orbits). The tool was developed by CNES to support the French Space Operations Act (FSOA) [Republique Française, 2008], its Technical Regulations have been mandatory since 2010 [Lazare, 2013]. The software allows efficient long-term propagation of LEO, GEO, and GTO types orbits based on semi-analytical models, statistical analysis and assessment of protected regions criteria. The main input parameters (general) for the performed

STELA simulations to understand the future scenario were the following:

- Orbit parameters (*zp, za, i, Ω, ω, M*): mean values in the reference frame Celestial Mean of Date (MOD).

- Initial date: the future launch date was set.

- Object characteristics: total mass of the spacecraft, mean cross sectional area used to compute the solar radiation pressure force (Reflectivity Area) and the atmospheric drag force (Drag Area), the reflectivity coefficient, and the drag coefficient. The reflectivity coefficient, used to compute the solar radiation pressure force, was selected with mean value (i.e. 1.5) between 1 (pure absorption) and 2 (pure specular reflection) as suggested in [Wertz et al., 2011] for LEO.

- Atmospheric Model: empirical model NRL-MSISE-00 (already set in STELA) for the density calculation.

- Solar Activity: Variable solar flux vs. time, this includes the future mean prediction given by NOAA and NASA till 2318 [CNES, 2013]

Table 4.2: Object characteristics for STELA simulations performed.

Object characteristics	
Mass (*kg*)	$m_{S/C}$
Reflecting area (*m²*)	A_{mean}
Reflectivity coefficient	1.5
Drag area (*m²*)	A_{mean}
Drag coefficient	2.2

Regarding the "Parameters Advanced section" the default parameters, already set in STELA were adopted (see Table 4.3).

Table 4.3:   Advanced Parameters settings for STELA simulations performed.

Algorithms	Settings
Integrator step	24 h
Atmospheric drag	Enabled
Solar radiation pressure (SRP)	Enabled
Third body perturbations (Sun and Moon)	Enabled
Earth perturbation	Zonal order 7x0

The re-entry altitude was maintained at 120 km as the default settings, when reached the simulation stopped automatically.

The computation of mean cross sectional area was obtained with STELA Mean Area Tool drawing a simplified model of the spacecraft considering the random tumbling orientation model.

Before analysing the future scenario, the confidence of STELA for de-orbit simulations was evaluated, particularly in situations of uncertainty in the spacecraft geometry. The purposes of this analysis were the comparison of real data (TLE) from already decayed and re-entered satellites (without any propulsion, just natural decay), with respect to STELA simulation propagation; the understanding of the influences of orbit parameters and perturbations; the proper configuration for geometry to be adopted.

Table 4.4:   Mission case studies with spacecraft mass and main orbit parameters.

Mission	Orbit type	Mass (*kg*)	Perigee (*km*)	Apogee (*km*)	Inclination (*deg*)
Uosat-1	SSO	52	532	537	97.46
Tiros-02	LEO	127	609	744	48.56
OV1-10	SSO	130	631	758	93.41
OPS7353	SSO	130	527	751	99.01

The TLEs for the decayed satellites (listed in Table 4.4) have been provided by the NORAD Two-Line Element Sets Current Data via Data Request [Kelso, 2014].
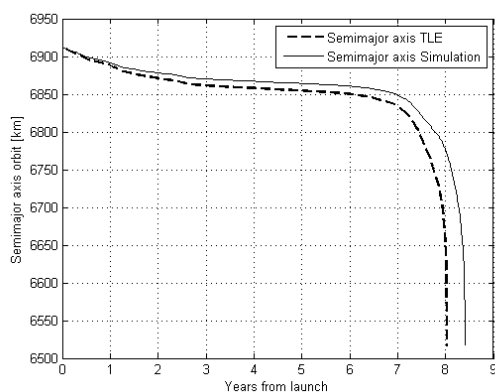
Figure 4.1: Decrease of semi-major axis of Uosat-1 during years, real satellite data (*dashed*) and STELA simulation (*continuous).*
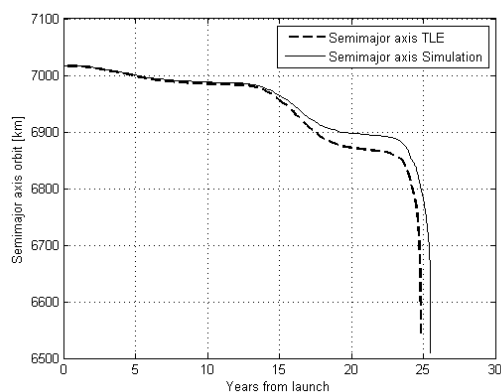
Figure 4.2: Decrease of semi-major axis of OPS7353 during years, real satellite data (*dashed*) and STELA simulation (*continuous*).

The case studies are all Micro and Minisatellites.

As can be seen from Fig. 4.1 and 4.2, the simulation trend is conservative (more time needed for re-entry) with respect to the real data, this gives confidence and margins for the results on future simulation.

As can be seen in Table 4.5 the error on time for Uosat-1 and OPS7353, both in Sun-Synchronous Orbits, is near or even below the 5%. The error encountered in the simulation is related to different uncertainties; one of them is the atmospheric model accuracy prediction of the density. The NRL-MSISE-00 is influenced by the accuracy of the solar cycles and geomagnetic activity used as inputs. The density uncertainty is of 15% for mean activity conditions, as stated in [ESA SDM WG, 2015].

Another uncertainty is the cross-sectional area for atmospheric drag that can vary over time depending on the orientation of the S/C, while for the simulations, random tumbling mean values have been adopted. The error due to the area uncertainty is very evident for OV1-10, in this case there was high uncertainty in the geometry data
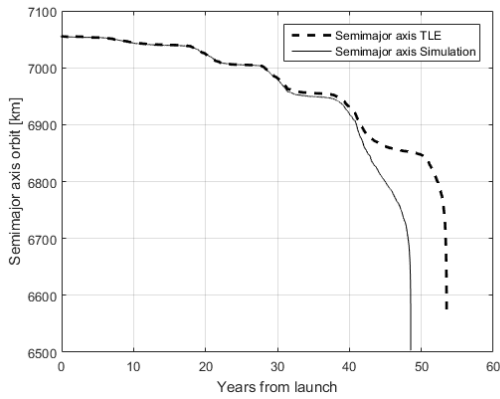
Figure 4.3: Decrease of semi-major axis of Tiros-02 during years, real satellite data (*dashed*) and STELA simulation (*continuous*).
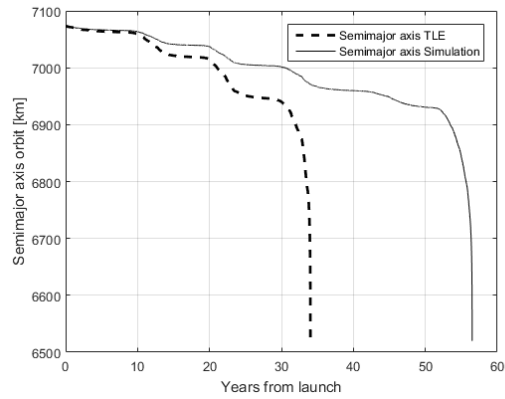
Figure 4.4: Decrease of semi-major axis of OV1-10 during years, real satellite data (*dashed*) and STELA simulation (*continuous*).

(lack of information for this military satellite) and consequently the value computed for the drag area was not very reliable.

In the case of Tiros-02, which had an orbit inclination of 48.5 deg, the simulation underestimates the real TLE data, despite the simulation time is just 10% shorter than the real time. However this satellite fits in the critical inclination group, identified in STELA in the ranges 40 to 80 deg and 110 to 130 deg with most sensitive inclinations close to 41.6 deg [Lamy et al., 2012].

Table 4.5: Relative error on time (years) for the simulation with reference to the real value at different semi-major axis during decay.

Semi-major axis (*km*)	Uosat-1	Tiros-02	OV1-10	OPS7353
Initial-5km	17,54% (6907km)	-1,00% (7050km)	37,51% (7068 km)	11,11% (7012km)
6878	43,17%	-3,22%	65,63%	24,82%
6828	4,36%	-15,09%	66,13%	2,72%
6778	5,19%	-12,69%	65,93%	2,46%
6728	4,35%	-10,40%	65,96%	2,60%
6675	4,47%	-9,55%	66,01%	2,83%
6628	4,66%	-9,37%	66,07%	2,78%
Final data	4,75% (6516km)	-9,33% (6562km)	66,11% (6516km)	2,80% (6539km)

These inclinations lead to resonance effects due to various perturbations with significant effect on the lifetime. STELA recommendation for this inclination range

95

is to run several simulations and process them statistically [Le Fèvre et al., 2014]. This is relevant to consider for the de-orbit propagation of future satellites if they fall in this group.

4.2   Results and discussion

In this section the results obtained from the performed STELA simulations for the de-orbit analysis of future satellites are presented. The satellites considered are planned to be launched in the time frame 2015-2020 (launch date stated) and they are divided in different orbit subgroups (SSO, Polar, LEO general) as mentioned before.

The main aim of this work is helping in defining top-level requirements for the design of passive devices to de-orbit a range of different spacecraft at the end of life; for this reason, the satellites have been divided into classes depending on their mass. Medium (above 1000 kg) and larger classes have not been considered since they are out of the purpose of this study. These spacecraft are out of the target for passive drag devices, because they are already equipped with propulsion subsystem and they need a controlled re-entry, as some components (e.g.: titanium tanks) are most likely to survive the re-entry. Medium and larger spacecraft are not fully demisable during re-entry, however, if their demisability could be improved, drag augmentation devices with larger sails could potentially be integrated on these platforms.

4.2.1   Expected compliance scenario

The expected scenario, presented in Fig. 4.5, identifies the de-orbit time compliance taking in account only the future launches for LEO and not the satellites already on-orbit.

This study was performed by considering the natural decay of these future missions, as its purpose was to identify which missions would need to employ de-orbit technologies. It is noted that some of the future missions may be already intending to either use a de-orbit device or the satellite's propulsion to achieve de-orbit.

The column chart presented shows the results for the mass classes: pico, nano, micro, mini and small. As can be seen in Fig. 4.5, picosatellites are not relevant as the amount is not significant and anyway they comply with the 25 years requirements. The nanosatellites, in this group fit the cubesats, are generally compliant as usually they are in very Low Earth Orbit (e.g: launched from the ISS); however 15% of them will require some kind of passive device to re-enter within the 25 years. Furthermore more attention shall be paid on this class considering the potential increase in the coming years confirmed by different projections, SpaceWorks foresees a CAGR (Compound Annual Growth Rate) equal to 23.8% average [Buchen and DePasquale, 2014].

The microsatellites non-compliant are comparable in number to the nanosatellites but the mass is significantly heavier and so the potential impact they could have as source of debris is greater; another aspect to take into account is that most of them don't have any propulsion subsystem or propulsion capabilities for an effective controlled re-entry.

More than 50% of the minisatellites will not comply with the requirements, which makes them an interesting target for the passive devices, also considering that their propulsion capabilities are limited. In addition, the drag device is an attractive option considering the relatively low additional mass with respect to the fuel mass needed to re-enter.

The small satellites are the less compliant to the re-entry time, however most of them (probably all) are equipped with propulsion subsystem and the higher quantity
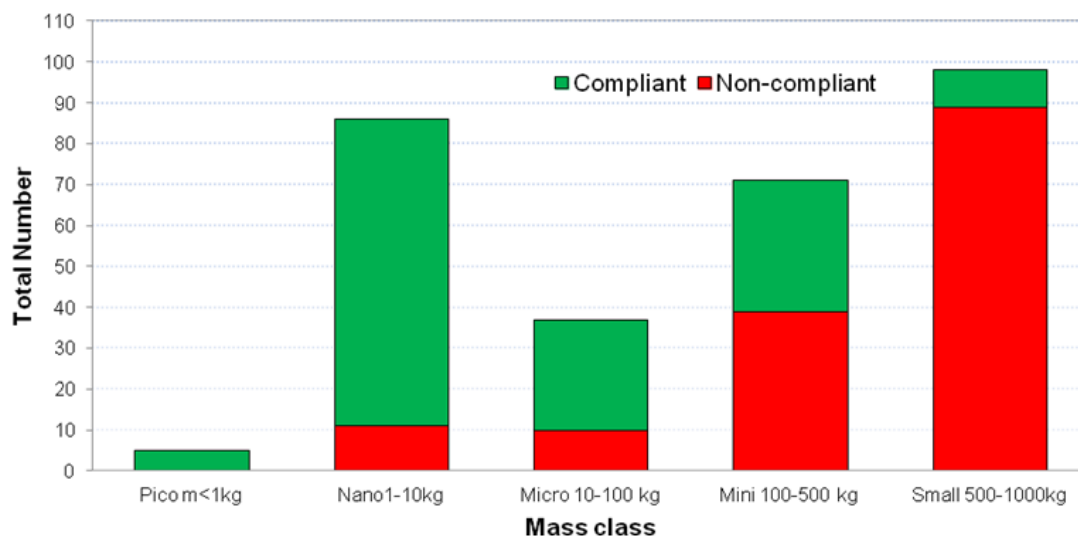
Figure 4.5: Compliance with 25 years re-entry for planned satellites 2015-2020 in LEO for all the orbit type categories: SSO, Polar, LEO general. Assumes no specific de-orbit measures are used. Note that OneWeb constellation of 700 LEO satellites has not been included in the study, since it was performed before the public announcement (in addition OneWeb states that these satellites will be designed to be compliant with debris guidelines).

is related to the presence of satellite constellations (e.g.: Iridium-NEXT on polar orbit). Nevertheless some passive solutions can be implemented as back-up option.

The bubble charts (Fig. 4.6, 4.7, 4.8) show a more detailed insight of the compliance distribution depending on the altitude and mass in the different orbit subgroups. It can be seen clearly where there will be a concentration of satellites in the next years.

Looking at the SSO chart (Fig. 4.6), a sparse distribution with different variety of spacecraft is identified. A constellation of 14 satellites is evident at 500 km; this is the Terra Bella (formerly Skybox imaging) constellation which results compliant if the target altitude is confirmed. Overall, on sun-synchronous orbits, half of the satellites will be compliant with the 25 years and half of them not, so de-orbit methods with scalable design are needed.
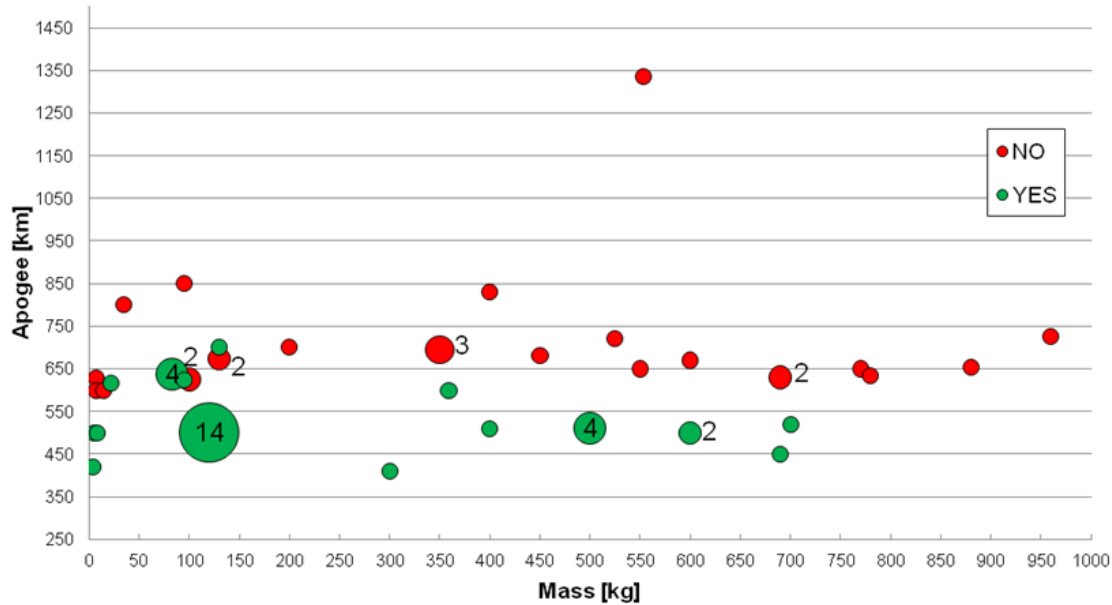
Figure 4.6: Distribution of satellites' compliance with 25 years re-entry considering mass and altitude for Sun-Synchronous Orbits, the size of the bubble represents the satellites number (number is 1 if not shown). Assumes no specific de-orbit measures are used.

For polar orbits (Fig. 4.7), the situation is different since fewer satellites fall in this group; however this orbit type is mostly used for communication satellites. The main constellation is in fact Iridium-NEXT (72 satellites to substitute the old Iridium), non-compliant if no de-orbit methods are implemented. In addition, the presence of four other satellites can be observed at the same altitude, this is the Ionosfera spacecraft constellation.

The last plot (Fig. 4.8) shows the LEO satellites which don't fit with the previous subgroups. For this group, the results presented consider only S/C with mass below 300 kg. It has been decided to focus on lighter masses for two reasons: firstly there are only few satellites with heavier masses, four of them around 400 kg are compliant and six Globalstar-SG are not but the drag effect is not significant on the planned altitude (around 1400 km); secondly, in this way, a more accurate scenario
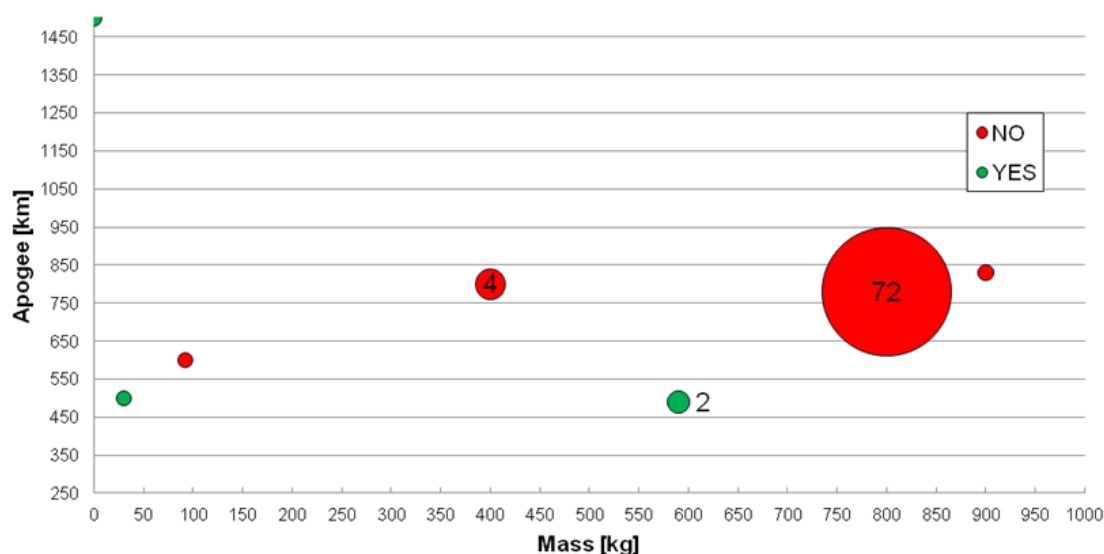
Figure 4.7: Distribution of satellites' compliance with 25 years re-entry considering mass and altitude for Polar Orbits. Assumes no specific de-orbit measures are used.

is depicted.

There is a noticeable concentration of nanosatellites, mostly cubesat type (QB50 with 50 S/C and EDSN-cubesats with 10 S/C), around 400 km and easily compliant due to the very low altitude. Another constellation in line with the re-entry requirement is CYGNSS with 8 microsatellites at 500 km of altitude.

More of interest for the purpose of this work is looking at the concentration of non-compliances. Three main groups can be identified: ORBCOMM OG2 with 11 new satellites, FORMOSAT constellation with 6 satellites at 750 km (and the other half compliant at 500 km), and the 4 Russian MKA-FKI satellites at 800 km. In addition, it is relevant to note how many different nanosats and microsats will be positioned in higher orbit than the commonly used one (see green bubbles for comparison) and so they will need drag disposal strategies.
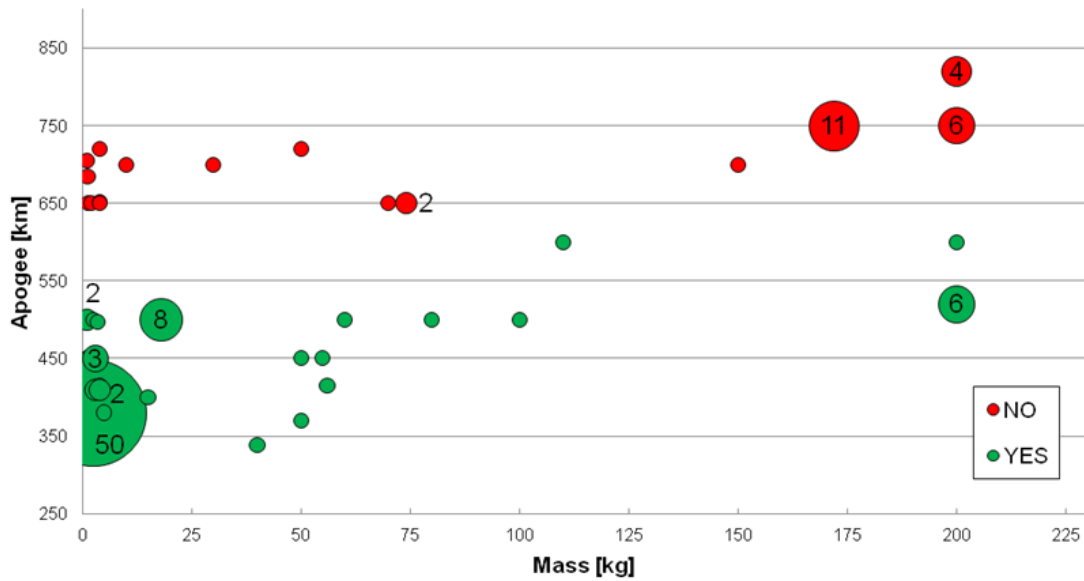
Figure 4.8: Distribution of satellites' compliance with 25 years re-entry considering mass below 300 kg and altitude for LEO (non-SSO or Polar orbit type). Assumes no specific de-orbit measures are used.

4.3 Summary

The future market for passive de-orbit systems in LEO has been investigated.

The process of filling the database gaps has not been an easy task as this relied on the information publicly available, so despite a good amount of data the numbers are underestimated. STELA has been confirmed a valid tool for de-orbit analysis, in particular considering the uncertainty in the spacecraft geometry and on-orbit perturbation given by the models.

The study performed showed that the natural decay is not enough to achieve the compliance: more than 60% of future spacecraft between 10 and 1000 kg (micro, mini, small satellite) will need more than 25 years to re-enter after the EoM if no de-orbit measures are applied. This represents a potential market for passive drag augmentation devices; in particular two mass categories stand out as target: micro

and minisatellites, with back-up option to be considered for the small satellites.

A further confirmation about the low compliance rate to the disposal requirement of these classes is given in [Frey et al., 2016]. The recent study on the level of adherence to SDM, performed by the ESA space debris office, shows that only 30% of objects in orbit between 10 and 1000 kg is currently compliant with the 25 years.

Chapter 5

Failure Analysis of Satellites' Subsystems

This chapter is derived from the journal article *Failure analysis of satellite subsystems to define suitable de-orbit devices* [Palla et al., 2016]. This work was also previously presented at the IAC 2015 within the Space Debris Symposium.

The study was performed together with the MSc student M. Peroni who carried out the statistical analysis to compute the subsystems' reliabilities for his individual research project [Peroni and Kingston, 2015]. The topic *Reliability study for LEO satellites* was proposed as MSc thesis and the PhD work included co-supervising the MSc student.

When evaluating the utility of different debris mitigation methods, it is useful to understand which spacecraft subsystems are most likely to fail and how this may affect the operation of a de-orbit system. This also helps the consideration of which components are the most relevant or should be redundant depending on the satellite mass class.

The results obtained can guide the identification of the activation procedure for

a de-orbit strategy and the level of integration it should have with the host satellite in order to be activated before a total failure.

5.1 Methodology

This work was based on a sample of recently launched satellites belonging to small mass classes. Failure analysis of satellite subsystems was performed using a statistical approach. The study was carried out by using the satellite database SpaceTrak$^{\text{TM}}$ which provided anomalies and failures for spacecraft subsystems.

The process followed in this work was firstly to extract the failure data per spacecraft, developing a separate database; then to perform a Kaplan-Meier analysis followed by Weibull distribution estimation in MATLAB for the different subsystems reliabilities; finally to combine the different subsystem reliabilities depending on the de-orbit strategies (presented in Section 2.3).

Following the reliabilities study a trade-off analysis to guide in the de-orbit methods selection was performed.

5.1.1 Spacecraft failures database

The sample extracted from SpaceTrak$^{\text{TM}}$ was composed of satellites in LEO, MEO, and Elliptical orbits, with mass lower than 1000 kg, launched between the 1$^{\text{st}}$ January 2000 and the 31$^{\text{st}}$ December 2014. MEO and Elliptical orbits satellites were added to the sample to obtain more failures data considering that their design and level of technology is similar to the LEO ones.

Spacecraft above 1000 kg were not taken into account as they were considered to require targeted re-entry due to the likelihood that some components may survive the re-entry. Suborbital vehicles and cargo missions were also not included since

they were out of the scope of this work.

For each spacecraft in the sample the key parameters collected from the database were: (1) S/C name, (2) S/C bus, (3) Launch Date, (4) Mass, (5) Failure Event Type and Date, (6) Retirement Date, (7) Re-Entry Date. The last three parameters obviously did not necessarily occur for all the spacecraft.

In addition a new parameter, not available in the database, was added: this confirms if a propulsion subsystem is on-board or not. Some assumptions were taken to speed up the research: spacecraft with mass lower than 3 kg were considered with no propulsion. This was based on analysis of available information on proposed S/C < 3 kg: the majority do not have chemical propulsion sufficient to perform de-orbit; moreover most cubesats do not carry a significant propulsion subsystem. Spacecraft with mass higher than 500 kg instead were considered equipped with propulsion subsystem. In Table 5.1 the amount of spacecraft with or without propulsion subsystem considered in the sample is shown.

The completion of the database with information about the propulsion subsystem was performed using different sources, in particular Gunter's Space Page [Krebs, 2015], Earth Observation Portal [ESA, 2015b], SatFlare [SatFlare, 2015], RussianSpaceWeb [Anatoly, 2015].

Table 5.1:   Spacecraft of the sample equipped with propulsion subsystem or not.

Spacecraft	Propulsion	No propulsion
798	380	418

The SpaceTrak[TM] database identifies five states [Seradata, 2014] for each satellite subsystem: one fully operational state, three degraded states (Class IV, Class III-LR, Class II), and one complete failure state (Class I) that brings the satellite to retirement. For the purpose of this study Class I (i.e. "death" of the satellite) and

Class II (i.e. major failure on the satellite subsystem) were considered.

As stated in the SpaceTrak^{TM} User Manual [Seradata, 2014] the failures and anomalies in the database are only included during the designed operational life, up to a maximum of 15 years, whichever is the shorter period.

Starting from the subsystem failure classification of SpaceTrak^{TM} five different failure typology groups were derived:

- TTC: telemetry, tracking, and command together with control processor failures and OBDH issues;

- POW: electrical distribution, batteries, and solar arrays issues;

- ATT: gyro, reaction wheel, attitude control, thrusters, and fuel anomalies;

- MECH: mechanisms, structures, thermal, and antenna deployment failures;

- PAY & UNK: payload and unknown problems.

The satellites were divided into classes depending on their mass (nano, micro, mini, small); however due to the small number of failures new broader classes were used:

- Up to 1 kg: equivalent to picosatellites and lighter;

- 1-10 kg: corresponding to nanosatellites;

- 10-100 kg: corresponding exactly to the microsatellites as classified by SpaceTrak^{TM};

- 100-1000 kg: equivalent to mini and small satellites, to be noted that for satellites without propulsion the upper limit is 500 kg.

Despite this new division it was found impossible to perform the statistical analysis for some typology groups and for some mass classes because there were not enough failure data.

Table 5.2: Spacecraft of the sample equipped with propulsion subsystem and respective number of failures (Class I and II) by typology group.

Mass Class	Total S/C	ATT failures	Mech. failures	TTC failures	POW failures
1 - 10 kg Nano	6	0	0	0	1
10 - 100 kg Micro	53	1	2	0	2
100 - 500 kg Mini	196	9	7	7	3
500 - 1000 kg Small	125	17	3	6	6

Table 5.3: Spacecraft of the sample not equipped with propulsion subsystem and respective number of failures (Class I and II) by typology group.

Mass Class	Total S/C	ATT failures	Mech. failures	TTC failures	POW failures
0.1 - 1 kg Pico	17	0	1	4	0
1 - 10 kg Nano	281	3	7	4	10
10 - 100 kg Micro	100	1	1	4	5
100 - 500 kg Mini	20	3	1	0	0

5.1.2   Kaplan-Meier analysis and Weibull distribution

As mentioned in the literature review, the main features of the Kaplan-Meier analysis [Kaplan and Meier, 1958] are the management of the right-censored data and the suitability of analysing subjects who begin the study at different times.

These relevant aspects fit perfectly with the sample of satellite subsystems to analyse. In fact the dataset of the satellites is censored, this is when the satellite is retired or re-entered or at the end of the observation period; moreover the subjects - the satellites - are launched and then on-orbit in different times. An example of the scenario for the S/C sample is shown in Fig. 5.1.

As said before, the Kaplan-Meier estimator is a non-parametric analysis, so to calculate the failure rate a link with a parametric function is necessary. For this purpose the Weibull distribution was selected. To achieve this, the MATLAB software was used; once a table like Table 2.3 is given it can produce both the Kaplan-Meier plot and estimate the Weibull parameters for that particular step function.

Following the previous work performed by Saleh and Castet [Saleh and Castet, 2011] once the empirical data of subsystems failures were collected, then the Weibull
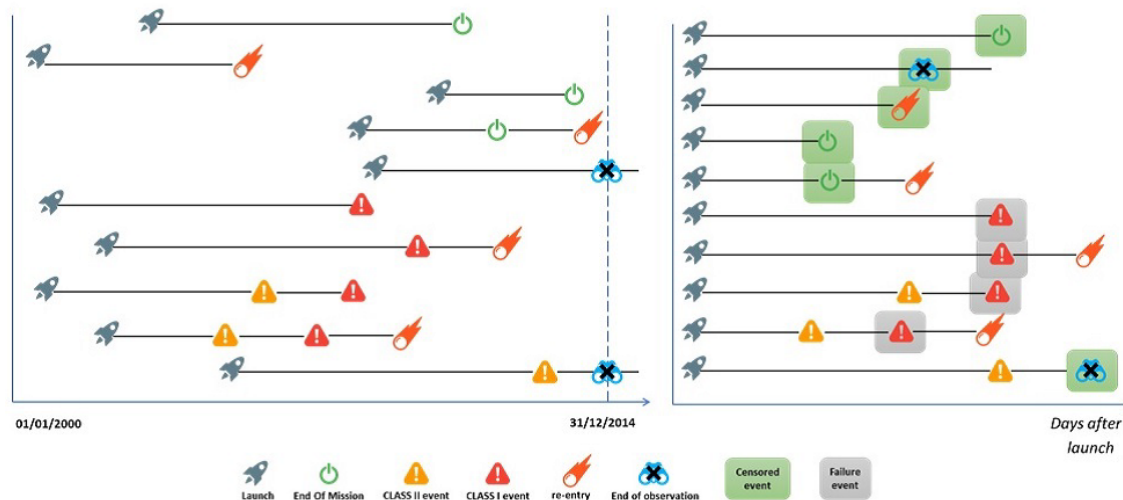
Figure 5.1: Spacecraft sample scenario: left - real situation for several spacecraft, right - all missions shifted to a common starting point and first Kaplan-Meier event (Courtesy of M. Peroni).

distribution was used for the data fit and to extrapolate future trend (see Fig. 5.2).

Saleh and Castet considered a database of 1584 Earth-orbiting satellites launched between January 1990 and October 2008, including also GEO satellites [Castet and Saleh, 2009].

Their work shows that a Weibull distribution fits the failure behaviour of the S/C subsystems well; however the sample is considered too broad for the purposes of this work, as the application, the development, testing and also the operational environment of micro and smaller satellites is significantly different compared to the geostationary satellites (including meteorological spacecraft in GEO).

In this case instead the focus is on LEO satellites and the reliability analysis is performed on the subsystems divided by mass class and S/C equipped with propulsion or not, because the purpose is to assist in the selection of the de-orbit method (and this can vary depending on the size and design of the satellite).

The following equation represents the Weibull reliability function for the satellite
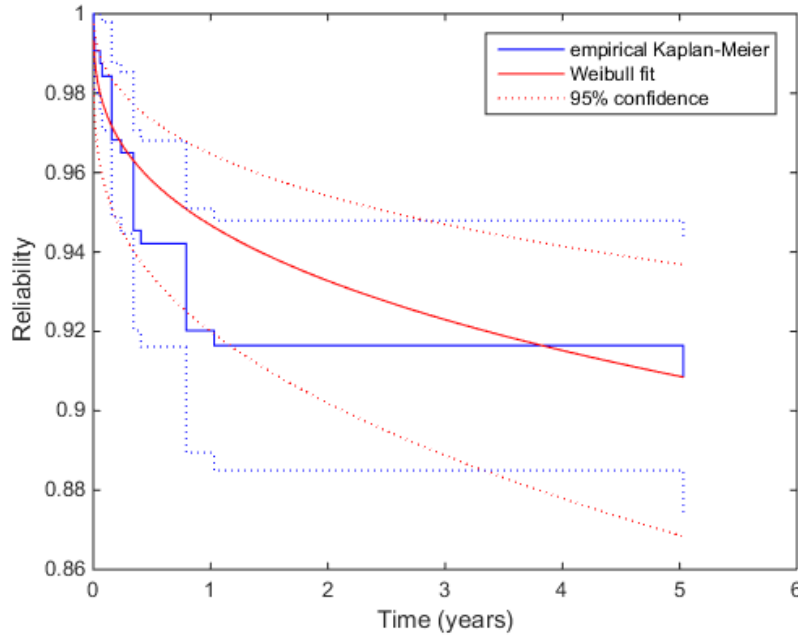
Figure 5.2: Example of Kaplan-Meier plot and corresponding Weibull distribution for attitude subsystem (ATT) of S/C with propulsion, mass range 100-1000 kg.

or subsystem reliability. β is the shape parameter (dimensionless) and θ is the scale parameter (days), see Table 5.4.

$$R(t) = e^{-(\frac{t}{\theta})^{\beta}} \qquad (5.1)$$

The β parameter gives insight of the failure trend: if $\beta < 1$ the rate will decrease with time (this is the case of infant mortality), if $\beta > 1$ the failures will increase with time.

The θ parameter gives an estimation of the time in which the component has a 63.2% probability of failure[2] [Bentley, 1999]. Another important aspect of the Weibull function is that even if the sample is relatively small it can give good

---

[2]This means that by the time θ there is a 63.2% probability that the component will fail, i.e. if there were 100 components only 36.8% would survive until that time.

confidence when used for extrapolation [Saleh and Castet, 2011].

5.1.3 Subsystems vs. de-orbit strategies

The last phase of the study combined the subsystems (typology groups) reliabilities and matched them with the de-orbit strategies.
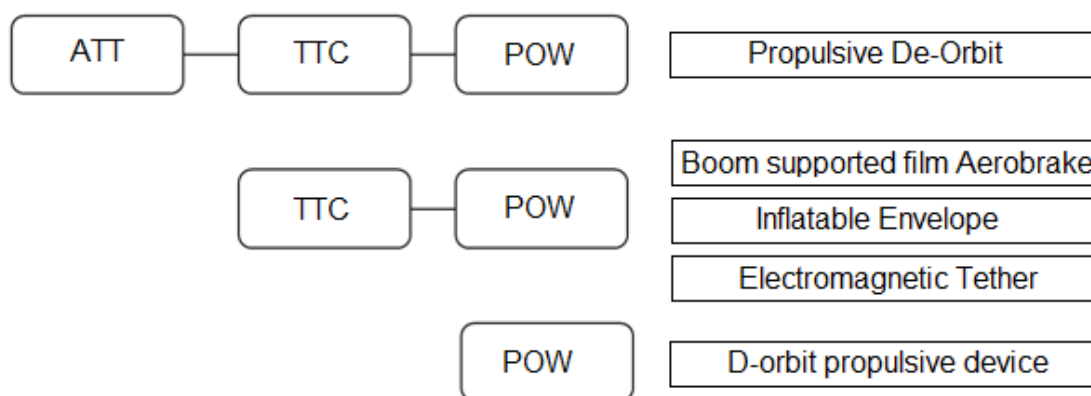
Figure 5.3: Combinations of subsystems vs. de-orbit strategies.

The de-orbit strategies considered were propulsive de-orbit (chemical or electrical), drag augmentation devices, electromagnetic tether, and solid propulsion but independent from the spacecraft (D-Orbit[TM] propulsive device [Rossettini, 2015]).

The selection and combination of subsystems reliabilities is related to the following question: "Which subsystems are required to be functional at EoM for the disposal strategy selected?"

After a technical evaluation the combinations of subsystems presented in Fig. 5.3 were analysed.

The subsystems taken into account belong only to the satellite host and not to the de-orbit methods; for example, a passive drag device will have specific mechanisms to deploy the sail, but the MECH subsystem of the spacecraft is not needed to activate the deployment and so it was not included in the reliability combination.

All the combinations considered were series systems; this means that the overall system reliability is the product of the individual subsystem reliabilities, assuming that the individual reliabilities are independent from each other [Bentley, 1999].

$$R_{syst} = R_1 \times R_2 \times ... \times R_n = \prod_{i=1}^{n} R_i \qquad (5.2)$$

5.2   Results and discussion

Before going into the detailed subsystems reliabilities, the spacecraft overall reliabilities were calculated (these consider also failures unknown or related to the payload).
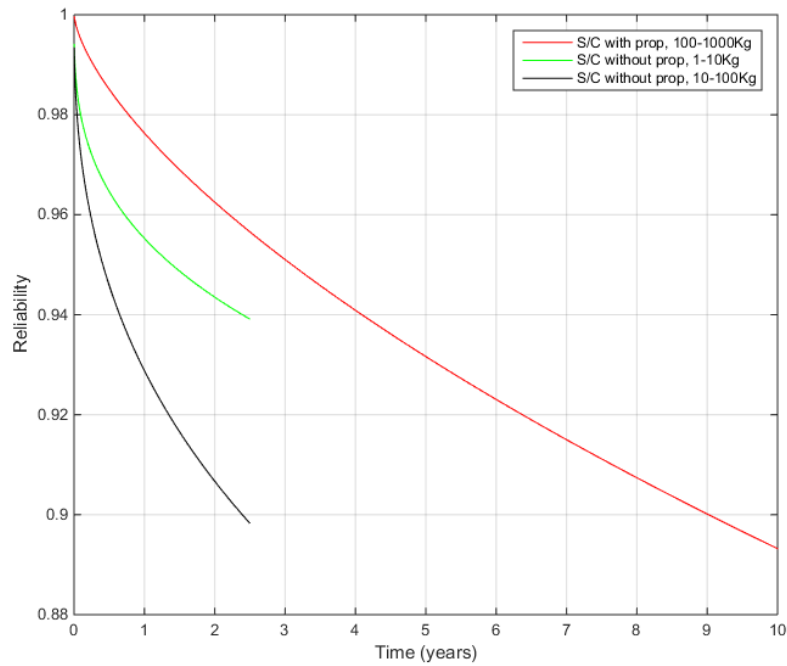
Figure 5.4: Weibull reliabilities comparison for S/C by mass classes, the different time scale to simulate the Weibull distributions is derived from a sample of re-entered spacecraft (with or without propulsion subsystem).

In Fig. 5.4 it is interesting to see the stronger infant mortality for smaller space-

111

craft without propulsion, as expected.

As can be seen, spacecraft without propulsion have a trend that stops at 2.5 years, while the bigger ones with propulsion it stops at 10 years. The time scale selected for the Weibull distributions have been in fact calculated by M. Peroni [Peroni and Kingston, 2015] from a sample of re-entered spacecraft (177 in total) in the period 2000-2014 considering the third quartile (i.e. the 75th percentile) and the standard deviation of their lifetimes (separating data into S/C with propulsion 67 and S/C without it 110).

The different timespans allow taking into account the design life of the missions and so the reliability performances. The same time scale is then used for the subsystems reliabilities.

5.2.1   Subsystems reliabilities

In this section the Weibull reliabilities for the different subsystems and mass classes obtained by means of the statistical analysis are presented.

It is relevant to note that the reliabilities calculated do not take into account human factors and design errors but simply the anomaly or part/component failure which cause the spacecraft subsystem (Class II) or mission (Class I) to fail. The failures can be due to moving parts, solid-state electronics, or other components, in a number of different subsystems; in this way the inherent reliability is related to the technology type. However, it must be noted that it is the end result that is critical, for instance if the AOCS fails it is not important if it failed due to a mechanism or other, it still cannot be used for the de-orbit.

When analysing a spacecraft subsystem (e.g.: ATT) it is relevant to note that the Class II event considered is only the failure event of that specific subsystem,

Table 5.4: Weibull fit parameters extrapolated by MATLAB.

Subsystem	Mass class [*kg*]	θ [*days*]	β [-]
Spacecraft	No propulsion 1-10	2.7441×10^6	0.3456
	No propulsion 10-100	2.1781×10^5	0.4077
	Propulsion 100-1000	9.3126×10^4	0.6733
ATT	No propulsion 1-10	/	/
	No propulsion 10-100	/	/
	Propulsion 100-1000	1.5427×10^6	0.3480
MECH	No propulsion 1-10	7.6463×10^7	0.2999
	No propulsion 10-100	/	/
	Propulsion 100-1000	2.0766×10^{10}	0.2072
TTC	No propulsion 1-10	1.1193×10^{10}	0.2458
	No propulsion 10-100	7.9801×10^5	0.5017
	Propulsion 100-1000	5.4928×10^5	0.5353
POW	No propulsion 1-10	1.2799×10^6	0.4112
	No propulsion 10-100	8.8481×10^5	0.4548
	Propulsion 100-1000	6.3973×10^4	0.9846

while the Class I (failure of the S/C depending on any subsystem) is always taken into account. Fig 5.5 show a graphical representation of what was just described.

As can be seen some mass classes are missing (e.g.: S/C without propulsion with mass > 100 kg), this is due to the lack of relevant data for that class.

The attitude subsystem for spacecraft with propulsion and mass class 100-1000 kg is the only one obtained for the different groups analysed. Although a comparison is not possible, it is interesting to look at the reliability decrease, which is below 90% just after 6 years of lifetime (Fig. 5.6). This is relevant to consider when the disposal reliability threshold is calculated as it requires to maintain a probability of 0.9 for a successful disposal [ESA SDM WG, 2015]. For this reason if the de-orbit strategy selected needs the attitude subsystem to work at the time of disposal it is better to have a reliability far above the 90% as this is going to be combined with other probabilities (e.g.: reliability of the de-orbit strategy itself, probability
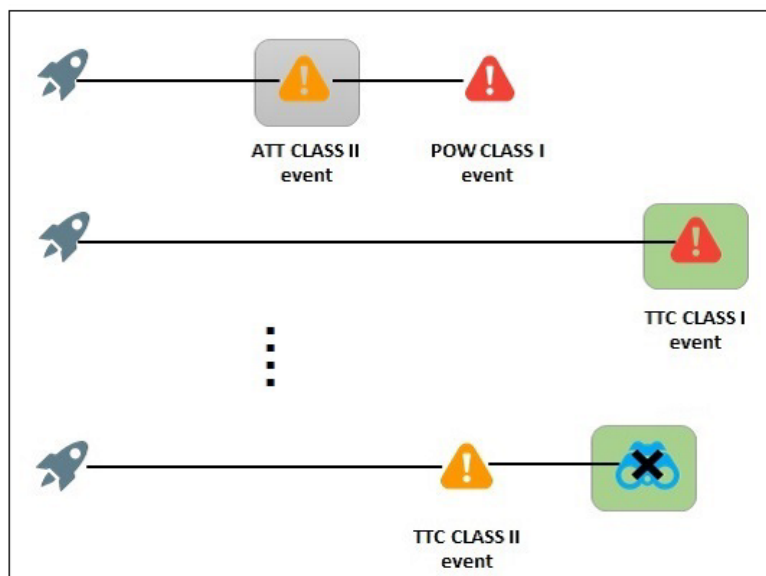
Figure 5.5: Example scenario of failure analysis of S/C subsystem. In this case analysis for ATT (Courtesy of M. Peroni).
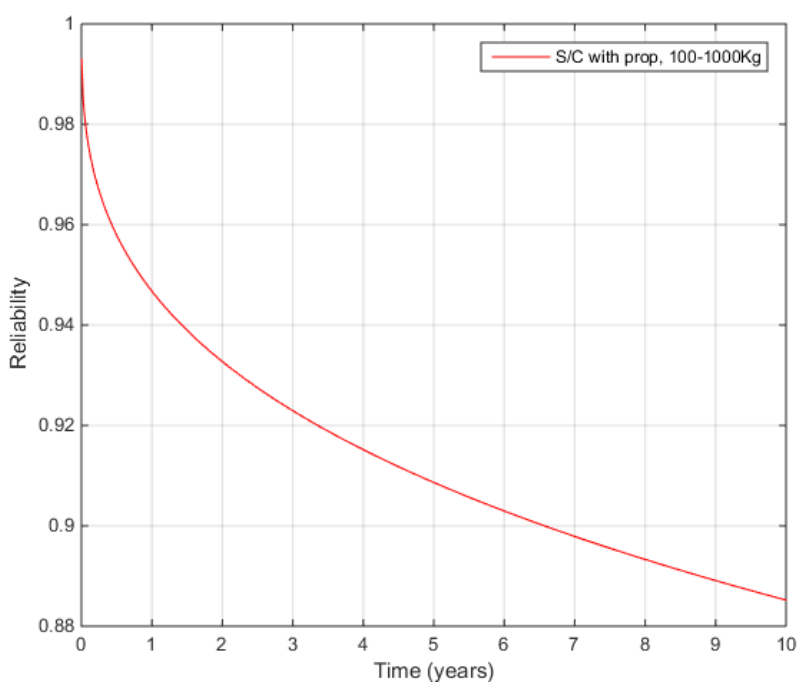
Figure 5.6: Weibull reliability for Attitude subsystem (ATT) of S/C with propulsion.
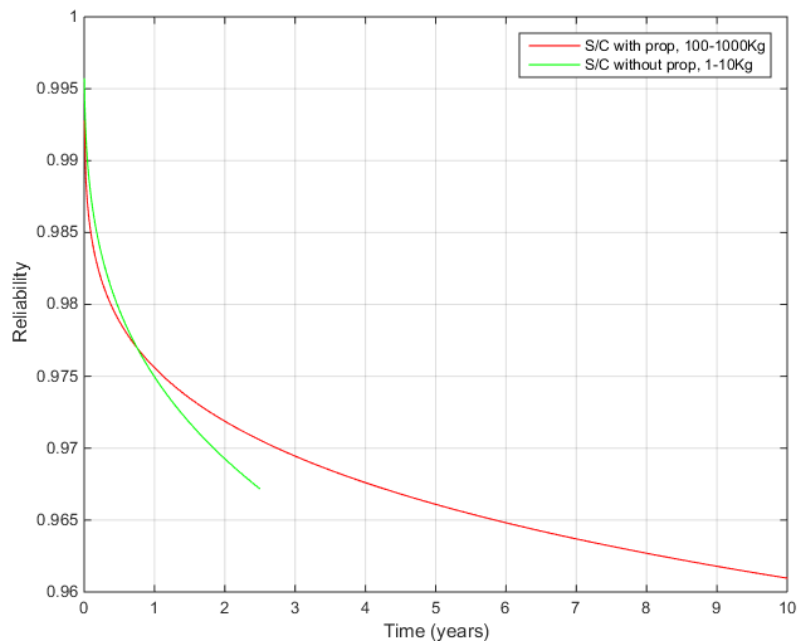
Figure 5.7: Weibull reliabilities comparison for Mechanisms subsystem (MECH) by mass classes.

of achieving the disposal, etc.).

In the case of mechanism and thermal subsystem (Fig. 5.7) the trends are always above 96% for the time scale considered.

TTC and POW subsystems (see Figs. 5.8 and 5.9) seem to have higher reliability compared to the ATT subsystem for spacecraft with propulsion. Spacecraft not equipped with propulsion have reliability above 95% for the time scale considered, with TTC more reliable than the POW. From the POW trends it is clear that bigger spacecraft with more redundancy and higher budget availability have more reliable Power subsystems, however the failure rate has a constant decreasing rate.

Both TTC and POW subsystems are crucial for the accomplishment of a space mission, and they are for the EoM disposal as well, because the capability of achieving the disposal by the de-orbit strategy is strongly dependent on them.
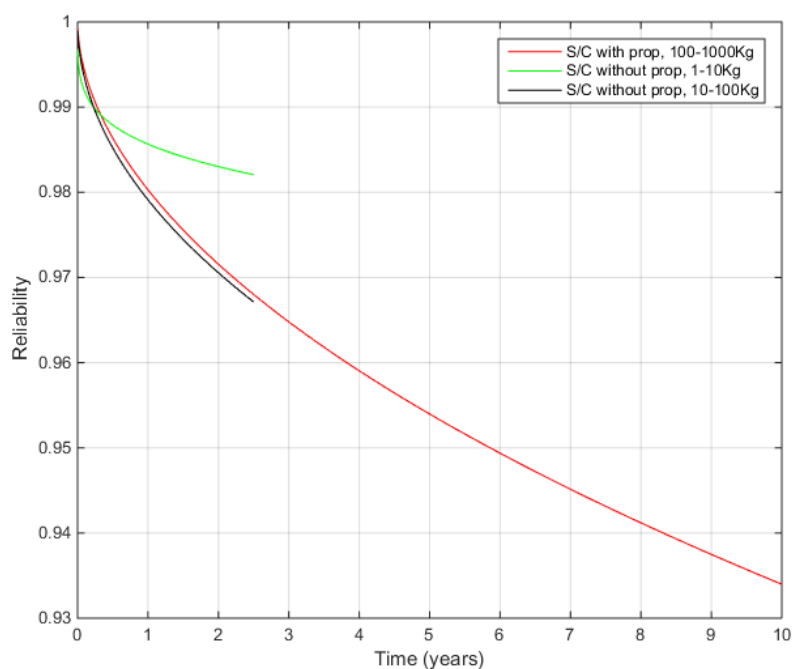
Figure 5.8: Weibull reliabilities comparison for TT&C subsystem (TTC) by mass classes.

5.2.2 Combined reliabilities

As mentioned in the methodology section the different combinations are subsystems in series. The combinations evaluated and the de-orbit strategies considered are the ones presented in Fig. 5.3.

In particular it is interesting to look at the difference in the trends when adding in series the ATT subsystem with respect to the case of TTC & POW combination only (see Fig. 5.10). This suggests to select a different de-orbit strategy than the propulsive de-orbit, in particular in the case of long missions. An option could be the drag-augmentation devices, which need only power supply and TT&C to operate.

The passive drag device seems definitely a good solution for S/C without propulsion, if just the reliability trends are considered (see Fig. 5.10). The combined reli-
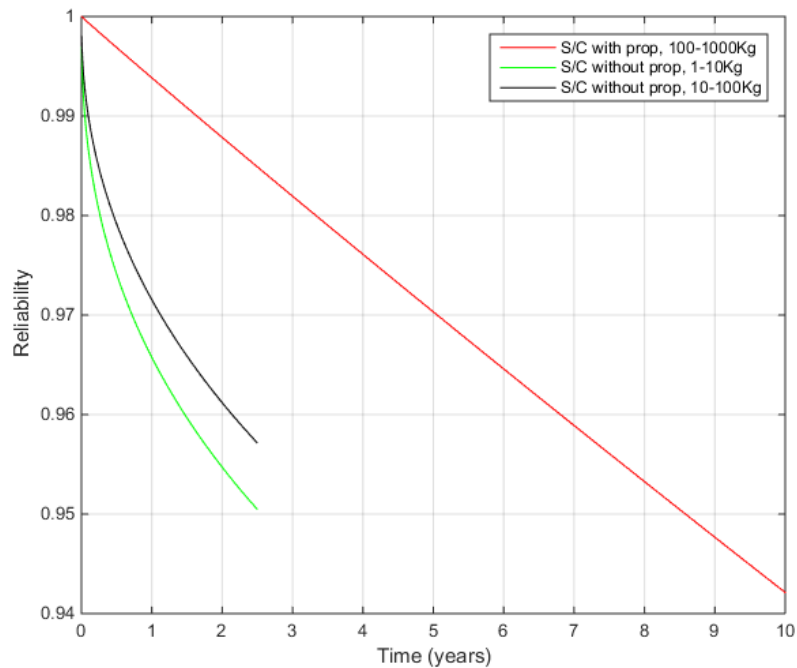
Figure 5.9: Weibull reliabilities comparison for Power subsystem (POW) by mass classes.

ability of the subsystems (TTC & POW) required for this strategy is always above 92% for the selected time scale and in general above 90% up to 7 years.

The trends presented in Fig. 5.11 are useful when evaluating the D-Orbit[TM] propulsive device, as mentioned before this strategy needs only the power line from the spacecraft host to charge its own batteries.

Clearly shorter mission duration is likely to lead to a higher reliability for a given set of spacecraft equipment, due to the decreasing reliability over time. An aim of this work is to inform decisions about suitable choice of de-orbit approach, and also appropriate timing of the end of a mission.
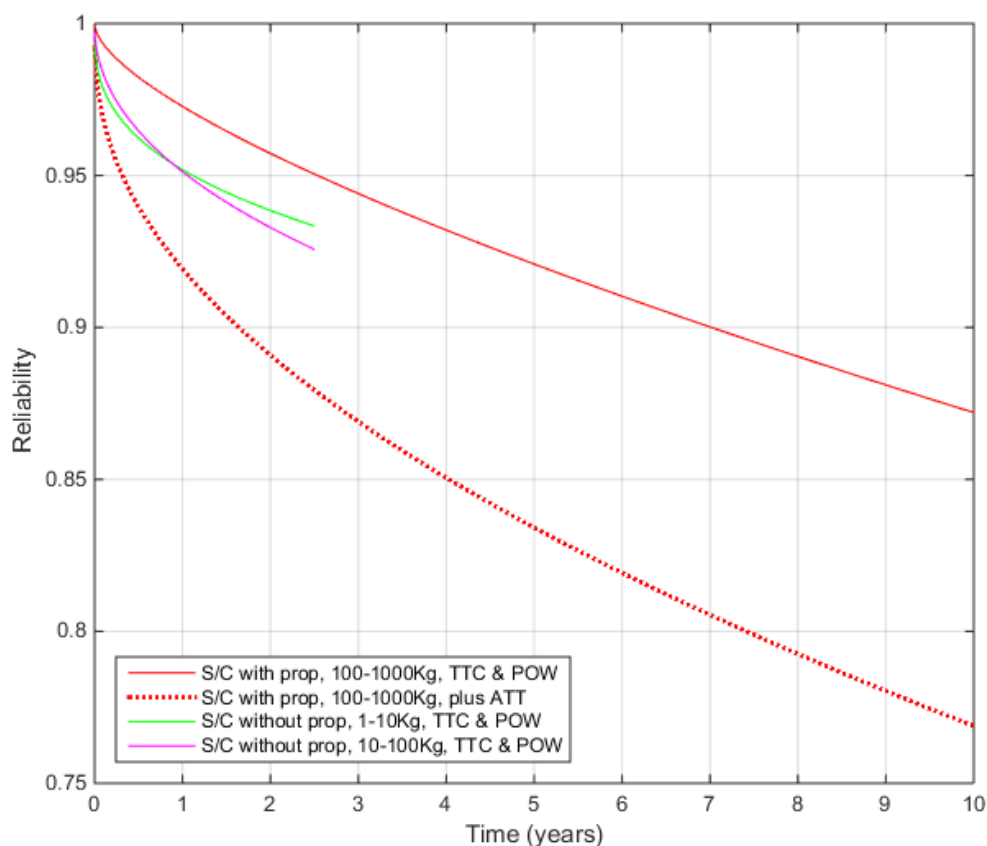
Figure 5.10: Weibull combined reliabilities TTC & POW & ATT vs. TTC & POW by mass classes. These trends are useful for the drag-augmentation device.

5.2.3 Trade-off analysis

Deciding which type of de-orbit strategy can fit with a specific LEO mission is a complicated matter, with many variables to take into account. For this reason a trade-off analysis was performed.

The reliability of the subsystems is indeed not the only factor to consider for the de-orbit strategy selection. Aspects related to the technology of the disposal strategy (e.g.: TRL, physical properties, reliability of the disposal method itself), the mission (e.g.: orbit parameters, duration), and the spacecraft need to be considered.
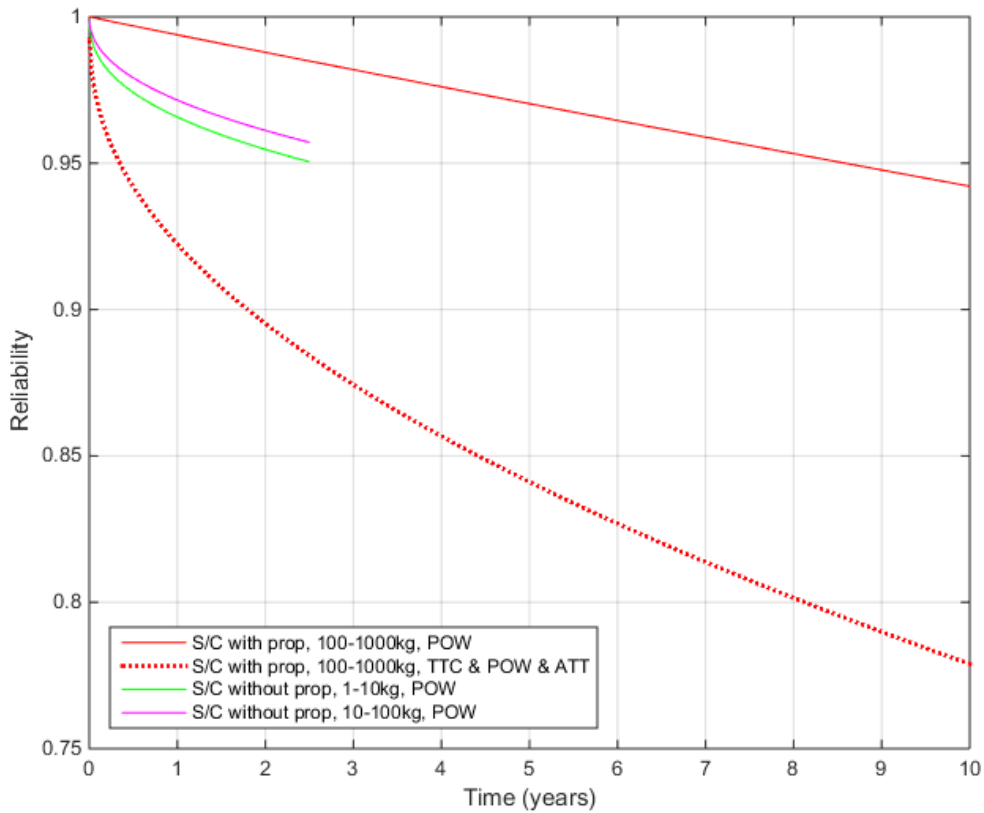
Figure 5.11: Weibull combined reliabilities TTC & POW & ATT vs. POW only by mass classes. These trends are useful for the D-Orbit$^{\text{TM}}$ propulsive device.

The aim of this work is to assess the impact of subsystem reliabilities on the function of different de-orbit methods. Clearly the reliability and safety of the de-orbit methods themselves are also of great importance in achieving an effective de-orbit solution, however the assessment of these reliabilities is outside the scope of this work.

In this analysis the focus is on the application and integration of the de-orbit strategy with respect to the spacecraft host.

The orbit altitude is not considered, the assumption is an altitude where all the de-orbit strategies can be used. However, it must be clear that some de-orbit

119

technologies are only effective below certain orbit altitudes (e.g.: drag augmentation concepts) or at specific inclination (e.g.: electric tether).

For each disposal strategy (see section 5.1.3) the trade-off parameters are:

- Feasibility: about the implementation and integration of the de-orbit strategy with the host spacecraft (5 = very easily);

- Mass: incidence of the de-orbit strategy mass to the spacecraft mass (5 = no incidence);

- TRL: in space missions and tests (5 = good heritage equivalent to TRL 8/9).

In addition the combined reliabilities relevant for each strategy at three time periods (2.5, 5, and 10 years) were included.

The minimum value, which is 0, has been assigned to the lowest combined reliability detected (77% for the TTC & POW & ATT for S/C with propulsion in the 100-1000 kg mass class at 10 years); the maximum value, which is 5, to the highest reliability observed (98% POW for S/C with propulsion in 100-1000 kg mass class at 2.5 years), see Table 5.5.

Table 5.5: Trade-off table for decision making in the selection of the de-orbit strategy by S/C classes.

Class	De-orbit strategy	Feasib.	Mass	TRL	$R(t)$ at 2.5 y	TOT	$R(t)$ at 5 y	TOT	$R(t)$ at 10 y	TOT
Prop 100-1000 kg	Propulsive	5	4	5	2.6	**16.6**	1.4	**15.4**	0	**14**
	Electr. tether	2	3	2.5	4.3	**11.8**	3.6	**11.1**	2.4	**9.9**
	Film aerobrake	4	3	4	4.3	**15.3**	3.6	**14.6**	2.4	**13.4**
	Inflatable env.	2	4	1.5	4.3	**11.8**	3.6	**11.1**	2.4	**9.9**
	Prop. D-Orbit	5	2	3	5	**15**	4.8	**14.8**	4	**14**
No prop 1-10 kg	Electr. tether	2.5	3	2.5	3.8	**11.8**				
	Film aerobrake	4	3	4	3.8	**14.8**				
	Inflatable env.	1	2	1.5	3.8	**8.3**				
No prop 10-100 kg	Electr. tether	3.5	4	2.5	3.6	**13.6**				
	Film aerobrake	4	4	4	3.6	**15.6**				
	Inflatable env.	3	3	1.5	3.6	**11.1**				
	Prop. D-Orbit	4	3	3	4.5	**14.5**				

The trade-off is aimed at LEO spacecraft but uses the overall reliability data derived previously, which includes MEO spacecraft as discussed before in section 5.1.1.

Considering the main purpose of this analysis, the parameters are selected to be the most relevant for evaluating suitability for integration with the spacecraft host.

For bigger spacecraft with propulsion the conventional de-orbit propulsive method seems still the best solution; however the trade-off results show a drop over time for this strategy. In fact despite the high ranking of the parameters not related with the reliability, a crucial result of the study is that the attitude subsystem reliability decreases the final result over time. As can be seen it is then worthy consider the D-Orbit$^{\text{TM}}$ propulsive device as a good alternative, in particular for long missions, provided an appropriate reliability of such a device can be demonstrated. Indeed, the TRL parameter for this disposal device was set lower than other methods because of the current status of the technology.

The drag-augmentation device, in particular the boom supported film aerobrake, provides the best solution for nano and microsatellites without propulsion, with good values as well for spacecraft with propulsion.

5.3 Summary

The results obtained can guide the identification of the activation procedure for a de-orbit strategy and the level of integration it should have with the host satellite in order to be activated before a total failure or before the failure of the subsystems necessary for its operation.

The reliability analyses accomplished give a more detailed insight into the LEO satellites compared to the work performed by Saleh and Castet. The purpose is in

fact to guide the selection of the de-orbit strategy.

Spacecraft equipped with a propulsion subsystem show a higher reliability than the ones without; however the attitude subsystem has the worst reliability and this is particularly relevant for the selection of the disposal method. On the other hand the power subsystem seems very reliable for the class 100-1000 kg with propulsion, but for smaller satellites without propulsion instead it is the worst.

The reliabilities calculated take into account the anomaly or part/component failure which causes the subsystem to fail, on the other hand human factors and system engineering design errors are not included. However, some might be included in the unknown failures used to calculate the overall spacecraft reliability.

After the reliabilities were combined in series and system design parameters were added, a trade-off analysis was performed. From the study two de-orbit strategies emerged as alternatives to the well-known propulsive de-orbit: drag-augmentation device for nano and microsatellites; D-Orbit$^{\text{TM}}$ propulsive device as good alternative for bigger satellites with propulsion.

The focus was on the assessment of the impact of spacecraft subsystems on the different de-orbit methods, then the strategy selection is left to the satellite's owner, who must consider the reliability and safety of the de-orbit method itself.

In addition, it is worth noting the need of a constant monitoring and data sharing using a common format for failures attribution at international level. This would improve the knowledge of satellites reliability especially for organizations that are ready to launch many micro and nanosatellites.

Chapter 6

Future Applicability of Drag Augmentation Systems

This chapter is derived from the IAC 2016 conference paper *Applicability of drag augmentation systems to enable future LEO spacecraft compliance with debris mitigation guidelines* [Palla and Kingston, 2016a]. The starting point are the results of expected non-compliance obtained in the market forecast analysis presented in Chapter 4.

This part of the research investigates the additional drag area required for the sample of expected non-compliant spacecraft to be launched in LEO, in order to review the applicability of the DAS baseline design.

First, the decay model used, its validation with orbital decay analysis tools, and the spacecraft sample analysed are presented. This is followed by the investigation to verify if the satellites of the sample would achieve the compliance with the additional drag area provided by the Cranfield DAS with their current design.

6.1   Methodology

In this study the sample is composed of LEO spacecraft with launch date between 2015-2020, which are not expected to be compliant with the 25 years ESA re-entry requirement [ESA SDM WG, 2015]. As mentioned before, the sample was derived from the previous work performed on market forecast and future scenarios.

In order to investigate the cross sectional drag area required to be compliant, the first step was the satellite decay model selection, followed by the calculation of the ballistic coefficient and the mass-to-area ratio required at different altitudes (range from 500 to 850 km).

The second step undertaken was the validation of the simplified model. This was performed with the software adopted for verifying the compliance with mitigation guidelines [IADC, 2007] or regulations [Lazare, 2013]: STELA, designed by CNES [CNES, 2013] and DRAMA [ESA, 2014b], in particular the tool OSCAR, developed by ESA Space Debris Office.

For this purpose a suitable test case was selected and the variations with different starting dates were analysed. The additional area, needed to achieve a re-entry in less than 25 years, was then evaluated for the sample of future non-compliant spacecraft.

In parallel the drag areas achievable with the current DAS design (Icarus, DOM) for the different satellites were calculated. Finally the two drag areas (the S/C area only, the S/C with the DAS design applied) were compared.

6.1.1   Simplified decay model and BC calculation

The model for the satellite lifetimes calculation is a simplified decay model for circular orbits. The atmospheric scale height and average density values, function of the constant solar flux, were extracted from the tables in the new SMAD [Wertz

et al., 2011]. Two cases were considered: solar mean and solar minimum. The density and scale height were calculated with linear interpolation for the different altitudes from the reference values.

If the satellite's lifetime is imposed at 25 years after the EoM, the ballistic coefficient required for the specific orbit altitude can be obtained (see Fig. 6.1). This is the upper limit to achieve a compliant re-entry time due to the action of natural perturbations. Indeed, as described in [Dolado-Perez and Revelin, 2015], most of the LEO objects achieved the compliance exactly because of the natural decay.

$$L = 25 years = \frac{-H}{\Delta a} \tag{6.1}$$

H is the scale height, which is fixed for different altitudes and dependent on those; Δa represents the approximate rate of change in semi-major axis:

$$\Delta a = \frac{-H}{L} = -2\pi \frac{\rho \, r^2}{BC} \frac{1}{P} \tag{6.2}$$

where r is the orbit radius and P is the orbit period. Having obtained Δa, the BC[3] can be calculated.

$$BC = \frac{m}{A \, C_D} \tag{6.3}$$

The drag coefficient C_D was considered fixed and with a value of 2.2. In this way the mass-to-area ratio is known. The drag coefficient is roughly bounded between 2 and 4 [Vallado and Finkleman, 2014], the value selected represents the average in case of spherical surface. C_D is definitely a source of uncertainty and the area itself varies during the decay, however the aim is to obtain a reference value.

In addition in our case the major effect on the decay time is produced by the

---

[3]Note that sometimes the ballistic coefficient is defined as $C_D A / m$
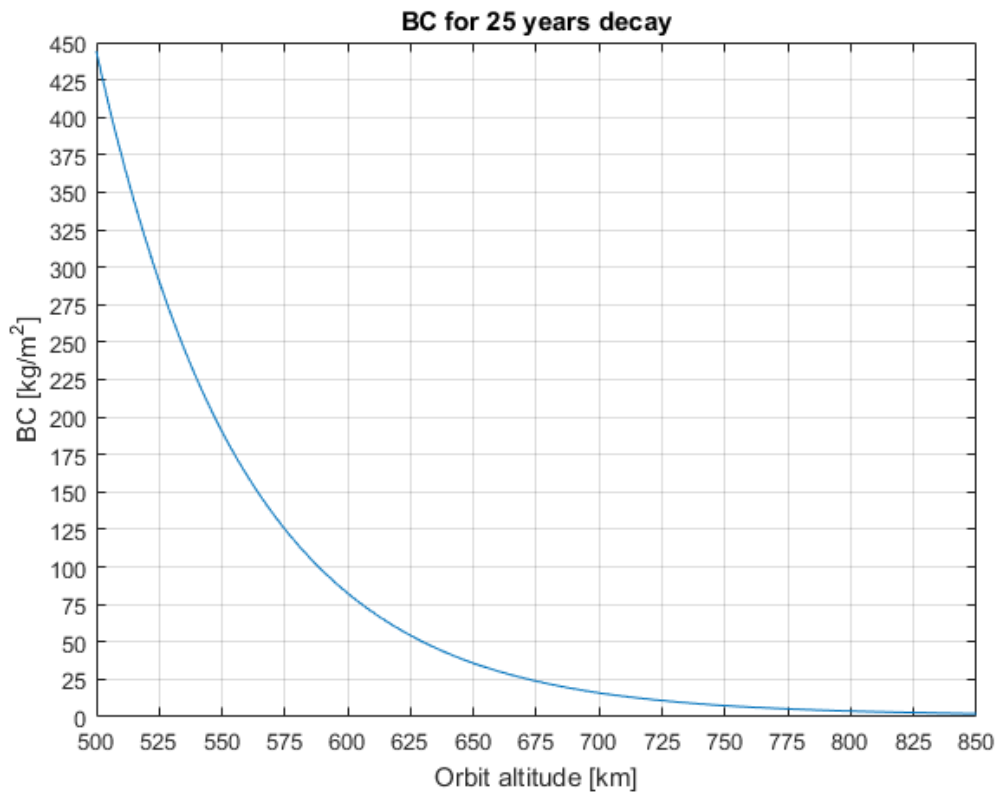
Figure 6.1:   Ballistic coefficient limit at different altitudes to achieve a 25 year re-entry in solar mean conditions.

solar flux variation predictions, as confirmed in [Vallado and Finkleman, 2014].

6.1.2   Model evaluation with test case

The simplified decay model was validated with a test case both in STELA and DRAMA orbital decay simulation tools. STELA and DRAMA were chosen because they were specifically developed by CNES and ESA, respectively, for verifying the space debris mitigation requirements. The main purposes of this analysis were:

- the evaluation of the BC [kg/m^2] limit at 25 years,

- the differences between the simplified model and the models in STELA and

DRAMA,

- the variations with different starting point (dates) for the decay during the solar cycle.

The orbit selected for the test case was a sun-synchronous orbit with altitude of 650 km, the object characteristics are presented in Table 6.1. The mass selected was 100 kg, fitting with the target S/C of the DAS, and the drag area was calculated to keep the same mass-to-area ratio for 25 year decay, as the simplified model with solar mean.

Table 6.1:   Spacecraft object characteristics, used as input for STELA and DRAMA simulations.

Parameter	
Mass (kg)	100
Reflectivity area (m^2)	1.2739
Reflectivity coefficient	1.5
Drag Area (m^2)	1.2739
Drag coefficient	2.2
m/A (kg/m^2)	78.5

The lifetime values that we expected to find in the STELA and DRAMA simulations were close to the 25 years as in the simplified model.

In the case of solar minimum, which affects the atmospheric scale height and the density, the m/A value obtained with the simple model at 650 km of altitude is instead 10.4 kg/m^2. If we consider the same re-entry time limit of 25 years and the same S/C mass, the resulting cross sectional area is then much larger. In this case the lifetime values expected to be found in STELA and DRAMA were much lower than the 25 years, because this m/A represents the worst case scenario, i.e. a drag area much larger than the real need.

6.1.2.1 STELA analysis

The simulations performed with STELA software were set with the input parameters mentioned before (orbit parameters and object characteristics) and the default for the advanced parameters [CNES, 2013]. The input for the solar activity was the variable solar cycle (input file included in the STELA package), which are past measurements (from 1956) and future mean prediction given by NOAA and NASA, up to year 2318.

Five cases were considered:

1) Start date at solar maximum;

2) Start date at solar mean (decreasing trend);

3) Start date at solar minimum;

4) Start date at solar mean (increasing trend);

5) Mean solar flux SFU constant $= 140$ $[10^{-22}W/m^2/Hz]$, geomagnetic index Ap $= 15$, this is the only case where the solar activity input is fixed.

Apart from Case 5), the only variation is the starting date for the decay. The date set for the Case 1) is 01/12/2022, the other dates follow corresponding to the solar flux condition desired.

When applied the solar minimum input the constant flux is set SFU $= 75$ $[10^{-22}W/m^2/Hz]$ and Ap $= 8$, as considered in [Wertz et al., 2011].

6.1.2.2 DRAMA analysis

The simulations with DRAMA were performed with the tool OSCAR, which allows to analyse the orbital decay of a spacecraft after the EoM with different disposal

strategies. The input for the orbit parameters and spacecraft object characteristics (see Table 6.1) were the same used for STELA simulations.

Here the focus was on the variations of decay time using different solar and geomagnetic activity forecast. The following cases were simulated:

1) Start date at solar maximum, solar forecast: latest prediction, recommended in [BSI Standards Publication, 2011b] with 25% confidence interval for best and worst cases;

1B) Start date at solar maximum, solar forecast: ECSS sample solar cycle, recommended in the ECSS standard [ECSS Secretariat, 2008];

1C) Start date at solar maximum, solar forecast: Monte Carlo method [BSI Standards Publication, 2011b] with samples from 5 cycles as recommended by the SDM Handbook [ESA SDM WG, 2015];

4) Start date at solar mean (increasing trend), solar forecast: latest prediction;

5) Mean solar flux SFU constant $= 140$ $[10^{-22}W/m^2/Hz]$, same conditions as STELA Case 5)

In the case of solar minimum input area, to achieve the 25 years re-entry, the same simulations have been run to compare them with the STELA results. In Case 5) the SFU index is equal to 75 $[10^{-22}W/m^2/Hz]$.

6.1.3   Non-compliant spacecraft sample

The sample is composed by LEO spacecraft with mass lower than 1000 kg and launch date between 2015-2020, the last update on the dataset was in November 2015. Larger satellites classes are out of the purpose of this work. The data were derived

from the results obtained in the market forecast analysis presented in Chapter 4, the rough data were previously extracted from Spacetrak^{TM} database [Seradata, 2014].

The spacecraft considered are not expected to be compliant with the 25 years requirement if no de-orbit strategy is applied after the EoM; basically their re-entry by natural decay exceeds the limit.
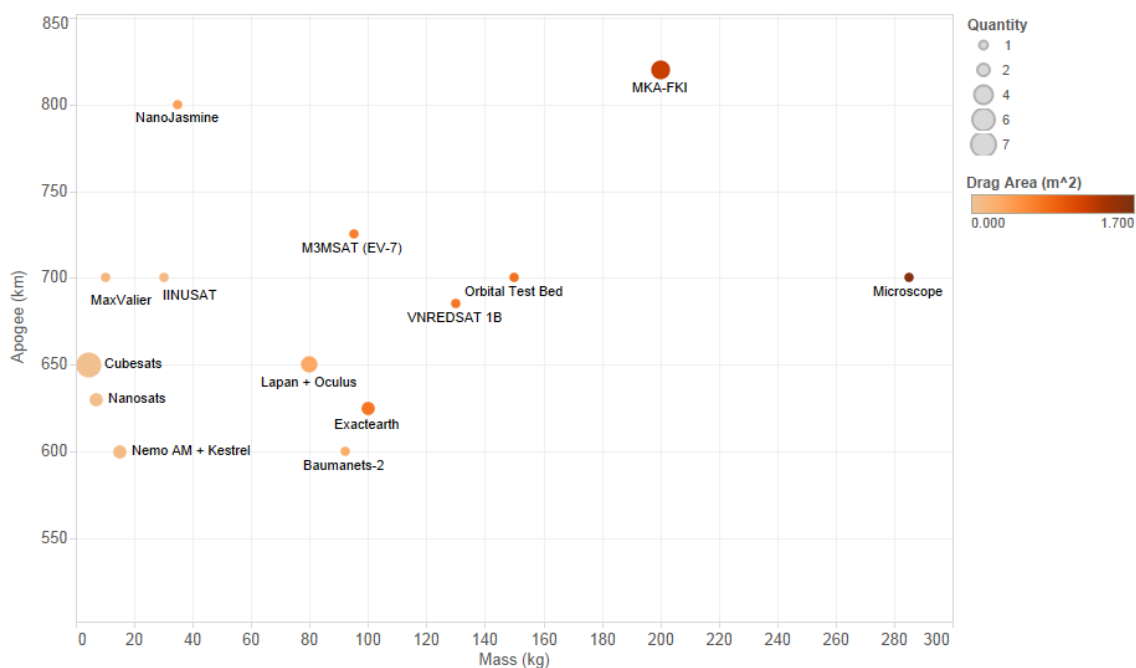
Figure 6.2: Distribution of expected non-compliant spacecraft without propulsion subsystem, assumes no de-orbit measures are adopted.

From the sample, there were 298 spacecraft with data retrievable for mass, planned orbit, and bus dimensions, of which 145 were the non-compliant ones. We then excluded 8 S/C because the planned orbit is above 850 km, which is out of the scope of the DAS. The parameters, just mentioned, were needed to calculate the m/A expected and the one needed to achieve the compliant re-entry for each spacecraft. In the sample there were 28 expected non-compliant spacecraft without propulsion (Fig. 6.2), while there were 109 equipped with propulsion subsystem (Fig. 6.3).
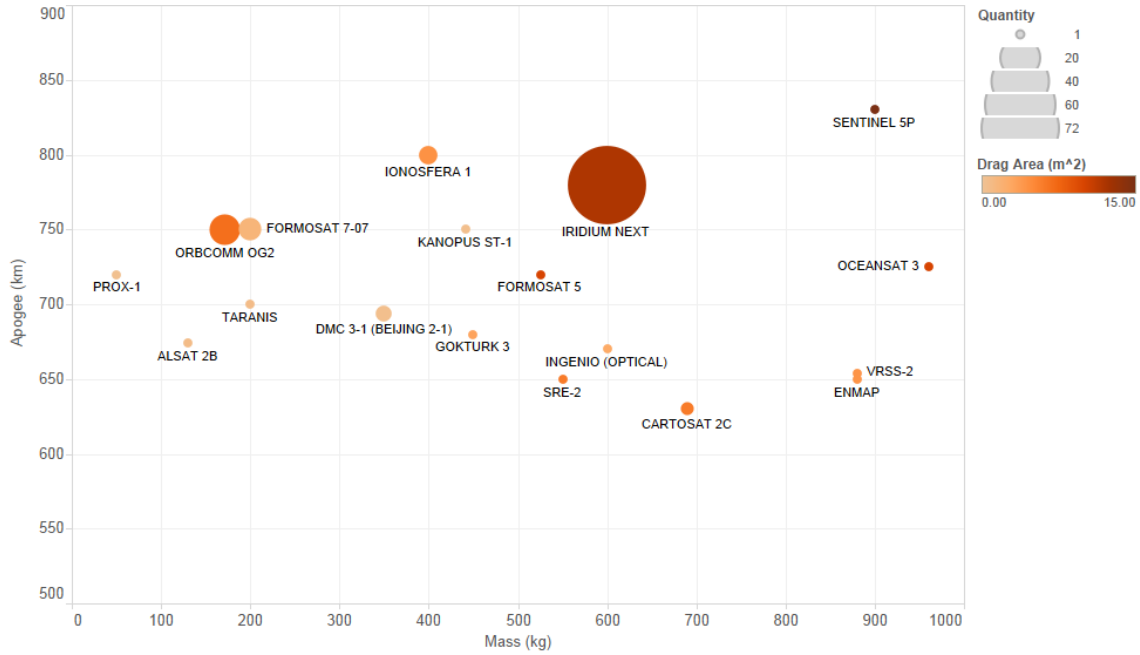
Figure 6.3: Distribution of expected non-compliant spacecraft equipped with propulsion subsystem, assumes no de-orbit measures are adopted. Note: the classes considered are below 1000 kg.

In Fig. 6.2, 6.3 the mass distribution of the spacecraft analysed with respect to the planned orbit altitude is presented. The size of the dot represents the number of spacecraft at the specific altitude and with the same mass, e.g.: the future constellation of IRIDIUM and the ORBCOMM S/C can be easily recognized by the reader. The variation of the colour is related to the value of the expected cross sectional drag area of the satellite, the darker the colour the larger the area.

6.2   Results and discussion

In this section we present the results of the simulations in STELA and DRAMA to validate the simplified decay model used to calculate the mass-to-area ratio needed to be compliant with the 25 years requirement, then we investigate and compare

the drag area that can be provided with the DAS designs to the non-compliant spacecraft sample.

6.2.1   Simulations results

The results obtained for the STELA and DRAMA simulations are here discussed. The focus is on the differences in orbital decay time varying the start date of de-orbit and selecting different solar flux models.

6.2.1.1   STELA results

In Table 6.2 the results obtained are presented. For the case of m/A input with Solar minimum condition, as expected, the years required for re-entry are much less than the simple model. In STELA in fact the solar cycle varies, except for the last case where the SFU and Ap have been imposed constant (see plots in Appendix C). In the case of Solar mean the results are consistent with the decay model for circular orbit. A variation in the decay time is detectable depending on the time of decay, this is less than one year among the cases with variable solar flux, less than two years with respect to the constant mean solar flux conditions.

Table 6.2:   STELA simulation results for test case with different starting point for decay during solar cycle.

STELA simulations	Case 1	Case 2	Case 3	Case 4	Case 5
Duration with Solar mean A/m input (years)	21.9	22.3	22.65	21.82	21.09
Duration with Solar min A/m input (years)	1.38	6.84	3.49	1.78	19.35
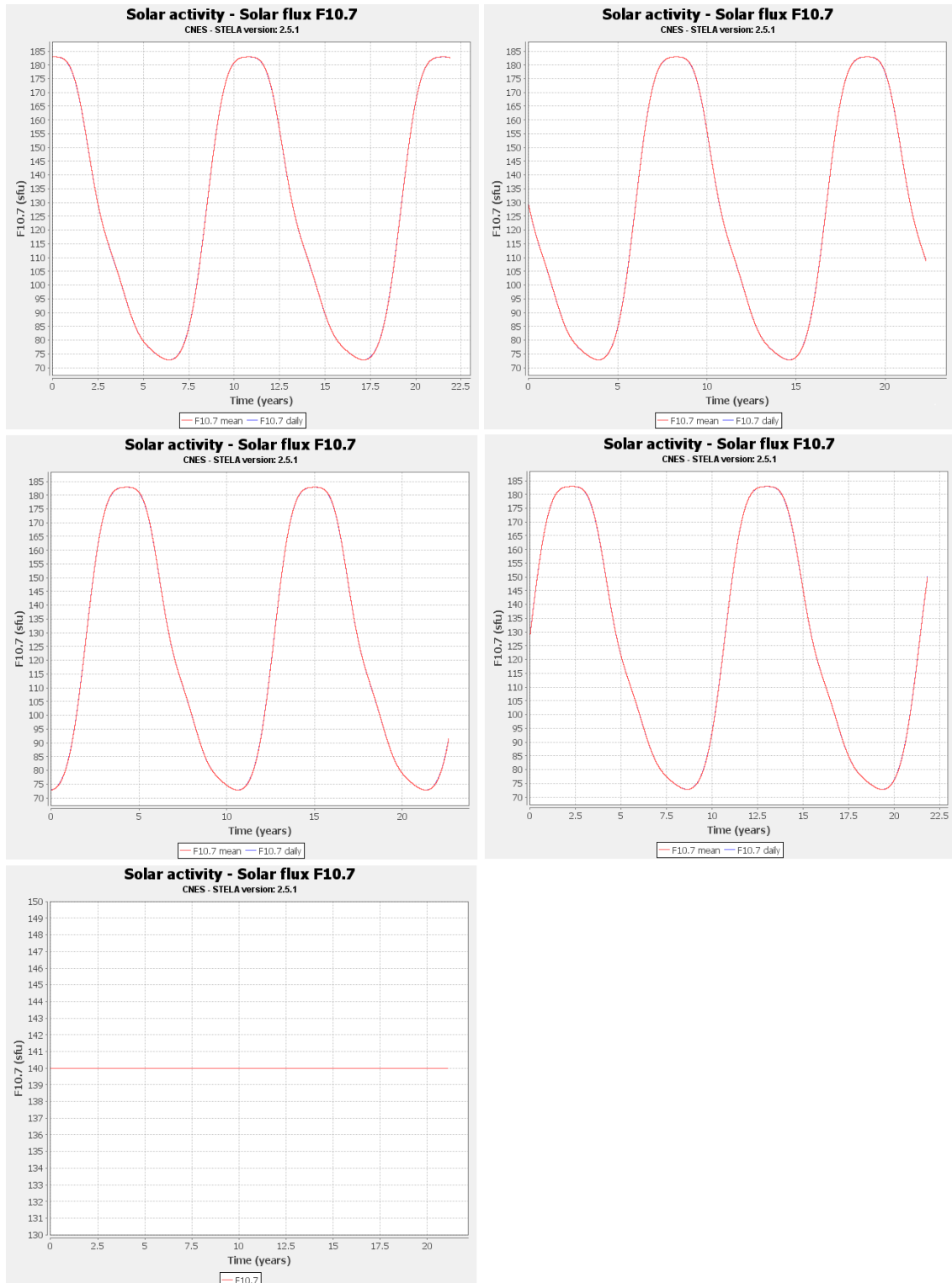
Figure 6.4: Solar activity fluxes for the 5 cases considered in STELA. In order from left to right, top to bottom.
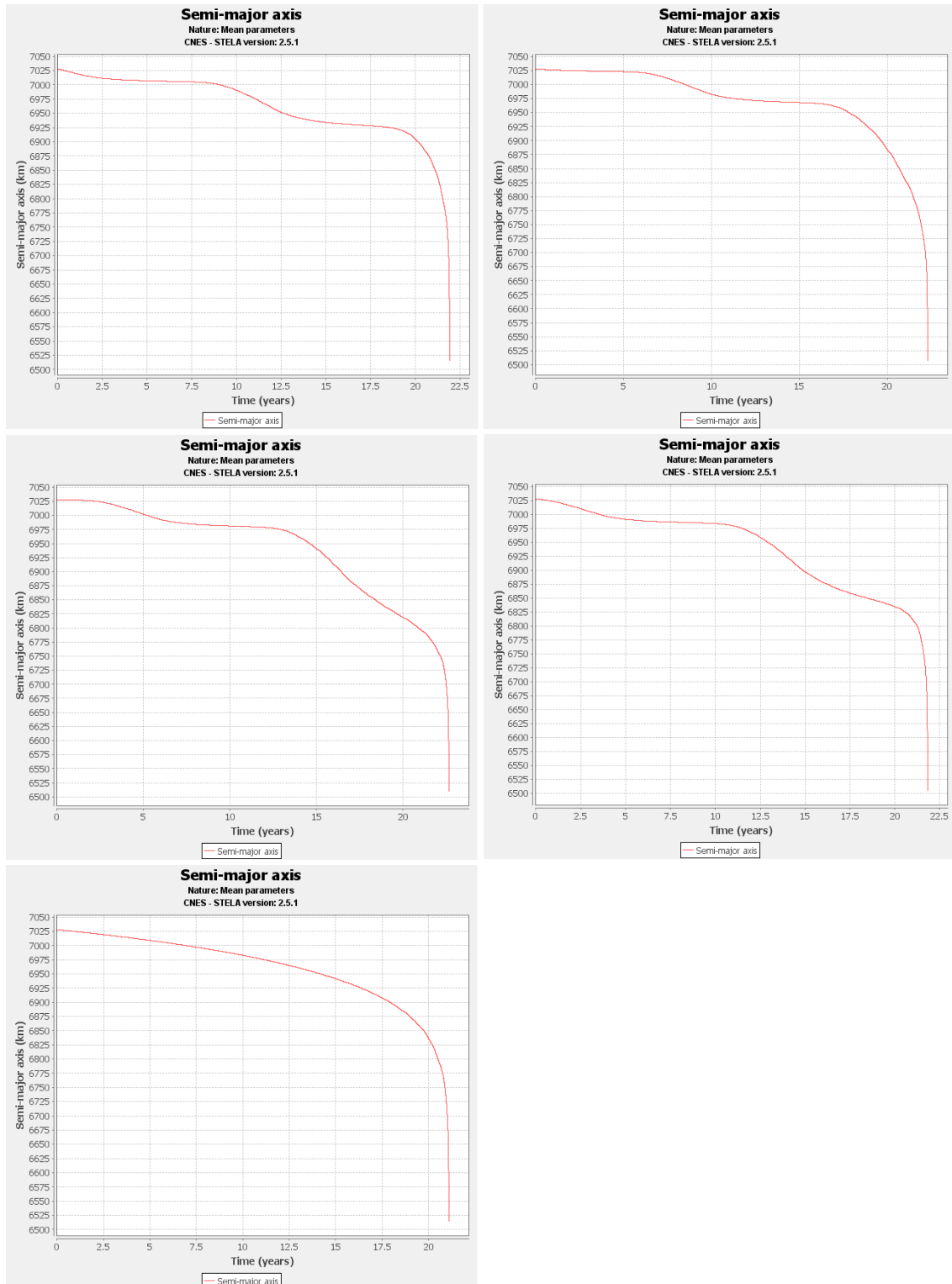
Figure 6.5: Semi-major axis vs. time for the 5 cases considered in STELA, object characteristics in Table 6.1. In order from left to right, top to bottom.

6.2.1.2   DRAMA results

In the STELA simulations (Table 6.2) can be seen that the difference in the results is less than two years (in solar mean conditions), for this reason here the focus was on the variations using different solar and geomagnetic activity forecast.

Table 6.3:   DRAMA simulation results for test case with different solar forecast models.

DRAMA simulations	Case 1	Case 1B	Case 1C	Case 4	Case 5
Duration with Solar mean 25 y A/m input (years)	34, 25 (best), 44 (worst)	22.2	16.83	34.99	21
Duration with Solar min 25 y A/m input (years)	2.8, 1.84 (best), 3.85 (worst)	1.49	1.18	2.92	18.21

With respect to the STELA simulations, which had the same solar activity prediction data, here the results vary and some of them exceed the allowed 25 years re-entry time (see Table 6.3). This happens with the latest prediction for the solar activity forecast in all the cases (nominal, best, worst). This model takes into account available up-to-date information on solar and geomagnetic activity provided by ESA, so this varies depending on the latest updates and would be more relevant for short-term predictions.
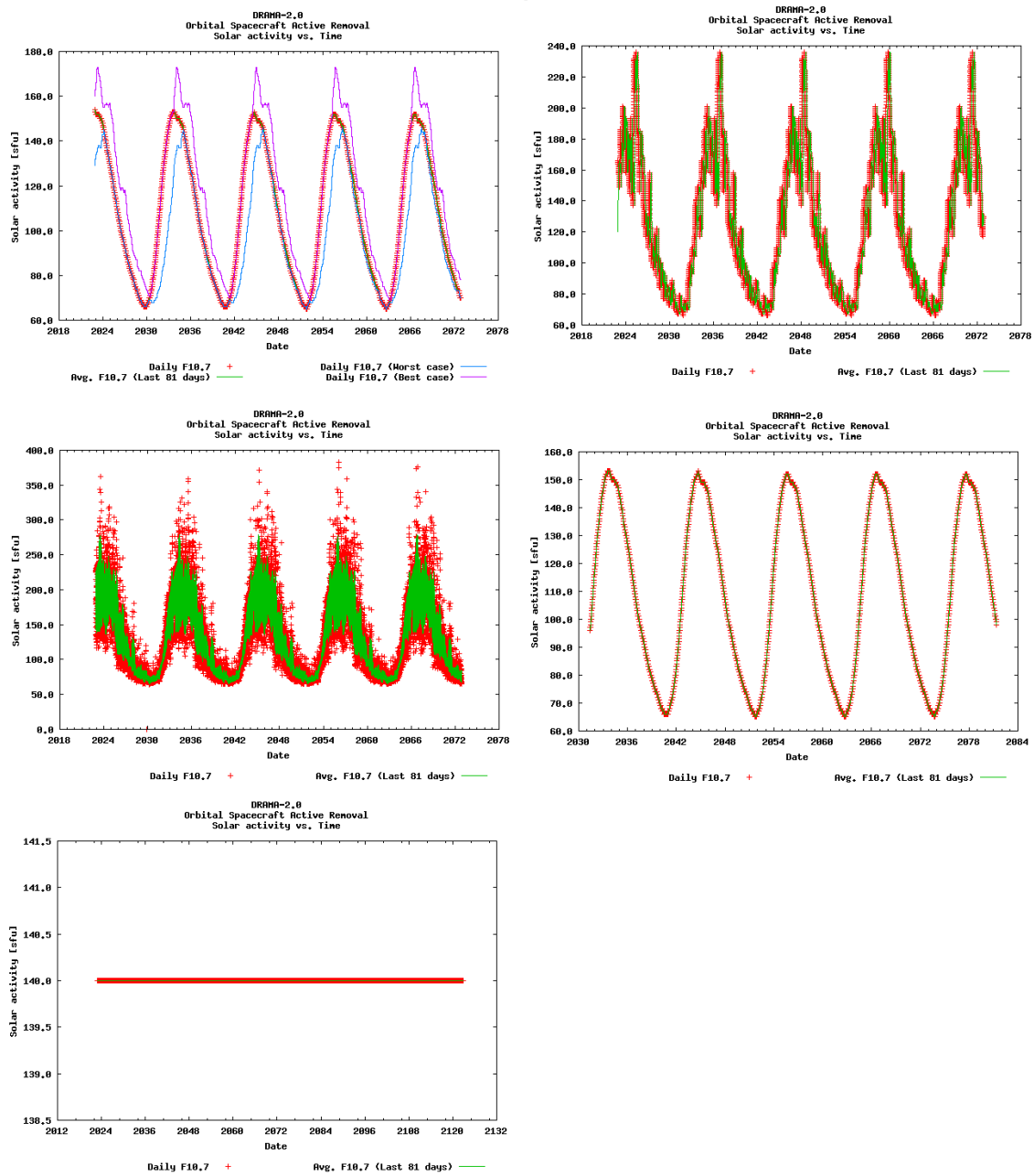
Figure 6.6: Solar activity fluxes for the 5 cases considered in DRAMA. In order from left to right, top to bottom.
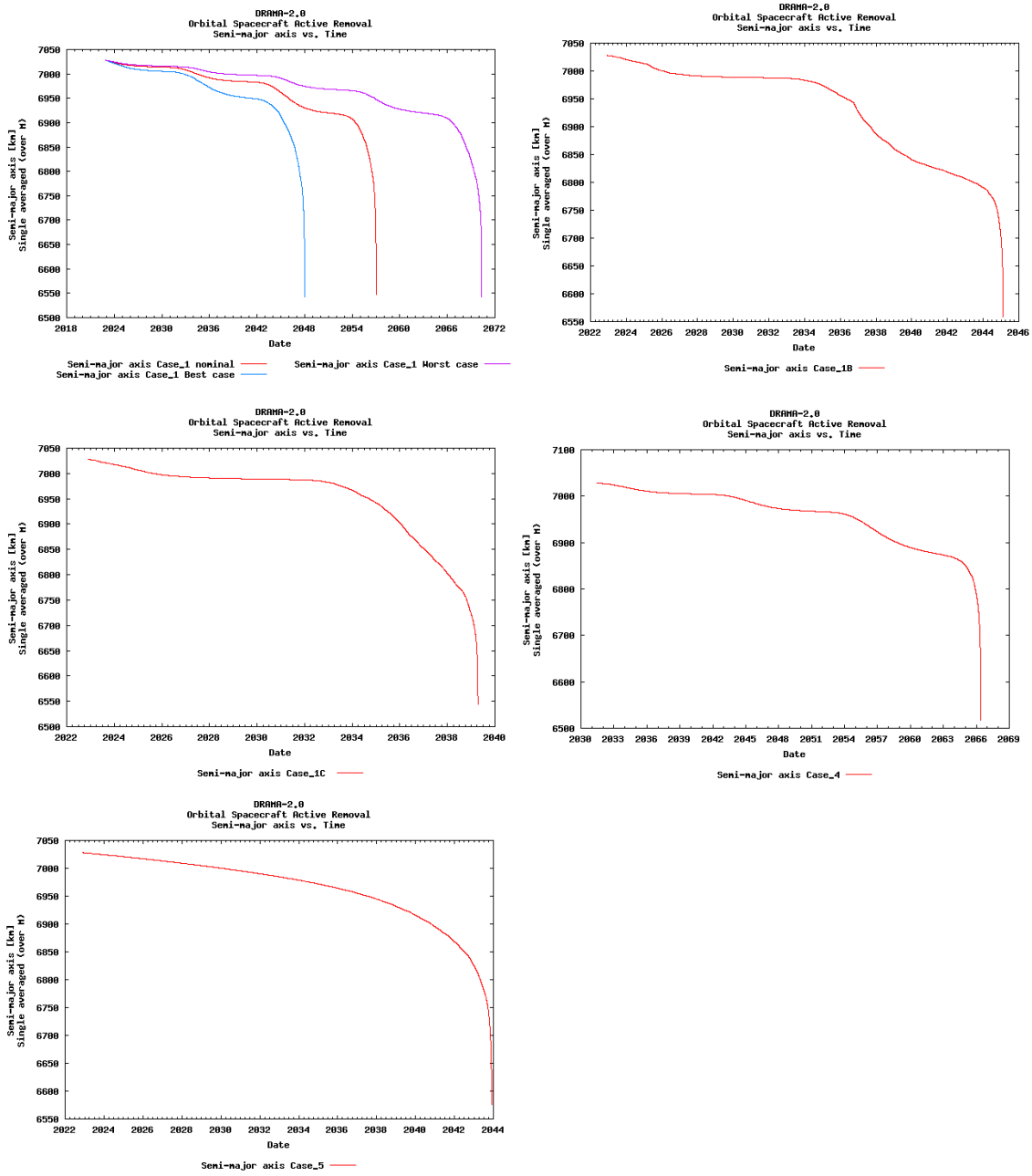
Figure 6.7: Semi-major axis vs. time for the 5 cases considered in DRAMA, object characteristics in Table 6.1. In order from left to right, top to bottom.

Since the aim is to use the simple model as a tool, later on it has been decided

137

to compute the BC and so the mass-to-area ratio limit at 22 years and then use this value in the simulations to have some margins. As the simple decay model makes use of equations fitted to pre-computed orbit lifetime estimation data, the margin suggested by the ISO on *Space systems - Estimation of orbit lifetime* [BSI Standards Publication, 2011b] is 10%. This has been applied and rounded to the 25 years limit (i.e.: 3 years).

The same cases have been run with the different mass-to-area ratio input (69.1 kg/m^2) to achieve a decay in less than 22 years. As can been seen in Table 6.3 the only predictions exceeding the limit are the worst and nominal case of the latest forecast.

Table 6.4:   DRAMA simulation results for test case with solar mean 22 y A/m input. Plots reported in Appendix.

DRAMA simulations	Case 1	Case 1B	Case 1C	Case 4	Case 5
Duration with Solar mean 22 y A/m input (years)	32.22 22.92 (best), 43.54 (worst)	15.39	13.55	28.48	18.51

6.2.2   Applicability of current DAS designs

The outcome of this work is to understand the scalability of the current DAS design types (Icarus, DOM), to achieve this the applicability and advantages/drawbacks of these designs must be evaluated with respect to the spacecraft that can eventually adopt one of them as de-orbit strategy. For this reason the two different configurations were evaluated for the non-compliant spacecraft sample.

The main point is to verify if the satellites, with the current DAS designs, would

achieve the compliance and if not what could be modified or which alternative solutions are available.

The input area for the m/A is the average cross sectional area of the spacecraft in random tumbling condition. This was computed with the STELA Mean Area Tool, before running the simulations to determine the orbital lifetime.

The m/A needed, instead, is the one calculated with the simple decay model for 25 years (see section 6.1), so this is the maximum ratio to achieve the re-entry within the time limit (if the ratio is lower the re-entry time is shorter).

This was obtained both for solar mean and solar minimum conditions, in the second case the area needed to achieve the re-entry requirement is much larger. Indeed, the simulations with solar minimum flux are not relevant because they represent an extreme condition, the worst case which could affect the atmospheric density and cannot happen in reality (as constant SFU value).

In this way, keeping the same S/C mass, the additional area needed was obtained. The mass of the DAS payload was not included in the updated mass-to-area ratio but considered within the overall spacecraft mass.

In parallel the area achievable with the current DAS design types - Icarus and DOM - were derived.

In the case of Icarus, the input for the area model are the two sides of the spacecraft (when cubic, parallelepiped shape) or the sides where the device can be integrated. The two measures are the drivers for the length of the stowed booms, and so these relate to the sail overall surface per side (see Fig. 6.8).

In the case of the DOM, the area of the deployed sails is not dependent on the spacecraft sides, because the design is not based on a rectangular frame but on a self-contained unit. This design is more flexible, so the applicable area was calculated depending on the required area needed to achieve the compliance and the current
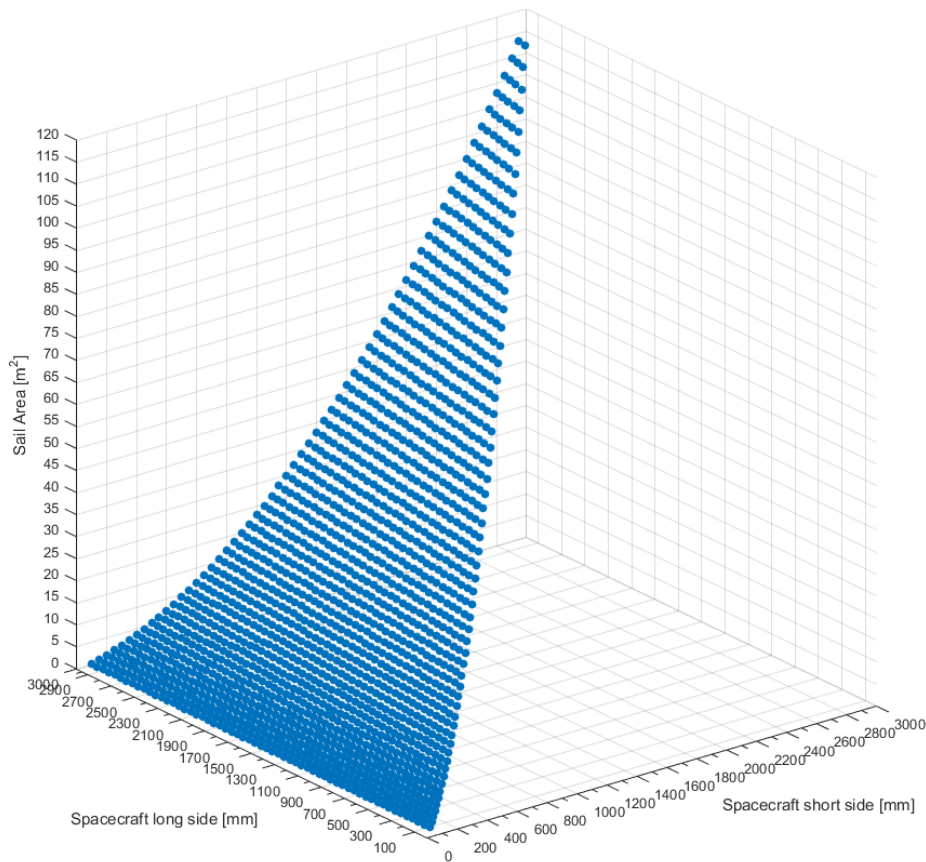
Figure 6.8: Sail area achievable with Icarus design.

limits of the DOM.

A more detailed analysis of the area achievable and the design of the DAS is performed in Chapter 7.

6.2.2.1 Spacecraft without propulsion subsystem

In this section the additional area needed and the one achievable with the Icarus and DOM designs are compared and discussed for the spacecraft not equipped with propulsion subsystem.

As can be seen from Fig. 6.9 all the satellites (of the sample) with planned altitudes below 700 km would achieve the compliance to the 25 years re-entry if the

Icarus DAS is applied as de-orbit strategy.

This is evident looking at the green bars, representing the random tumbling area given by the Icarus deployed thin film, which cover the red ones, representing the additional area needed to decay within 25 years.

The random tumbling area is calculated applying a factor of 2, as advised in ISO 27852:2011 [BSI Standards Publication, 2011b] when estimating the cross-sectional area with tumbling modes. This means that the effective geometric area deployed by Icarus DAS, as indicated by the labels in Fig. 6.9 is double.

For altitudes above 700 km, the area achievable with Icarus design is clearly not enough, this is the case of seven spacecraft (IINUSAT, M3MSAT, NANOJASMINE, 4 MKA-FKI). In the case of IINUSAT a slight modification of the design would allow to deploy a larger area, indeed the area needed is really close to the one achievable; in the case of NANOJASMINE instead would be more difficult as the orbit altitude is higher (800 km).
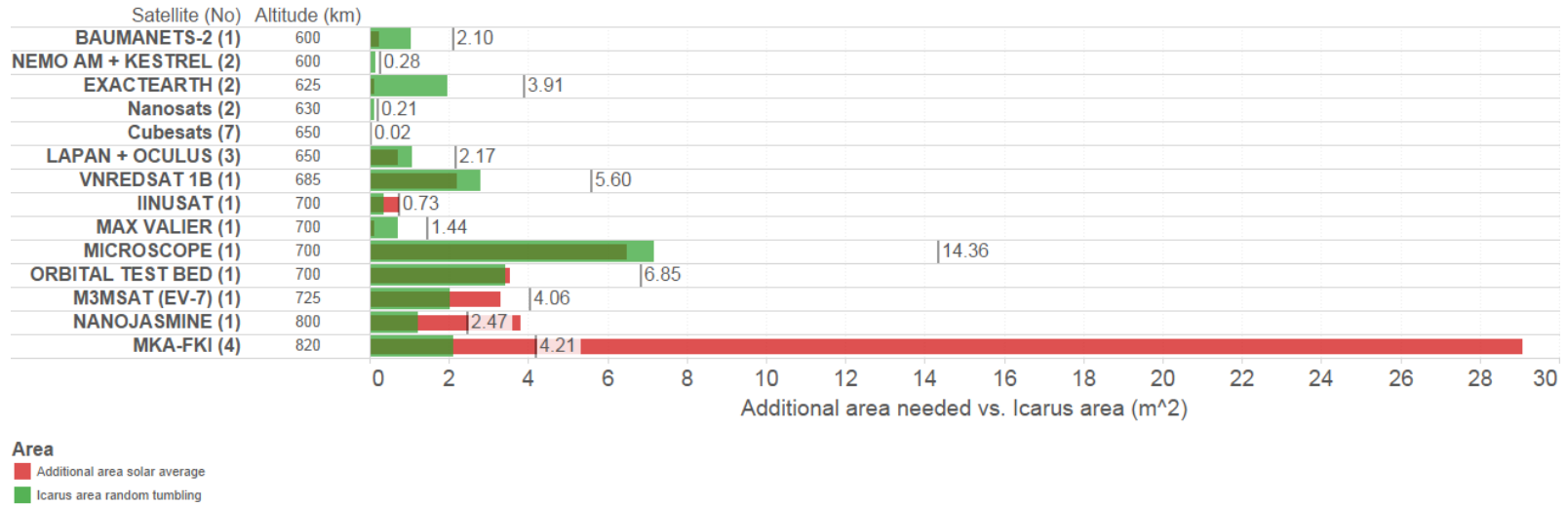
Figure 6.9: Additional drag area needed (red bar) for re-entry in 25 years with respect to the added random tumbling area with Icarus design (green bar) for the spacecraft without propulsion. The reference line with label (for each bar) is the effective Icarus area deployable.
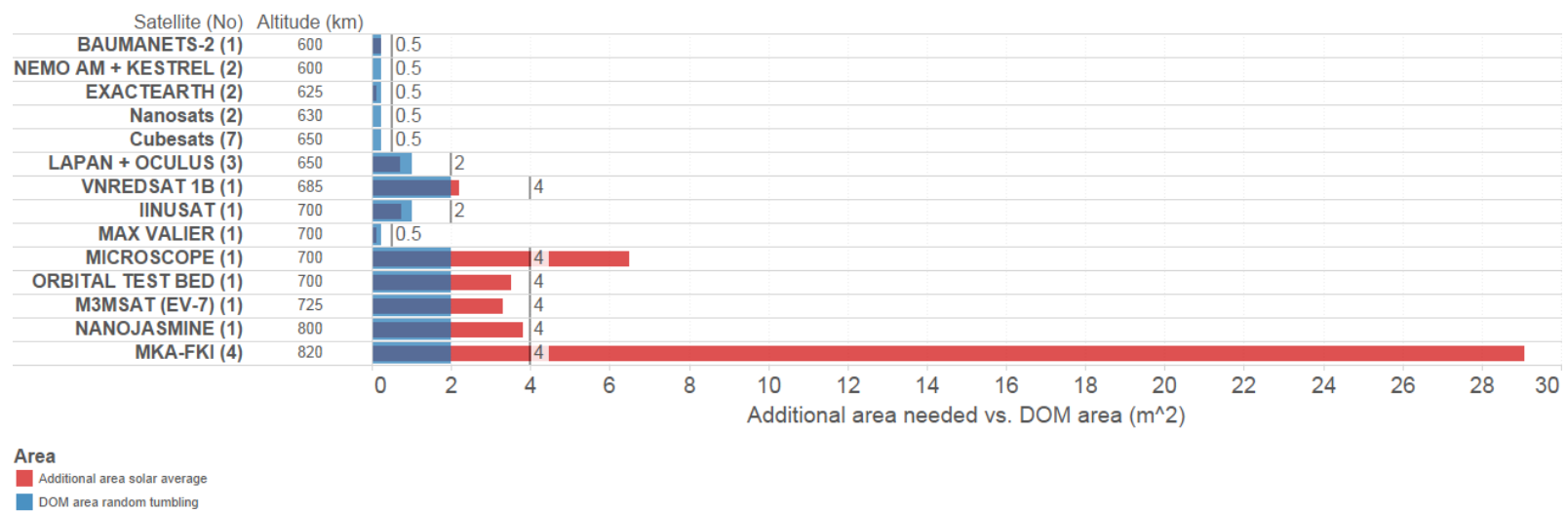
Figure 6.10: Additional drag area needed (red bar) for re-entry in 25 years with respect to the added random tumbling area with DOM design (blue bar) for the spacecraft without propulsion. The reference line with label (for each bar) is the effective DOM area deployable.

The satellites MKA-FKI would need a different de-orbit strategy, there are also uncertainties on the programme itself (first cancelled then restarted, according to the available on-line resources [Krebs, 2015]) and the expected orbit (might be higher).

The drag area that could be deployed on the satellite named ORBITAL TEST BED is indeed almost matching the missing area, this could be achievable with a modified shape of the sail quadrants.

The sail size achievable for the recently launched MICROSCOPE looks difficult to be implemented, however the area needed is actually half of it, moreover a drag tether (IDEAS) has already been designed and integrated on the S/C by Airbus DS [Rasse, 2015] to achieve a faster re-entry.

The cross sectional area needed for nanosats and cubesats is quite small and it is easily obtainable. However, the additional mass of the Icarus frame would affect this type of satellites; in addition, the small size of components needed for the Icarus DAS on cubesats, make this concept not really a feasible solution for this class. The alternatives can be developing an ad hoc design for cubesats already integrated in the S/C structural frame, or using a different DAS design as the DOM, more compact and with lighter structure.

On this purpose Fig. 6.10 can be observed. The figure represents the same sample of spacecraft with no propulsion subsystem and their area needed compared with respect to the DOM area (blue bar). The DOM design is much more flexible and doesn't depend on the spacecraft sides available, despite protrusions in the proximity of the deployed envelope shall be avoided.

As can be seen from the labels, the effective geometric areas selected are 0.5 m^2, 2 m^2 and 4 m^2. These values were chosen considering the additional area required and based on DOM standardized dimensions available to the customer.

The DOM design could cover the gap of Icarus for cubesats and other nanosats

and gives the adaptability that Icarus doesn't allow (as for IINUSAT for example).

The Icarus design is definitely a good solution for the spacecraft that fall in the drag area range between 1 and 7 m^2. At Cranfield we have already demonstrated that we can test and qualify this strategy with similar sail dimensions (on TechDemoSat-1 [Kingston et al., 2014] and on Carbonite-1 [SSTL, 2015]). In addition, similarly to the DAS on-orbit, these satellites planned orbit altitudes are in the range 650-750 km and sun-synchronous.

6.2.2.2   Spacecraft equipped with propulsion subsystem

The spacecraft of this group are equipped with a propulsion subsystem so, provided that the additional propellant is loaded and all the subsystems are fully functional, they can achieve an active de-orbit re-entry or at least lower the orbit to achieve a natural decay within the limit. The DAS is then considered as a back-up strategy.

The dimensions of these S/C buses allow bigger volume envelope, however, the size of the sail is rather large, and so the testability aspect is definitely compromised.

Looking at the coloured bars in Fig. 6.11 a deployable surface of less than 10 m^2, achievable with Icarus design, would be sufficient for around 20 satellites: all the spacecraft with planned altitude below 680 km and the ORBCOMM OG2 constellation with 11 S/C recently launched (22/12/2015).

For the constellations FORMOSAT and IONOSFERA the additional area is far above the one feasible with the Icarus design type, the main reason is due to the orbit altitude. The IRIDIUM constellation, instead, with the ELITE bus, has enough room for a very large sail, however this is not feasible in reality, moreover, given the number of satellites in the constellation (72), a direct re-entry is the most advisable solution.

Fig. 6.12 shows the additional area that can be achieved using the DOM design

on the same group of spacecraft. As can be seen, except two cases (ALSAT 2B and PROX-1), the DOM does not appear to be a good solution for de-orbiting these spacecraft. The DOM sail area is not dependent on the spacecraft panel size, however the limit is due to the length of the booms deployable in 1g environment (testability requirement).

The limit imposed on the area achievable with the current DOM design is 6 m^2 considering that two devices, each with a deployable sail area of 3 m^2 (1.2 m boom length), could be integrated on the spacecraft.

If the DOM sail area can be instead maximized, with a configuration perpendicular to the velocity vector, most of the spacecraft with expected altitude below 700 km would obtain the required area to achieve the compliance.
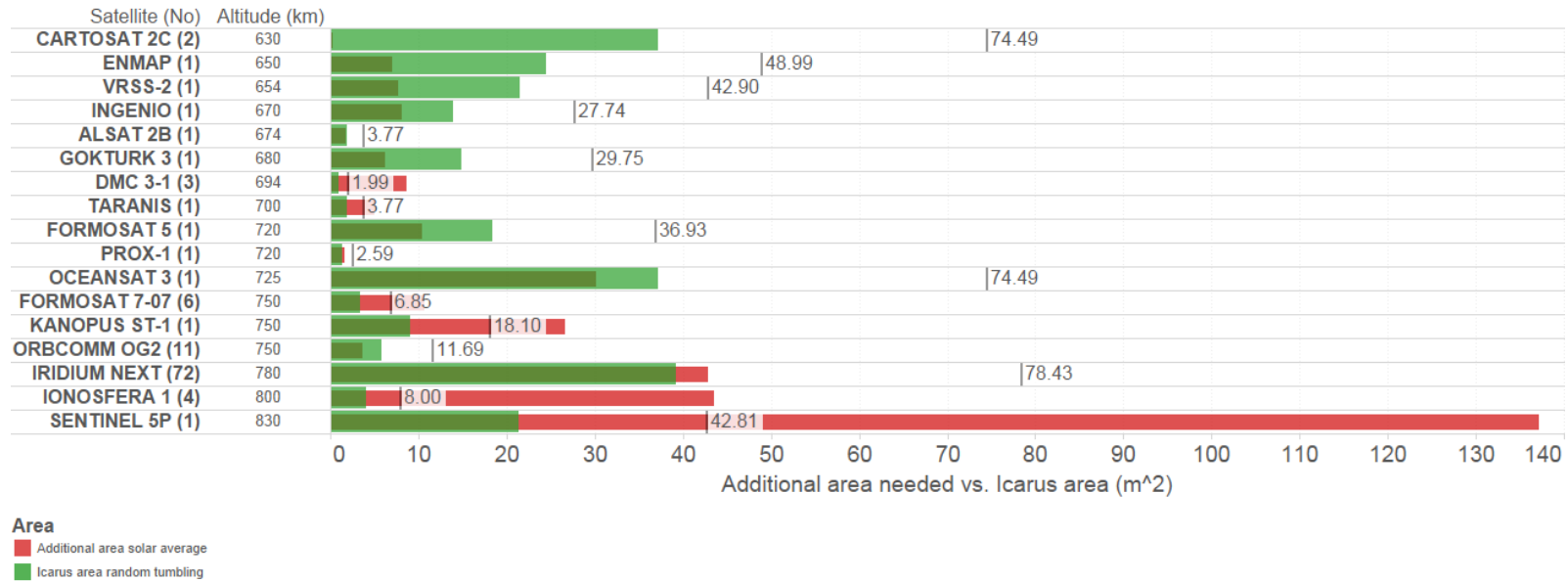
Figure 6.11: Additional drag area needed (red bar) for re-entry in 25 years with respect to the added random tumbling area with Icarus design (green bar) for the spacecraft equipped with propulsion subsystem. The reference line with label (for each bar) is the effective Icarus area deployable.
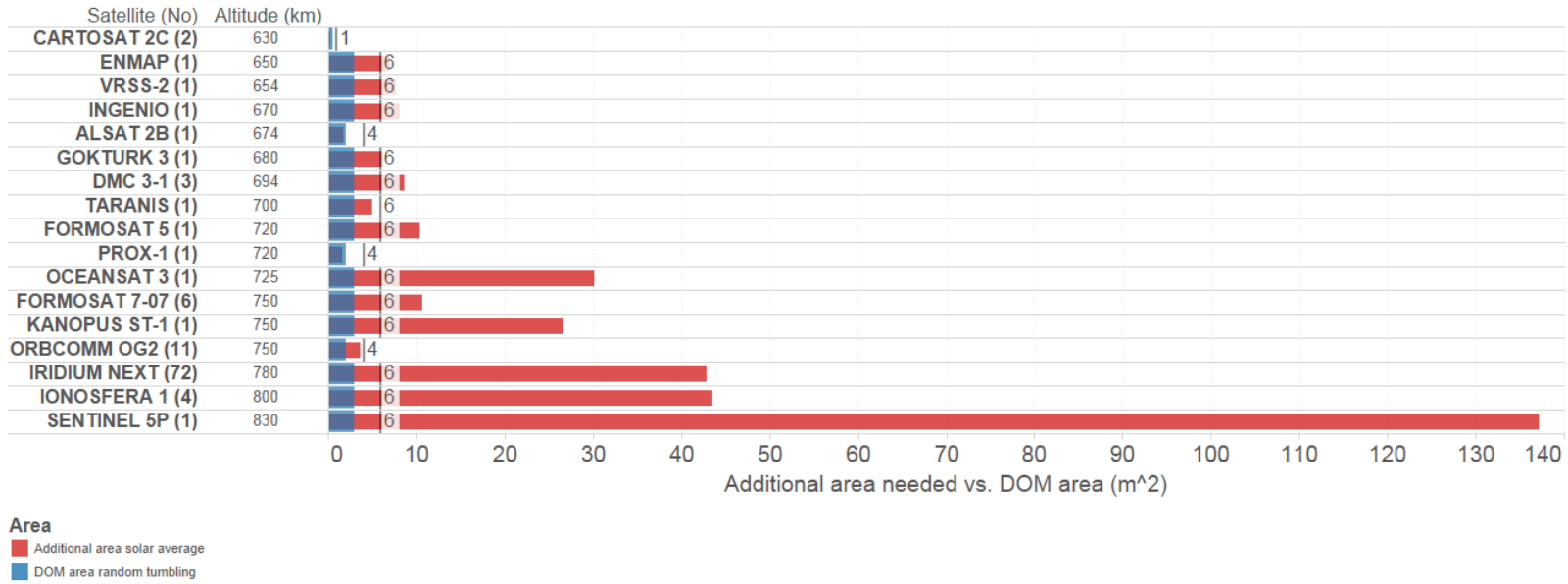
Figure 6.12: Additional drag area needed (red bar) for re-entry in 25 years with respect to the added random tumbling area with DOM design (blue bar) for the spacecraft equipped with propulsion subsystem. The reference line with label (for each bar) is the effective DOM area deployable.

6.3   Summary

The additional drag area, required to be compliant with the 25 re-entry requirement, for a sample of spacecraft to be launched in LEO has been investigated.

The simplified decay model was validated with STELA and DRAMA orbital decay simulators, proving that this model can be used as an easy tool to quickly verify the requirement compliance. The main differences were detected with the latest prediction model for the solar activity in DRAMA; considering the updated input affects the model, we suggest to use it for short term predictions of the satellite's decay.

When computing the BC limit for a specific spacecraft is advisable to have a 10% margin in the de-orbit time. In this way the additional area needed will increase slightly, but at the same time the re-entry is assured to be compliant, despite the solar flux variations.

The Icarus design type showed a good suitability with the population of spacecraft without propulsion 20 out of 28 S/C would achieve the compliance, if this DAS type is selected as de-orbit strategy; in the group of S/C with propulsion the achievable compliance instead is lower (only 20 out of 109 S/C). S/C in the range 500-1000 kg allow to deploy very large sail area, however this is not feasible both for the testability and taking in account the DAS mechanism relies on tape spring energy (no motor for deployment).

The Icarus design is instead a good solution for the spacecraft that need a cross sectional drag area in the range between 1 and 7 m^2, which are basically almost all the S/C without propulsion subsystem analysed and 16% of the other group.

The DOM design is instead suitable for nanosats and microsatellites with no propulsion and altitudes below 700 km. In particular, when there's limited surface

available on the S/C panels, the DOM layout could be integrated while the Icarus configuration cannot.

Chapter 7

Development of a Family of Scalable DAS

This chapter is derived from the conference papers *Development of a Family of Scalable Drag Augmentation Systems* [Palla et al., 2017a] presented at the 2017 IEEE Aerospace Conference and *Development of Commercial Drag-Augmentation Systems for Small Satellites* [Palla et al., 2017b] presented at the 7$^{\text{th}}$ European Conference on Space Debris.

Moreover, part of this work was performed in the framework of the ESA CleanSat programme (under AO/1-8287/15/NL/MT). As mentioned before, the objective of the CleanSat programme is to mature and develop suitable BB, by means of technology assessment and concurrent engineering studies (e.g.: CDF), to ensure future LEO platforms comply with SDM requirements [ESA, 2015a].

The main objective of Cranfield BB is the development of a family of drag augmentation system (DAS) modules to enable small satellites in LEO to comply with SDM requirements. This is, indeed, the main aim of this PhD research.

The CleanSat study helped evaluating the design options, manufacturing, AIT

and operational factors to define the DAS modules and guiding to achieve commercial readiness for the technology.

The chapter presents and discusses the compliance of the DAS with respect to the consolidated requirements as agreed during the CleanSat CDF study. Following this, the design justification and performance analyses to meet the requirements are described.

The design is investigated in terms of scalability by performing a design parameters analysis on the Cranfield DAS already developed. The scalability of the design is then evaluated with respect to the spacecraft platforms and determining the DAS compatibility with them. This specific part of the study was performed together with the MSc student D. Grinham who analysed the DAS compatibility with a range of spacecraft platforms for his individual research project [Grinham and Kingston, 2016]. The topic *Drag Augmentation Systems Design Study* was proposed as MSc thesis and the PhD work included co-supervising the MSc student.

The input of the CleanSat study together with the research work and the analysis performed by D. Grinham led to the definition of refined designs and new concepts.

The results of the performance analysis, both on the heritage and new DAS design, are then presented. The evaluation of the performance focuses on specific mission case studies and on the effects of the orbital environment.

7.1   Synthesis of requirements

In this section we present the customer's requirements matured during the CDF for the CleanSat BB study. The match between the internal requirements, presented in Chapter 3, and the top-level requirements from the potential customer's perspective (e.g.: satellite integrators) is shown and discussed.

The key drivers used during the design process (i.e.: internal requirements) were: reliability, low mass, low cost, simple design and interfaces, easy testability, safety, scalability, and avoidance of additional debris production.

Table 7.1 lists the requirements established during the first CDF meeting and their verification method. These requirements are based on inputs from key players in the European space industry, and are intended to capture the customer's perspective (typically for a Large System Integrator, LSI). In some cases, the requirements are actually targets rather than strict requirements, however expressing them as requirements gives a clear statement of potential user needs and expectations.

7.1.1   Requirements discussion

As can be seen from Table 7.1 the Cranfield design drivers, described in Chapter 3, matched with different top-level requirements. These are safety and reliability, system level requirements in terms of command, power, state modes, interfaces to ensure minimum impact, and physical properties (mass, area-to-mass ratio implying scalability).

In particular, in terms of safety the host spacecraft must be assured that there is negligible risk (<0.001) that the DAS will jeopardise the primary mission. The critical items were identified performing a FMECA. The resulting probability of severe impact on host mission is very low, so no high criticality items were identified.

The reliability of the DAS maintains a strict 95% as it is assumed a required overall spacecraft system reliability of 90% according to [BSI Standards Publication, 2011a] and specified in the ESA SDM Verification Handbook [ESA SDM WG, 2015]. To verify the reliability for the DAS produced so far, the approach has been to use repeated deployments of Qualification Models to characterise the behaviour

Table 7.1: Consolidated requirements as agreed at CDF for CleanSat study. Verification methods: D = design, A = analysis, T = test. Compliance status: C = Compliant, PC = Partially compliant, NC = Non compliant.

ID	Requirement topic	Requirement description	Verification	Compliance
BB13-CU-01	Command	The device shall deploy as commanded by the host spacecraft.	D	C
BB13-CU-02	Demisability	The device shall be fully demisable, with no debris over 15 Joules (kinetic energy) reaching the surface.	D, A	C
BB13-CU-03	Safety	The risk of premature deployment of the device shall be 0.001 (goal=10^{-4}) or less.	D, A	C
BB13-CU-04	Reliability	The reliability of the device (predicted successful deployment at end of host's nominal mission, evaluated at time of integration) shall be superior to 95%.	D, A, T	C
BB13-CU-05	Performance	Once deployed the device shall ensure de-orbit of the host spacecraft within 25 years. Two test cases shall be used to demonstrate compliance: (1) 500 kg mass, (2) 200 kg mass, both at 600-800 km altitude.	D, A	PC
BB13-CU-06	Deployed area	Random tumbling of the spacecraft shall be assumed to estimate the effective area of the deployed device.	A	C
BB13-CU-07	Area-to-mass ratio	The ratio between deployed surface area and subsystem mass shall be better than 1 m^2/kg (threshold), 2.5 m^2/kg (goal)	D, A	C
BB13-CU-08	Functional	The device shall be capable of deploying successfully on a host spacecraft rotating at up to 0.2 deg/s about any axis.	D, A	C
BB13-CU-09	Functional	The device shall not require any electrical power from the host spacecraft once deployed.	D	C
BB13-CU-10	Lifetime	The device design shall be compatible with 10 years ground storage, without need for complementary re-acceptance testing at the end of the storage period.	D, A, T	NC
BB13-CU-11	Lifetime	The device shall be able to operate successfully after an operational host satellite period of 10 years in LEO.	D, A, T	NC
BB13-CU-12	Environment	The device shall ensure the expected performance under the radiation conditions observed during the operational lifetime and the disposal phase.	D, A	PC
BB13-CU-13	Environment	The device shall ensure the expected performance under the ATOX environment of a worst-case of de-orbit from 600 km, 25 year re-entry time.	D, A	PC
BB13-CU-14	Environment	The device shall ensure the expected performance under the debris/meteoroid environment of a worst-case of de-orbit from 800 km, 25 year re-entry time.	D, A	C
BB13-CU-15	States	The device shall have three primary discrete states: stowed, deploying and deployed.	D	C
BB13-CU-16	Subsystem	The device shall be a separate sub-system with clearly defined interfaces to the host.	D	C
BB13-CU-17	Cost	Target figures for threshold and goal were defined by the LSIs.	A	C
BB13-CU-18	Mass	The device mass shall be inferior to 5 kg as a goal, 10 kg as a maximum.	D	C
BB13-CU-19	Volume	The volume of the undeployed device shall not exceed 10 litres.	D	C

and proper functionality of the designs, then a small number of deployments of the Flight Units for acceptance. To determine the appropriate number of deployments to be performed during functional qualification testing, the ECSS-E-ST-33-01C on Mechanisms [ECSS Secretariat, 2009b] has been referred to. For mechanisms, the number of ground test cycles recommended are based on the number of cycles expected to be experienced by the flight unit.

The requirements which focus on the physical properties help the designer to perform an independent assessment of the DAS de-orbit performance, and to evaluate if/how including the device in the host spacecraft design. Both the DOM and the Icarus designs are compliant with the area-to-mass ratio threshold. The Icarus ratio improves with increasing size, while the DOM is compliant also with the goal. This is discussed in the following section on the design parameters analysis and scalability. The requirements on mass and volume are also achieved with the current DAS designs.

The random tumbling condition was assumed in all the analyses performed. This requirement guarantees assurance for the 25 years re-entry because the mean cross sectional area is smaller than an aerostable configuration (i.e.: when the sail surface is perpendicular to the velocity direction), and so there's margin when computing the decay time, however this implies a considerable larger sail surface to deploy.

At the current TRL the DAS is able to meet most of the requirements, however the two most challenging aspects to assess were the compliance with the lifetime required for storage on ground and pre-deployment storage on orbit, and the DAS performances under the effect of the orbital environment.

The storage lifetime of 10 years was difficult to verify and was accepted as a goal. A 10 year storage period on ground may not be achievable, moreover verification of this requirement may be incompatible with other requirements. A servicing may be

needed to check and re-tension the safety protection band on the DAS.

The compliance for the storage time on orbit requires either assumptions about a nominal host mission or definition by the customer of their specific mission plan, here instead it is 10 years fixed time. Moreover, there could be potential for degradation of some DAS components during the nominal mission (if 10 years is assumed). The stored energy within the tape spring could be reduced, particularly due to repeated thermal cycling in orbit, and the tightly stowed sail layers could stick to each other under the combined vacuum and thermal cycling conditions in orbit. Furthermore, the pyrotechnic cutters do not meet the required lifetime, and indeed it is understood that pyrotechnic devices in general are limited in terms of storage life.

To demonstrate compliance with the lifetime requirements, significant further analysis and testing to validate practical component lifetimes are required.

For what concern the demisability, the DAS is compliant by design. All of the design concepts are of low mass, and this mass is predominantly aluminium. The units only use very small amounts of high melting point materials such as stainless steel. It is not therefore expected that there will be any issues regarding the demisability.

Materials used are well known and qualified for space use and so for the radiation conditions, except for cutters which are not currently qualified for the required duration.

The analyses performed to assess the DAS performance in orbit include several case study missions (500 kg and 200 kg LEO satellites) and they evaluate the potential reduction of orbit lifetime after EoM, the effects of atomic oxygen erosion and the debris risk during the de-orbit phase (see Sections 7.4 and 7.5).

7.2   Design parameters analysis

The main phases of this work encompass an analytical study on the design parameters of the DAS concepts focusing on the scalability; identifying the spacecraft constraints from a customer's perspective; determining the DAS compatibility with respect to the satellite platforms.

This analysis helps to verify the compliance to specific requirements on the DAS physical properties: area-to-mass ratio (BB13-CU-07), mass (BB13-CU-18), volume (BB13-CU-19).

7.2.1   Methodology

The physical properties which drive the scalability of the DAS with respect to the spacecraft integration are the mass, the volume of the device, and the deployed area achievable. These represent key requirements, as we have seen in Section 7.1, also in term of performance of the DAS concept for the satellite's orbital lifetime.

The main physical properties are directly dependent on the main design parameters of the DAS concepts, which are: the material properties for both the designs presented, the size of the frame driven by the lengths of the spacecraft sides in the case of the Icarus frame, the boom lengths and the thickness of the Kapton sail in the case of the DOM unit.

These parameters are cross-correlated: for example the boom length determines the sail area and affects the applied loads on the central structure, but also defines the number of sail foldings and so the stowed volume.

The applicable DAS design constraints are derived from the spacecraft platform size and configuration, orbit, and target re-entry time.

7.2.1.1   Icarus parameters

In the case of the Icarus design the cross-correlation is determined by the spacecraft sides/edges available for the frame. The boom length and the base of the trapezoidal sail are then calculated as a function of the side length. From these, the area of the deployable sails can be derived.

The design of the Icarus concept is largely driven by the spacecraft sides/edges available for the frame. The sail area is then constrained by the length of the shortest side of the S/C panel to be attached as this dictates the length of the booms which deploy the sail.

The Icarus design doesn't adapt well for satellites where the panel dimensions (perpendiculars sides) are largely different from each other, such as in the ESEO spacecraft.

For these reasons, specific design constraints have been imposed on the panel side lengths:

- the maximum ratio between the longest side and the shortest side of the frame is 2;

- the difference between the two sides of the frame is less than 1 m.

7.2.1.2   DOM parameters

In the case of the DOM, the cross-correlation is determined by the arc length of a polar curve, which is actually the length of the boom when rolled around the central spool. In our model, this is an example of Archimedean spiral (Fig. 7.1).

From the general equation for a spiral in polar coordinates, the radial distance from the origin is:

$$r = r_i + h\theta \tag{7.1}$$
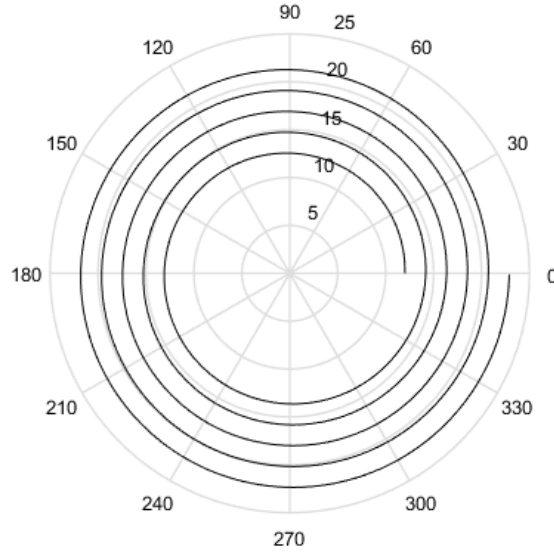
Figure 7.1: Example of Archimedean spiral for booms stowing with boom length 516 mm and external diameter of 45 mm. Note: four booms and sail thickness included.

where r_i is the initial radial offset (i.e. the starting point of the spiral), in our case is the radius of the spool, h is the incremental offset per revolution and θ is the subtended angle. The increment in the radius at each turn is then $2\pi h$. In this way the arc length of polar curve is given by [Wolfram Research, 2016]:

$$L(\theta) = \int_0^n \sqrt{r^2 + \left(\frac{dr}{d\theta}\right)^2}\, d\theta \qquad (7.2)$$

where n is the angle of revolution and $dr/d\theta$ is the incremental offset h as shown in the following:

$$L(\theta) = \int_0^n \sqrt{(r_i + h\theta)^2 + h^2}\, d\theta \qquad (7.3)$$

After integrating the function above, we obtain the length of the boom as function of the angle of revolution. With the length we can then compute the external stowed

Table 7.2: Input and Output for DOM design parameters.

Input parameters	Output parameters
Spool diameter	Boom length
Boom and sail thickness	External diameter stowed
Depth of foldings	Number of foldings
Numbers of booms	Area of the sail
Materials properties	Mass of booms and sail

diameter D_e, which includes the booms and sails, and the deployed sail area A_s:

$$D_e = 2(r_i + nh) \tag{7.4}$$

$$A_s = 2L^2 \tag{7.5}$$

The other parameters that can be obtained from the computation of the arc length in the case of the DOM design are presented in Table 7.2.

Another relevant parameter that can be computed is the constant torque generated by the tape spring booms during the deployment:

$$M^* = -\frac{\alpha E b^3 (1 - \nu)}{12(1 - \nu^2)} \tag{7.6}$$

this is referred as the steady-state bending moment for the equal sense of bending, where E is Young's modulus, ν is Poisson's ratio, b is the thickness of the boom and the angle α is shown in Fig. 7.2. It was found that the radius of the longitudinally curved fold region r is in good approximation equal to the initial transverse radius of curvature R [Seffen and Pellegrino, 1999]. In the case of the DOM the tape spring booms have a C-shape cross section and the radius of the spool is approximately equal to R, which, in this way, causes the natural folding of the booms and prevents

jamming during the deployment.
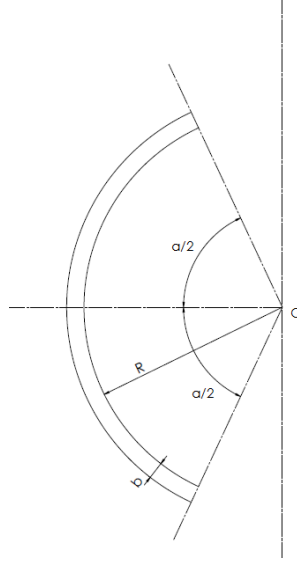
Figure 7.2: C-shape section of boom arm.

Having the material properties, the moment can be calculated depending on the geometric parameters, allowing to tailor the geometry to produce a targeted moment [Ploss and Hobbs, 2013]. Then also the potential energy, stored in each tape spring boom during the coiling process, can be calculated as in [Seffen and Pellegrino, 1999] with:

$$U = \frac{\alpha \theta E b^3 (1 - \nu)}{12(1 - \nu^2)} \tag{7.7}$$

this is the case for equal sense of bending.

7.2.1.3 Spacecraft platforms features

As we have seen in the CDF requirements (Table 7.1), the user/customer perspective is a relevant aspect to investigate the scalability of the DAS already developed, and to identify what is required from the DAS in terms of interfaces. For this reason

161

the platform characteristics needed to determine the DAS compatibility have been extracted from the sample of expected non compliant LEO spacecraft (re-entry > 25 years) analysed in Chapter 4 and Chapter 6. The spacecraft sample considered matches with the target classes for the DAS, i.e.: LEO satellites with mass below 1000 kg and with planned orbit altitude below 800 km.

The main objectives of the analysis of the spacecraft platforms features were: identifying what the customer will require from a DAS, how to best interface the DAS with the platform, and determining the constraints on the device coming from the host satellite [Grinham and Kingston, 2016].

The main features to determine the Icarus and/or DOM compatibility with respect to the spacecraft are: S/C mass, S/C class, presence of protrusion on panels, solar array configuration (body mounted/deployable wings). Analysing more in details the sample of uncompliant S/C, the following features were detected as constraints on the DAS:

- Satellite mass class: this constrains the type of device to be used. E.g.: Nanosatellites are less compatible with Icarus frame design, while the DOM Unit is more feasible for this group.

- Geometric shape: this can restrict the compatibility of the DAS; in particular for the Icarus frame (with the current design), which is designed to fit around or on rectangular spacecraft panels.

- Length ratio compatible with Icarus: this is a limit for Icarus frame concept. The drag area achievable is constrained already by the shortest side of the spacecraft panel, moreover our internal constraints on the design are the maximum ratio between the longest side and the shortest side (< 2) and the difference in the side dimensions (< 1 m).

- Panel access: a spacecraft panel may have protrusions in the form of optical payloads, deployable antennas, thrusters, which can prevent the deployment of the drag sail and booms for the DOM unit or affects the mechanical interfaces for the Icarus concept.

- Number of panel edges available: this affects the Icarus concept, its implementation may be prevented if one edge/side of the panel is obstructed.

- Solar panel deployable wings: they can interfere with the DAS deployment and limit the deployable drag area. In addition, in case of an aerostable configuration, the DAS should be in a plane parallel to the solar panels to maximize the cross sectional drag area (Note: this doesn't apply for random tumbling).

- Solar panel body mounted: this reduces the area available for mounting the DOM Unit, the same limitation affects the Icarus frame for the sides and corners of the panel. Assumption considered: once the DAS is deployed after the EoM, the panels can be covered by the sail.

- Satellite orbital parameters: they affect the DAS in terms of drag area needed to be produced to comply with the 25 years re-entry requirement.

7.2.2   Scalability evaluation

In this section the cross-correlation of the design parameters, which drive the scalability for the two different DAS concepts, is presented. Following this the design compatibility with respect to the spacecraft platforms is discussed.

The list of Matlab codes developed for the correlation of the design parameters are reported in Appendix D.

163
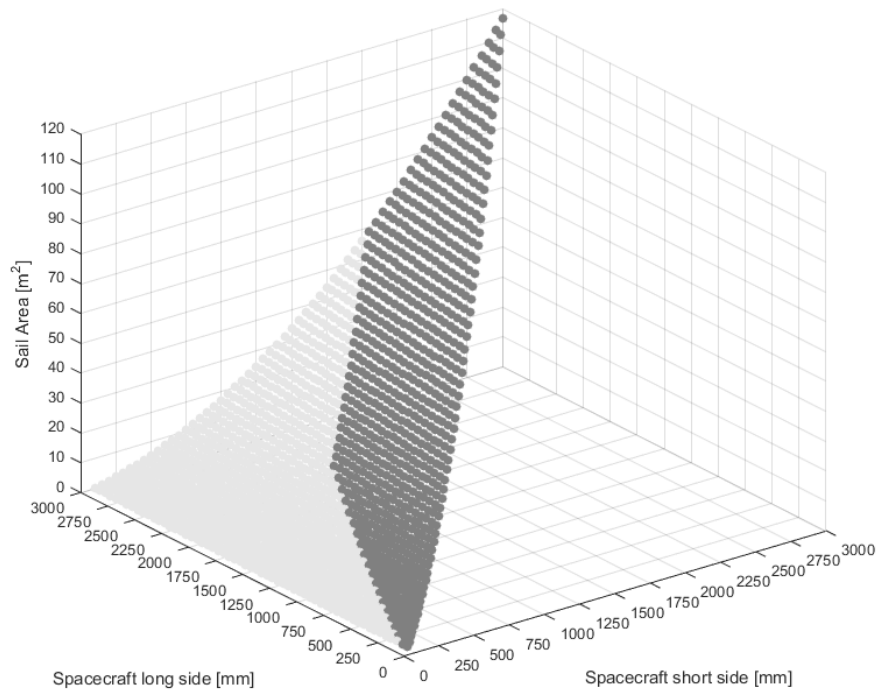
Figure 7.3: Sail area achievable with Icarus frame design: dark grey is the one considered imposing the constraints.

7.2.2.1   Icarus scalability

Focusing on the Icarus design, this has a simple interface resulting in a low impact on the host satellite, the advantage of this design is that it can be incorporated at a late stage in the development of the satellite.

Despite the relatively simple integration the sail area deployable is restricted by the length of the shortest side of the spacecraft mounting panel (see Fig. 7.3).

As can be seen in Fig. 7.3, the area analytically achievable can be very large, however this is not feasible both for the testability aspect and taking into account that the DAS relies on tape spring energy (no motor for deployment).

In Fig. 7.4 an enlargement of Fig. 7.3 is presented to show the sail area feasible
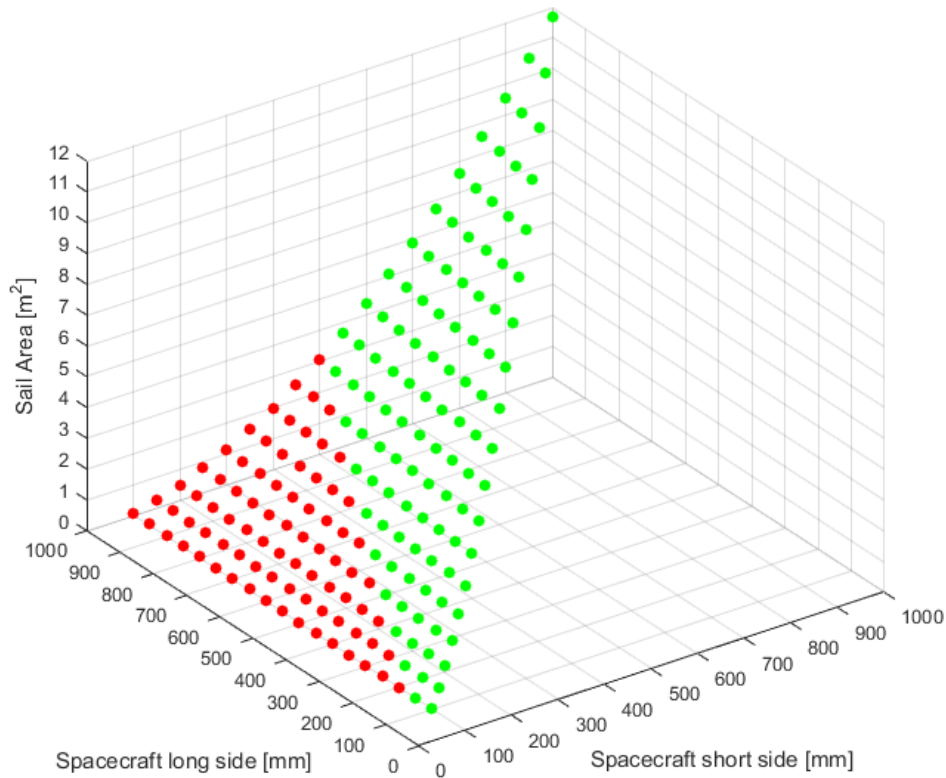
Figure 7.4: Sail area most likely feasible with Icarus design: green is the one considered imposing the constraints.

with the current Icarus design.

Scaling down this design concept would be rather infeasible and inefficient in term of area-to-mass ratio, instead the greater the mass of the satellite and room available for the frame, the more efficient the Icarus design is. In fact Icarus-1 with a bigger sail area than Icarus-3 (more than double surface) has a much better ratio (1.4 m^2/kg for Icarus-1 vs 0.9 m^2/kg for Icarus-3, see Table 3.8). The frame concept is definitely less mass efficient than DOM Unit but it can be scaled up better, without losing any cross sectional drag area already provided by the spacecraft panels.

It should be noted that, from the point of view of the Icarus design, it is possible to mount the frame so it "overhangs" the sides of the satellite panel, removing the

shortest side constraint. The frame does not need to be fully mounted on a panel, so if there are no constraints from the satellite side, a square frame could be attached to a rectangular panel. It is recognised that this configuration is less likely to be possible from the host satellite point of view, but there are no restrictions from the Icarus design side.

7.2.2.2   DOM scalability

As can be seen from Fig. 7.5 the impact of the mass of the DOM unit is very low, in particular when increasing the surface of the sail deployed. The area-to-mass ratio of the device, when in deployed configuration, is already above 1 m^2/kg with a mass of 0.5 kg and then it improves with longer booms. This is a good threshold value considering that allows the compliance with the requirement BB13-CU-07 (area-to-mass ratio) discussed with the LSIs.

An initial mass has been imposed to the aluminium cuboid assembly without sail and booms. This includes the central spool and the supporting structure composed by the main housing, the boom arm guides, and the release mechanism. The initial mass is same as the DOM engineering model already developed for the ESEO; however this should be feasible up to a boom length of 1.2 m for which the spool and main structure were initially developed, in case of longer booms and bigger sail then it would need to be re-adjusted.

It was found in [Ploss and Hobbs, 2013] that a boom length of 1.2 m is at the very limit for an open section self-supporting tape spring design in 1g conditions.

The sail area, which is a crucial parameter for the purpose of the DAS, increases very rapidly when the boom length is beyond 0.8 m (see Fig. 7.6), whereas the stowed diameter does not increase proportionally, therefore it is more efficient to have a longer boom length. This shows the suitability of the DOM unit to be scaled
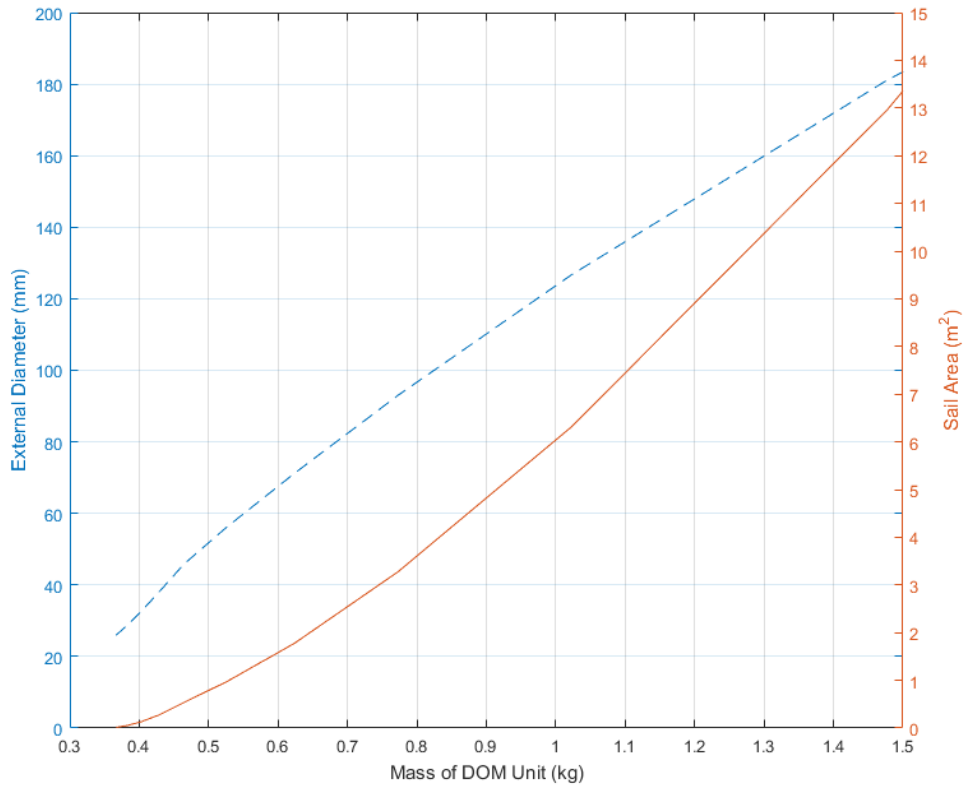
Figure 7.5: Cross correlation among the design parameters (mass, stowed booms diameter, deployed sail area) for DOM Unit concept.

up. However this would not be possible to be performed in-house due to facilities constraints, so external suppliers and different routes need to be sought.

As the DOM concept is a self-contained unit, considering the external diameter as a reference value, the mounting area needed on the host spacecraft will be very small, resulting in a minimal impact on the spacecraft design. In this correlation we considered a unit with four booms (with fixed thickness) and four sail quadrants, so the thickness varies as function of these values; however a different design option might use different number of booms.

We have seen in the Icarus vs DOM comparison that one of the main constraints affecting the DOM is the presence of protrusions on the S/C panel which prevent the sail from deploying. By adapting the DOM design considering this weakness,
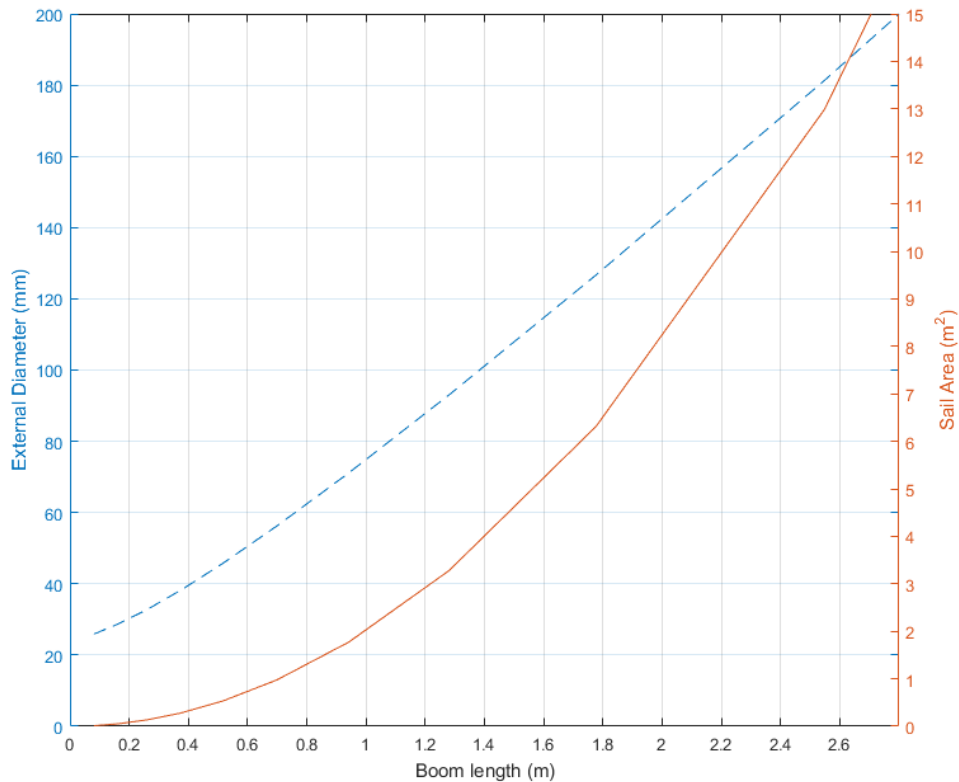
Figure 7.6: Cross correlation among the design parameters (boom length, stowed booms diameter, deployed sail area) for DOM Unit concept.

the number of satellites that are compatible can greatly increase [Grinham and Kingston, 2016].

The DOM can be evolved into a corner concept removing one sail segment.

In Fig. 7.7 the design considered is with 4 booms and 3 sails, this is suitable for the corners of a S/C panel.

In this case the ratio area deployed and device mass is slightly worse than the current design as the booms number is the same and one sail is instead removed. Nevertheless, the area deployed is fully exploited as in this case the additional area doesn't overlap the S/C panels.

Another option is the DOM evolution concept with just two sails and three
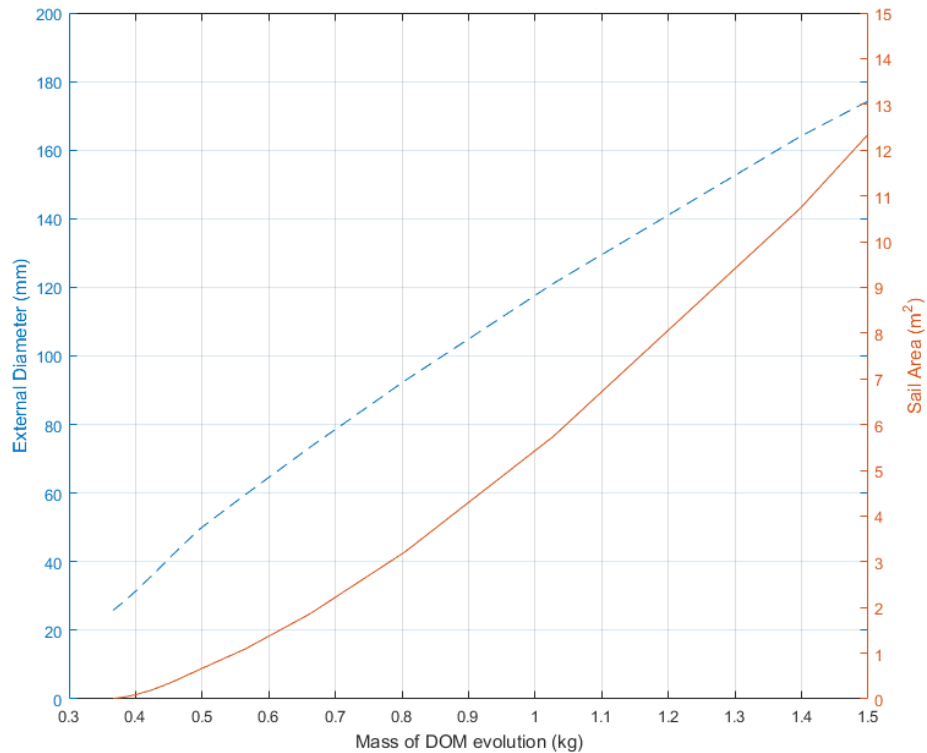
Figure 7.7: Cross correlation among the design parameters for DOM with 4 booms and 3 sails.

booms for deployment (Fig 7.8), it can be attached on the side avoiding corners and exploiting the whole additional drag area, moreover multiple device can be mounted on different sides.

These DOM evolution concepts are presented more in details in section 7.3.1.

For what concern the bending moment, this is of the order of 0.1 Nm, precisely 96.1696 Nmm using equation 7.6. The material properties of the Copper Beryllium were considered ($E = 130000$ N/mm^2 $v = 0.3$) and the geometry of the DOM booms for ESEO.

This is valid, using the equation for steady-state bending moment, since the transverse radius of curvature R of the uncoiled tape spring is approximately equal to the average coiling radius, however with longer boom arms this is not applicable
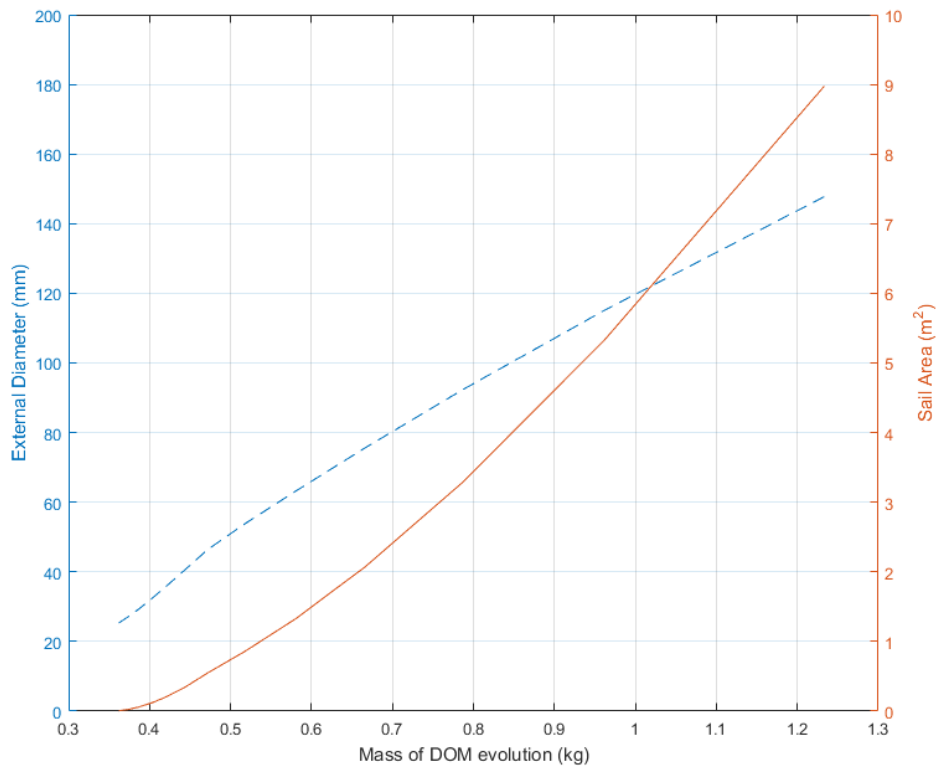
Figure 7.8: Cross correlation among the design parameters for DOM evolution concept with 3 booms and 2 sails.

any more.

Calculations were adopted for comparison with tape springs of Copper Beryllium tested by Seffen [Seffen and Pellegrino, 1999]. The results for the steady-state bending moments matched.

This theoretical result of ∼0.1 Nm is also consistent with the torque wrench (attempted) measurement for the DOM PFM, where the stowing torque was found to be considerably less than the bottom of the measurable scale of 2 Nm.

The potential energy stored during the coiling process is directly proportional to the number of booms and function of the angle of rotation θ to store the boom around the spool and this varies with the boom length. The stored energy varies

between 3 to 30 J considering the range presented in Fig.7.5. This is useful to then calculate the deployment impact on the spacecraft, i.e. the disturbing moment due to the DAS DOM Unit.

7.2.2.3   Design scalability vs. platforms

Having performed a critical analysis of the DAS design concepts and using the information derived from the customer, i.e.: the spacecraft features and requirements, and the Cranfield supplier, i.e.: the design parameters, a method to help in the selection of the most appropriate DAS for the customer's satellite has been developed (see Fig. 7.9).

The flow diagram was developed by D. Grinham to categorize the satellites into three different groups: Icarus compatible, DOM compatible, incompatible.

In this way the spacecraft compatibility with any DAS can be identified. The input needed for the flow diagram are the following satellite data coming from the customer:

- Orbital altitude

- Satellite mass

- Satellite configuration

    - Shape

    - Dimension

    - Drag area

    - Panel protrusions

    - Solar panel placement

Once the customer has provided the satellite data above, the following parameters can be calculated:

- Additional drag area required for 25 years compliance

- Mass class

- Panel edges available

- Panel dimensions compliant with DAS

- Available Icarus sail area

- Sail area required for DOM

    - Boom length required

    - Mounting area required

- Surface area available on panel

- Icarus compliant

- DOM complaint

This represents a tool to quickly identify the compatibility of the Icarus or DOM designs with the selected spacecraft. When using the flow diagram for a specific spacecraft there will be a point at which it becomes compatible with one of the concepts, however the spacecraft may be compatible with both the DAS concepts so the path continues through the diagram to allow the most appropriate selection. It may also be possible that none of the DAS developed so far is suitable for the satellite, in which case the flow chart brings to the incompatible result.
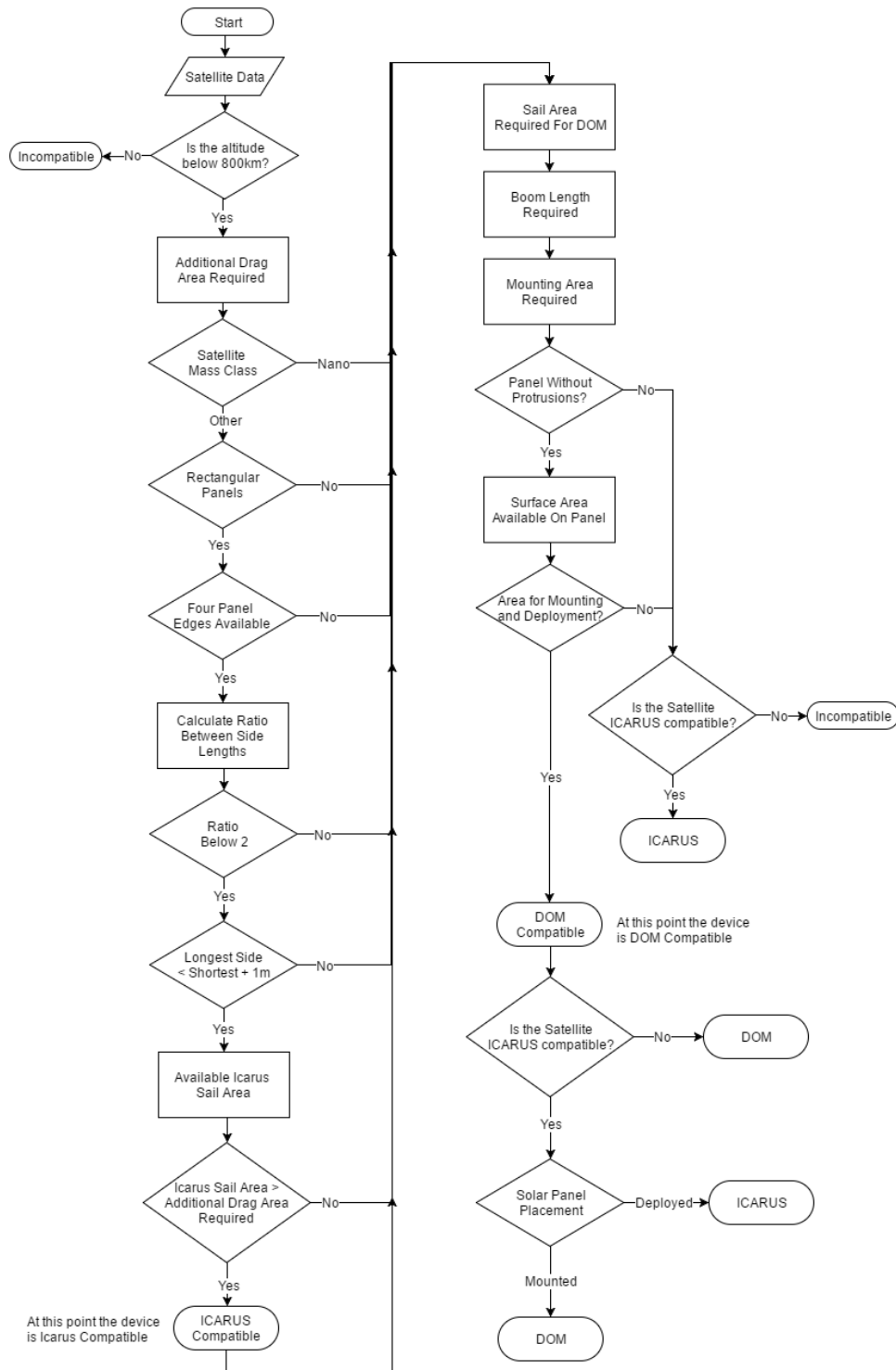
Figure 7.9:   Flow diagram for DAS selection (Courtesy of D. Grinham).

Apart from understanding whether a DAS is suitable for a specific mission, this will help the designer to define the interface requirements between spacecraft and DAS payload.

In addition the diagram highlights the spacecraft constraints, these weaknesses can be turned into strengths to develop potential adaptive concepts. The Icarus and the DOM designs can be combined in a hybrid design in order to reduce the limitations of the respective individual concepts.

This would improve the scalability with respect to the original Icarus concept as the drag sail area produced is no longer constrained by the panels shortest side length, it is instead driven by the boom length.

Moreover, the current concepts can be adapted to minimize the constraints imposed onto the device, as discussed and shown in the parameters correlation in Fig. 7.7.

7.3   New design concepts

The new concepts are being developed considering the gap in the family of heritage designs.

For example there is a gap in the family of DAS for a device that is compatible with a satellite that may not have rectangular panels, or four edges available and also does not have a panel that is free of protrusions [Grinham and Kingston, 2016].

7.3.1   DOM evolution concept

One of the main constraints on the DOM is that it cannot be deployed when there are protrusions on the spacecraft panel, because they prevent the sail from fully deploying. Moreover, part of the DOM sail overlaps with the panel, losing a percentage

of the additional drag area.

We have seen in the DOM scalability analysis (section 7.2.2.2) that this constraint can be removed by adapting the DOM design to a corner configuration, and still maintaining good performances in terms of area-to-mass ratio and volume of the device.

The DOM can be adapted by removing one of the four triangular sail segments (Fig. 7.10). By positioning the DOM on the corner of a satellite panel, the booms can be oriented to allow for the three remaining sails to deploy without obstructing any protrusions such as antenna, sensors, etc.
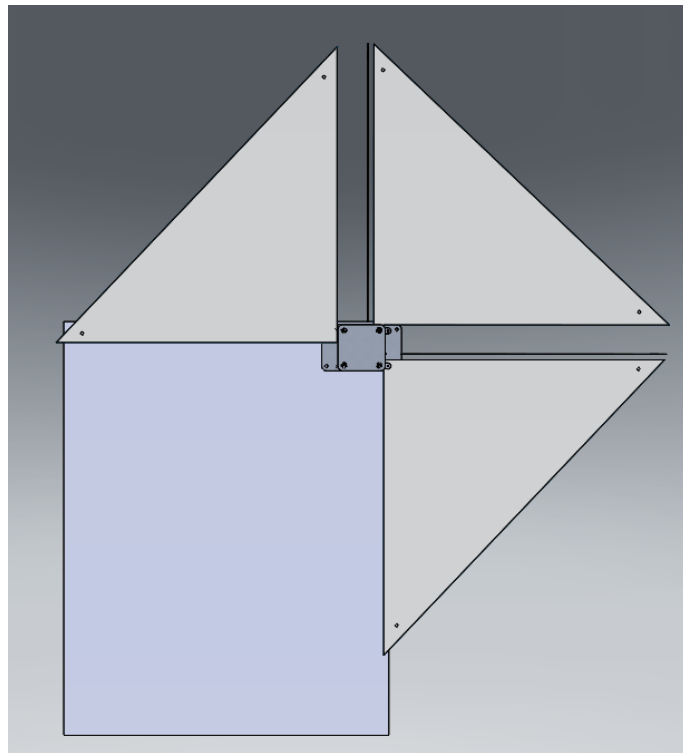
Figure 7.10: DOM evolution concept for corners.

This configuration loses the symmetry. Nevertheless, as the device is small and light, multiple DOMs could be placed around the panel to maximise the additional drag area (e.g.: on opposite corners to gain more symmetry in the configuration).

In addition to the removal of one of the sails, the design can be modified to deploy only three booms and two sail segments. The DOM evolution can then be positioned on the edge of the panel instead of the corner, to accommodate protrusions in the corners. As emerged during the CDF study, quite often on the corners are placed thrusters for attitude control.
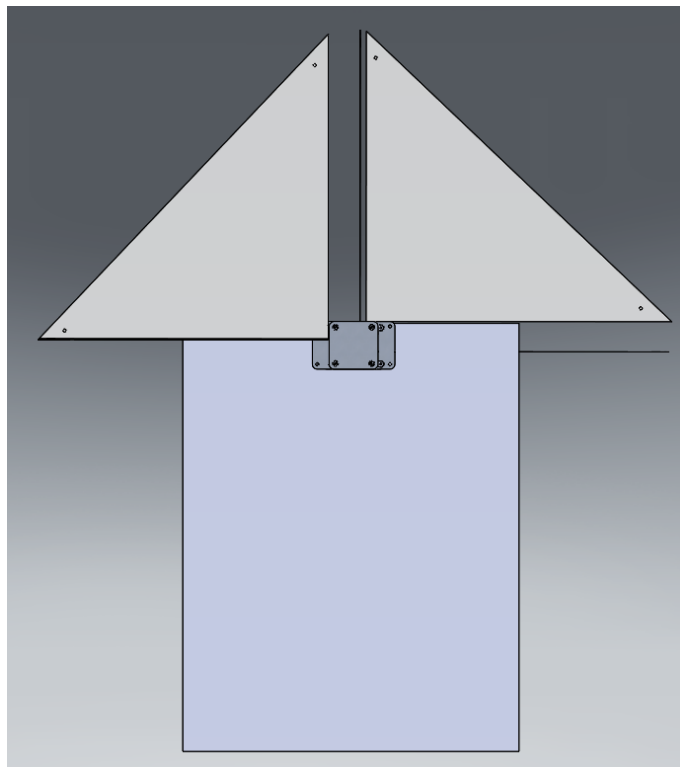
Figure 7.11: DOM evolution concept for edges.

With the reduction of wasted sail area and a boom, it reduces the overall mass of the device, which can potentially make it more compact.

Another modification can be implemented in the design of the DOM or DOM evolution to gain additional area. By modifying the sail shape into a fan shape, i.e. the triangular sail becomes a sector of a circle, an area growth of approximately 57% can be obtained. This was previously tested by A. Krammer [Krammer and Kingston, 2014] on a prototype of the DOM; the deployment tests performed with

the "fan" sail showed no sagging. However, the additional material needs to be stowed, increasing the number of folds (and so the sail thickness between booms) required.

The DOM evolution design is able to scale for larger and smaller satellites. As we mentioned before, for larger spacecraft platforms more devices can be implemented to increase the sail area.

7.3.2   Hybrid concept

This concept is derived from component technologies used in Icarus and DOM and conceptually builds on the strengths of each to improve scalability, versatility (i.e. adaptability) and manufacturability. The hybrid concept is at an earlier design stage and requires development to achieve TRL 6 alongside the other DAS.

The philosophy of the hybrid concept is to achieve a design composed of discrete self-contained modules, which can be integrated in a variety of configurations to adapt to different host satellite architectures. The modules derived from the heritage designs are:

- Boom module with release mechanism: allows different lengths of boom and can contain a sail quadrant if required;

- External sail cartridge: allows different widths and lengths of sail.

The boom module is based on the DOM design, but will contain either a single boom and no sail, or two booms and only one sail segment. Longer booms can be stored within the same size of the unit.

The external sail cartridge is derived from the Icarus concept. One of the main issues of Icarus-1 was the sail folding pattern, which was very time consuming other

than complicated to reproduce. In Icarus-3 the pattern was simplified, however, this still required a meticulous sequence for a correct folding. The reason to look for a repeatable and easy folding is also dictated by the testability. There is in fact the need of performing many deployment tests (see 3.7 for the DOM) to demonstrate the functionality of the DAS without tearing or damaging the aluminized Kapton membrane.

The cartridge would contain the stowed sail membrane, and would be integrated between two boom module units. In this way, when the firing command is sent, the two booms deploy pulling the sail out of the cartridge. The sail can be rolled on a thin rod or spool within the cartridge, reducing the complexity of the folding patterns required and simplifying the stowing process.

The shape of the sail membrane stowed in the cartridge can be rectangular as
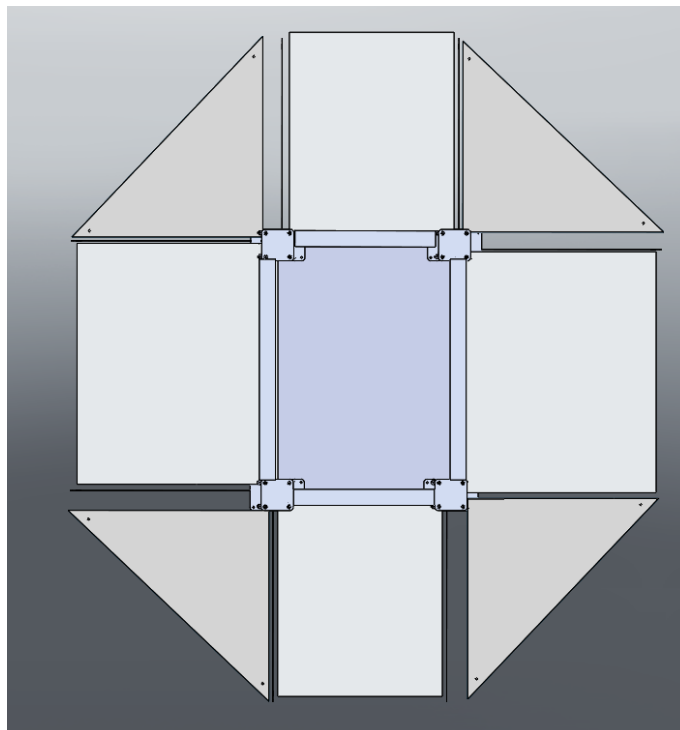
Figure 7.12: Hybrid concept with eight booms.

showed in Fig.7.12 or trapezoidal, like the Icarus ones. The two modules (boom and cartridge) can be set-up into different configurations depending on the satellite host platform.

The concept can be used as a single edge device (2 boom modules plus one sail cartridge). If more edges are available then multiple devices can be mounted and connected to each other. Also, this allows flexibility if the spacecraft panel is for example hexagonal instead of rectangular.

The hybrid design concept allows a higher compatibility with different spacecraft and is more scalable than the original Icarus, the sail area is now constrained only by the boom length (as in the DOM).

7.4   Mission performance analysis

The compliance to the performance requirement BB13-CU-05 was assessed by means of two main case studies (see Table 7.3), which were proposed and agreed during the CDF session:

1. 500 kg S/C with solar panel deployable wings, and with AstroBus platform features and geometry;

2. 200 kg S/C with body-mounted solar panels, similar to the Myriade platform geometry.

The 25 year requirement constraint is the driver for the mission case studies. For each of the two S/C configurations the following analyses were performed:

- Maximum altitude: S/C at 800 km of altitude with no DAS, to estimate the area of the sail needed to re-enter in 25 years.

Table 7.3: Spacecraft characteristics used as input for STELA simulations

S/C characteristics		
Mass	500 kg	200 kg
S/C body	1.0 m x 1.0 m x 1.8 m	0.6 m x 0.6 m x 1.1 m
Solar array	2 deployable (0.9 x 1.4) m^2 each	Body mounted
Drag area random tumbling	3.56 m^2	0.84 m^2
Mass-to-area ratio	140.45 kg/m^2	238.10 kg/m^2

- Existing design limit: S/C with largest DAS area achievable with heritage design, to compute the maximum orbit altitude to ensure 25 year re-entry.

- New design and alternative configuration limit: same as before but with the new design concepts applied.

The preliminary assessment was performed with a simplified decay model for circular orbits, and then verified with the CNES tool for end of life analysis STELA [CNES, 2013].

In the decay model the atmospheric scale height and average density values, function of the constant solar flux (solar mean), were extracted from the tables in [Wertz et al., 2011]. The density and scale height were calculated with linear interpolation for the different altitudes from the reference values. The satellite's lifetime was imposed at 25 years after the EoM, then, with the assumed CD (2.2), the required mass-to-area ratio for the specific orbit altitude was obtained.

In STELA we assumed a mean constant solar flux to avoid dependence of the results with the simulation date. All the simulations were set with the starting date on the 2016-12-01 and time T 00:00, however considering average solar activity, this does not affect the results. The orbits considered are sun-synchronous and circular ($e = 0$).

For the second and third groups of analyses, the achievable sail area was computed with the current Icarus design for the two case studies, and with the DOM evolution designs for the 500 kg S/C case.

The mass-to-area ratio of the S/C was then re-calculated for a random tumbling configuration (factor of 2 assumed as in [BSI Standards Publication, 2011b]), including also the expected additional mass of the DAS. Using the previous model, the altitude limit for the 25 years maximum re-entry time is then obtained, a verification with STELA followed, as before.

7.4.1   Maximum altitude
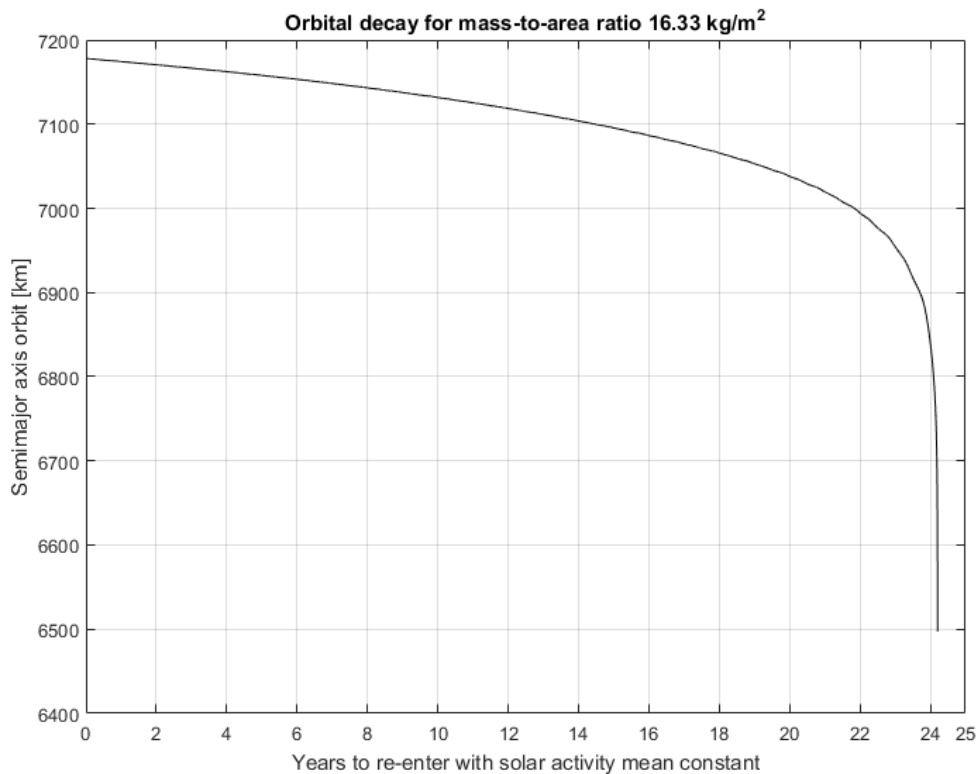
Figure 7.13: Decrease of semi-major axis for S/C with m/A=16.33 kg/m^2 and required sail area above 50 m^2 to comply with the 25 years requirement.

The mass-to-area ratio is initially obtained from the simple model, and then refined with STELA simulations. As can be seen in Table 7.4 the drag sail area required for the 500 kg S/C results above 50 m^2 in case of random tumbling configuration. As expected, the area needed for the 500 kg case to be de-orbited within 25 years from 800 km of altitude (see Fig. 7.13) is not feasible with the current existing designs.

Table 7.4: Summary of results for 500 kg S/C and 200 kg S/C for extreme case at 800 km altitude. Note: Total drag area is considered as random tumbling drag area.

Maximum altitude 800 km results		
Spacecraft case	**500 kg**	**200 kg**
Mass-to-area ratio needed	16.33 kg/m^2	16.33 kg/m^2
Total drag area needed	30.61 m^2	12.25 m^2
Drag sail area	54.12 m^2	22.81 m^2
STELA decay time	24.19 y	24.18 y

For the smaller spacecraft the drag sail area required is 23 m^2 for a S/C with random tumbling orientation. Despite the smaller area required when compared with the 500 kg S/C, this is still not achievable with the current existing designs. If aerostability can be achieved, the drag area needed to be provided by the sail is halved; only in this case a refined DAS design could be feasible and would allow a compliant re-entry.

7.4.2 Existing design limit

As mentioned before, the achievable sail area was computed with the current Icarus design for the two spacecraft case studies. In Table 7.5 the performance results achievable with the Icarus design are presented.

Two configurations (Fig. 7.14, 7.15) were considered for the 500 kg S/C:

(A) Sail deployed in a plane parallel to the solar panels;
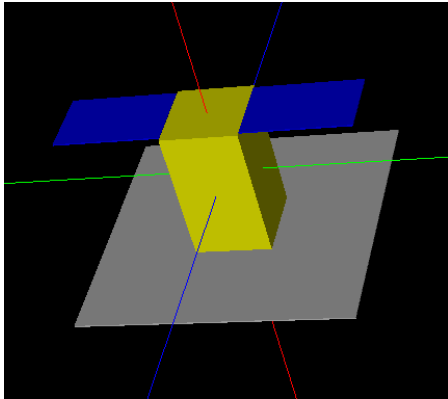
Figure 7.14: Configuration A: Sail deployed in a plane parallel to the solar panel deployable wings.
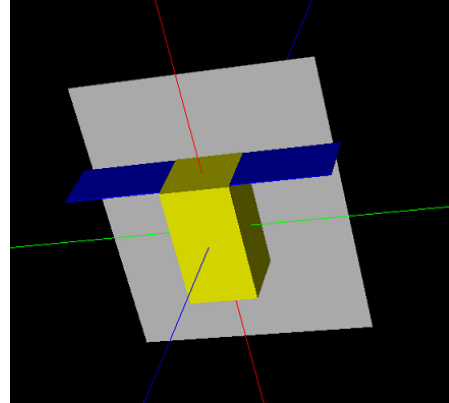
Figure 7.15: Configuration B: Sail deployed in a plane perpendicular to the deployable wings.

(B) Sail deployed in a plane perpendicular to the solar panels.

Table 7.5: Summary of results for 500 kg S/C and 200 kg S/C applying existing DAS Icarus design. Note: Total drag area calculated with STELA random tumbling model.

Existing design limit - Icarus			
Spacecraft case	**500 kg - A**	**500 kg - B**	**200 kg**
Drag sail area	11.69 m^2	13.77 m^2	4.50 m^2
Total drag area	7.97 m^2	8.7 m^2	2.79 m^2
DAS mass	6.18 kg	7.01 kg	3.30 kg
Total m/A	63.51 kg/m^2	58.28 kg/m^2	72.87 kg/m^2
Limit altitude 25 y	685 km	692 km	674 km
STELA decay time	24.77 y	24.81 y	24.75 y

As expected, the random tumbling area of configuration B is better than configuration A (see Fig. 7.16); however, the sail deployment is more constrained, in particular should be taken into account where the frame is going to be attached (on the side, and not the edges) to avoid interference with the deployed wings. In this case having a dihedral angle for the sail and booms deployment would be probably beneficial.
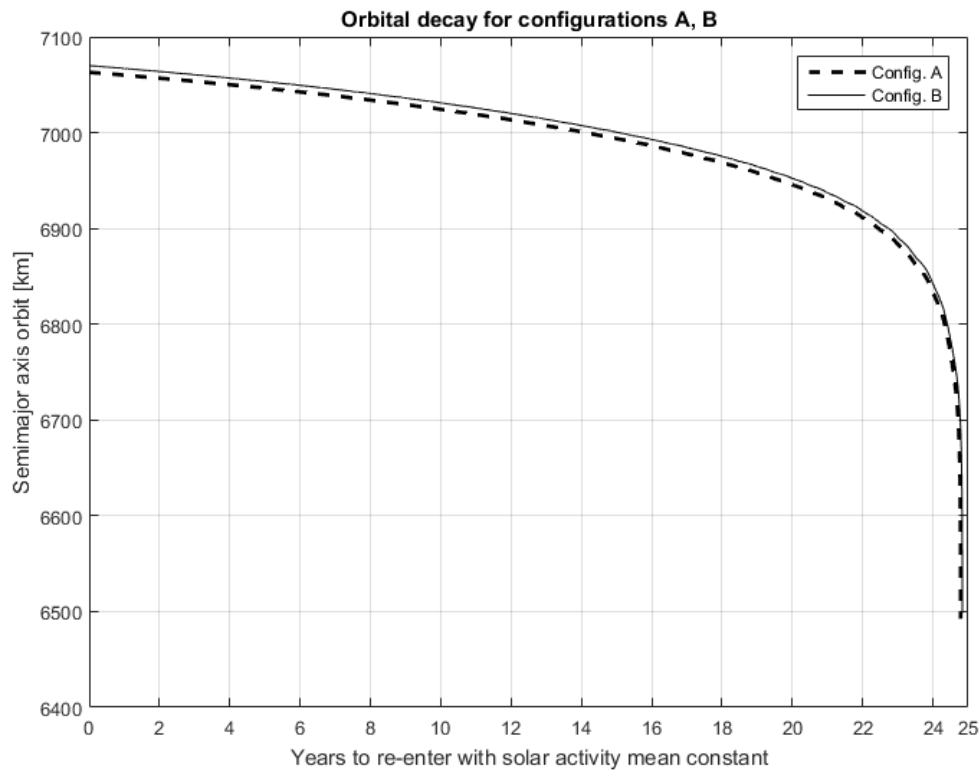
Figure 7.16: Decrease of semi-major axis for 500 kg S/C with existing DAS Icarus design and achievable max altitude to comply with the 25 years requirement.

The configuration selected for the 200 kg (see Fig. 7.17) is instead the one that maximizes the achievable area with the S/C geometry. The configuration for this case resembles the S/C with the Icarus-1 and 3 currently on-orbit.
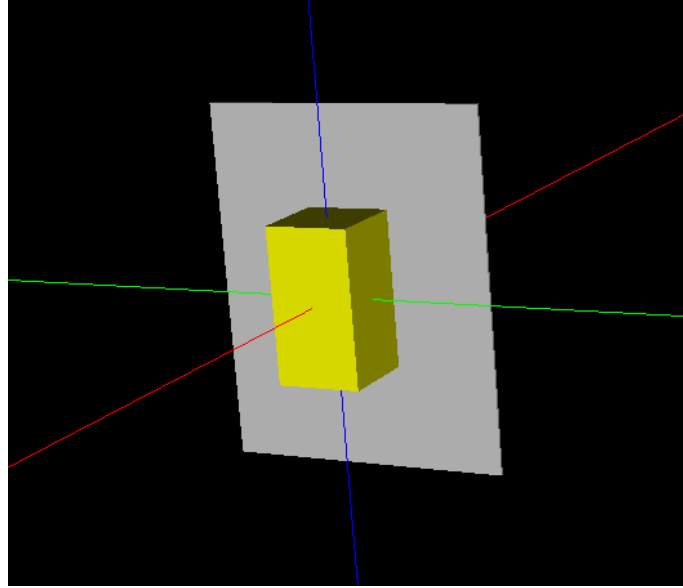
Figure 7.17: Configuration with maximum sail area achievable with existing Icarus design for 200 kg S/C case.

7.4.3   New design limit

The achievable sail area was computed with the proposed DOM evolution design for the 500 kg S/C case (see Table 7.3 for S/C features) only. This case is the most demanding in term of DAS performance.

Different configurations were analysed to evaluate the performances in terms of limit altitude to comply with the 25 year requirement, and area-to-mass ratio. The following configurations were chosen:

- DOM evolution design with standard sail shape and corner configuration;

- DOM evolution design with "fan" sail shape (scalloped sails) and corner configuration;

- DOM evolution design with "fan" sails with two different configurations.

It must be clear that the achievable sail area is not necessary additional area to

the S/C drag surfaces, there can be overlapping with solar panels in parallel planes and/or other panel surfaces.

In the DOM evolution designs considered the limit is given mainly by the length of the boom to be self-supported in 1 g. This is a limit to be easily testable in 1 g, however if this constraint can be removed the upper limit of the sail area could be increased. Care will be needed, however, to confirm that the testing performed is still valid and robust. For this reason the maximum boom length considered in the DOM evolution designs is 1.5 m, however 1 m boom length gives more confidence at the current stage of the DOM design. The mass of the DOM evolution was calculated from the design parameters analysis performed as shown in Section 7.2.2.2.

Table 7.6: Summary of results for 500 kg S/C applying DAS with DOM corner configuration 1.5 m booms. Note: Total drag area calculated with STELA random tumbling model.

DOM evolution design limit - corner configuration		
Configuration	**Standard corners**	**Fan corners**
Drag sail area	6.75 m^2	10.61 m^2
Total drag area	5.36 m^2	7.29 m^2
DAS mass	1.80 kg	2 kg
Total m/A	93.62 kg/m^2	68.86 kg/m^2
Limit altitude 25 y	655 km	679 km
STELA decay time	24.88 y	24.91 y

In this configuration two DOM evolution devices are attached on opposite corners of the S/C panel parallel to the solar panels, resulting in a configuration similar to Icarus in terms of deployed drag area. In this case the two DOM deployed sails are slightly overlapping each other, however this is not a problem if the two DOM are integrated with plate supports of different thickness (or one sunk in the panel and the other not). In this way the sails deploy in parallel but different planes.

To gain additional drag area, without modifying the design adopted in the pre-
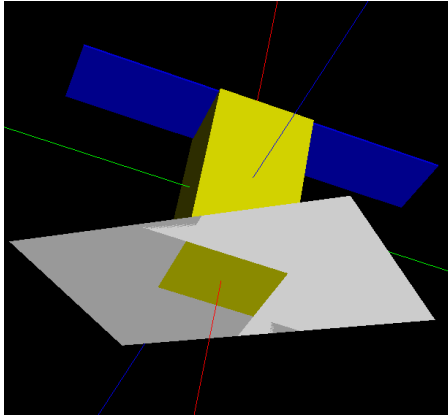
Figure 7.18: Configuration with two DOM 1.5 m booms - Sails deployed in a plane parallel to the solar panel deployable wings.
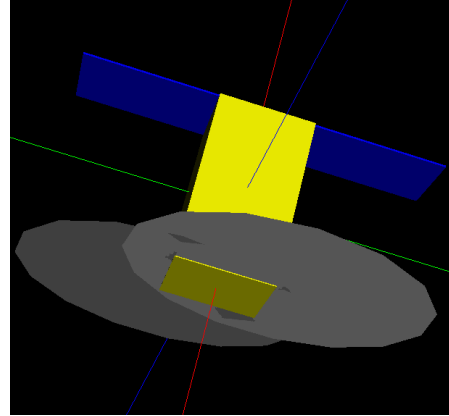
Figure 7.19: Configuration with two DOM 1.5 m booms with scalloped sail - Sails deployed in a plane parallel to the solar panels.

vious configuration, the triangular sail shape can be modified in a "fan" shape, i.e. the external edge will be circular instead of straight.

As can be seen in Table 7.6, the main advantage of this design is a better area-to-mass ratio of the device, having the same boom length and only minor additional mass given by the sail. The additional sail area respect to the standard triangular shape is given by a factor of $\pi/2$. As a consequence, the altitude limit to meet the 25 years requirement is higher.

The DOM evolution design is pretty flexible and different configurations can be used depending on the S/C and presence of appendages, protruding parts, etc. In Table 7.7 two example of possible configurations analysed are presented.

The first configuration (Fig. 7.20) has three DOM evolution devices: two of them with 1.5 m boom length and three sails each (corner configuration type design), the other with 0.9 m boom and edge configuration. All the three devices deploy their sails in planes perpendicular to the solar panels.

The second configuration (Fig. 7.21) is composed by two DOM with 1.5 m boom

Table 7.7: Summary of results for 500 kg S/C applying DOM evolution design with two examples of different configurations. Note: Total drag area calculated with STELA random tumbling model.

	DOM evolution design limit	
	Configuration 1	**Configuration 2**
Description	3 DOM evolution devices: 2 DOM evolution 1.5 m booms on corners, sails deploy perpendicular plane to solar panels; 1 DOM on edge 0.9 m booms on S/C edge, sails deploy in another perpendicular plane to solar panels.	2 DOM evolution devices: 1.5 m booms on S/C edges, sails deploy parallel plane with solar panels but no overlapping area.
Total drag area	7.44 m^2	6.79 m^2
DAS mass	2.53 kg	1.5 kg
Total m/A	67.54 kg/m^2	73.86 kg/m^2
Limit altitude 25 y	680 km	673 km
STELA decay time	24.78 y	24.74 y

length, each one with edge configuration (two sails and three booms). In this configuration the sails are deployed parallel to the solar panels but without any area shadowed by the deployable panel wings.
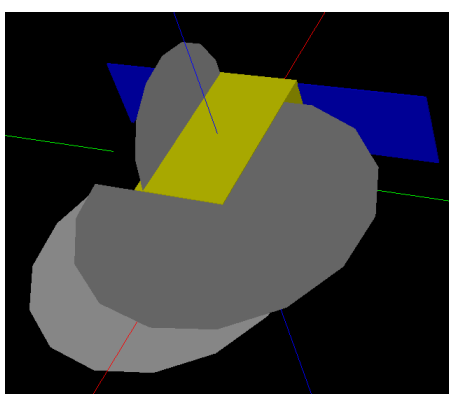
Figure 7.20: Configuration 1 with three DOM evolution devices - Sail deployed in planes perpendicular to the solar panel deployable wings.
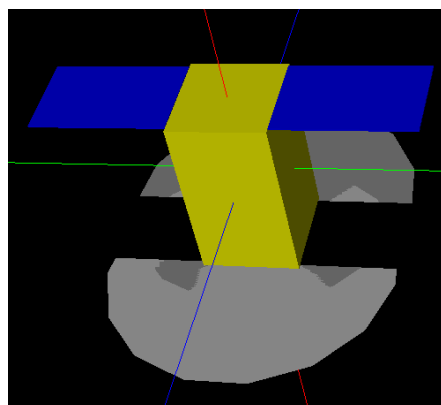
Figure 7.21: Configuration 2 with two DOM evolution devices - Sail deployed in a plane parallel to the solar panel deployable wings.

7.5   Orbital environment analysis

In this section the DAS performances against the effects of atomic oxygen erosion and the debris risk during the de-orbit phase are presented. The analyses performed are in response to the requirements BB13-CU-13 and BB13-CU-14.

7.5.1   ATOX analysis

The compliance to the ATOX environment requirement BB13-CU-13 was assessed to evaluate the degradation of the vapor-deposited aluminum (VDA) Kapton sail with respect to the orbital decay.

The case suggested to be analysed is a re-entry starting from an orbit altitude of 600 km and decay time of 25 years (see Table 7.8). This represents the worst case for the VDA Kapton sail (to be noted the VDA is on both sides of the sail), as the spacecraft will remain longer time in low and very low orbit, where the ATOX levels are higher.

Table 7.8: Summary of results for ATOX decay simulation.

ATOX case 600 km 25 y	
Spacecraft mass	500 kg
Mass-to-area ratio	192 kg/m^2
Random tumbling drag area	2.6 m^2
STELA decay time	23.84 y

The ATOX flux erodes spacecraft surfaces and also causes drag on the spacecraft. Since the same flux is responsible for both effects a relationship can be established between ATOX erosion rate and orbital energy loss for orbit heights where ATOX is the dominant atmospheric gas.

Figure 7.22 gives atomic ATOX fluence as a function of orbit altitude and solar
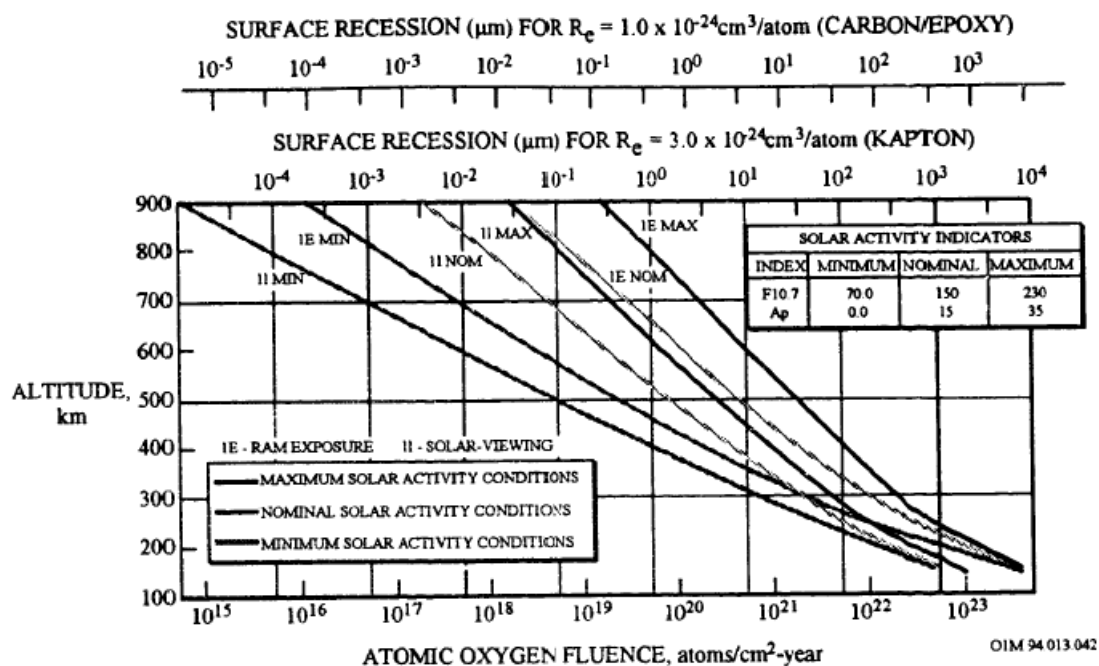
Figure 7.22: Atomic oxygen fluence for the ram (1E) and sun-facing (1I) directions, Figure 2-1, 4-1 from [Silverman, 1995].

activity for the ram (1E) and sun-facing (1I) directions. Considering a ram facing surface with average solar activity conditions the ATOX fluence (1E NOM) at different altitudes can be extrapolated from Fig. 7.22. From the decay profile obtained with STELA simulator the time spent at the different altitude ranges can be derived. In this way, having the ATOX reaction efficiency of the Aluminized Kapton (1 x 10^{-25} cm^3/atom, see Fig. 7.23.) from [Silverman, 1995], a preliminary estimation of the surface degradation can be performed.

For each 50 km altitude range considered (see Table 7.9) the value of fluence corresponds to the lowest altitude of the interval (worst condition than expected).

Since the spacecraft is assumed to be randomly tumbling, each side of the drag sail (both covered by VDA) is effectively exposed directly to the ATOX flux for only a quarter of the time (so for a 2-sided sail, the effective drag exposure is 2 x 1/4

190

Table 2- 1. Classification of AO Reaction Efficiencies (10^{-24} cm^3/atom) Data

0.01-0.1	.1-.9	1.0-1.9	2-4	>4
Al$_2$O$_3$ (<0.025)	Polysiloxane/ Kapton (0.3)	Various forms of Carbon (0.5-1.3)	Kapton H Polyimide (3.0)	Silver
Al/Kapton (0.1)	Siloxane /Polyimide (0.3)	Epoxies (1.7)	Polycarbonate Resin	
Diamond (0.021)	Polysilane/ Polyimide (0.3)	Polystyrene	Polyester	
ITO/aluminized Kapton (0.01)	401-C10 (flat black)	Polybenzimidazole	Polysulphone	
SiOx/aluminized Kapton (0.01)	Z-306 (flat black)	Kevlar/Epoxy	Mylar	
Al$_2$O$_3$, 700Å on Kapton H (<0.02)		LDEF Carbon/Epoxy (˜1.0)	Polyethylene	
Silicones	Apiezon Grease		Tedlar, clear (3.2)	
Fluorpolymers	Tedlar (white)		Z-302(glossy black)	
Teflon FEP	Osmium (bulk)		STS Carbon/Epoxy (2.1-2.6)	
MgF$_2$ on Glass				
Mo (0.006)				
S Glass/Epoxy (0.14)				

Figure 7.23: Materials ATOX erosion yield ranges [Silverman, 1995].

= 1/2 which is the effective drag area factor assumed for a randomly tumbling flat surface).

Although from this first rough estimate it can be seen that the total surface degradation exceeds the thickness of the VDA Kapton sail (which is 25 μm); the initial erosion on any one surface is barely 1 μm for the first half of the de-orbit period (note that the estimate uses worst case assumptions of erosion rate). However, this is still close to the thickness of the Al coating of the sail and so it is possible that the sail will begin to erode more quickly around this time.

Design precautions, which could be included to mitigate this effect, include using thicker Al coatings and/or multiple layers or thicker aluminised Kapton. Nevertheless, undercutting of aluminized Kapton is not predictable. In addition, the material is perforated (and will suffer micrometeoroid damage), which is advantageous during

191

Table 7.9: Surface degradation for aluminised Kapton with decay profile of ATOX simulation 600 km 25 y decay.

Altitude range (km)	ATOX fluence (atoms/cm^2 year)	Time at h (years)	Time (% years)	Surface deg (cm)	Surface deg (μm)
600-550	4.00E+20	12.5	52.15	0.0005	5
550-500	8.00E+20	5	20.86	0.0004	4
500-450	1.00E+21	3	12.52	0.0003	3
450-400	2.50E+21	2	8.34	0.0005	5
Below 400	1.00E+22	1.5	6.26	0.0015	15
Tot degradation				0.0032	32

depressurization at launch but at the same time it can lead to faster degradation. On this purpose, the topic requires further study, moreover the data available on the degradation on the VDA Kapton are sparse and the effects are not well known.

However, it must be noted that the decay profile considered is the worst case not only for the degradation of the VDA Kapton sail, but also in term of mass-to-area ratio of the S/C. Indeed, the resulting random tumbling area is 2.6 m^2 for a S/C of 500 kg mass, this drag area is even smaller than the one simulated in the mission case studies without any DAS on-board (see Table 7.3). This means that:

1. the AstroBus S/C (i.e. the 500 kg S/C), even without any DAS, would decay much faster from 600 km of altitude and so it would be less affected by degradation;

2. if we do not consider the AstroBus configuration but an hypothetical S/C, the resulting tumbling area would include only a very small sail area other that the spacecraft surfaces.

7.5.2   Debris risk analysis

The case analysed to assess the risk of debris collision (requirement BB13-CU-14) with the DAS is a re-entry starting from an orbit altitude of 800 km and decay time of 25 years. This is the worst case in terms of debris environment. The decay profile is the same as the 500 kg S/C case presented in Fig. 7.13 (see Table 7.4). The case represents the debris risk for the (maximum 25 years) deployed lifetime only.

MIDAS tool within DRAMA was used to assess the collision risk and impact flux. The orbit altitude was assumed to be constant for distinct time intervals, so
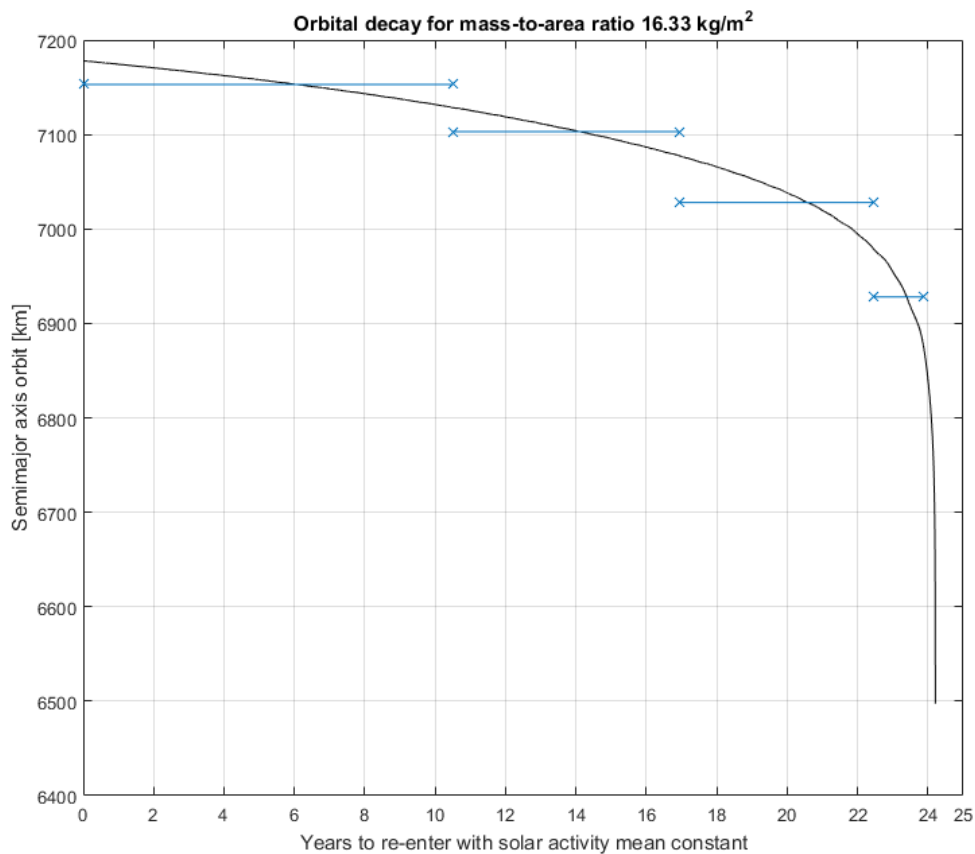
Figure 7.24: Decrease of semi-major axis from 800 km with constant time intervals considered.

multiple target orbits were defined (see Fig. 7.24).

The worst case for the impact vs sail area has been considered, i.e. the 500 kg S/C, which needs a bigger sail area than the 200 kg ones.

The critical size (diameter) of the particle that will lead to (partial and complete) failure of the sail was selected with respect to the boom width of the DOM design.

The reference width is 28 mm and the critical size is debris with diameter d above 1/4 of the boom width, i.e. 7 mm. The debris range considered in the simulation is 7 mm to 1 m, it is assumed that size above 1 m will damage also the S/C so they are already assessed by the S/C integrator.

Table 7.10: Summary of boom surface area for the simulation performed.

Parameter	Value
Area sail (m^2)	54
Boom length (m)	5.196
Boom width (m)	0.028
Single boom area (m^2)	0.145488
Total 4 booms (m^2)	0.581952

The surface defined for the impact flux analysis is a random tumbling plate with cross sectional area equivalent to the sum of the exposed area of four booms. The length of the booms is equivalent to the one needed to deploy a sail of 54 m^2 (see Table 7.10), which would allow a S/C like the 500 kg AstroBus to be de-orbited within 25 years.

Table 7.11: Time intervals with constant altitude as shown in Fig. 7.24 and collision risk results.

Interval	Altitude range (km)	Average a (km)	Time from launch (years)	Time at average h (years)	Cumulative P of collision
1	800-750	7153	10.5	10.5	P<0.0014
2	750-700	7103	16.93	6.43	P<0.0007
3	700-600	7028	22.47	5.54	P<0.0004
4	600-500	6928	23.86	1.39	P<0.00004

194

The sail area is not considered as source of debris, in fact, as described in [Nock et al., 2013] and [Visagie et al., 2015], the potential impact will only leave a hole to the VDA Kapton surface.
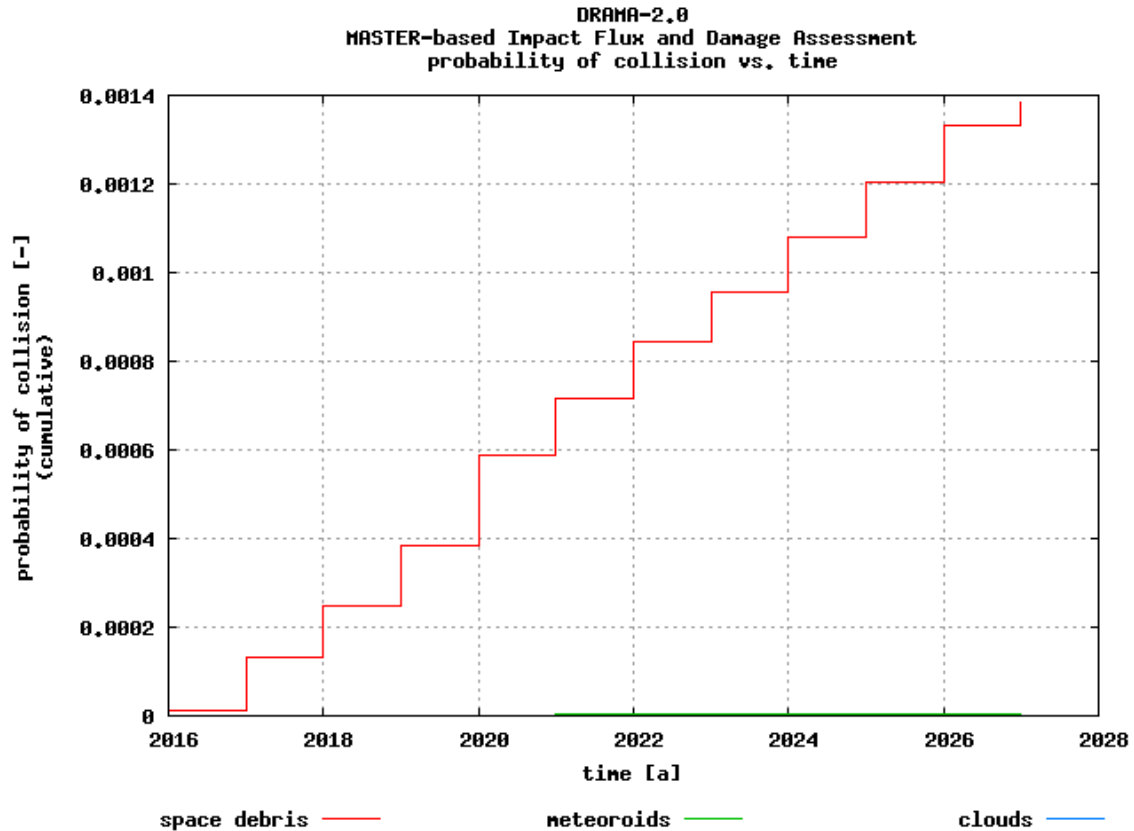
Figure 7.25: Cumulative probability of collision vs time for Interval 1: 775 km altitude for 10.5 years. Note that the cumulative probabilities for meteoroids and clouds cannot be seen since they are more than 2 orders of magnitude smaller than the debris probability.

The scenario considered in MIDAS is "business as usual". The sources considered during the simulations are: space debris (i.e. explosion fragments, collision fragments, launch and mission related objects, etc.), debris clouds (e.g. events comparable to the collision of Iridium-33 and Cosmos-2251), and meteoroids. In Table 7.11 the different time intervals with constant altitude and correspondent

195
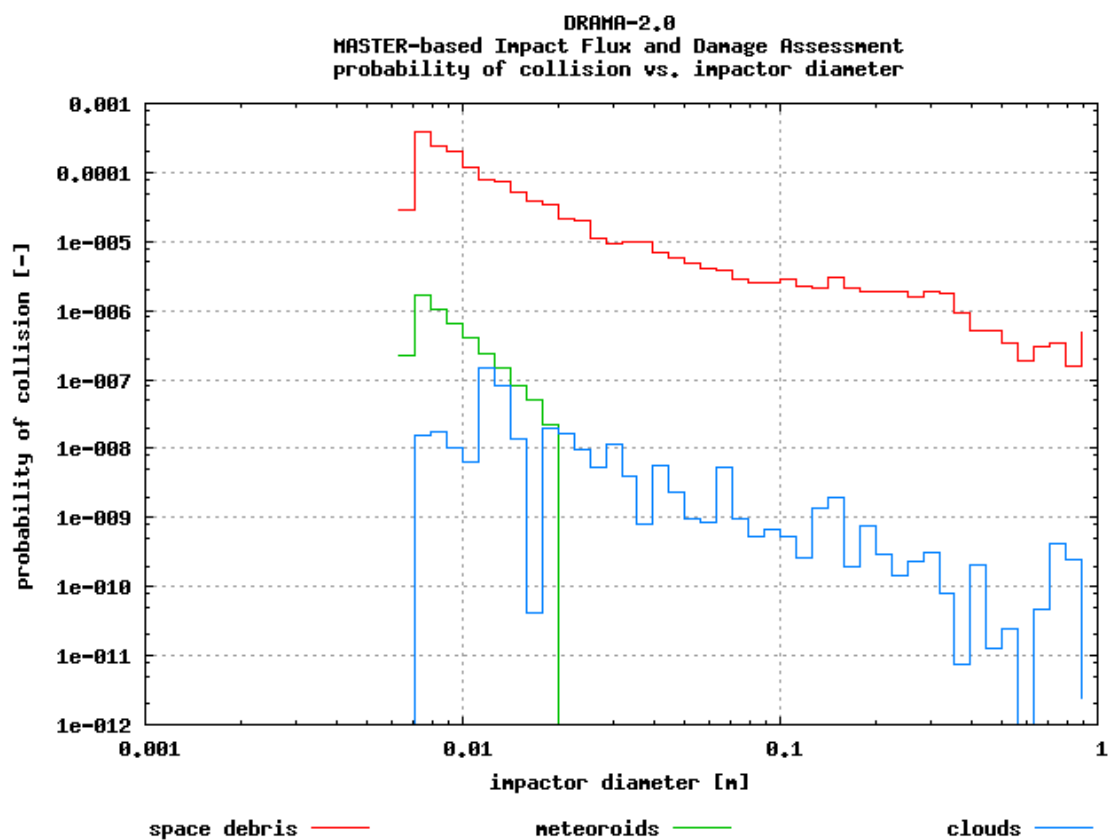
Figure 7.26: Differential probability of collision vs impactor diameter for Interval 1.

results for cumulative probability of collision are shown. As expected, the first interval at 775 km, it is the one with highest risk; however, the probability of collision remains below 0.0014 (see Fig. 7.25).

7.6   Summary

The requirements definition for typical LEO satellites of interest to European LSIs and their detailed analysis show there appears to be a valid role for drag augmentation systems to de-orbit spacecraft in significant LEO regions.

From the design parameters study emerged that the Icarus frame concept is less mass efficient than the DOM Unit but it can be scaled up better.

In the case of the DOM Unit, the sail area increases very rapidly with longer booms, whereas the stowed volume does not increase proportionally. This shows the suitability of the DOM unit to be scaled up.

The satellite categorisation flow diagram developed creates a simple and effective way of categorising a satellite, to allow for easy determination of which of the DAS proposed by Cranfield are compatible and also suggests which de-orbit device is best suited for the satellite.

Risks such as atomic oxygen erosion, damage by other debris and micrometeoroids have been quantified and can be mitigated. Storage lifetime on ground and in-orbit before deployment requires significant further analysis and testing to validate practical component lifetimes.

The study has provided useful input to explore new concepts based on the heritage designs. The DOM Evolution concept, especially with several units installed on one satellite, is probably the most effective method in the short-term for increasing a satellite's drag area. The most promising concept for development is a hybrid concept using components of the two Cranfield DAS heritage designs.

The work is progressing towards the development of hybrid designs based on the two heritage concepts; this will allow Cranfield to offer a family of devices that between them are compatible with a huge range of satellite platforms and could

act as almost off the shelf components that can be selected and easily scaled and implemented onto a customer's satellite.

Chapter 8

Critical Evaluation

In this chapter a critical evaluation of the research outcomes is performed. The contribution to the scientific knowledge and technological advancement in the research field are also presented here.

8.1   Future scenarios for passive de-orbiting

The study on future scenarios investigated the potential spacecraft market for drag augmentation systems. This was to determine the real need for passive de-orbiting and if the development of this type of technology is appropriate.

This shows a different perspective compared with the studies available in the literature [Rasse, 2015] [Harkness et al., 2014], [Kuwahara et al., 2013]; they, in fact, focus on the development of the device/technology itself or target a specific type of satellite (e.g.: drag sail for cubesat), with little or no discussion on the wider market need.

Completing the database by retrieving the needed data from publicly available information has not been an easy task. A good starting point was the use

of SpaceTrak^{TM} database, which was then updated with further data collected from different sources. However, spacecraft integrators, operators, and owners are not usually keen to release information on long term plans for future launches, even less on spacecraft configurations; for this reason, despite a good amount of data, the numbers are underestimated. For example, at the time of the analysis, the large and mega constellations plans were still not publicly announced. Nevertheless, considering the number of satellites involved (e.g.: 648 for OneWeb), mega-constellation will need a proper planning and controlled EoL disposal, which could be achieve only with active de-orbit.

On the other side, a balancing effect is given by delays and changes that often affect space programs. Short term data are easier to retrieve and they are most likely to reflect the real mission in terms of orbit parameters and spacecraft bus.

The confidence in the STELA de-orbit simulator was gained by comparing the real TLE data of decayed satellites with respect to the simulations data. STELA has been confirmed a valid tool for de-orbit analyses, in particular considering the uncertainty in the spacecraft geometry and the influences of the input parameters which affect the orbit propagation.

From the analysis emerged that more than 60% of spacecraft, falling in the small satellite classes, will need to apply a de-orbiting strategy to achieve the re-entry within 25 years. This future scenario is further confirmed by the low compliance rate to SDM (about 30%) of small satellites already on-orbit [Frey et al., 2016].

8.2   Failure analysis of satellites' subsystems

Chapter 5 presents a reliability analysis of spacecraft launched during a certain time period. The reliability is analysed by subsystem and it is then used to assess the

suitability of different de-orbit strategies, based on the required subsystems to be active during the de-orbit device activation or manoeuvre.

The analysis of satellites' subsystems failures was already performed by Saleh and Castet, but in a more general way, encompassing all satellites in all Earth orbits to assess general, rather than specific, reliabilities.

Here instead the reliability study is specifically focussed on guiding the de-orbit strategy selection, with a more targeted classification of satellites and their failures.

The comments received by the journal reviewers on this research work support the novelties just mentioned:

"This work is novel as it explores which de-orbit device is more appropriate based on reliability data".

"The concept that you are presenting is certainly of interest. De-orbiting poses a complicated problem because it is so intertwined with other mission considerations, and many alternatives exist. There is a need for a set of guidelines on which alternative will be best. In addition, satellite and mission designers can make use of the outcome of this paper".

It must be emphasised that the attribution of failure/anomaly to the specific subsystem, part, component poses a significant challenge and this can affect the analysis results. As pointed out in the SCAF (S/C Anomalies and Failures) workshop 2014 organized by D. McKnight, subsystems failures and anomalies do not have a framework/process for sharing them in the space community and quite often the real cause is unknown. If a common format for failure determination could be achieved this would improve our understanding of the satellite's reliability and the effects of the space environment which could trigger the anomalies.

The approach followed does not consider the reliability of the de-orbit method itself, only the host spacecraft subsystems that are required for the de-orbit method.

This does not assume that the de-orbit device/method selected is perfectly reliable, indeed the reliability and safety of the de-orbit methods themselves are also of great importance in achieving an effective de-orbit solution, however the assessment of these reliabilities was outside the scope of this work. The reliability of the DAS was instead relevant in the requirements analysis and in the DOM development.

As expected, spacecraft equipped with propulsion subsystem show a higher reliability than the ones without; however, the attitude subsystem has the worst reliability and this is particularly relevant for the selection of the de-orbit strategy.

After the reliabilities were combined in series and the trade-off analysis was performed, propulsive results the preferred choice by large spacecraft and boom supported film aerobrake for smaller spacecraft.

The outcome of this study together with the forecast scenario have identified particular target classes of satellite to which passive drag augmentation devices are most suitable for de-orbit. In this way the next phase of the PhD, which was the evaluation of the applicability of the design and review the requirements of the de-orbiting system, was performed in the most rigorous and robust way.

8.3   Future applicability of DAS

In Chapter 6, the additional drag area required to achieve a re-entry within 25 years for the sample of non-compliant spacecraft is evaluated.

The sample was obtained from the forecast analysis and then used as input for this study. For this reason, we need to take into account that the total number of spacecraft can be underestimated, and at the same time, some spacecraft of the sample have already been launched (the time frame for the sample was 2015-2020).

The additional drag area needed was then compared with the sail area that can

be provided to the spacecraft using an available DAS design, i.e. the Icarus design and the DOM design. In this way, we link up the target spacecraft market for passive drag de-orbiting with the DAS design currently available. This is useful because it allows understanding the scalability needed for Icarus and DOM, and the modifications required to apply their design to a wider range of satellite platforms.

In a nutshell, it allows quantifying the benefit of making use of the DAS on real spacecraft.

The calculation of the BC limit for the 25 years was performed with a simplified decay model for circular orbits, with atmospheric scale height and density values functions of the constant solar flux. Before employing it for the drag area calculation, it was validated with a test case in STELA and DRAMA orbital decay simulators.

The model showed a good match with STELA results: the decay in STELA is shorter with 2-3 years difference depending on the starting date. The main differences, instead, were detected in DRAMA when using the latest prediction model for the solar activity. The latest predictions results are rather pessimistic (longer re-entry time, i.e. lower solar flux) when compared with the other solar flux models used, moreover, they are affected by the updated input on the solar flux data. The latest predictions seem more suitable for short term orbit propagation, instead of using them for a 25 year limit decay assessment, which covers anyway two solar cycles within the de-orbiting time.

Despite the differences described, the simplified model can be a useful and easy tool to quickly verify the requirements compliance, in particular in the preliminary phases of a mission.

When computing the BC limit for a specific spacecraft is advisable to have a 10% margin in the de-orbit time, as suggested by the ISO for lifetime estimation [BSI Standards Publication, 2011b]. This is because the model makes use of equations

fitted to pre-computed orbit lifetime estimation data. The additional area needed will increase slightly, but the re-entry is assured to be compliant with the 25 years, despite the solar flux variations.

Another factor which deserves attention is the random tumbling configuration for the cross sectional area calculation. This assumption was taken since the effects of aerostability (i.e. the aerodynamic torques act to turn the sail so that it is perpendicular to the flow) haven't been quantified properly for the DAS. Some work was performed for Icarus-1 [Hobbs et al., 2013], derived from [Roberts and Harkness, 2007], selecting a shallow rectangle based pyramid configuration for the sail; however, this is not sufficient to guarantee the maximization of the drag area in the velocity direction. The detailed configurations of the spacecraft in the sample are not known, these are required to quantify the stability effect on the system. Moreover, the DOM does not have a pyramidal sail configuration, which instead could provide some stability effects as showed in [Long and Spencer, 2016].

Furthermore, the random tumbling assumption appeared afterwards in the CleanSat study. A specific requirement from the LSIs was to assume random tumbling configuration to estimate the effective deployable area.

Nevertheless, further work on the topic would be beneficial to optimize the sail design configuration and the positioning on the spacecraft.

The work was particularly useful for the CleanSat study and to give an overview to the LSIs and ESA of the capabilities of the current design with respect to the spacecraft platforms.

8.4   DAS payload projects

The practical work involved two different DAS payload: Icarus-3 for SSTL Carbonite-1 and DOM for ESA ESEO mission.

8.4.1   Icarus-3 for Carbonite-1

Icarus-3 allowed the use of STELA tool on a real project with better understanding of the geometrical modelling and input parameter influences on the results.

The involvement in the project included performing orbit decay calculation and report delivery for the SSTL satellite with Icarus-3.

The work performed allowed gaining further confidence in the use of STELA tool. This was particularly useful considering the piece of research on the future scenarios where STELA was used extensively to calculate the decay times. Understanding the influences of the input parameters and how they affect the results (e.g.: drag coefficient variation, solar flux cycle) was a fundamental aspect. In addition, the modelling of the spacecraft from available CAD drawings was a good practice to determine how to simplify the geometry, without compromising the integrity of the results.

It must also be reminded this is a real case application of de-orbit analysis. Indeed, the calculations performed to simulate the orbital decay using Icarus-3 and predict the re-entry time of Carbonite-1 were reported in a technical note delivered to the UK Space Agency. The document was needed to obtain the launch licence for the satellite Carbonite-1. This probably represents the first case in which a passive drag-augmentation payload has been used to meet the SDM requirements needed to achieve the launch licence.

8.4.2   DOM for ESEO

In parallel with the research work performed, there has been full involvement, as DOM Payload Engineer, in the development and delivery of the De-Orbit Mechanism.

The DOM represents a complete project work from the analysis to design, test and delivery. It gave better insight on real engineering issues with respect to the main aim of the thesis.

The work involvement started at the beginning of the PhD, in phase B of the mission just before the Preliminary Design Review (PDR) milestone. During this phase, the DOM was just a prototype model. The Critical Design Review (CDR) was achieved in 2015. This milestone was reached after the development of the engineering model (EBB model) and the test campaign performed to qualify it and demonstrate its suitability for flight. After a period on-hold due to delays in the satellite integration, the DOM Test Readiness Review (TRR) was performed and successfully passed in January 2017. This led to the flight model building followed by the acceptance test campaign. The delivery of the PFM is scheduled in June.

Having followed a rigorous process for flight qualification for a specific mission, the development of the De-Orbit Mechanism represents an advancement from a technological point of view in the field of design solutions for SDM.

The DOM is actually a technological demonstrator, however, a design based on the DOM refinement can be applied on light microsats and nanosatellites, which will be a relevant market share in the near future.

8.5   Development of a family of scalable DAS

8.5.1   CleanSat building block

The objective of the *CleanSat: technology assessment and concurrent engineering in support of LEO platform evolutions* was to mature specifications for Building Blocks for future LEO spacecraft [ESA, 2015a].

Cranfield Space Research group proposed a *Building Block on Drag-Augmentation System Modules for Small Satellites* submitting a proposal to the ESA AO on 16th July 2015.

The proposal was prepared thanks to different input from this research, for example, the analyses performed for the future scenarios for passive devices were included, and the project work for the DOM and Icarus-3 highlighted the technological background.

The proposal was successfully accepted, this shows the relevance and significance of the work performed and the planned activities both for the agency and the major players of the European space industry.

The CleanSat study fitted perfectly with the final phase of the PhD. The final steps were the requirements definition of the DAS, and developing further the current heritage designs into a family of COTS products to commercialise.

A further justification about the relevance of the research performed and the Cranfield CleanSat study is given in the recent *ESA Compendium of potential activities for Clean Space*. Here a specific activity on *prototype and qualification of a drag augmentation de-orbiting subsystem* is proposed (and budgeted) with the aim to bring the technology from a TRL 5 to a TRL 7.

8.5.2 Requirements analysis

The requirements analysis performed during the CDF study showed a good matching between Cranfield internal DAS requirements and top-level requirements from customer's perspective.

The work was useful to identify the customers' needs with respect to the potential technology offered. In the previous research works performed on drag sails, quite often this aspect is not properly evaluated, with the risk of developing a technology that will not be exploited in the near future.

At the current TRL, the DAS is compliant with most of the requirements.

Risks such as atomic oxygen erosion, and damage by other debris and micrometeoroids were quantified and can be successfully mitigated. Nevertheless more detailed analyses would allow to quantify processes which may degrade the sail once deployed and before final demise, and identify design changes to achieve the required performance.

The storage lifetimes on ground and in-orbit before deployment require significant further analysis and testing to validate practical component lifetimes. More time is definitely needed to perform life testing of components for ground and on-orbit storage and quantify the factors for potential degradation of the DAS performances.

8.5.3 DAS family

The main aim was to develop drag augmentation devices for de-orbiting a range of different spacecraft at the end of life, so to have a product family design.

The investigation of the scalability of the concepts already developed was fundamental to evaluate the design options which provide optimal matches for a range

of satellite sizes and platform configurations.

The design parameters analysis together with the customer's requirements study provided useful input to explore new concepts based on the heritage designs; these concepts are evolutions of the DOM and hybrid designs. The hybrid design combines aspects of the Icarus and the DOM concepts to reduce the limitations of the respective individual devices and improve scalability, adaptability and manufacturability.

The interest on the DAS family development has grown not only in Europe but also in other contexts, for example the article presented at the IEEE Aerospace conference in US was peer reviewed and then accepted.

In addition, this work is helping to achieve commercial readiness for the technology. This will enable development of a commercial DAS offering that will be an attractive solution for small satellite integrators, allowing them to meet debris mitigation requirements. Indeed, currently there is interest in commercializing the DAS device.

Chapter 9

Conclusions

This chapter summarizes how the PhD objectives have been achieved. Recommendations for future research work are also provided.

9.1 Summary of achievements

The aim of this research was to develop drag augmentation systems for de-orbiting small spacecraft at the end of life, to ensure they comply with Space Debris Mitigation requirements. This has been achieved through specific, measurable and realistic objectives.

1. **Assess the feasibility for potential commercial use of DAS**

   This was achieved by identifying the current status of SDM guidelines/requirements and their implementation by space agencies and different countries; by evaluating the current markets forecast, which showed a growth of micro and smaller satellite, making them a target for passive de-orbiting devices; by reviewing the de-orbiting strategies and their pros and cons.

2. **Identify and review the state of the art on drag de-orbiting**

A review of the current technologies for passive drag augmentation de-orbiting was performed. Cranfield technological heritage was evaluated looking at limitations and advantages of the designs developed so far. In addition, practical work involved the Icarus-3 payload, currently on-board Carbonite-1.

3. **Determine the need for passive de-orbiting in the future**

   The study on future scenarios investigated the potential spacecraft market for drag augmentation systems. This was performed by developing future launches database; by computing satellites' decay with STELA, by identifying future spacecraft compliances with SDM. More than 60% of future spacecraft between 10 and 1000 kg will need to employ de-orbit strategies; they represent a target for passive drag augmentation devices.

   Novelty: wider market need for passive de-orbiting.

   Publication: *Forecast analysis on satellites that need de-orbit technologies: future scenarios for passive de-orbit devices* [Palla and Kingston, 2016b].

4. **Assess satellites' subsystems failures**

   The assessment was achieved by compiling a database of subsystems failures, by analysing statistically the subsystems reliabilities, by combining the reliabilities as function of the subsystems needed by de-orbit strategies, by performing a trade-off analysis to guide the strategy decision.

   Novelty: detailed insight into LEO satellites reliabilities with the purpose of guiding the de-orbit strategy selection.

   Publication: *Failure analysis of satellite subsystems to define suitable de-orbit devices* [Palla et al., 2016].

5. **Assess the applicability of DAS design**

   The design applicability was assessed by developing a simple model for prelimi-

nary drag area calculation, by validating the model with STELA and DRAMA, by calculating the additional area needed vs the area provided by DAS for S/C sample.

Novelty: Link between the target spacecraft market for passive drag deorbiting and the DAS designs available; quantifying the benefit of making use of the DAS on real spacecraft.

Conference paper: *Applicability of drag augmentation systems to enable future LEO spacecraft compliance with debris mitigation guidelines* [Palla and Kingston, 2016a].

6. **Analyse requirements of DAS**

The requirements were analysed considering the customer's needs (coming from CleanSat study) with respect to the internal design drivers. The compliance of the DAS baseline designs was assessed by means of performance analyses, review of design, testing (performed or planned).

Conference paper: *Development of Commercial Drag-Augmentation Systems for Small Satellites* [Palla et al., 2017b].

7. **Evaluate the scalability for a DAS family**

This was achieved by performing a design parameters analysis on the Icarus and DOM concepts, and by assessing their compatibility with spacecraft platforms. The design parameters analysis together with the requirements analysis provided useful input to explore new concepts based on the heritage designs; these concepts are evolutions of the DOM and hybrid designs.

Novelty: development path for a scalable family of DAS; helping to achieve commercial readiness for DAS offering.

Conference paper (peer-reviewed): *Development of a Family of Scalable Drag*

213

Augmentation Systems [Palla et al., 2017a].

8. Develop DOM payload technological demonstrator

The DOM design was refined from prototype model to EBB model, EBB and PFM have undergone full test campaign for flight qualification, now the DOM PFM is ready for delivery.

Novelty: the development of the De-Orbit Mechanism represents an advancement from a technological point of view in the field of design solutions for Space Debris Mitigation.

9.2   Future work

This research work has laid the foundation for a commercialisation of a family of DAS. However, several areas need to be addressed before the DAS technology will be ready for commercial use.

In short term MSc individual research projects will focus on new design, testing, and materials performances for the DAS. Specifically the following thesis projects were proposed and have just started:

- *De-orbit mechanism redesign*: the development and prototyping of the hybrid design is the focus of this project. This will be based on an iterative process between CAD modelling, lab prototyping and testing.

- *Materials selection and performance for drag sails*: materials alternatives for the DAS devices need to be investigated; this involves both sail material and mechanism components. The materials performances and degradation on orbit (with respect to e.g.: atomic oxygen, radiation environment, debris impact) will be analysed.

- *Drag augmentation systems design study*: this will focus on scaling up the DOM evolution concept, with possible prototyping. It will also investigate possibilities to combine drag augmentation and propellant-based de-orbit strategies, and how such approaches can be optimised.

The outcomes of these projects can help bringing the new design concepts to higher TRL (possibly TRL 6), quantifying processes which may degrade the sail once deployed and identifying design changes to achieve the required performance. Indeed, during the CleanSat study, it emerged that the deployed lifetime performance required further study.

Moreover, recommendations for further work and a long term development plan should focus on:

- Hybrid concept: development to a comparable level of maturity as the existing Icarus and DOM concepts;

- Storage lifetime: quantify processes which may degrade the DAS while stored on-ground and on-orbit (e.g.: perform life testing of components);

- Attitude dynamics: understand effects of a deployed DAS on attitude and to what extent aerostability may increase its effectiveness;

- Market analysis: continued study of potential markets for DAS to ensure that the engineering design meets commercial needs;

- Flight opportunities: identify opportunities for technology demonstration of new designs.

Furthermore, the planned observation campaign for the deployment of Icarus-1 and Icarus-3, and evaluation of the subsequent effect on the orbits of the TDS-1 and Carbonite-1 satellites, will allow validation of the operation of the DAS technology.

Successful demonstration of on-orbit deployment and confirmation of the increased drag effect produced, would justify that TRL 9 has been achieved for this design of DAS.

References

Airtec (2017). The CYPRES Cutter. `https://www.cypres.aero/products`. Last accessed 17/03/2017.

AlmaSpace (2013). ESEO Mission Analysis Report. Technical report.

Anatoly, Z. (2015). RussianSpaceWeb. `http://www.russianspaceweb.com`. Last accessed 20/01/2015.

Antonetti, S., Ferrario, L., Toson, E., and Rossettini, L. (2015a). Implementation of Debris Prevention and Reduction Measures by an Independent Propulsive Decommissioning Device. In *66th IAC 2015 proceedings*, Jerusalem, Israel.

Antonetti, S., Rossettini, L., and Ferrario, L. (2015b). Contributing to Orbital Sustainability with an Independent Decommissioning Device for Satellite and Space Launcher Implementing Space Debris Mitigation Measures. In *5th CEAS Air & Space Conference*, Delft.

Bentley, J. P. (1999). *Introduction to reliability and quality engineering.* Harlow: Addison-Wesley, 2nd edition.

Bonnal, C. (2016). A brief historical overview of space debris mitigation rules. In *Clean Space Industrial Days*, ESTEC, ESA.

Brooks, D. R., Gibson, G. G., and Bess, T. (1974). Predicting the Probability that Earth-Orbiting Spacecraft will Collide with Man-Made Objects in Space. In *American Astronautical Society, Scientific Technology Series*, volume 3.

BSI Standards Publication (2011a). ISO 24113:2011 Space systems - Space debris mitigation requirements.

BSI Standards Publication (2011b). ISO 27852:2011 Space systems - Estimation of orbit lifetime.

Buchen, E. and DePasquale, D. (2014). 2014 Nano/Microsatellite Market Assessment. Technical report, SpaceWorks Enterprises, Atlanta, GA.

Castet, J.-F. and Saleh, J. H. (2009). Satellite and satellite subsystems reliability: Statistical data analysis and modeling. *Reliability Engineering & System Safety*, 94(11):1718–1728.

Castet, J.-F. and Saleh, J. H. (2010). Beyond reliability, multi-state failure analysis of satellite subsystems: A statistical approach. *Reliability Engineering & System Safety*, 95(4):311–322.

Chobotov, V. A. (2002). Orbital Debris Hazards Assessment and Mitigation Strategies. In Smirnov, N. N., editor, *Space debris: hazard evaluation and mitigation*, pages 1–23. Taylor and Francis.

Christensen, I., Vaccaro, D., and Kaiser, D. (2010). Market Characterization: Launch of Very-Small and Nano Sized Payloads Enabled by New Launch Vehicles. In *61st IAC 2010 proceedings*, Prague, Czech Republic.

CNES (2013). STELA User's Guide.

D-Orbit (2015). D-Orbit Decommissioning Device. `http://www.deorbitaldevices.com/site/our-technology/`. Last accessed 01/08/2015.

Dolado-Perez, J., Morand, V., Le Fevre, C., Handschuh, D., and Philippe, T. (2014). Analysis of mitigation guidelines compliance at international level in low earth orbit. In *65th IAC 2014 proceedings*, Toronto, Canada.

Dolado-Perez, J. and Revelin, B. (2015). The Effect of Uncertainties on the Effectiveness of Mitigation and Remediation. In *66th IAC 2015 proceedings*, Jerusalem, Israel.

Doncaster, B. and Shulman, J. (2016). 2016 Nano/Microsatellite Market Forecast. Technical report, SpaceWorks Enterprises, Atlanta, GA.

ECSS Secretariat (2008). ECSS-E-ST-10-04C Space environment.

ECSS Secretariat (2009a). ECSS-E-ST-10-02C Verification.

ECSS Secretariat (2009b). ECSS-E-ST-33-01C Space Engineering - Mechanisms.

ESA (2014a). Clean Space. `http://www.esa.int/Our_Activities/Space_Engineering/Clean_Space`. Last accessed 15/01/2014.

ESA (2014b). DRAMA Software User Manual.

ESA (2015a). CleanSat : Technology assessment and concurrent engineering in support of LEO platform evolutions, ESA-TEC-SC-SOW-2015-001.

ESA (2015b). Earth Observation Portal. `https://eoportal.org/web/eoportal/satellite-missions`. Last accessed 20/01/2015.

ESA (2016). Clean Space - The Challenge. `http://www.esa.int/Our_Activities/` `Space_Engineering_Technology/Clean_Space/The_Challenge`. Last accessed 30/03/2017.

ESA Clean Space (2016). Cleansat presentation. In *Clean Space Industrial Days*, ESTEC, ESA.

ESA Director General's Office (2014). ESA/ADMIN/IPOL(2014)2 - Space Debris Mitigation for Agency Projects.

ESA Education (2014). ESEO mission. `http://www.esa.int/Education/ESEO_` `mission`. Last accessed 30/03/2017.

ESA SDM WG (2015). ESSB-HB-U-002 ESA Space Debris Mitigation Compliance Verification Guidelines.

ESA Space Debris Office (2017). Scanning and Observing Space Debris. `http://www.esa.int/Our_Activities/Operations/Space_Debris/Scanning_` `and_observing2`. Last accessed 25/04/2017.

FAA (2013). 2013 Commercial Space Transportation Forecasts.

Foust, J. (2008). If you build it who will come? Identifying markets for low-cost small satellites. In *22nd Annual AIAA/USU Conference on Small Satellites*, Logan, Utah.

Fraysse, H., Morand, V., Le Fevre, C., Deleflie, F., Wailliez, S., Lamy, A., Martin, T., and Perot, E. (2012). Long term orbit propagation techniques developed in the frame of the french space act. *Journal of Aerospace Engineering, Sciences and Applications*, 4(4):1–16.

Frey, S. and Lemmens, S. (2017). Status of the space environment: current level of adherence to the space debris mitigation policy. In *7th European Conference on Space Debris proceedings*, ESA/ESOC, Darmstadt, Germany.

Frey, S., Lemmens, S., Virgili, B. B., and Flohrer, T. (2016). Level of Adherence to SDM Guidelines. In *Clean Space Industrial Days*, ESTEC.

Grinham, D. and Kingston, J. (2016). *Drag Augmentation Systems Design Study.* Msc thesis, Cranfield University.

Harkness, P., McRobb, M., Lützkendorf, P., Milligan, R., Feeney, A., and Clark, C. (2014). Development status of AEOLDOS - A deorbit module for small satellites. *Advances in Space Research*, 54(1):82–91.

Hobbs, S., Kingston, J., Roberts, P., Juanes, C., and Sewell, R. (2013). De-Orbit Sail Design for Techdemosat-1. In *6th European Conference on Space Debris proceedings*, ESA/ESOC, Darmstadt, Germany.

IADC (2007). IADC Space Debris Mitigation Guidelines.

Innocenti, L. and Soares, T. (2013). Clean Space Initiative: Status of Implementation. Technical report, ESA.

Janhunen, P. and Toivanen, P. (2016). Electrostatic plasma brake for deorbiting. In *Clean Space Industrial Days*, ESTEC.

Kaplan, E. L. and Meier, P. (1958). Nonparametric Estimation from Incomplete Observations Source. *Journal of the American Statistical Association*, 53(282):457–481.

Kelso, T. (2014). NORAD Two-Line Element Sets Current Data. `http://www.celestrak.com/NORAD/elements/`. Last accessed 01/12/2014.

Kessler, D. J. (2009). Significance of the "Kessler Syndrome" Today. `http://webpages.charter.net/dkessler/files/KesSym.html`. Last accessed 25/04/2017.

Kessler, D. J. and Cour-Palais, B. G. (1978). Collision frequency of artificial satellites: The creation of a debris belt. *Journal of Geophysical Research*, 83(A6):2637–2646.

Kingston, J., Hobbs, S., Roberts, P., Juanes-Vallejo, C., Robinson, F., Sewell, R., Snapir, B., Llop, J. V., and Patel, M. (2014). Use of CYPRES^{TM} cutters with a Kevlar clamp band for hold-down and release of the Icarus De-Orbit Sail payload on TechDemoSat-1. *Acta Astronautica*, 100:82–93.

Klinkrad, H. (2006). *Space Debris: Models and Risk Analysis*. Springer Science & Business Media, Chichester, UK.

Klinkrad, H. (2015). Hazard of Orbital Debris. In Pelton, J. N. and Allahdadi, F., editors, *Handbook of Cosmic Hazards and Planetary Defense*, pages 808–834. Springer International.

Krammer, A. and Kingston, J. (2014). *ESEO DeOrbit Mechanism: Synergy between theoretical aspects of payload design and practical engineering application from a systems perspective*. Msc thesis, Cranfield University.

Krebs, G. D. (2015). Gunter's Space Page. `http://space.skyrocket.de/`. Last accessed 20/01/2015.

Kuwahara, T., Yoshida, K., Yuji, S., Tomioka, Y., Fukuda, K., and Sugimura, N. (2013). A series of de-orbit mechanism for active prevention and reduction of space debris. In *64th IAC 2013 proceedings*, Beijing.

Lamy, A., Morand, V., Le Fevre, C., and Fraysee, H. (2012). Resonance Effects on Lifetime of Low Earth Orbit Satellites. In *23rd International Symposium on Space Flight Dynamics*, Pasadena.

Lazare, B. (2013). The French Space Operations Act: Technical Regulations. *Acta Astronautica*, 92:209–212.

Le Fèvre, C., Fraysse, H., Morand, V., Lamy, A., Cazaux, C., Mercier, P., Dental, C., Deleflie, F., and Handschuh, D. a. (2014). Compliance of disposal orbits with the French Space Operations Act: The Good Practices and the STELA tool. *Acta Astronautica*, 94:234–245.

Ley, W., Wittmann, K., and Hallmann, W. (2009). *Handbook of Space Technology*. John Wiley and Sons.

Long, A. C. and Spencer, D. A. (2016). Stability of a Deployable Drag Device for Small Satellite Deorbit. In *AIAA/AAS Astrodynamics Specialist Conference*, Long Beach, California.

Longley, J. (2015). How to make an Icarus drag sail. Technical report, Cranfield Space Research Group.

NASA Safety Standard (1995). Guidelines and Assessment Procedures for Limiting Orbital Debris.

Niehuss, K. O., Euler, H. C., and Vaughan, W. W. (1996). Statistical Technique for Intermediate and Long-Range Estimation of 13-Month Smoothed Solar Flux and Geomagnetic Index. *NASA Technical Memorandum TM-4759*.

Nock, K. T., Aaron, K. M., and McKnight, D. (2013). Removing orbital debris with less risk. *Journal of Spacecraft and Rockets*, 50(2):365–379.

Palla, C., Grinham, D., and Kingston, J. (2017a). Development of a family of scalable drag augmentation systems. In *2017 IEEE Aerospace Conference*, Big Sky, Montana.

Palla, C. and Kingston, J. (2016a). Applicability of drag augmentation systems to enable future LEO spacecraft compliance with debris mitigation guidelines. In *67h IAC 2016 proceedings*, pages 1–11, Guadalajara, Mexico.

Palla, C. and Kingston, J. (2016b). Forecast analysis on satellites that need de-orbit technologies: future scenarios for passive de-orbit devices. *CEAS Space Journal.*

Palla, C., Kingston, J., and Hobbs, S. (2017b). Development of Commercial Drag-Augmentation Systems for Small Satellites. In *7th European Conference on Space Debris procedings*, ESA/ESOC, Darmstadt, Germany.

Palla, C., Peroni, M., and Kingston, J. (2016). Failure analysis of satellite subsystems to define suitable de-orbit devices. *Acta Astronautica*, 128:343–349.

Pardini, C., Hanada, T., and Krisko, P. H. (2009). Benefits and risks of using electrodynamic tethers to de-orbit spacecraft. *Acta Astronautica*, 64:571–588.

Peroni, M. and Kingston, J. (2015). *Reliability study for LEO satellites to assist the selection of End of Life disposal methods.* Msc thesis, Cranfield University.

Petros, E. (2016). Space Debris Mitigations in National Space Legislation. In *Clean Space Industrial Days*, ESTEC, ESA.

Ploss, M. and Hobbs, S. (2013). *ESEO De-Orbiting Device: Concept Exploration and Deployable Boom Arm Design.* Msc thesis, Cranfield University.

Rasse, B. (2015). Satellite Inflatable Deorbiting Equipment. In *Technical Day on De-Orbit Strategies*, ESTEC.

Republique Française (2008). LOI no 2008-518 du 3 juin 2008 relative aux opérations spatiales. *Journal officiel de la république française*, (1 sur 129).

Roberts, P. C. E. and Harkness, P. G. (2007). Drag sail for end-of-life disposal from low Earth orbit. *Journal of Spacecraft and Rockets*, 44(6):1195–1203.

Rossettini, L. (2015). D-Orbit - Solution for our future. In *Technical Day on De-Orbit Strategies*, ESTEC.

Saleh, J. H. and Castet, J.-F. (2011). *Spacecraft Reliability and Multi-State Failures: A Statistical Approach*. John Wiley and Sons, first edit edition.

SatFlare (2015). SatFlare. `http://www.satflare.com`. Last accessed 20/01/2015.

Seffen, K. a. and Pellegrino, S. (1999). Deployment dynamics of tape springs. *Proceedings of the Royal Society A: Mathematical, Physical and Engineering Sciences*, 455:1003–1048.

Seradata (2014). SPACETRAK User Guide v1.4. `http://www.seradata.com/`. Last accessed 30/03/2017.

Silverman, E. M. (1995). Space environmental effects on spacecraft: LEO materials selection guide, NASA Contractor report 4661, part 1. Technical report.

SSTL (2015). EO & Science Platforms CARBONITE-1. `http://www.sstl.co.uk/Products/EO-Science-Platforms/CARBONITE-1`. Last accessed 01/09/2015.

Tanizawa, K. and Miura, K. (1978). Large displacement configurations of bi- axially compressed infinite plate. *Transactions of the Japan Society for Aeronautical and Space Sciences*, 20(50):177–187.

Taylor, R. and Hobbs, S. (2013). *Conceptual development of a de-orbiting payload for micro-satellites in LEO.* Msc thesis, Cranfield University.

Tripepi, G. and Catalano, F. (2004). L'analisi di sopravvivenza con il metodo di Kaplan-Meier. *Giornale Italiano di Nefrologia.*

United Kingdom (1986). Outer Space Act.

Urgoiti, E. (2016). Development of Commodity for removal of expended elements using Electro-dynamic Tether. In *Clean Space Industrial Days*, ESTEC.

Vallado, D. a. and Finkleman, D. (2014). A critical assessment of satellite drag and atmospheric density modeling. *Acta Astronautica*, 95:141–165.

Visagie, L., Lappas, V., and Erb, S. (2015). Drag sails for space debris mitigation. *Acta Astronautica*, 109:65–75.

Wertz, J. R., Everett, D. F., and Puschell, J. J. (2011). *Space Mission Engineering: The New SMAD.* Space technology library. Microcosm Press.

Wertz, J. R. and Larson, W. J. (1999). *Space mission analysis and design.* Microcosm Press; Kluwer Academic Publishers, Torrance,CA; Dordrecht.

Wolfram Research (2016). Arc Length. `http://mathworld.wolfram.com/ArcLength.html`. Last accessed 10/11/2016.

Woodburn, J. and Lynch, S. (2005). A Numerical Study of Orbit Lifetime. In *AAS/AIAA Astrodynamics Specialists Conference*, number AAS 05-297, Lake Tahoe.

Zanutto, D., Lorenzini, E. C., Mantellato, R., Colombatti, G., and Sanchez-Torres, A. (2012). Orbital debris mitigation through deorbiting with passive electrodynamic drag. In *63rd IAC 2012 proceedings*, Naples, Italy.

Appendix A

DOM CAD and tables

A.1   DOM CAD drawings

4x Ø 4Interface

78

135

54

42

2

11

100

UNLESS OTHERWISE SPECIFIED: DIMENSIONS ARE IN MILLIMETERS SURFACE FINISH: TOLERANCES: LINEAR: ANGULAR:	QUANTITY		MANUFACT. INDICATIONS		DO NOT SCALE DRAWING		REVISION	Numb.
	1				*Cranfield* UNIVERSITY Space Research Centre			
	NAME	SIGNATURE	DATE			TITLE		
DRAWN	CP		27/05/14			ESEO DOM Assembly		
CHK'D								
APPVD								
MFG								
Q.A.			MATERIAL: Aluminium, Steel, Plastic			DWG N. Assembly 1		A3
			WEIGHT: $PRPSHEET:{Peso}			SCALE:1:2	SHEET 1 OF 1	

C. Palla

UNLESS OTHERWISE SPECIFIED: DIMENSIONS ARE IN MILLIMETERS SURFACE FINISH: TOLERANCES: LINEAR: ANGULAR:	QUANTITY		MANUFACT. INDICATIONS	DO NOT SCALE DRAWING		REVISION	Numb.
	1			Cranfield UNIVERSITY Space Research Centre			

	NAME	SIGNATURE	DATE			TITLE
DRAWN	CP		19/5/2014			ESEO DOM Top plate
CHK'D						
APPVD						
MFG						
Q.A.			MATERIAL:	DWG N.		A3
			Alu 6061	3		
			WEIGHT: 0.0323 kg	SCALE:2:1	SHEET 1 OF 1	

2x∅3 L7

5

7

32

7

9,5

13,5

A

A

B

B

∅2

∅2

SECTION B-B
SCALE 2 : 1

5

7

SECTION A-A
SCALE 2 : 1

4x∅2 L5

6,4

R12

6,4

7

∅10

11,6

21

| UNLESS OTHERWISE SPECIFIED: DIMENSIONS ARE IN MILLIMETERS SURFACE FINISH: TOLERANCES: LINEAR: ANGULAR: | QUANTITY | | | MANUFACT. INDICATIONS | DO NOT SCALE DRAWING | | REVISION | Numb. |

QUANTITY: 1

Cranfield UNIVERSITY Space Research Centre

	NAME	SIGNATURE	DATE			TITLE
DRAWN	CP		15/05/2014			
CHK'D						ESEO DOM Spool
APPVD						
MFG						
Q.A.				MATERIAL:	DWG N.	

MATERIAL: Alu 6061

DWG N.: 1

A3

WEIGHT: 0.03617 kg | SCALE: 2:1 | SHEET 1 OF 1

6,4

4x⌀4

4x⌀2,4

6,4

⌀11

⌀65

1,5

Note: The 4 small holes shall be suitable for M2 x 4mm
Socket Countersunk Screws   (DIN 7991)

UNLESS OTHERWISE SPECIFIED: DIMENSIONS ARE IN MILLIMETERS SURFACE FINISH: TOLERANCES: LINEAR: ANGULAR:	QUANTITY 2		MANUFACT- INDICATIONS	DO NOT SCALE DRAWING	REVISION	Numb.

Cranfield UNIVERSITY   Space Research Centre

	NAME	SIGNATURE	DATE			TITLE
DRAWN	CP		15/05/2014			
CHK'D						ESEO DOM Spool Plate
APPV'D						
MFG						
Q.A.			MATERIAL: Alu 6061			DWG N. 2

A3

WEIGHT: 0.0129 kg   SCALE: 2:1   SHEET 1 OF 1

SECTION A-A

SECTION B-B

	NAME	SIGNATURE	DATE			
DRAWN	CP		26/01/2016			
REVISION	CP		13/09/2016			
REVISION	CP		02/02/2017			

UNLESS OTHERWISE SPECIFIED:
DIMENSIONS ARE IN MILLIMETERS
SURFACE FINISH:
TOLERANCES:
  LINEAR:
  ANGULAR:

QUANTITY

1

MANUFACT.
INDICATIONS

DO NOT SCALE DRAWING   REVISION   3

Cranfield UNIVERSITY   Space Research Centre

TITLE

ESEO DOM Bottom Plate - Back side

MATERIAL:
Aluminium

DWG N.
5.3

A3

WEIGHT   SCALE:1:1   SHEET 1 OF 1

A.2   DOM verification matrix

Table A.1: Verification Matrix.

Requirements	Subsystem/ Prototype	EBB	PFM
	Status	Status	Status
PHY-EIDA-4100 DOM Payload mass in flight configuration shall be limited to 1.5kg	/	Verified, DDF Parts list	Verified
PHY-EIDA-4200 The Volume of the payload shall be limited to L:140mm W:80mm H:56mm	/	Verified, DDF Drawings, Inspection	Verified
INT-EIDA-5111 The payload shall be designed to operate without performance degradation considering unregulated power supply bus with voltage in the range 18V to 25.2V ± 1%.	/	Verified Electrical Test in AS during TRR	TBV
INT-EIDA-5112 The payload shall utilize the ground wires of the power bus interface as primary return, i.e. structure shall not be used as an intentional return path for either signal or power distribution.	/	Verified Electrical Test in AS during TRR	TBV
INT-EIDA-5115 Power consumption shall be limited to 25.2W (25.2 maximum voltage with 1A current)	/	Verified Electrical Test in AS during TRR	TBV
INT-EIDA-5116 Power cut-offs will not degrade the device.	Verified	Verified Electrical Test in AS during TRR	TBV
INT-EIDA-5119 DC resistance across the electrical bond between any two adjacent parts, shall not exceed 2.5 mΩ	/	/	TBV
INT-EIDA-5120 Isolation of input power lead and return from chassis shall be equivalent to a parallel combination of a resistor of 1MΩ minimum and a capacitor C<50 nF	/	Verified Electrical Test in AS during TRR	TBV
DES-EIDA-5221 The following failure modes, for units at all levels of integration, shall be prevented.	Verified FMEA_DOM	Verified FMEA_DOM	Verified FMEA_DOM

ENV-EIDA-5231 The unit shall be designed to withstand the environment it will encounter during its lifetime without degradation of its performance, and without detrimental influence on the spacecraft or any other unit...	Verified TREP Prototype	Verified TREPs	TBV
ENV-EIDA-5233 The payload shall be designed to withstand the low frequency longitudinal and lateral vibration environment spectra experienced at the platform-to-equipment interface	/	Verified DOM-TREP-Vibration	Verified DOM-TREP-Vibration
ENV-EIDA-5234 The payload shall be designed to withstand the high frequency random environment spectra experienced at the platform-to- equipment interface...	/	Verified DOM-TREP-Vibration	Verified DOM-TREP-Vibration
ENV-EIDA-5235 The payload shall be designed to withstand the Shock Response Spectrum...	/	Verified DOM-TREP-Vibration	Justified in DOM-TREP-Vibration PFM
ENV-EIDA-5236 The payload shall withstand the pressure variation inside the satellite during the ascent phase with the associated maximum depressurization rate of 5.0 KPa/s	/	Verified DOM-TREP-Vacuum	TBV in TVC test
ENV-EIDA-5320 Temperature ranges for operational and non-operational modes shall be defined as: Non-operative: -40°C MIN +85°C MAX,Operative:-25°C MIN +70°C MAX	Partially verified DOM-TREP-Electrical (similarity test)	Verified DOM-TREP-Functional	TBV in TVC test
ENV-EIDA-5340 The payload shall withstand without failure or degradation thermal cycling/vacuum tests considering the temperature limits specified in ECSS-E-ST-10-03C.	Partially verified DOM-TREP-Electrical (similarity test)	/	TBV (April 2017)

237

		Verified DOM-TPRO &TREP-Vacuum	
ENV-EIDA-5410 The payload will be vacuum tested to the effects of depressurization from 1bar to vacuum will not impede the operation of the mechanism.	/	Verified DOM-TPRO &TREP-Vacuum	TBV
INT-EIDA-6110 The payload shall be designed so that correct operation will continue in the presence of RF emissions from the ESEO spacecraft	Verified (similarity)	/	/
INT-EIDA-6120 The payload shall be designed so that it will be resistant to damage during launch by telemetry and other transmissions from the launcher or launch support services	Verified (similarity)	/	/
PRA-EIDA-8310 The supplier shall perform the following analyses and present the results in the review documentation: Structural analysis, Thermal analysis, Functional test	Verified Structural Analysis report	Verified TREP-Functional Structural Analysis report	Verified on EBB

Appendix B

Kaplan-Meier and Weibull Fit

The Kaplan-Meier plots and the corresponding Weibull distributions for each subsystem and specific spacecraft class are presented here.
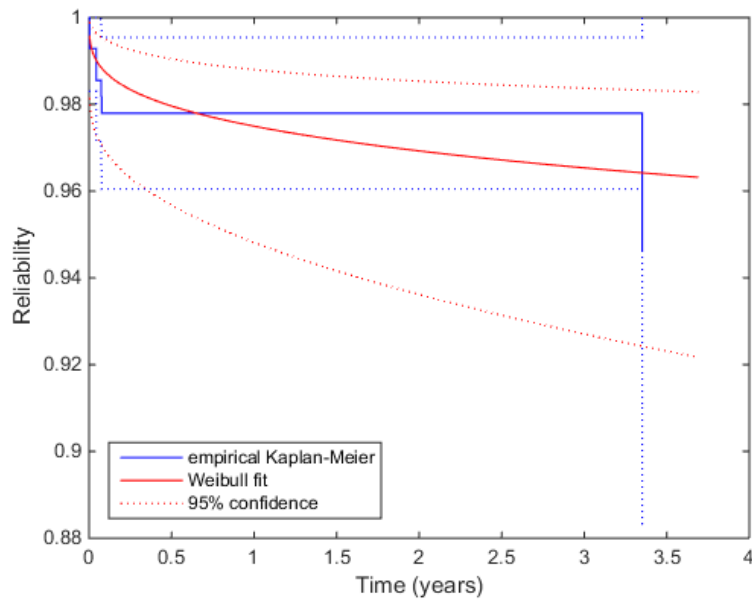
Figure B.1: Kaplan-Meier plot and corresponding Weibull distribution for mechanism subsystem (MECH) of S/C without propulsion, mass range 1-10 kg.
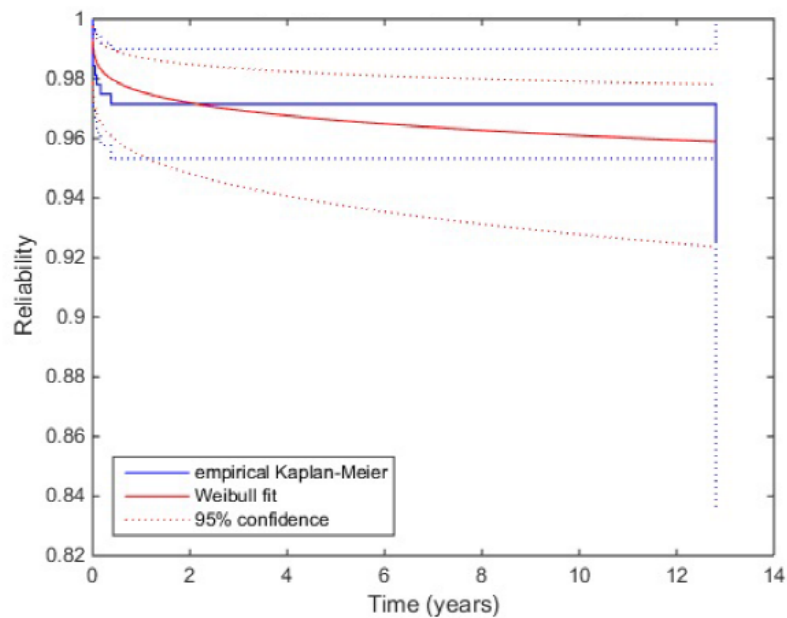

Figure B.2: Kaplan-Meier plot and corresponding Weibull distribution for mechanism subsystem (MECH) of S/C with propulsion, mass range 100-1000 kg.

Figure B.3: Kaplan-Meier plot and corresponding Weibull distribution for TT&C subsystem (TTC) of S/C without propulsion, mass range 1-10 kg.

Figure B.4: Kaplan-Meier plot and corresponding Weibull distribution for TT&C subsystem (TTC) of S/C without propulsion, mass range 10-100 kg.
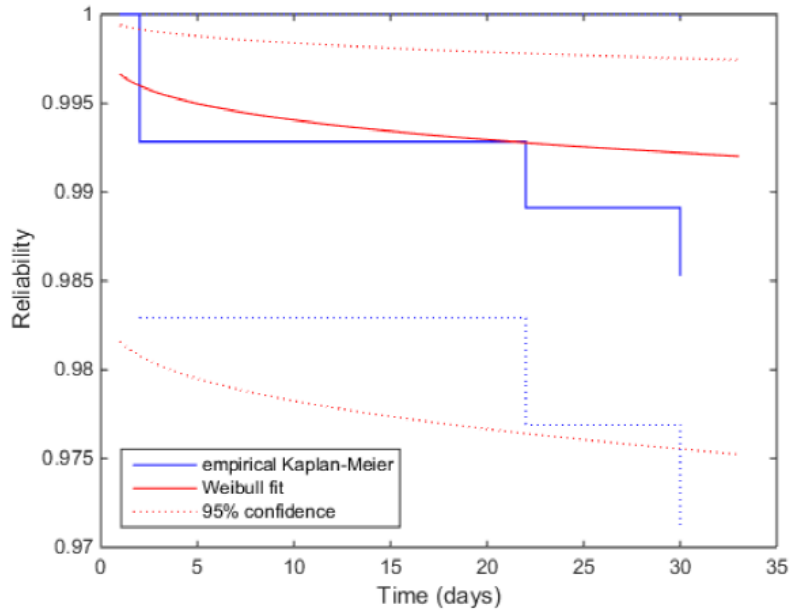
Figure B.5: Kaplan-Meier plot and corresponding Weibull distribution for TT&C subsystem (TTC) of S/C with propulsion, mass range 100-1000 kg.
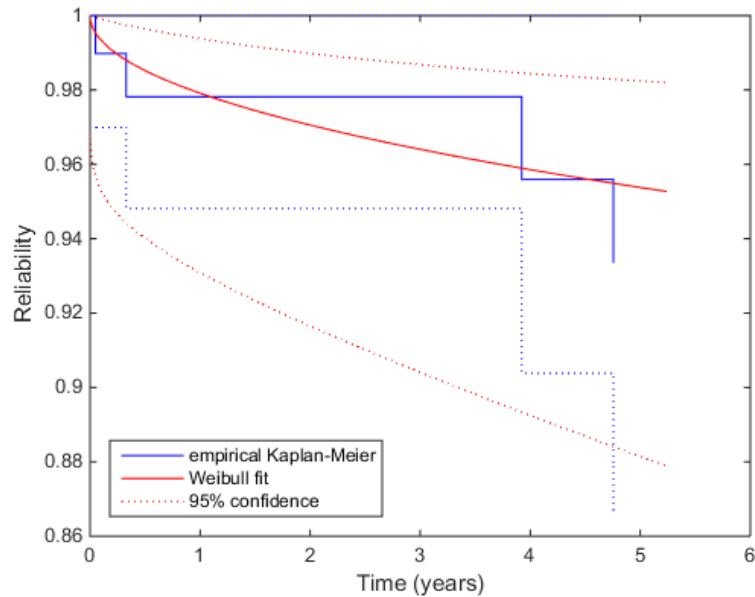

Figure B.6: Kaplan-Meier plot and corresponding Weibull distribution for power subsystem (POW) of S/C without propulsion, mass range 1-10 kg.

Figure B.7: Kaplan-Meier plot and corresponding Weibull distribution for power subsystem (POW) of S/C without propulsion, mass range 10-100 kg.
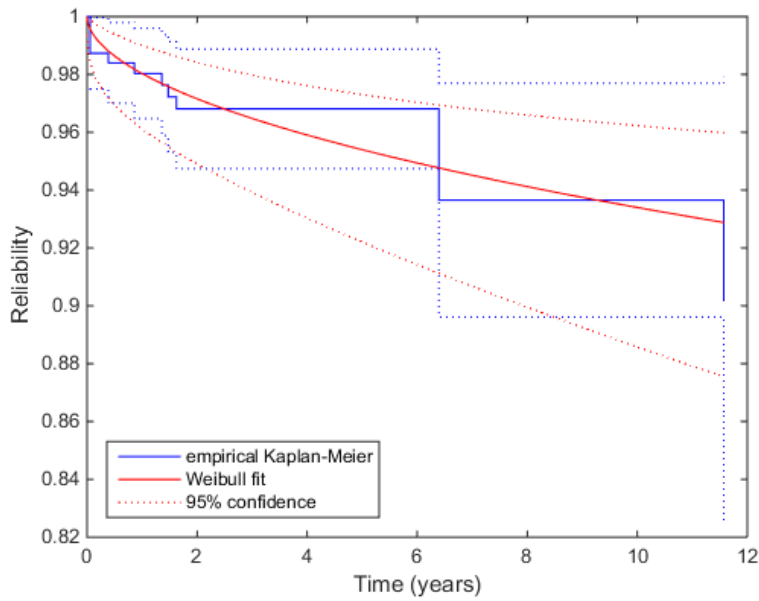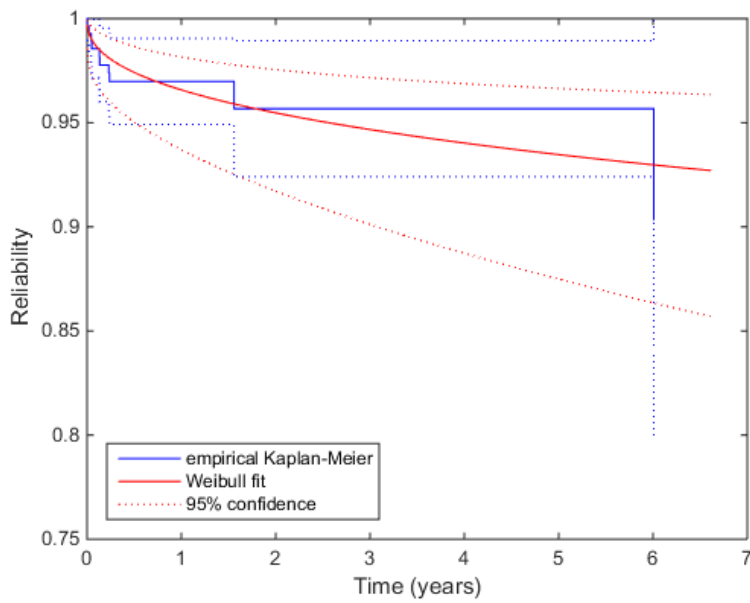

Figure B.8: Kaplan-Meier plot and corresponding Weibull distribution for power subsystem (POW) of S/C with propulsion, mass range 100-1000 kg.
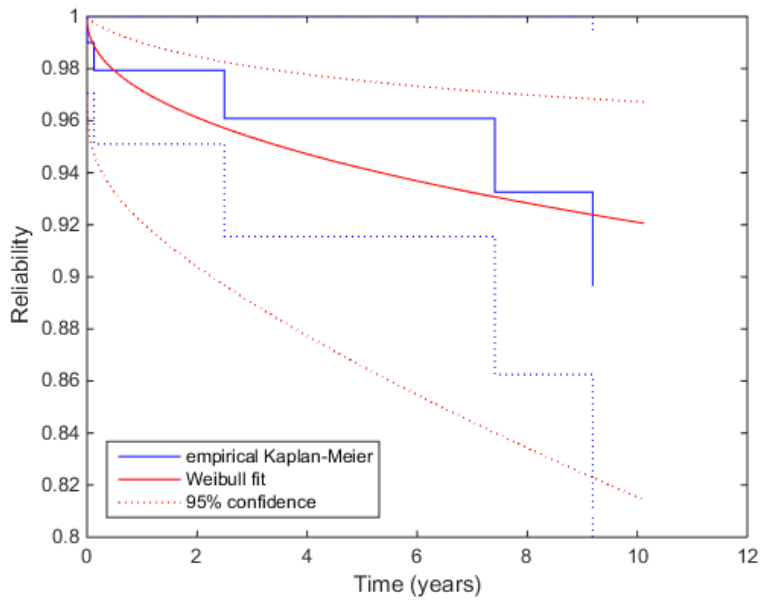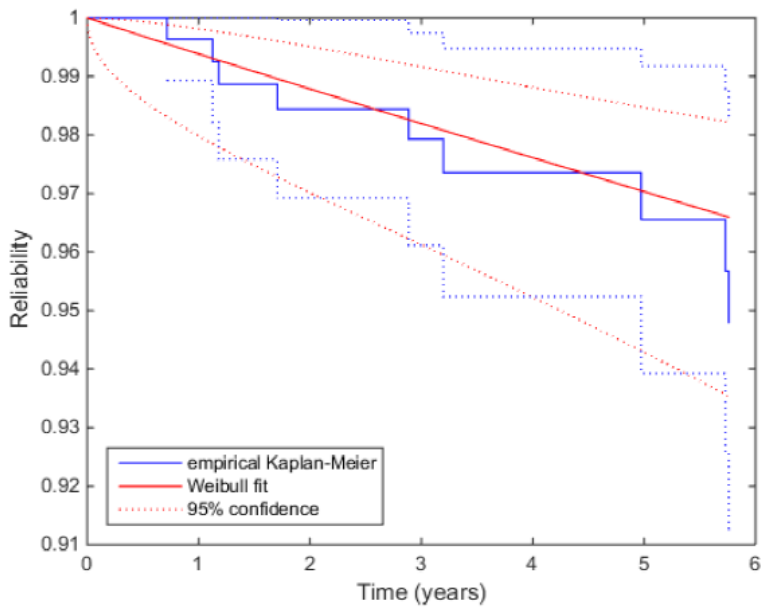
Appendix C

Simulations STELA and DRAMA

C.1 Simulations record examples

Two record datasheets containing the input data for the STELA simulations and the results obtained are showed here.

Input							
Simulation	DMC_3		Kanopus V		VENUS	Dubaisat-3	Gokturk-3
Parameter	Value		Value	Value	Value	Value	Value
Simulation Info							
Simul duration [years]	100		100	50	100	100	100
Orbit parameters (mean) from TLE on orbit							
Reference frame	Celestial Mean of Date		Celestial Mean of Date	Celestial Mean of Date	Celestial Mean of Date	Celestial Mean of Date	Celestial Mean of Date
Date	2015-06-15T00:00:00.000		2015-08-15T00:00:00.000	2015-08-15T00:00:00.000	2016-02-15T00:00:00.000	2017-06-30T00:00:00.000	2019-06-30T00:00:00.000
zp [km]	674.00		510.00	510.00	720.00	600.00	680.00
za [km]	694.00		510.00	510.00	720.00	600.00	680.00
i [deg]	98.20		97.40	97.40	98.27	97.16	98.16
RAAN Ω [deg]	0.00		0.00	0.00	0.00	0.00	0.00
ω [deg]	0.00		0.00	0.00	0.00	0.00	0.00
M [deg]	0.00		0.00	0.00	0.00	0.00	0.00
Object characteristics							
Satellite Class	Mini		Mini	Mini	Mini	Mini	Mini
Mass [kg]	350.00		400.00	400.00	300.00	359.00	450.00
Reflectivity Area [m^2]	0.4000		0.3500	0.8000 solar panel	2.0700	3.1000	
Reflectivity coeff	1.50		1.50	1.50	1.50	1.50	1.50
Drag Area [m^2]	0.4000	tumbling	0.3500	0.8000	2.0700	3.1000	3.1000
Drag coeff	2.2		2.2	2.2	2.2	2.2	2.2
m/A	875		1142.857143	500	144.9275362	115.8064516	145.1612903
Atmospheric drag							
Atmospheric model	NRLMSISE-00		NRLMSISE-00	NRLMSISE-00	NRLMSISE-00	NRLMSISE-00	NRLMSISE-00
Solar activity	Variable (file)		Variable (file)	Variable (file)	Variable (file)	Variable (file)	Variable (file)
Advanced							
Algorithm	Default		Default	Default	Default	Default	Default
Reentry Altitude [km]	120		120	120	120	120	120
TT-UT1 [s]	67.184		67.184	67.184	67.184	67.184	67.184
Output*							
Parameter	Value		Value	Value	Value	Value	Value
Compliance Criteria							
Effective simul duration [years]	>100		41.3	19.07	95.16	16.32	57.23
					But have propulsion for change orbit 410		
Date					1.75		

Figure C.1: Records of STELA decay simulations of planned minisatellites to be launched in SSO.

Input					
Simulation	Case_1	Case_2	Case_3	Case_4	Case_5
Parameter	Value	Value	Value	Value	Value
Simulation Info					
Simul duration [years]	50	50	50	50	50
Orbit parameters (mean) from TLE on orbit					
Reference frame	Celestial Mean of Date	Celestial Mean of Date	Celestial Mean of Date	Celestial Mean of Date	Celestial Mean of Date
Date	2022-12-01T00:00:00.000	2025-06-01T00:00:00.000	2029-06-01T00:00:00.000	2031-06-01T00:00:00.000	2015-12-01T00:00:00.000
zp [km]	650.00	650.00	650.00	650.00	650.00
za [km]	650.00	650.00	650.00	650.00	650.00
i [deg]	98.00	98.00	98.00	98.00	98.00
RAAN Ω [deg]	0.00	0.00	0.00	0.00	0.00
ω [deg]	0.00	0.00	0.00	0.00	0.00
M [deg]	0.00	0.00	0.00	0.00	0.00
Object characteristics					
Satellite Class	Mini	Mini	Mini	Mini	Mini
Mass [kg]	100.00	100.00	100.00	100.00	100.00
Reflectivity Area [m^2]	1.2739	1.2739	1.2739	1.2739	1.2739
Reflectivity coeff	1.50	1.50	1.50	1.50	1.50
Drag Area [m^2]	1.2739	1.2739	1.2739	1.2739	1.2739
Drag coeff	2.2	2.2	2.2	2.2	2.2
m/A	78.5	78.5	78.5	78.5	78.5
Atmospheric drag					
Atmospheric model	NRLMSISE-00	NRLMSISE-00	NRLMSISE-00	NRLMSISE-00	NRLMSISE-00
Solar activity	Variable - Start at Solar MAX	Variable - Start at Solar average (decreasing)	Variable - Start at Solar min	Variable - Start at Solar average (increasing)	SFU=140 Ap=15
Advanced					
Algorithm	Default	Default	Default	Default	Default
Reentry Altitude [km]	120	120	120	120	120
TT-UT1 [s]	67.184	67.184	67.184	67.184	67.184
Output*					
Parameter	Value	Value	Value	Value	Value
Compliance Criteria					
Effective simul duration [years]	21.9	22.3	22.65	21.82	21.09

Figure C.2: Records of STELA sensitivity analysis varying the decay starting date.

C.2   Plots

The plots obtained with STELA and DRAMA for the sensitivity analysis considering the area-to-mass ratio input for 25 y Solar minimum and 22 y Solar mean are presented here.
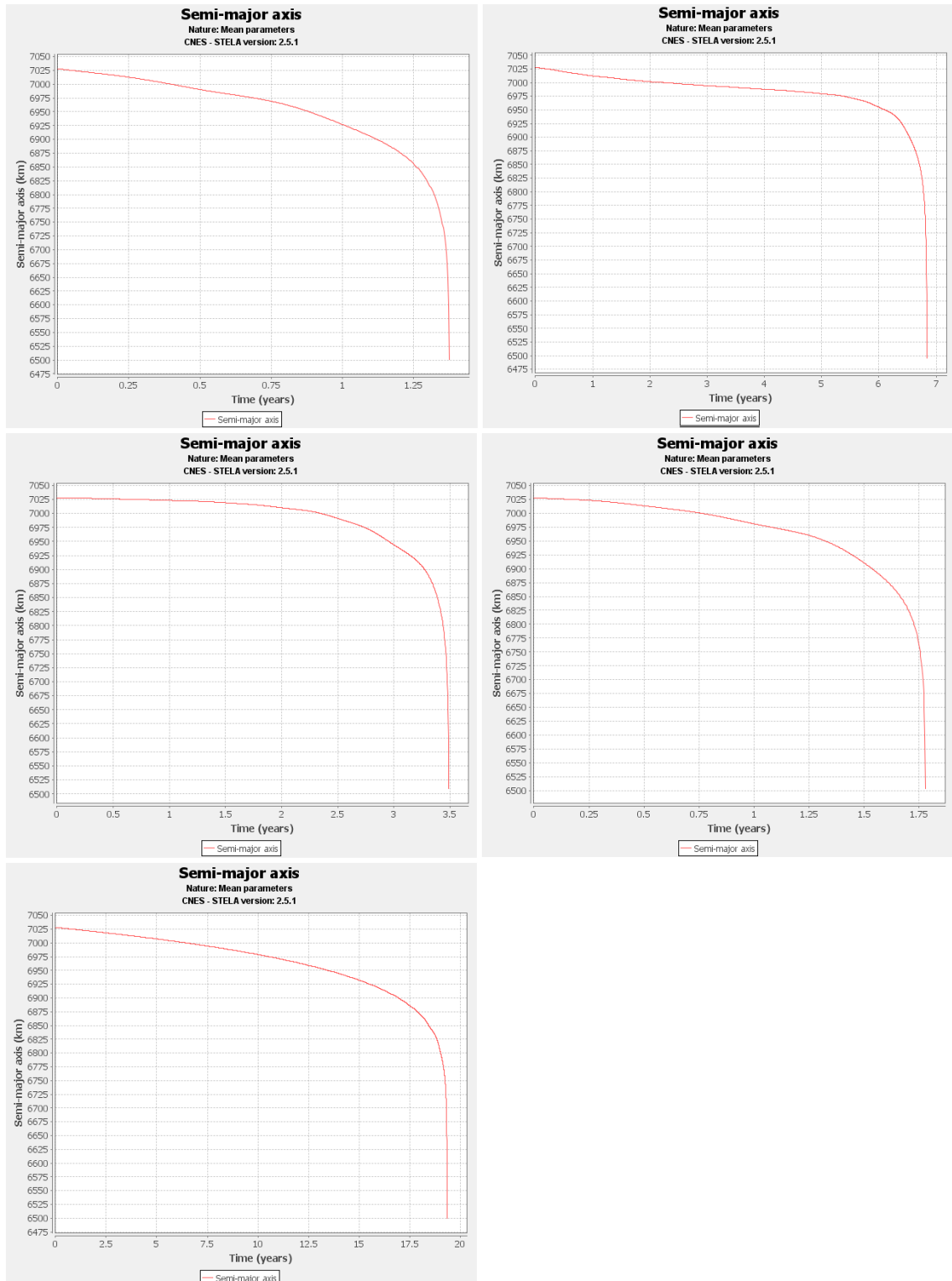
Figure C.3: Semi-major axis vs. time for the 5 cases considered in STELA with Solar minimum 25 y A/m input. In order from left to right, top to bottom.
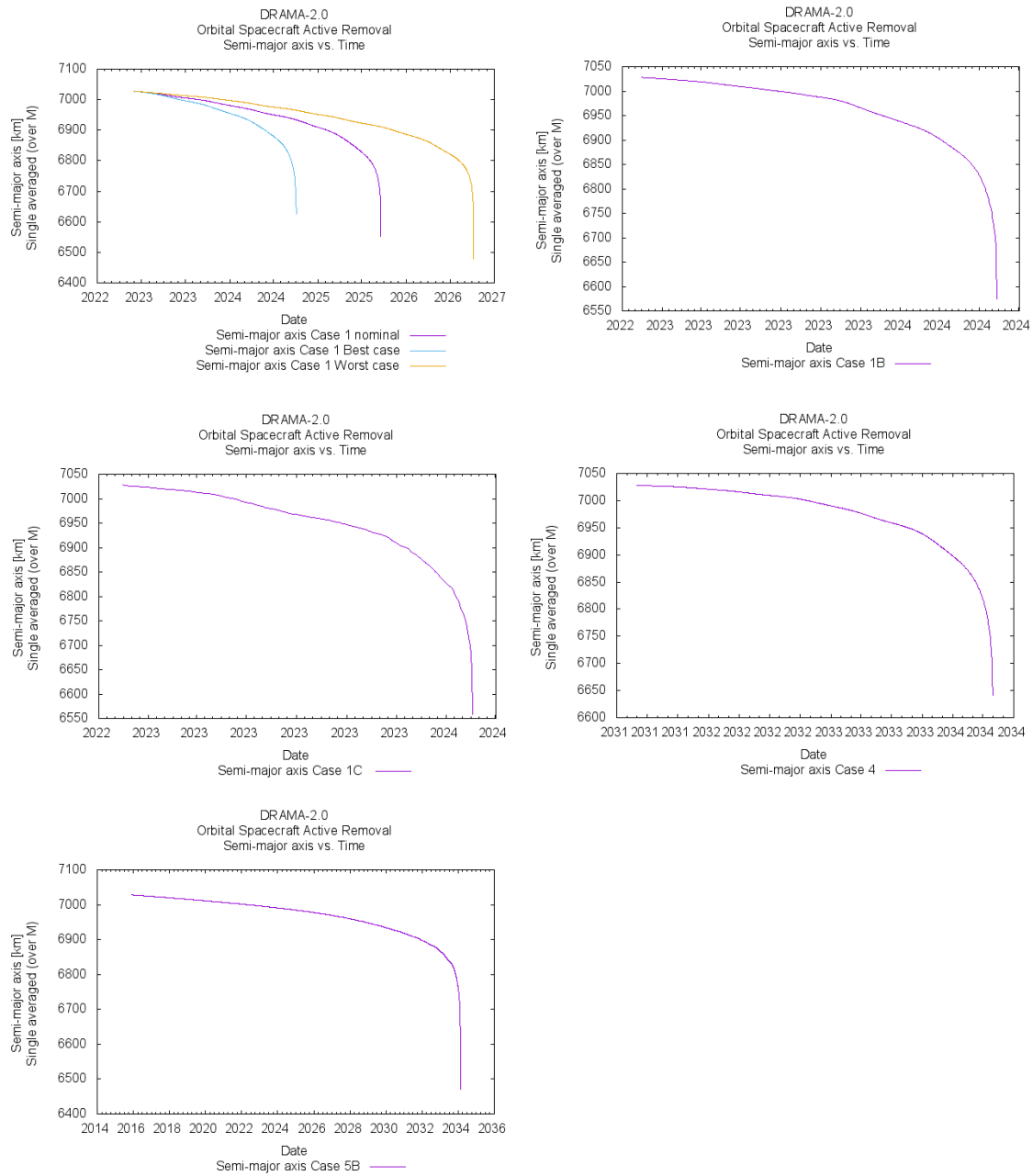
Figure C.4: Semi-major axis vs. time for the 5 cases considered in DRAMA with Solar minimum 25 y A/m input. In order from left to right, top to bottom.
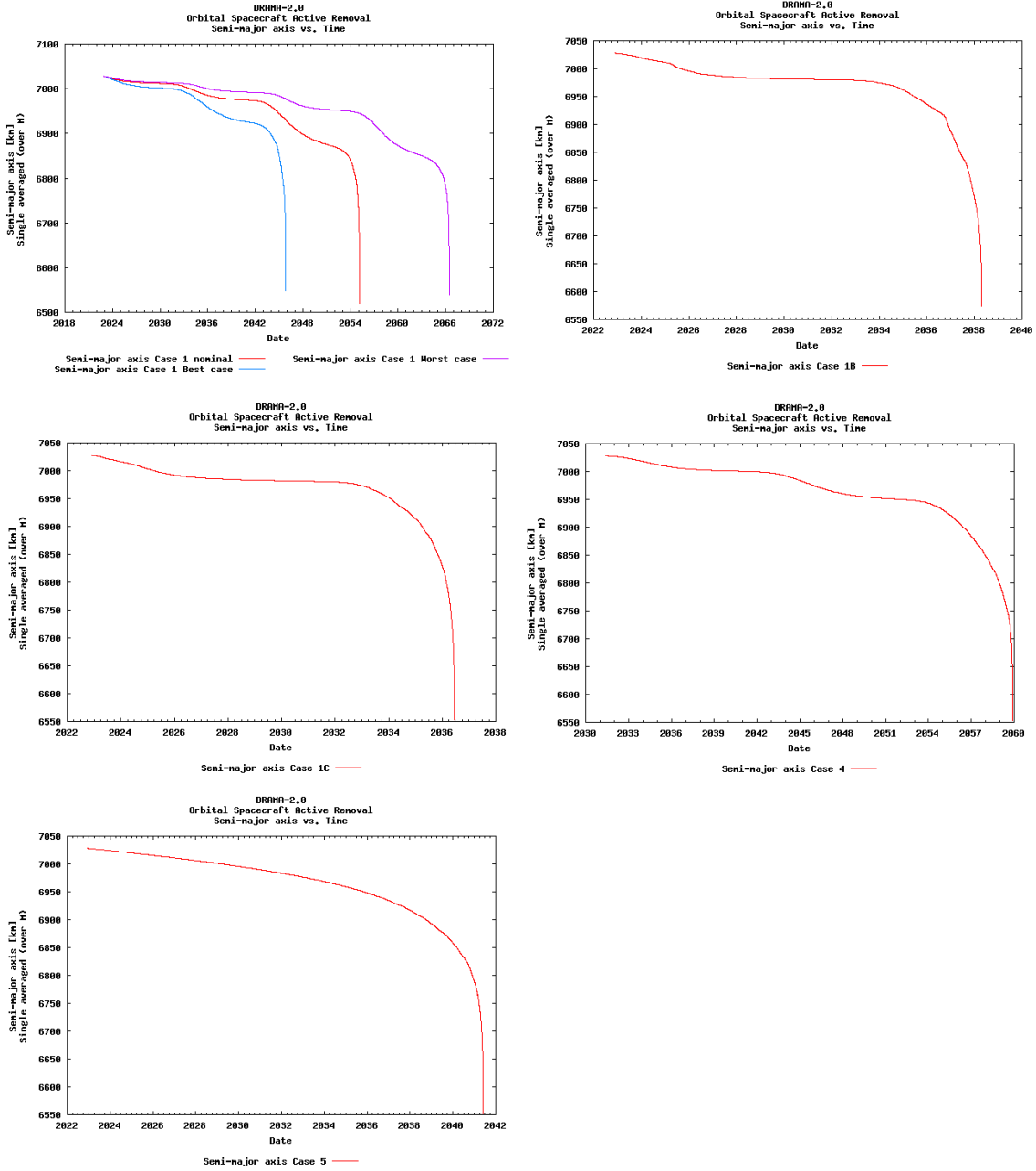
Figure C.5: Semi-major axis vs. time for the 5 cases considered in DRAMA with 22 y A/m input, (see Table 6.4). In order from left to right, top to bottom.

Appendix D

Matlab Codes

The Matlab codes used in the thesis are listed here with their main purposes. Full codes available on request.

control_deorb Computes and plots Δv and propellant mass fraction for direct re-entry, Fig. 2.8 and 2.9.

contr_failure Plots relative contribution of each subsystem to satellite failure from Castet and Saleh data, Fig. 2.10.

Failure_analysis Computes and plots Kaplan-Meier function, Fig. 2.16.

figure_zpconf Computes and plots altitude of perigee vs time from STELA data results for Icarus-3, Fig. 3.10.

figure_a Plots semi-major axis vs time for different DOM-ESEO configurations, Fig. 3.20.

figure_a_comparison Reads and plots semi-major axis from TLE data vs time and from STELA simulation vs time. Used in figures of Chapter 4.

weibull_fit_kaplan_meier Kaplan-Meier analysis from recorded data on S/C classes and their subsystems. Computes and displays Weibull fit parameters. Used in Fig. 5.2 and Appendix B.

weibull_plot_trends Plots Weibull reliabilities using Weibull fit parameters calculated. Used in figures in section 5.2.1.

weibull_comb_probabilities Computes and plots Weibull combined reliabilities, Fig 5.10 and 5.11.

Sail_Area_general Computes and saves drag area achievable with Icarus design concept, used in Chapter 6.

plot_area_side Plots sail area achievable with Icarus design from recorded file, Fig. 6.8.

spoolradius_cp Computes boom length and stowed diameter for DOM, plots Archimedean spiral Fig. 7.1.

Plot_area_drag Plots sail area achievable with Icarus design with design constraints, Fig. 7.3 and 7.4.

crosscorrel_DOM Computes and plots cross correlation boom length, sail foldings, stowed diameter, mass and deployed sail area for DOM/DOM evolution. Used for figures in section 7.2.2.2.

figure_a_comparison Plots semi-major axis vs time for mission performance analysis, Fig. 7.13 and 7.16.